The Arabian killifish (*Aphanius dispar*) as a novel model for mycophysiological studies.

Submitted by Atyaf Saied Hamied to the University of Exeter
as a thesis for the degree of
Doctor of Philosophy in Biological Sciences
In May 2018

This thesis is available for Library use on the understanding that it is copyright material and that no quotation from the thesis may be published without proper acknowledgement.

I certify that all material in this thesis which is not my own work has been identified and that no material has previously been submitted and approved for the award of a degree by this or any other University.

Signature: Atyaf S. HAMIED

Abstract

Candida albicans is a commensal fungal pathogen that grows in yeast and hyphal forms in the human gut. *C. albicans* causes mucosal and cutaneous diseases that can result in significant mortality following systematic infections and it also exhibits drug resistance. Zebrafish have been an excellent model to investigate *C. albicans* infections because of their transparency and the availability of many transgenic lines. However, there is a limitation in using zebrafish as a model because the fish embryos cannot survive at 37°C therefore it is not suitable for studying Candida infections at physiological relevant human body temperature. In this thesis, the normal embryonic development of Arabian killifish (*A. dispar)* is investigated, revealing that embryogenesis was divided into 32 stages based on diagnostic patterns of development. *A. dispar* can also found to tolerate a wide range of temperatures and salinities. This suggests that *A. dispar* could be developed as a novel model to investigate host-pathogen interactions. The tolerance of *A. dispar* to high temperatures may in part be attributable to brown pigment cells with a highly fluorescent character that may have developed to allow the fish to adapt to live within extreme environmental conditions with strong sunlight and a wide range of temperatures (Chapter 3). In terms of Candida infections, this study examined *A. dispar* as a model to test *C. albicans* pathogenicity. The survival of *A. dispar* embryos following Candida infection showed a dose dependent relationship. We also found that *A. dispar* can survive longer than zebrafish after infection. Furthermore, *C*. *albicans* cells were observed to undergo a transition from yeast to hyphae at 37°C. An investigation of the ability of mutant strains of *C. albicans* with defects in cell wall mannosylation revealed a significant impact on virulence, host mortality, and the fishes' immune response. The present study found that although the deletion of *O*- and *N*-mannan from the cell wall of *C. albicans*, affected fungal burden (attenuation), and the survival of the infected embryos *per se* was significantly decreased in the infections of the mutant strains compared to the WT. This data confirms the importance of the mannosylation state of the cell wall in triggering an immune recognition event (Chapter 4). *A. dispar* is also shown to be suitable for studying the effectiveness of

antifungals. Fluconazole treatment of infected embryos and eggs promoted greater rates of survival at high doses, alongside a significant reduction of *C. albicans* CFUs (Chapter 4). When looking at the Candida-host interaction, we directly observed phagocytosed yeast cells within macrophages. Various detection methods were used to follow macrophages and neutrophils including Western blotting, immunostaining and histological staining (Sudan black and FITC-tyramide) allowing the monitoring of the time course of the immune cells. A biphasic response of macrophages was detected by L-plastin Western blotting, suggesting activation of two different type of macrophage: activated macrophage (M1) and alternative macrophage (M2). We also assayed reactive oxygen species (ROS) within infected embryos using a fluorescent probe (H_2DCFDA), revealing the accumulation of the fluorescent probe at the sites of infection. Quantitative and qualitative analyses of the oxidative and immune response using the H_2DCFDA and qPCR were also accomplished within *A. dispar* embryos after infection with both the WT and mutant strains of *Candida albicans* (WT, *pmr1*Δ*, mnt1-mnt2*Δ*,* and *och1*Δ). The results confirmed that the mutant strains did not activate a host oxidative stress response nor immune cell accumulation when compared to WT, suggesting that the immune response is less activated against these mutants.

Finally, a new transgenic line of *A. dispar* fish was developed using Beta-actin-DsR-LoxP-GFP. The new transgenic *A. dispar* is suggested to be an ideal model for real time observation of host-pathogen interactions and for investigation of molecular functions of the immune response.

Overall these results improve our understanding of the use of a new transparent fish model to study fungal pathogenesis and demonstrates the potential advantages of using this species in future studies of bacterial, fungal and viral pathogens at a physiologically relevant temperature for human infection. Such a model could lead us to investigate in more depth the key interactions between pathogens and their host and permit the screening and development of new antifungal therapies (that might target the pathogens directly or target the host immune system).

Acknowledgements

First and foremost, I would like to express my sincere thanks to my advisors Dr. Tetsu Kudoh and Dr. Mark Ramsdale for the continuous support of my Ph.D study and related research. I appreciate all their contributions of time, patience, motivation, and their great guidance that helped me in all the time of research and writing of my thesis. I would like to express my gratitude to Dr. Steven Bates of the University of Exeter, Robert T. Wheeler of the Maine University, Dr. Paul Martin of the Bristol University and Dr. Robert Kelsh of the Bath University for their generosity and assistance.

I would like to thank members of the Tetsu lab. I would also like to acknowledge my colleagues in the microbiology lab, Sarah Duxbury and Lauren Ames for their assistance during my lab work. Thanks to John Dowdle and Anke Lange, the lab managers, for their kind help and cooperation. Thanks to my kind colleagues at the University of Exeter; especially, Seta Noventa, Carole Lee and Ruth Cooper for their great support and assistance. Thanks to the team of the Aquatic Resources Centre for their support and assistance. The biggest thanks go to my sponsor, the Iraqi government for giving me this great opportunity to do my PhD at the University of Exeter and support throughout my study period.

Finally, I would like to thank my family. Words cannot express how grateful I am to my mother and father and my sisters for supporting me for everything, your encouragement for me was what sustained me thus far. I would especially like to thank my beloved husband, Qusay Alnedawy for supporting me and for all of the sacrifices that you've made on my behalf. To my beloved daughters Sarah and Arwa, I would like to express my thanks for being such brilliant girls and for always encouraging me up.

Table of Contents

	Page
Title	1
Declaration	1
Abstract	2
Acknowledgments	4
Table of Contents	5
List of figures	11
List of tables	15
List of appendices	15
List of Abbreviations	16
Chapter 1: Introduction	20
1.1 Candida species	20
1.2 A unique fungus: *C. albicans*	21
1.3 Virulence factors and pathogenicity	22
1.3.1 Adherence to the host tissue	24
1.3.2 Morphogenesis	26
1.3.3 Invasion of *C. albicans*	27
1.3.4 Secreted hydrolases	28
1.3.5 pH sensing and metabolic adaptation	29
1.3.6 Biofilm formation	29
1.4 Fungal Cell Wall	31
1.4.1 Fungal cell wall components	31
1.4.2 *C. albicans* mannosylation	33
1.5 Innate immunity	35
1.6 Phagocytosis	36
1.6.1 Phagocytosis and macrophages	37
1.6.2 Macrophage-specific gene expression	38
1.6.2.1 L-plastin	39
1.6.2.2 Irf8	40
1.6.2.3 Csf1r	40
1.6.3 Phagocytes (neutrophils)	41

1.6.3.1 Mpx 41
1.6.3.2 CXCR4 42
1.7 Reactive oxygen species (ROS) 43
1.7.1 Nox1 43
1.8 The interplay between *C. albicans* and innate host defense 44
1.9 Antifungal reagents 46
1.10 Limitation of animal models research for Candida albicans at 37˚C. 47
1.10.1 Zebrafish in some studies 49
1.10.2 A. killifish (*A. dispar*) 50
Chapter 2- Materials and Methods 54
2.1 Organisms group, strains, plasmids, and primers. 54
2.1.1 *C. albicans* strains 54
2.1.2 Bacterial Strain 55
2.1.3 Fish models 55
2.1.4 Plasmids 56
2.1.5 Primers 57
2.2 Fish Care and Maintenance 58
2.2.1 Arabian killifish (*Aphanius dispar*) 58
2.2.2 Medaka (*Orizias latipes*) 58
2.2.3. Zebrafish (*Danio rerio*) 59
2.3 Microinjection technique 59
2.4 Media and Culture 60
2.4.1 Media and culture for *C. albicans* 60
2.4.2 Media and culture of Bacteria 60
2.4.3 Long-term storage of *C. albicans* strains 61
2.5 Molecular Techniques 61
2.5.1 *E. coli* preparation 61
2.5.2 Transformation of *E. coli* 61
2.5.3 Isolation of plasmid DNA 61
2.5.4 Gel electrophoreses to resolve DNA fragments 62
2.5.5 Generation of transgenic fish 62

2.6 Gene expression analyses using in situ hybridization 63
2.6.1 Preparation of in situ probes 63
2.6.1.1 Preparation of template DNA using digestion and purification of plasmid DNA 63
2.6.1.2 Preparation of template DNA using PCR 64
2.6.1.3 Probe synthesis using template DNA 64
2.6.2 Preparation of samples 65
2.6.3 In situ hybridization 65
2.7 qPCR 66
2.7.1 *C. albicans* Culture Preparation 66
2.7.2 *A. dispar* embryo infections 66
2.7.3 Isolation of RNA samples 67
2.7.4 Reverse transcription 67
2.8 Protein analysis 68
2.8.1 Western blotting 68
2.8.1.1 Western blotting materials 70
2.8.2 Immunohistochemistry 70
2.8.2.1 Paraffin sectioning 70
2.8.3 Immunofluorescence staining of macrophages and Candida cells. 71
Chapter 3 74
3.1 Abstract
3.2 Introduction 75
3.3 Materials and Methods 77
3.3.1 *Aphanius dispar* care and maintenance 77
3.3.2 Dechorionation 78
3.3.3 PTU 78
3.3.4 In situ probe synthesis 78
3.3.5 In situ hybridization 79
3.3.6 Imaging 80
3.3.7 Statistical analysis 80
3.4 Results 81
2.4.1 Normal embryonic development in A. killifish (*A. dispar*) 81

3.4.2 Influence of water temperature on embryonic development 88
3.4.3 Influence of water salinity on the embryonic development 89
3.4.4 The brown pigment in *A. dispar* is highly fluorescent 91
3.5 Discussion 100
Chapter 4 104
4.1 Abstract
4.2 Introduction 106
4.3 Experimental procedures 109
4.3.1 *C. albicans* strains and growth conditions 109
4.3.2 Maintenance of Arabian killifish and embryo collection 109
4.3.3 Microinjection 109
4.3.4 Enumeration of fungal burdens 110
4.3.5 Calcofluor staining 110
4.3.6 Histological analysis of *C. albicans* colonization in *A. dispar* 110
4.3.7 Immunofluorescence Staining 111
4.3.8 Western blotting 111
4.3.9 Direct *A. dispar* egg infection 112
4.3.10 *A. dispar* survival and killing assay (Fluconazole serial dilution) 113
4.3.11 Growth analysis of *C. albicans* strains 113
4.4 Results 114
4.4.1 Dose dependent lethality assay using *A. dispar* embryos infected with *C. albicans* 114
4.4.2 Injection of *A. dispar* with *C. albicans* at different temperatures 115
4.4.3 The *A. dispar* embryo show higher tolerance to Candida infection than zebrafish 116
4.4.4 Dynamics of fungal burden of the *C. albicans* infected in the *A. dispar* embryos with human body temperature. 118
4.4.5 *C. albicans* can infect both brain and yolk in *A. dispar* 119

embryos
4.4.6 *C. albicans* can develops hyphae in the *A. dispar* embryo 120
4.4.7 Examination of *C. albicans* invasion in *A. dispar* 121
4.4.8 Visualization of *C. albicans* infection using red-fluorescent *C. albicans* line infected in the live *A. dispar* embryos 122
4.4.9 Time-course of infection in *A. dispar* embryos 124
4.4.10 Attenuation of virulence in the *C. albicans* mannosylation mutants 126
4.4.11 *C. albicans* can infect chorion of the *A. dispar* 130
4.4.12 *C. albicans* infection in the *A. dispar* are suppressed by fluconazole in a dose and time dependent manner 134
4.4.13 Effect of fluconazole on the number of CFU of *C. albicans* within *A. dispar* embryos 137
4.5 Discussion 139
4.5.1 Utility of *A. dispar* as a model 139
4.5.2 Utility of *A. dispar* as a model to screen mutants 142
4.5.3 *A. dispar* as a model to investigate antifungal drug therapy 144
Chapter 5 Infection and the immune response of *A. dispar* embryos 147
5.1 Abstract 147
5.2 Introduction 148
5.3 Experimental procedures 153
5.3.1 RNA-sequence of *A. dispar* to reveal immune function 153
5.3.2 Removing the chorion 153
5.3.3 Survival rates in infected zebrafish embryos 154
5.3.4 Sudan Black and tyramide-FITC staining of embryos to reveal neutrophils 154
5.3.5 Immunofluorescence staining 154
5.3.6 Morpholino knockdown 155
5.3.7 Western blot analysis of L-plastin expression in infected 155

embryos
5.3.8 Time-lapse fluorescent imaging of *A. dispar* embryos 156
5.3.9 RT-PCR 156
5.3.9.1 RNA isolation, cDNA synthesis, and expression assay 156
5.3.9.2 Primer design 156
5.3.9.3 Primer optimisation 157
5.3.9.4 Amplification efficacy and primers specificity 157
5.3.9.5 qPCR quantification of *A. dispar* samples 158
5.3.9.6 Data analysis 158
5.3.9.7 ROS detection 158
5.3.10 Production of transgenic *A. dispar* 159
5.4 Results 159
5.4.1 Analysis of total RNA of *A. dispar* 159
5.4.2 Assays of wild-type and Casper zebrafish killing by *C. albicans* 160
5.4.3 Sudan Black (SB) stained granulocytes in *A. dispar* embryos 162
5.4.4 Rapid and specific dissemination of macrophages in response to Candida infection 164
5.4.5 Suppression of *irf8* and *cxcr4* expression blocks the development of macrophages 167
5.4.6 Immunofluorescence analysis of microglial cell distribution 169
5.4.7 Time-course of phagocytosis in *A. dispar* embryos 171
5.4.8 Deletion of mannan from the *C. albicans* cell wall affected macrophages-*L-plastin* levels 172
5.4.9 Direct real-time visualisation of Candida-host immune cell interactions in vivo 172
5.4.10 Macrophages show tissue specific response in relation to interact with *C. albicans* 174
5.4.11 Reactive Oxygen Species (ROS) detection within *A. dispar* embryos 175
5.4.12 Induction of the immune response and gene 178

expression is required for elimination of the fungal Infection
5.4.13 Development of the transgenic *A. dispar* fish 180
5.5 Discussion 181
Chapter 6- General discussion 190
6.1 Normal embryonic development 190
6.2 *A. dispar* as a model to investigate fungal infection 192

List of Figures

Figure		Page
1.1	Simplified fungal phylogeny.	21
1.2	The mechanisms of pathogenicity in *C. albicans.*	24
1.3	Fungal adhesion is promoted by secretion of specialized cell surface protein, adhesins that anchor cells to surfaces.	25
1.4	Morphogenesis of *C. albicans* within innate immune cells (macrophages).	27
1.5	biofilm formation	30
1.6	The arrangement of *C. albicans* cell wall components.	31
1.7	A simplified model of the Candida yeast cell wall.	33
1.8	Structures produced by *C. albicans* mannosylation mutants (N- and O-linked glycosylation).	35
1.9	Arabian killifish (*Aphanius dispar*)	51
2.1	Injection of diluted *C. albicans* into *A. dispar* embryos.	60
3.1	Normal embryonic development in *A. dispar.*	83

3.2	Developmental stages in *Aphanius dispar* showing stage from somitogenesis to organogenesis.	85
3.3	Development stages from organogenesis to hatching.	87
3.4	Influence of water temperature on the growth of *A. dispar* embryos.	88
3.5	Influence of water salinity on the growth of *A. dispar* embryos.	90
3.6	Influence of water salinity on the length of *A. dispar* embryos.	91
3.7	Development of fluorescent pigment cells in the trunk.	92
3.8	Development of fluorescent pigment cells in the head.	93
3.9	Development of fluorescent pigment cells in the yolk.	94
3.10	Characterisation of fluorescent pigment cells with different filter combinations.	95
3.11	Leucophores do not contain melanin.	97
3.12	Leucophores in *A. dispar* are brighter than in medaka.	98
3.13	Fluorescent pigment cells express gch	99
4.1	*A. dispar* killing assay by *C. albicans*	115
4.2	Injection into the *A. dispar* at (26°C, 30°C, 37°C and 38.5°C)	116
4.3	Fungal burden in the yolk of *A. dispar* and zebrafish at 30 °C	117
4.4	Human body temperature is required to evaluate the infection in *A. dispar*.	118
4.5	Injection *A. dispar* embryos into the hindbrain and	119

	yolk with 1X10^8 cells/ml *C. albicans*	
4.6	Morphogenesis of *C. albicans* in crushed embryos	120
4.7	Morphological transition of *C. albicans* (CAF2-dTomato) cells attached to *A. dispar*.	122
4.8	Whole mount immunofluorescence of hyphal growth of *C. albicans* in life embryos stained with anti-rabbit-R2 antibody.	123
4.9	Candida CAF-dTomato and GFP proteins in the yolk of *A. dispar* and Zebrafish embryos.	125
4.10	Growth curve of *C. albicans* mutant's cells from culture growing in YPD for 22 hours.	127
4.11	Growth profile of *C. albicans* mutant and parental strain at 37°C and 40°C.	128
4.12	Human body temperature is required to evaluate the infection in *A. dispar*.	129-130
4.13	Infection of *A. dispar* eggs with different condition.	131
4.14	Evaluation of CAF2-dTomato *C. albicans* protein within infected embryos under different condition of media/serum and salinity.	133
4.15	Localization of *NGY152, och1*Δ*, mnt1-mnt2*Δ and *pmr1*Δ of *C. albicans* cells in the infected *A. dispar* embryos model.	134
4.16	The Protective Role of FLC with different doses against *C. albicans* Strains in the *A. dispar* Infection Model.	136
4.17	Fungal burden during *A. dispar* infected with *C. albicans.*	138
5.1	Assessment of RNA integrity and quantification of RNA from *A. dispar.*	160
5.2	Pigment free mutants of zebrafish (Caspar) are less resistant to *C. albicans* infection than the WT	161

	embryo	
5.3	Sudan Black (SB)-stained neutrophils in *A. dispar* embryos.	163
5.4	Macrophages revealed by *L-plastin* marker within zebrafish and Arabian killifish embryos.	165
5.5	*L-plastin* labelled macrophages are significantly recruited during fungal infection in *A. dispar* embryos	166
5.6	*irf8* and *cxcr4*-MO injected embryos have no macrophages and randomly expression of macrophages with *cxcr4*-MO.	168
5.7	Survival curve of *A. dispar/irf8*-MO after *C. albicans* infection.	169
5.8	Visualization of microglia in the brain and spinal cord of *A. dispar* embryos	170
5.9	Time-course of *L-plastin* expression within activated macrophages following *C. albicans* infection.	171
5.10	Activation of *L-plastin* level by different *C. albicans* mutants	172
5.11	Direct real-time visualization of the Interaction between Candida and immune cells of *A. dispar*.	173
5.12	Fluorescence imaging of *C. albicans* and macrophages (*L-plastin*) within *A. dispar* embryos.	175
5.13	Whole mount ROS-detection in *A. dispar* embryos	176
5.14	Quantification of ROS in *A. dispar* embryos using H_2CFDA fluorescence intensity measurements in a microplate reader.	177
5.15	qPCR monitoring of immune response in *A. dispar* embryos after Candida infection.	179
5.16	Generation of transgenic Arabian killifish.	180

List of Tables

Table		Page
2.1	*C. albicans* strains used in this study	54
2.2	Organism models used in this study	55
2.3	Plasmids used in this study	56
2.4	General oligonucleotides used in this study for the qPCR	57
2.5	Primary and secondary antibodies used for western blots	69
2.6	western blot reagents	70
2.7	Primary and secondary antibodies used for immunofluorescence	73
5.3.9.2	Parameters for primer design	157
6.1	*C. albicans* kills organisms in a dose dependent manner	194
6.2	Summary comparison of *A. dispar* and *D. rerio* as models	207

List of Appendices

Appendix 1	Plasmid map of Ad_ptgs2	243
Appendix 2	Plasmid map of Ad_mpx	244
Appendix 3	Plasmid map of Ad_mfap1	245

Abbreviations

(1 Δg)	Single oxygen
. OH	Hydroxyl radicals
°C	Degrees Celcius
3’	Three prime
5’	Five prime
Amp	Ampicillin
ANOVA	Analysis of variance
ASW	Artificial Sea Water
bd	Blastodisc
BLAST	Basic Local Alignment Search Tool
bp	Base pair
bp	Base pair
BPS	Bathophenanthrolinedisulfonic acid disodium salt hydrate
BSA	Bovine serum albumin
BSI	Bloodstream infection
bv	Blood vesicle
CaCl2	Calcium chloride
ch	Chorion
CLRs	C-type lectin receptors
CNS	Sentral Nervous System
CSF1R	Colony Stimulating Factor 1 Receptor
CXCR4	Chemokines receptor 4
dl	Dorsal lip
DNA	Deoxyribonucleic acid
dNTP	Deoxyribonucleotide
EDTA	Ethylenediaminetetraacetic acid
ep	Epiboly
et al.	and others

EtOH	Ethanol
ey	Eye
fb	Forebrain
FLC	Fluconazole
g	Gram
g/L	Grams per liter
G-CSF	Granulocyte Colony- Stimulating Factor
GFP	Green fluorescent protein
GM-CSF	Macrophage colony-stimulating factor
GPI	Glycosylphosphtidylinositol
GPI	Glycosylphosphtidylinositol
GPI-CWP	Glycosylphosphtidylinositol- dependent Cell wall proteins
h	Heart
H2O	Water
H_2O_2	Hydrogen peroxide
hb	Hindbrain
HCl	Hydrochloric acid
hpf	Hour post fertilization
ICSBP	Interferon Consensus Sequence Binding Protein
Imo	Inflammatory monocytes
kb	Kilobases
KCl	Potassium chloride
KOH	Potassium hydroxide
L	Litre
l	Lens
LB	Luria broth media
LiCl	Lithium chloride
LPS	Lipopolysaccharide
M	Molar

MAP	Mitogen-activated protein
mb	Midbrain
mg	Milligram
mg/ml	Milligram per millilitre
MgCl2	Magnesium chloride
MgCl2	Magnesium chloride
ml	Millilitre
ml/L	Millilitre per litre
mM	Millimolar
M-MLV	Moloney Murine Leukemia Virus
MOPS	3-(N-Morpholino)-propanesulfonic acid
Mpo	Myeloperoxidase
NaCl	Sodium chloride
NADPH	Nicotinamide Adenine Dinucleotide Phosphate
NLRs	NOD-like receptors
nm	Nanometres
O_2-	Superoxide
od	Oil droplet
OD_{600}	Optical density at 600 nm
ov	Otic vesicle
p	Pigmentation
p	Pigmentation
PAMP	Pathogen-associated molecular pattern
PAMPs	pathogen-associated molecular patterns
PBS	Phosphate buffered saline
PCR	Polymerase chain reaction
PFA	Paraformaldehyde
pH	Measure of the acidity or alkalinity of

	a solution
PLPM	Posterior lateral plate mesoderm
Pmol	Pico molar
ppt	Part per thousand
PRRs	Pattern Recognition Receptors
PTU	1-phenyl 2-thiourea
RLRs	RIG-I-like receptors
RNA	Ribonucleic acid
RNS	Reactive nitrogen species
RO	Reverse Osmosis
ROS	Reactive Oxygen Species
rpm	Revolutions per minute
RPMI	Roswell Park memorial institute
RT-PCR	Reverse transcription polymerase chain reaction
S	Somite
SDF-1	Stromal cell-derived factor 1
TAE	Tris-acetate-EDTA
TLRs	Toll-like receptors
TLRs	Toll-like receptors
UV	Ultraviolet
V	Volts
WISH	Whole-mount in situ hybridization
Yo	Yolk
YPD	Yeast extract peptone media
YSL	Yolk syncytial layer
Mg	Micrograms
µg/ml	Micrograms per millilitre
µl	Microliter
µM	Micromolar

Chapter 1- Introduction

1.1 Candida species

In the past few decades, interest in fungal diversity has increased and has attracted more attention from scientists than in any period before. Although fungi are among the most important microorganisms in the world, currently there are significant differences between estimated species numbers for fungi and completed information on fungal diversity (Schmit, 2014). The total number of fungal species has been estimated to be 1.5 million species (Hawksworth, 2001). Fungi make up approximately 7% (611,000) of the total number of Eukaryotic species, which have been recently estimated at 8.7 million. Over 600 species of fungi are known to be human pathogens (Mayer *et al., 2013*) and cause life-threatening infections of billions each year (Gow *et al*., 2011; Hawksworth, 2001). Fungal Infections have markedly increased during the last three decades and fungal pathogens have emerged as a significant public health problem. During the 20th century, most common human fungal infections were caused by Candida species. Certain factors have contributed in the occurrence of mycotic infections, such as HIV/AIDS, the increased use of a broad spectrum of immuno-suppressive therapies, and also increases in life expectancy, which is a particularly important factor (Deorukhkar and Saini, 2015).

Candida species (Fig. 1.1) are a group of human pathogens and are the fourth most common cause of blood stream infection (BSI) in the United States (Hajjeh *et al.,* 2004). Approximately, 8% to 10% of these infections are acquired in hospitals (Pfaller *et al*., 2007; Wisplinghoff *et al*., 2004). There are around 200 recognized Candida species, but only 10% are considered pathogenic. The latter are the cause of life-threatening systematic infections in immunologically weak people (Turner and Butler, 2014).

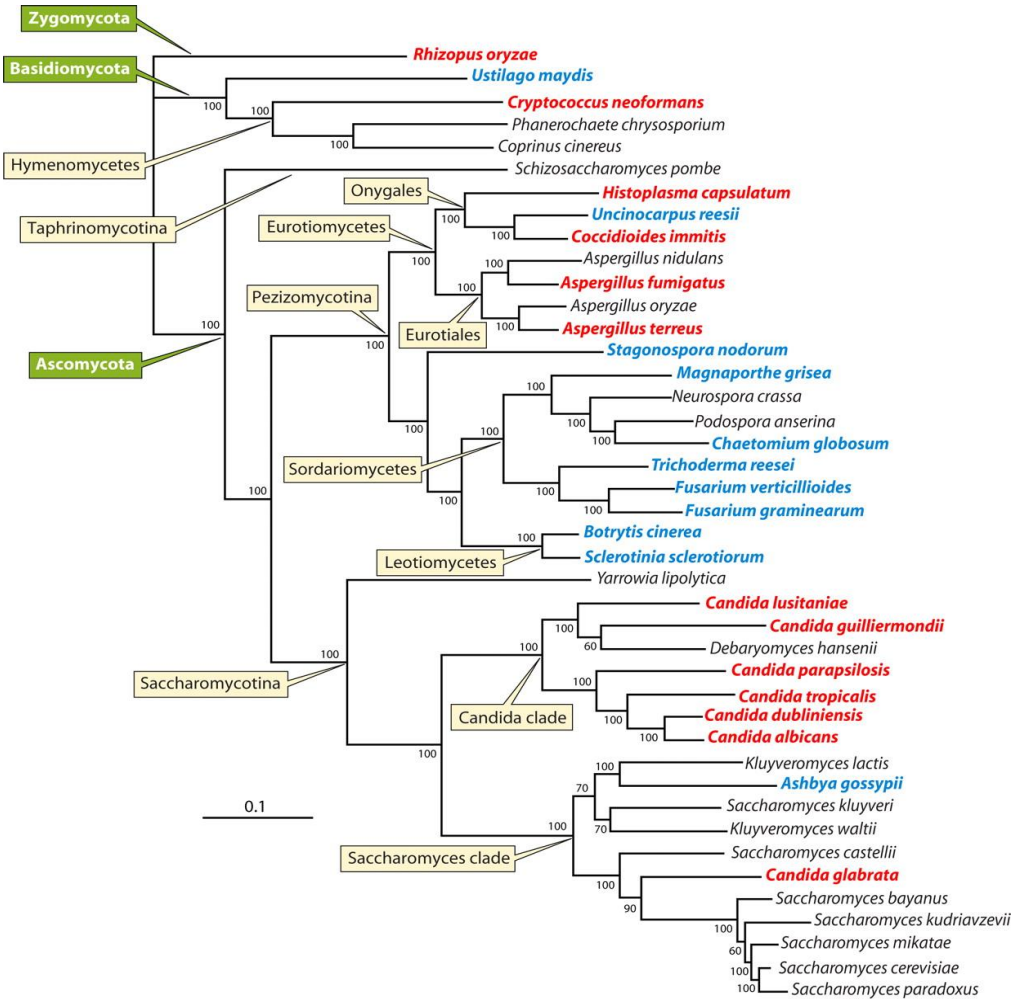

Figure 1.1 Simplified fungal phylogeny. The blue highlighted species indicate plant pathogens, and the red highlighted species indicate human fungal pathogens (Butler, 2010).

1.2 A unique fungus: *C. albicans*

The frequency of fungal infections is steadily increasing, contributing significantly to mortality and morbidity, especially in immuno-compromised patients. *C. albicans* is a major human pathogen that is responsible for wide variety of infections (Rolston, 2001), collectively called candidiasis. Candida as a genus is classified in the phylum: Ascomycetes; Class: Saccharomycetes; Order: Saccharomycetales and Family: Saccharomycetaceae. *C. albicans* is a common commensal on mucosal surfaces in the gastrointestinal and urgenitary tracts of the human

population, but frequently, causes superficial infections of the skin as well and can develop into life-threatening systemic disease. The fungus is controlled by the innate immune system, epithelial barriers, and as a result of interactions with the normal microbial flora (Calderone and Funzi, 2001; Gow and Hube, 2012; Moran *et al.,* 2012; Calderone and Clancy, 2012). It is Important to understand that Candida has versatility as a pathogen, and adapts as a commensal to various anatomically distinct sites (Miceli *et al*., 2011). *Candida* can actively cause a spectrum of diseases exceeding that of most other commensal microorganisms. The pathogenicity of *Candida* species is enhanced or mediated by impairing a host's resistance to infection, locally or systemically (Calderone and Funzi, 2001). In addition, opportunistic infections are facilitated by a range of key virulence factors.

1.3 Virulence factors and pathogenicity

Pathogenicity refers to the ability of microbes to infect and damage the host and cause disease. In this regard, host damage can result from the interaction between the host and pathogen for example as a direct action on tissue, or via expression of factors on both sides (Mayer *et al*., 2013). Infection by a fungus depends on its capacity to adapt to the host environment and to resist the activity of the host's defences.

Candida pathogenicity arises from several factors that underscore their versatility as pathogens. These factors are crucial components in enhancing the survival of Candida in several distinct sites in the human host, and when given the opportunity facilitate disease. The ability of Candida to cause disease is also influenced by a wide diversity of predisposing conditions that range from weakness in the host's defence to the use of ill-fitting dentures (Calderon and Fonzi, 2001; Ruiz-Herrera *et al.,* 2006; Mayer *et al.,* 2013). The different outcomes arising from pathogenicity *per se* are called virulence factors and they are expressed by *C. albicans*, contributing to the impact on the host. The survival or death of the host is determined during the host-microbe interaction by these factors, which can be induced or constitutively expressed. Virulence factors affect the ability of pathogens to expand and cause harm to the host (Khan *et al.,* 2010;

Casadevall, 2009). These factors include host recognition (adhesion), polymorphism or morphogenesis (transitions between unicellular yeast forms and filamentous forms), secreted proteinases and phospholipases.

Importantly, the virulence factors reported in a wide range of Candida species include an ability to secrete proteases at 37°C encouraging adherence, penetration of the tissue and dissemination, and resistance to the immune defence. Some research has explored the ability of Candida species to invade deep tissues (Khan *et al.,* 2010) (Fig. 1.2). Overall, pathogenicity is a complex phenomenon, and fungi usually require a combination of properties, because possession of a single virulence factor is often not enough to cause disease. Indeed multiple virulence factors are involved in the many steps required for the process of infection to initiate the pathogenicity (Brand, 2012).

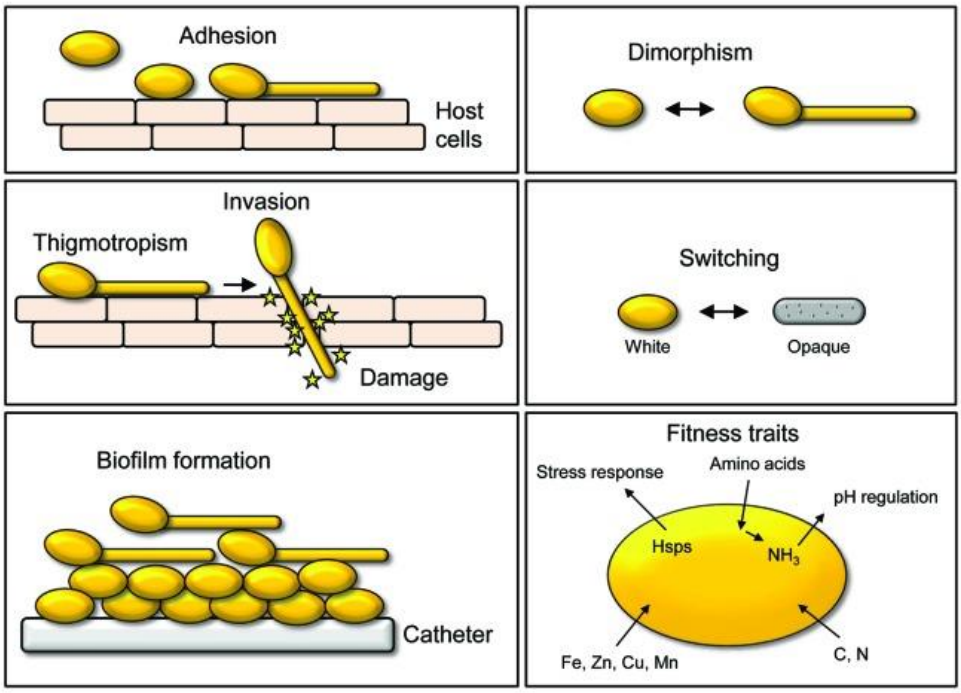

Figure 1.2 The mechanisms of pathogenicity in *C. albicans*. Candida yeast cells express numerous factors that promote adherence to the host cell, switches to a hyphal form and directed growth within tissues. Candida cells can invade through induced endocytosis, with penetration of the host assisted by the secretion of hydrolases. Mature biofilm matrix facilitates protection against antibiotic activity by reducing accessibility of cells to the drug. Some fitness traits implicated in pathogenicity include stress responses resulting from the expression of heat shock proteins, the uptake of amino acids and the utilization of distinct carbon, nitrogen and metal sources (Mayer *et al.,* 2013).

1.3.1 Adherence to the host tissue

The cell wall plays a crucial role in interacting with the environment, and *vice versa*. It is also important for adherence to other surfaces, and prevents cells from being washed away, especially under conditions of shear stress. The cell wall protects cells from hazards by producing extracellular polymers to facilitate biofilm formation and adhesion (Kojic and Darouiche, 2004; Verstrepen and Klis, 2006).

Adherence is one of the crucial determinants influencing fungal disease. Adhesins are biomolecules that facilitate the adherence of microbes to the host cells, which is an essential early step in the promotion of diseases. Adhesins are typically glycosylphosphtidylinositol-dependent cell wall proteins (GPI-CWP) (Chaffin *et al.,* 2008).

Four proteins (Hwp1, Ala1p/Als5P, Alslp) have been identified in *C. albicans* as adhesins. These GPI-anchored proteins are involved with attachment to the glucan in the cell wall and allow adhesion to specific tissues (Sundstrom, 2002).

Adhesins promote adhesion by binding specific amino acids or sugar remnants to the surfaces of cells (Fig. 1.3)

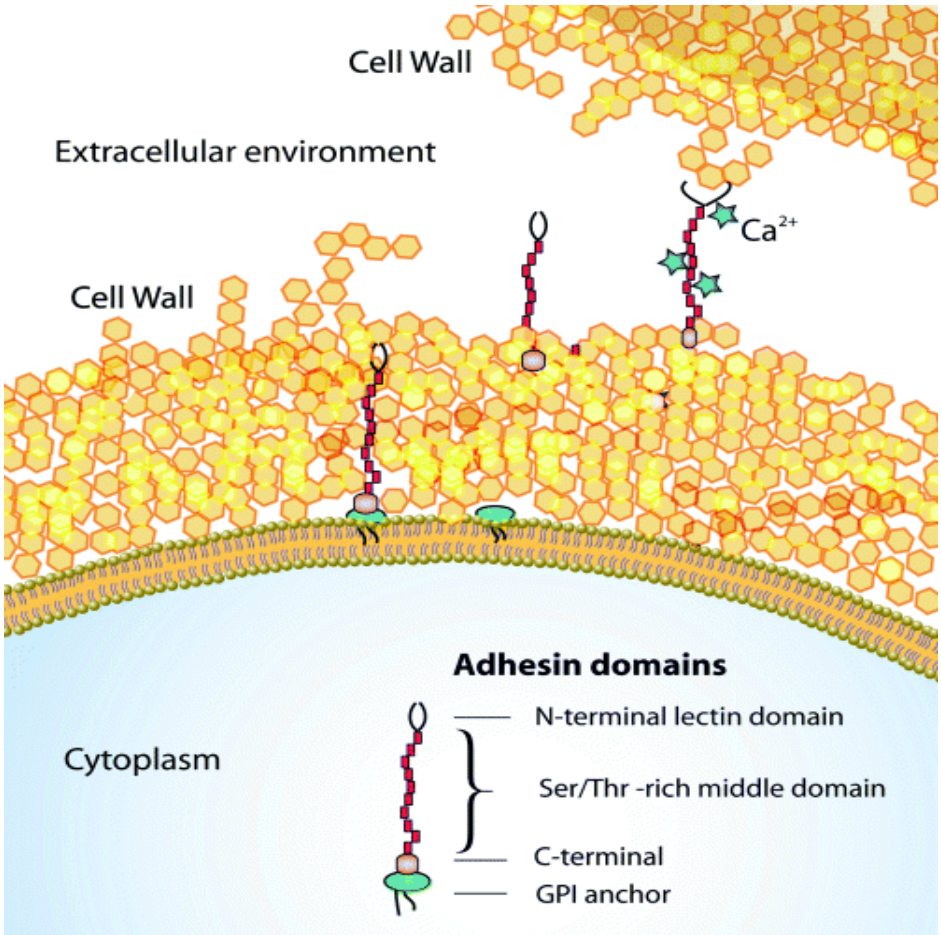

Figure 1.3 Fungal adhesion is promoted by secretion of specialised cell surface protein, adhesins that anchor cells to surfaces (Verstrepen and Klis, 2006).

In general, fungal adhesins possess three common domain structures:

1- The C-terminal part contains a glycosylphosphtidylinositol (GPI)-moiety which links the adhesin to the cell wall itself (Bony *et al.,* 1997).

2- The N- terminal part of adhesins contain a carbohydrate or peptide binding domain, protruding from the cell wall surface (Kobayash and Cutler, 1998; Rigden *et al.,* 2004).

3- The middle part of fungal adhesins are distinguished by their multiple serine and threonine-rich repeats that are encoded by conserved DNA sequences- Fungal adhesins have different modes of binding to another cell. These modes can be divided into two groups: the sugar sensitive group (lectin-like adhesions) and sugar- insensitive adhesion (Stratford, 1992).

The adhesins have a lectin-like carbohydrate binding domain in its N-terminus, which enhances the binding of the adhesin to the residual sugar on the cell surface (Guo *et al*., 2000; Stratford, 1992). Adhesions can be induced by several environmental triggers, such as carbon or nitrogen starvation, pH changes or ethanol levels (Sampermans *et al*., 2005).

1.3.2 Morphogenesis

C. albicans is a polymorphic fungus that can undergo transitions from unicellular yeasts to filamentous forms. *C. albicans* is often termed dimorphic, but more accurately as pleomorphic. This ability to switch growth mode contributes to its pathogenicity by increasing adherence, invasiveness, and elaboration of proteolytic enzymes, as well as antigen presentation (Fidel and Vazquez 1999). Environmental conditions play a key role in the growth mode of many fungal species (Whiteway and Bachewich, 2007).

Particular conditions can lead the cell to grow as yeast or hyphae, and the ability to switch from one form to another in response to external references is rapid (Whiteway and Bachewich, 2007).

The transition is facilitated by: nutrients, pH, a temperature of 37-40°C, CO_2 concentrations of approximately 5.5%, serum, biotin, and some amino acids. This transition is a requisite for pathogenicity. Unicellular forms are

more appropriate for dissemination in the host tissues, while filamentous forms are required for damaging and invading the tissues. Filamentous forms have a stronger capacity for adherence and display greater invasiveness of the host tissues. For instance, during phagocytosis, yeast cells produce hyphae and kill macrophages by secretion of hyphae-associated proteinases. These cells prevent hyphae from being killed by innate immune cells (Fig. 1.4). Additionally, hyphal cells have an ability to escape from the blood stream through the induction of phagocytosis by endothelial cells (Khan *et al.,* 2010). In addition to the yeast-hyphae modes, there are other distinct morphological forms, including the unique opaque-colony form with oblong cells characteristic of the mating process (Pujol, *et al.,* 2004). Chlamydospores are also produced relating to the pseudo-mycelium. Understanding of their biological roles remains inadequate and there has been little investigation in this area (Fabry *et al.,* 2003).

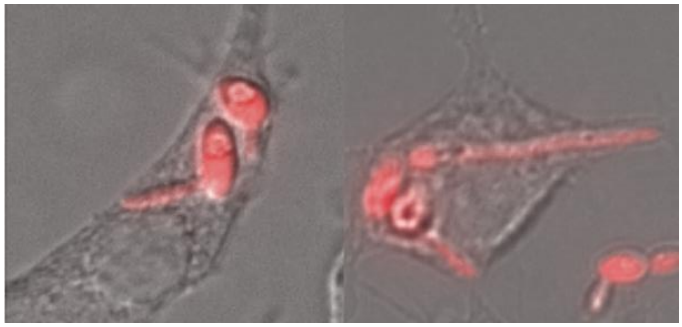

Figure 1.4 Morphogenesis of *C. albicans* within innate immune cells (macrophages). *C. albicans* can germinate rapidly and disrupt the macrophages after switching to a filamentous form (Jimenez-Lopez *et al*., 2013).

1.3.3 Invasion of *C. albicans*

C. albicans is a pathogen that is notable for its ability to utilize two distinct mechanisms for invasion and epithelial entry: induced endocytosis and active penetration (Zhu and Filler, 2010; Naglik *et al*., 2014). *C. albicans* can penetrate and degrade the mucosal tissue and vascular barriers, procuring nutrition at the infection site and eventually killing epithelial and endothelial cells. *C. albicans* can also invade epithelial cells by inducing epithelial cell endocytosis which is regulated by Mitogen-activated protein

(MAP) kinases that can trigger a switch from yeast cells to a more invasive hyphal form (Csank *et al.,* 1997). Candida cells stimulate the production of pseudopods by cells, which engulf the pathogen and pull them inside host tissues. This process requires binding to the epithelial cell surface proteins and is dependent on the active participation of the pathogen – since dead cells do not get taken up by this route (Zhu and Filler, 2010).

Candida viability is also required to achieve active penetration at different anatomical sites. Indeed, invasion via *C. albicans* not only depends on fungal viability and morphology, but also the type of anatomical site with different lineages of epithelial cells showing difference in their sensitivity to invasion. Candida thus invades and damages the epithelial cells via induced endocytosis and/or active penetration. Candida invades oral epithelial cells by both mechanisms, whereas gastrointestinal epithelial cell lines are only invaded by active penetration (Zhu and Filler, 2010; Dalle *et al.,* 2010; Naglik *et al*., 2014).

1.3.4 Secreted hydrolases

Hydrolytic enzymes are one of the most important virulence factors that affect *C. albicans* invasion and the avoidance of the host's defence. Most of the enzymes are extracellularly secreted, are required for survival, and promote infection at different sites by giving pathogens sufficient flexibility to cause pathogenicity. Hydrolytic enzymes help to degrade/digest host proteins and alter the structure of the cell membrane to facilitate adhesion, invasion, and avoidance of antimicrobial agents and host attack by targeting cells of the host's immune system (Bader *et al.,* 2004; Mayer *et al*., 2013; Naglik *et al.,* 2003). Three of the most important hydrolytic enzymes secreted by *C. albicans* are the aspartyl proteinases (Sap), phospholipases and lipases. Many studies have referred to the biologically important role of these hydrolytic enzymes, not only in *C. albicans,* but in other Candida species (eg. *C. parapsilosis, C. tropicalis* and *C. dubliniensis* (Naglik *et al.,* 2003; De Viragh *et al*., 1993). It is clear that enzyme secretion provides Candida with great flexibility and contributes to its success as an opportunistic pathogen.

1.3.5 pH sensing and metabolic adaptation

The high efficiency of fungi in causing diseases depends on their ability to adapt and grow within different environments and within distinct host niches that exhibit different pHs. In general, fungi are more acidophilic than other microorganisms including many common bacterial pathogens (Dana, 2009). Tolerance of a broad range of pHs is essential for pathogenicity of *C. albicans* which can encounter highly acidic (pH -2) conditions in the stomach, to mildly neutral and even alkaline conditions elsewhere. *C. albicans* can directly alter the environment pH, making a neutral environment with changing pH conditions. *C. albicans* can actively balance the extracellular pH (from either acidic or alkaline) resulting in the induction of a yeast-hyphal transition (Vylkova *et al.,* 2011; Mayer *et al*., 2013). The metabolic adaptation of Candida, is an important factor in a medical context because of its capacity to occupy diverse niches in the human host. Generally, human niches contain many different types of assimilable and non-assimilable carbon sources. *C. albicans* is able to grow and assimilate many of these carbon sources but primarily favours glucose (Ene *et al.,* 2014). To thrive within different human niches, Candida can exhibit remarkable metabolic flexibility in these niches.

1.3.6 Biofilm formation

Biofilms are defined as complex accumulations of microorganisms attached to a solid surface (Donlan and Costerton, 2002). Biofilms provide a niche for microorganisms, in which the latter are protected from antibiotic treatment and can create a source of permanent infection. They are the most common mode of growth of microorganisms both in nature and infectious states due to their high ability to resist antibiotics (Chandra *et al*., 2001). The formation of a biofilm is influenced by the species of Candida involved, by distinct patterns of morphogenesis, by environmental agents, and by the type and quality of contact surfaces. In general, a biofilm is a co-operating community of adherent cells that are attached to surfaces and develop by producing extracellular polymers that supply a structural matrix which may assist adhesion (Donlan 2001; Kokare *et al*., 2009; Kojic, Darouiche, Bader *et al*., 2004).

The fungal biofilm is a complex, but highly organized structure. Although there are few studies focusing on the formation of biofilms in Candida species, it has been studied more extensively in *C. albicans*. *C. albicans* biofilms have four distinct developmental phases (Hawser and Douglas, 1994; Kojic and Darouiche, 2004; Chandra *et al*., 2001):

(i) Early-phase spherical yeast cells, which allow *C. albicans* to adhere to the device surfaces.

(ii) The intermediate phase, where the basal layer of the matrix with proliferating cells is formed by yeast cells switching to a hyphal form.

(iii) The maturation phase with increased anchoring of cells, growth of pseudohyphae and hyphae concomitant with the production of extracellular matrix material, arranged to produce a three-dimensional architecture.

(iv) The dense network of cells (yeasts, pseudohyphae and hyphae) can slowly disseminate yeast cells from the matrix to seed new sites (Nobile and Johnson, 2015) (Fig.1.5).

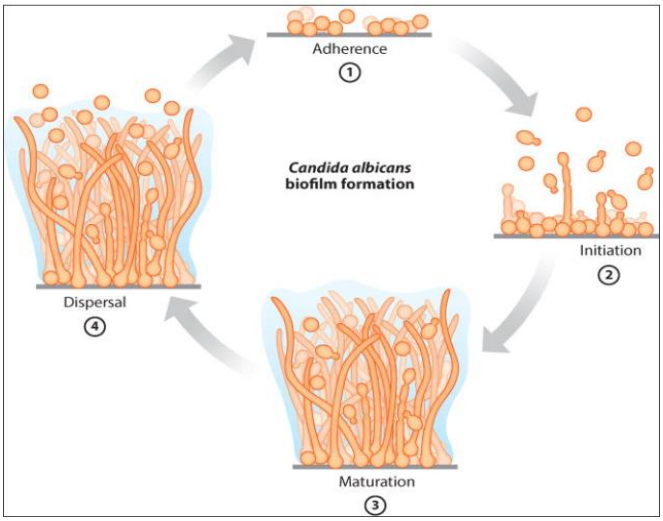

Figure 1.5 biofilm formation. Stages of biofilm formation and adherence to surfaces in *C. albicans:* (1) Adherence of yeast-form of Candida to the cell surfaces. (2) Proliferation cells initiated to form basal layer of anchoring Candida cells. (3) growth of filamentous form (maturation). (4) Dispersal stage to form new infected sites (Nobile and Johnson, 2015).

1.4 Fungal Cell Wall

The fungal cell wall is vital in maintaining cellular integrity and communicating with the environment, protecting it from environmental conditions and osmotic stress. The assessment and response to environmental change by the cell wall is mediated by a variety of cell wall sensor proteins (Fig. 1.6) (Freeman, 2015; Ruiz-Herrera *et al.,* 2017). The cell wall is critical for adhesion and biofilm formation, contributing substantially to virulence and pathogenicity. It also has vital properties for the invasion of tissue and protection against other microbes. In addition, it has a role in the regulation of host defence mechanisms (Free, 2015).

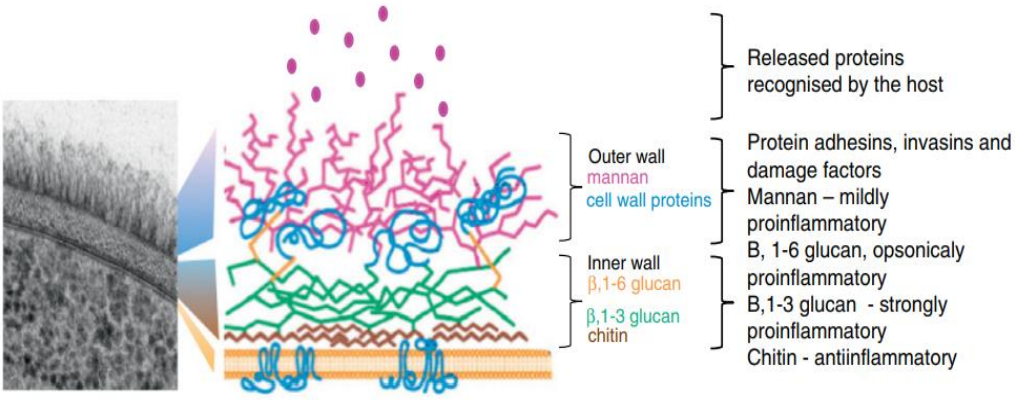

Figure 1.6: The arrangement of *C. albicans* cell wall components. The outer layer (protein and mannan) and the inner layer (glucan and chitin) (Nobile and Johnson, 2015).

1.4.1 Fungal cell wall components

The cell wall is a coherent structure composed of linear and branched polysaccharides, proteins and lipids (Klis *et al*., 2006; Karkowska-kuleta and Kozik, 2014). The major components of the fungal cell wall are chitin, chitosan, ß -1,3 glucan, ß -1,6 glucan, mixed ß -1,3/ß-1,4 glucan, α-1,3 glucan, melanin, and glycoproteins (Eisenman *et al*., 2005) (Fig. 1.7).

Plasma membrane-associated glucan synthases are responsible for synthesizing and extruding glucan into the cell wall space. Chitin is

extruded into the cell wall space by synthesizing from plasma membrane associated chitin synthases (Gow and Hube, 2012). Chitin is a linear polymer of N-acetyl-D-glucosamine (GlcNAC) including ß-1,4 bands (Lo *et al.,* 1998). In *C. albicans*, chitin is a minor component, around (0.6 to 9%): it is concentrated mostly at bud scars, but it is also scattered in the lateral walls during cell wall structure and linked (1-3)- (1-6) ß-glucan (Ueno *et al.,* 2013; Molano *et al.*,1980).

According to Calderone (1991), approximately (47 to 60%) of the total weight of the *C. albicans* cell wall is formed of ß-glucans. On the other hand, mannan forms the outer layer of *Candida albicans,* which constitutes about (12.2 to 22.9%) of the dry weight (yeast) and approximately 40 % of the total polysaccharide component the cell wall (Calderone, 1991). Mannan is a soluble immunodominant component in the *C. albicans* cell wall, typically present as a phosphomannoprotein complex. This fraction comprises homopolymers of D-mannose, phosphate, (1 to 2%) and proteins (3 to 5%). Mannoproteins are formed by binding mannan and cell wall proteins with different linkages: *N*-linked mannan links to asparagine, and *O*-linked mannans are bound to serine or threonine (Lo *et al.,* 1998). The architecture of the *C. albicans* cell wall represents a linkage between multiple components ß-(1-3)-glucan, ß-(1-6)-glucan, chitin and mannoproteins (Kollar *et al*., 1997). The polysaccharides are essential for structural function, while mannoproteins are responsible for cell wall permeability and appear to act as a filler. Mannoproteins and ß-1,6-glucans are attached over a remnant of glycosylphosphatidylinositol anchors that includes five α-linked mannosyl residues. The ß-1,6-glucan components have some ß-1,3-glucan branches that contribute to the reducing end of chitin (Kollar *et al.,* 1997; Lo *et al*., 1998).

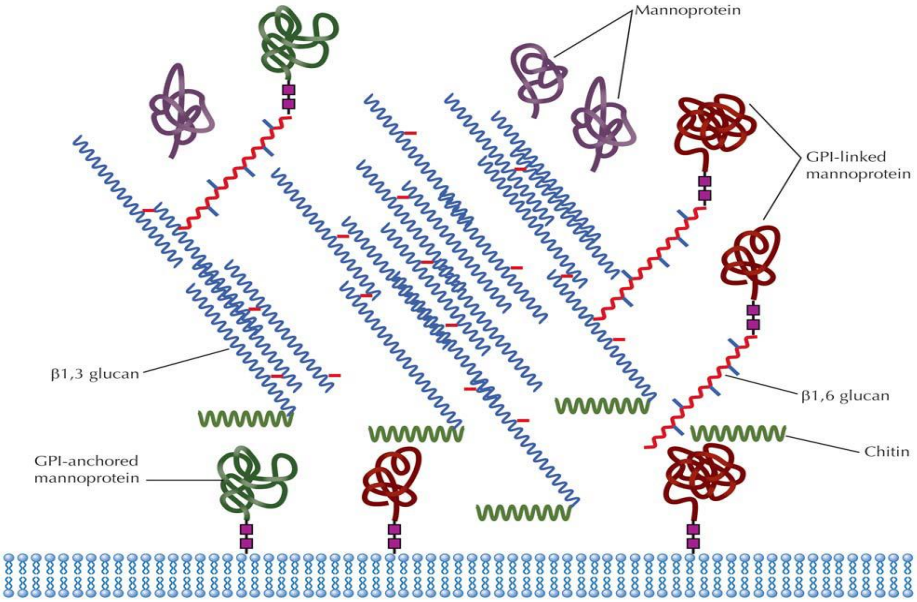

Figure 1.7: A simplified model of the Candida yeast cell wall.

To generate the mesh-like structure of the Candida cell wall, short branches of ß-1,3-glucan can be cross-linked to ß-1,6-glucan, with ß-1,3-glucans cross-linking to chitin. Mannoproteins have glycosylphosphatidylinositol (GPI) anchors which are covalently attached to ß-1,6-glucan. GPI anchors are attached to the plasma membrane and can sequester the cell wall proteins in the plasma membrane (Stuart and Charles, 2009).

1.4.2 *C. albicans* mannosylation

The fungal cell wall has numerous glycosylated mannoproteins at the surface, which are required for cell shape, and conferring upon the cell wall key physical and immunological activities. *O*- and *N*-linked mannosylation and phosphomannosylation are the most common modifications (Brand *et al.*, 2010; Hall and Gow, 2013; Kruppa *et al*., 2011; Netea *et al.,* 2006). The outer layer of polysaccharides is considered to be the first point of interaction between the pathogen and the host's immune system. Thus, there is an interplay between this component, an inner layer (including ß-glucan, chitin) and immune cells. *O*-mannosylated proteins play a crucial role in some important physiological processes. The formation of *O*-linked

carbohydrates was first studied in *S. cerevisiae* and later in *C. albicans* as human fungal pathogens (Prill *et al*., 2005). Prill *et al.,* (2005) and Hall and Gow, (2013) mention in their studies that *O*-mannan in *C*. *albicans* is a simple linear carbohydrate involved in a group of α-1, 2 linked mannose units. These residues are attached to the serine/threonine residues (hydroxyl group) by the enzymes Pmt1, Pmt2, Pmt4, Pmt5 and Pmt6.

Mnt1p and Mnt2p encode partially redundant α-1, 2 mannosyltransferases which are required for catalysing the addition of the second and third α-1, 2 mannose residues onto the α-mannose (Munro *et al.,* 2005). *O*-linked glycosylation is important for cell wall integrity (Timpel *et al*., 1998). In fungi, *O*-mannan is significantly affected after the disruption of *MNT1* and *MNT2* and becomes a short chain of mannose, which has an impact upon host-pathogen interactions and virulence. (Buurman *et al*., 1998). Loss of *PMR1* by gene disruption (a gene encoding a high affinity $Ca^{2+/}Mn^{2+}$ P-type ATPase) alters the morphology and growth rate of *C. albicans* as well as biofilm formation (Navarro-Arias *et al.,* 2016). The mutant is also more susceptible to perturbation by some agents such as Calcofluor (Hall and Gow, 2013). All of these outcomes might occur because of deficiency in the provision of co-factors to mannosyltransferases to regulate mannan synthesis and to attach glycoproteins (Papon *et al.*, 2013; Hall and Gow, 2013) since *pmr1*Δ has a fundamental role in Golgi-resident ion pumps to provide Mn^{2+} and Ca^{2+} ions which are essential for *O*- and *N*-mannosyltransferase activity (Castillo *et al*., 2008). After disruption of *O*- and *N*-mannan (*pmr1*Δ mutant), cells produce less dense fibrils, and a thinner and longer glucan-chitin layer (Hall and Gow 2013). With regard to the immune response, mannan reduction in the *C. albicans* cell wall promotes delays in the engulfment of cells by macrophages but no change in the rate of migration of immune cells and chemokines towards *C. albicans* (Lewis *et al.,* 2012; Keppler-ross *et al.,* 2010).

N- mannosylation mutants, such as *och1*Δ display no branching in the outer chain mannans but are attached to the branched mannans through an α-1,6 backbone (Bates *et al*., 2006) (Fig. 1.8). Deletion of *och1*Δ results in a considerable shortening of mannan fibrils, increased chitin and glucan levels and a thickening of the cell wall. This appears to be the result of an

enhanced ability of the cells to activate a so-called salvage pathway (Netea *et al*., 2006; Bates *et al.,* 2006). In general, deletion of *O*-and *N*- mannan results in an increase of pathogen recognition by host Dectin-1 following the enhanced exposure of the ß-glucan layer (Wheeler *et al*., 2008; Hall and Gow, 2013).

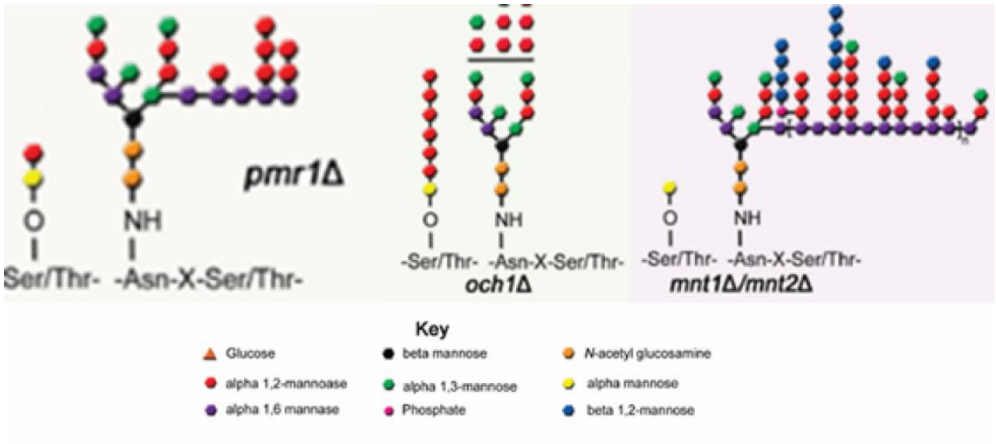

Figure 1.8: Structures produced by *C. albicans* mannosylation mutants (N- and O-linked glycosylation) (Hall and Gow 2013). Candida mutants display truncations in both *O*- and *N*-linked mannan that influence on the cell wall function and immune recognition.

1.5 Innate immunity

The human body is exposed to millions of microbes or pathogens daily. The immune system is responsible for protecting the body from infections by encountering pathogens and destroying them. The adaptation of the immune response is not specific to individual pathogens, but depends on the ability to recognize them and act quickly to attack them. This process is achieved by a group of proteins such as pentraxins (homopentameric proteins) or antibodies (associated with adaptive immunity) and phagocytic cells (associated with innate immunity) (Medzhitov *et al*., 1997; Chaplin, 2010). Fundamentally, the immune system is organized into two overlapping responses to destroy the pathogens: (1) phagocytosis to promote intracellular killing and (2) production of cytokines and activation of

lymphocytes to produce antigen-specific immunity that presents peptide antigens to the lymphocytes. These innate responses are relatively rapid but not always effective, because they are non-specific. However, adaptive immune cells provide highly specific and effective protection against a wide variety of pathogens (David and Chaplin, 2010) in both the short-term and long-term. In addition, the short and long-term activation of pro-inflammatory regulates another part of the immune system function through creating immunoregulatory cytokines (Christ *et al.,* 2016). A core ability of the immune system is to distinguish between self and non-self. In view of this fact, whilst the immune system employs many different and efficient effector mechanisms to destroy a wide range of microbial cells it is crucial that the immune system is capable of avoiding the destruction of its own tissues by unleashing immune response mechanisms against the host's tissues. The avoidance of the reaction against its own tissue is expressed by both innate and adaptive immune responses. This ability to avoid the destruction of self-tissue is referred to as self-tolerance (Chaplin, 2006; Chaplin, 2010).

1.6 Phagocytosis

Phagocytosis is a unique, complex and multifaceted process. Phagocytosis is involved in normal growth and development and is involved with autophagy, inflammation, tissue repair and reconstruction, and the clearance of senescent cells. The success of the immune response against fungal infections depends on numerous factors, including the manner of infection, the host's immune defence (status), readiness, and inoculum size. Any failure of the innate immune defence leads to dissemination of microbial infections. Qualitative and quantitative disturbance of phagocytosis can expose host tissues to a considerable number of infection factors (Erwig and Gow, 2016; Freeman and Freeman, 2014; Medzhitov and Janeway 2002). Immune recognition of pathogens is mediated by a distinct set of receptors that help identify infections by engaging pathogen-associated molecular patterns (PAMPs) (Thompson *et al*., 2011). PAMPs are recognized either directly, or by products generated from them

(Medzhitov and Janeway 2002). In other words, PAMPs play a significant part in activation of the innate immune cells response. This important role is achieved through recognition by Toll-like receptors (TLRs) and other pattern recognition receptors (PRRs).

PAMP recognition allows engagement of the PRRs and the presence of specific pathogens is indicated by the nature of their ligands. There are essentially three types of PRRs: humoral proteins (common in the plasma); endocytic receptors; and signalling receptors (which can be expressed intracellularly or on the cell surfaces) (Medzhitov and Janeway, 2002). Membrane-bound receptors, (cellular PRRs) are expressed on effector cells of the immune system, including Antigen Presenting Cells (APCs) as part of the adaptive immunity response, and surface epithelial cells that function as first response cells in the recognition of pathogens. After PAMP recognition, PRRs can be activated directly to signal the presence of microbial agents to the host by inducing and triggering proinflammatory and inflammatory cytokines and chemokines (Medzhitov and Janeway, 2002; Mogensen, 2009).

1.6.1 Phagocytosis and macrophages

Macrophages, discovered in the 19th century by Elie Metchnikoff during his investigation of phagocytosis (Gordon, 2007; Cooper and Alder, 2006) are key cells of the innate immune system that are distributed through the tissues of the body and participate in critical homeostatic and disease responses (Gordon and Plüddemann, 2017). Macrophages are essential to the regulation of the activity and proliferation of lymphocytes (Epelman *et al*., 2014; Jakubzick *et al*., 2008). Normal host defences are orchestrated by macrophages, which display a variety of cell surface receptors in order to direct migration (chemotaxis) to the infection sites, where they eliminate and clear pathogens by phagocytosis and subsequently present antigens to adaptive immune cells. Any inappropriate regulation of macrophages activity leads to human disease (Park *et al.,* 2011). This process of migration and pathogen clearance occurs through the action of specific

colony stimulating factore 1 (csf1) receptors tyrosine kinase by auto phosphorylation of csf1 during the infection (Pixley and Stanly, 2004).

Various studies have demonstrated that circulating monocytes give rise to a variety of tissue macrophages (Epelman *et al.,* 2014). These are created in the bone marrow from myeloid progenitor cells and then released into the peripheral blood *in vivo* (Elhelu, 1983). The subsequent development and differentiation of macrophages occurs during tissue repair (Ogle *et al.,* 2016) and contribute to the host's defence (Ebert, 1939; Takahashi, 2000; Gordon and Taylor, 2005). The morphological heterogeneity of monocytes is apparent in terms of variability of size, nuclear shape, and granularity.

In the last few years, understanding of the origin of macrophages has been drastically revised. It has been demonstrated that the major tissue-resident macrophages are established before birth (during embryonic development). During adulthood, independent replenishment is perpetuated by blood monocytes (Yona *et al*. 2013; Hashimoto *et al.* 1968; Ginhoux *et al.,* 2013). Tissue macrophages are quite heterogeneous in morphological form and function, depending on the tissue. So, for example there are microglia, in the central nervous system (CNS); Kupffer cells in the liver; osteoclasts in bone and alveolar and peritoneal macrophages in the lungs (Eligini *et al.,* 2015). Macrophages exhibit remarkable plasticity and flexibility in their activated states (Das *et al*., 2015; Mosser and Edwards, 2008) which are responsible for changes in macrophage physiology, depending on the environmental cues. The distinct functions of macrophages can be activated in response to environmental stimuli, leading to effective physiological changes, especially with regard to the induction of the pro-inflammatory or anti-inflammatory responses (Das *et al.,* 2015).

1.6.2 Macrophage specific gene expression

An appreciation of the literature on immune cell gene expression patterns is useful when trying to identify an appropriate marker gene for immune responses and cell types. Fortunately, the literature is rich in information on candidate macrophage and neutrophil marker genes. These gene markers are useful in identifying the abundance of macrophage or neutrophil

populations within a site of infection. For instance, *L-plastin* is a marker that can be used to distinguish macrophages from neutrophils, whereas CSF1R is utilised to maintain the development and migration of macrophages.

1.6.2.1 L-plastin

L-plastins are a family of human actin-bundling proteins (with distinct isoforms) that are expressed in proliferating mammalian cells. They seem to be induced following the tumorigenic transformation of cells (Lin *et al.,* 1993). L-plastin has also been identified as a fundamental constituent in cellular processes that are critical for innate immune cells (macrophages and neutrophils), eosinophils, osteoclasts, and T-cell and B-cell lymphocytes (Morley, 2012; Deady *et al*., 2006). Under physiological conditions, the expression of L-plastin is apparent in innate immune cells (macrophages and granulocytes), where it occurs as a phosphorylated protein in macrophages stimulated by exposure to bacterial lipopolysaccharide (LPS). Phosphorylation of L-plastin takes place on ser5 in macrophages activated by LPS (Hirata, and Shinomiya, 2006; Shinomiya *et al*., 1995). Ser5 phosphorylated L-plastin induces adhesion in neutrophils (Deady *et al*., 2014). Additionally, the L-plastin action is influenced by intracellular Ca^{+2} (Namba *et al.,* 1992). L-plastin therefore appears to help leukocytes to respond quickly to stimuli by inducing actin rearrangements in macrophages at the time of an immune response (Bañuelos *et al*., 1998).

In zebrafish biology, *L-plastin* is used as a marker for macrophages (Jones, 1998; Crowhurst, Layton, and Lieschke, 2008). The initiation of *L-plastin* expression occurs as macrophages disseminate over the yolk sac 20 hpf. The expression is dispersed along the body of the embryo and in the cranial mesenchyme at 28 hpf. The levels of *L-plastin* expression are however drastically reduced 5 dpf. Hence, *L-plastin* can be used to distinguish the macrophages from emerging granulocytic populations at an early stage of the Zebrafish's development. L-plastin constitutes approximately 1.8% of the overall cytoplasmic protein in macrophages, so is easy to detect (Bennett *et al*., 2001).

1.6.2.2 Irf8

The regulation of a range of immune responses (innate and adaptive) is achieved through the activation of interferon regulatory factor (IRF) family transcription factors (Kurotaki *et al.,* 2013). Irf8, or interferon consensus sequence binding protein (ICSBP), is one of nine members of the IRF family (Yanai *et al.,* 2012) that is implicated in the pathogenesis of myeloid neoplasia and is responsible for the regulation of cellular genes involved in stimulating immune responses (monocyte and macrophage differentiation) against viral and bacterial infections, as well as regulating cell growth (Zhao *et al.,* 2017; Shin *et al.,* 2011).

Irf8 is also a key regulator of autophagy in innate immune cells (macrophages) and is required for their maturation. Moreover, Irf8 has a major role in the resistance of innate immune cells to intracellular bacteria (Gupta *et al*., 2015). *In vivo* studies have revealed that the expression of Irf8 in macrophages is related to the differentiation of macrophages, whereas irf8 inhibits the differentiation of neutrophils. Thus, *Irf8* is specifically expressed in macrophages, but not in neutrophils. Knockdown of *Irf8* function in zebrafish leads to macrophage depletion and increased production of neutrophils (Li *et al*., 2011).

1.6.2.3 Csf1r

Colony stimulating factors (Csf1r) are essential haematopoietic growth factors that act as mediators of the immune response. Csf1r is a tyrosine kinase receptor that is produced by macrophages, monocytes and its committed progenitors (Charles *et al*., 1988). It is responsible for profound effects on the activity of leucocytes. In addition, the Csf1r receptor has an ability to mediate growth and survival effects of colony-stimulating factor 1 (Marvin *et al.,* 2010; Shi *et al*., 2006). There are more than 20 dissolvable factors that play a key role in the cell development, such as macrophage colony-stimulating factor (M-CSF), granulocyte colony- stimulating factor (G-CSF), granulocyte-macrophage colony-stimulating factor (GM-CSF) and multi-colony-stimulating factor (multi-CSF or IL-3). They are essential to different biological functions in tissues, as they have functional pleiotropy.

Inflammatory cytokines have a capacity for up-regulation of phagocyte expression of M-CSF and GM-CSF. They can therefore play a crucial role during infection time by stimulating production of other cytokines. In the steady-state, prior to infection, M-CSF is already produced but there is a rapid up-regulation of expression, depending on the response to different pathogens (Daniel *et al.,* 2004) For example, in response to bacterial infection, macrophages can migrate to the site of an infection to remove the debris of neutrophils which have infiltrated to clear the bacteria. Macrophages then express the granulopoiesis factor Gcsf (Hall *et al*., 2012). According to Panopoulos and Watowich (2008), G-CSF is fundamental for driving granulopoiesis in steady state and stress (infection) conditions.

1.6.3 Phagocytes (neutrophils)

Professional phagocytes include many types of leukocytes other than macrophages, including neutrophils, mast cells, and dendritic cells. Neutrophils are abundant leukocytes in the blood and are released from the bone marrow. They comprise the first line of defence against many pathogens (Silva and Correia-Neves, 2012). Neutrophils can migrate directly to infected sites to kill invading microorganisms immediately by different cytotoxic mechanisms. Neutrophils have an essential role in phagocytosis by eliminating pathogens during the inflammation phase (Furze and Rankin, 2008) and also have a fundamental role in the orchestration of the immune response through their capacity to exchange information with macrophages, and dendritic cells by soluble mediators or direct cellular contact (Rosales *et al*., 2016; Kobayashi and Deleo, 2009). Pathogen killing is achieved by several microbicidal functions of neutrophils, utilizing an NADPH oxidase complex to produce cytotoxic Reactive Oxygen Species (ROS) (Mantovani *et al*., 2011).

1.6.3.1 Mpx

Mpx gene is a myeloid-specific peroxidase (myeloperoxidase) gene in Zebrafish and is the closest homologue of *mpo* in mammals (Loynes *et al*.,

2010). During an inflammatory response, myeloperoxidase (Mpo) enzymes are released by activated neutrophils catalysing the production of hypochlorite via the conversion of chloride and hydrogen peroxide (Loria *et al.,* 2008). In zebrafish embryos, *mpx* is the most important marker for neutrophils which first reveals expression within the posterior lateral plate mesoderm (PLPM). Additionally, it has been suggested that Anterior Lateral Plate Mesoderm derived cells contribute to neutrophil production, due to clear *mpx* expression in both domains (Jin *et al.,* 2012). One study has implicated *mpx* in the control of lineages of granulocytes showing mature amyloid in granulocytes, along with a decrease of the cell numbers that express *L-plastin* (Forrester *et al*., 2012).

1.6.3.2 CXCR4

Leukocyte traffic is mediated via chemokines receptors, which are classified into two groups: haemostatic chemokines, which play a key role in controlling homeostatic leukocyte traffic; and inflammatory chemokines, which conscript leukocytes to infected tissues. During the development of stem cells, the process of migration must start from the generating zone to the developing organs in the differentiated organs. It is clear that the cell migration process is directed through small secreted proteins, called chemotactic cytokines or chemokines during the inflammation and immune response. Chemokines play a fundamental role in the recruitment of leukocytes to the infected sites. Cxcr4 is member of a group of proteins (8-14 kDa) that belong to a family of G-protein coupled receptors, with the major functions of cxcr4 including organogenesis during embryonic development, haematopoiesis, and activation of the immune response. Alongside the homeostatic chemokines SDF-1 and CXCL-12, *cxcr4* and *cxcr4* have a crucial role in developmental pathways by controlling leukocyte traffic and guiding cell migration during disease. Depletion of *cxcr4* within zebrafish results in considerable phenotypic alterations and interrupted cell migration in which granule cells locate ectopically away from the normal route of progenitor cell migration (Lu *et al*., 2002; Miller *et al.*, 2008; Raz and Mahabaleshwar, 2009; Walters *et al*., 2010).

1.7 Reactive oxygen species (ROS)

ROS are defined as oxygen-derived radicals, that play a crucial part as signalling messengers to activate the immune system and regulate the response to pathogens (Chande and Schieber, 2014). There are different reactive molecules that contain oxygen including hydrogen peroxide (H_2O_2), hydroxyl radicals ($^{\cdot}OH$), superoxide (O_2^-), and single oxygen O_2 ($^1\Delta_g$) (Li *et al.,* 2017). ROS can enhance the bactericidal activity of innate immune cells (macrophages) and play a critical in establishing host defence and inflammation (Kanayama and Miyamoto, 2007). Many enzymes such as NADPH oxidase Nox and amine oxidases along with the dysregulation of antioxidant enzymes such as catalase, Superoxide dismutase SOD, glutathione and thioredoxins are responsible for ROS generation in different tissues (Segal, 2008; Bae *et al*., 2011).

1.7.1 Nox1

The NADPH (nicotinamide adenine dinucleotide phosphate) oxidase (NOX) complex plays an essential role in maintaining human health through its ability to initiate the respiratory burst (Masoud *et al*., 2014). This process is accomplished by donating an electron from NADPH to molecular oxygen (O_2), leading to superoxide production (Paik *et al.,* 2011). Therefore, the biological function of NOX family enzymes is to generate Reactive Oxygen Species (Bedard and Krause, 2007), which are the key to immune defenses and ROS stress responses (Panday *et al*., 2015).

The NOX complex is associated with both membrane and cytosolic components allowing it to provoke immune responses to a wide diversity of viral and bacterial infections (Panday *et al.*, 2015). NADPH oxidase deficiency may cause immunosuppression (Huang *et al.*, 2004). However, excess ROS production via NOX can lead to a variety of lethal diseases, including cancer and autoimmune disease (Wang *et al*., 2011). Inhibition of apoptosis and viral diffusion may result from NOX mediated intracellular ROS accumulation (Panday *et al.,* 2015). In general, the enzymatic components of NOX contribute to a wide range of functions starting from host immune defence to cellular signalling.

Nox has an essential role in many non-pathological responses too, especially vascular Nox, which generates ROS to maintain normal health by regulating blood pressure (Bae *et al*., 2011; Cross and Segal, 2004).

1.8 The interplay between *C. albicans* and innate host defence

The interplay between a pathogen and the host defence mechanisms is influenced by a variety of receptors and signal transduction pathways (Mogensen, 2009) in both parties. The interaction between *C. albicans* and immune cells is initiated through the detection of *C. albicans* cell wall components, mainly proteins and carbohydrate polymers. Groups of host PRRs are responsible for recognizing microbial signatures (PAMPs) leading to the activation of specific intracellular signalling pathways involving Toll-like receptors (TLRs) (Mogensen, 2009). TLRs play a major role in the initiation of the host immune response. TLRs include different types of transmembrane proteins that possess an ectodomain that is capable of recognizing PAMPs, leading to the activation of downstream signalling pathways in different cells types, such as macrophages, plasmacytoid dendritic cells and inflammatory monocytes. The TLRs possess leucine-rich repeats and cytosolic Toll-IL-1 receptor (TIR) domains (Kawai and Akira, 2011; Qin *et al*., 2016; Naglik *et al.,* 2014).

The TLR family is divided into two groups: intracellular TLRs (such as TL3, TL7, TL8, and TL9), which are expressed exclusively in the endolysosome, endosome, lysosome and endoplasmic reticulum (ER) compartments, are able to recognize microbial nucleic acids. The other group consists of cell surface receptors (TL1, TL2, TL4, TL5, TL6) which are responsible for recognizing microbial membrane components such as proteins, lipoproteins, and lipids (Blasius and Beutler, 2010). Activation of TLR signalling pathways invoke particular responses, tailored to each PAMP (that are expressed by microbes) but also recognise conserved structures associated with tissue damage (Kawai and Akira, 2010). Generally, TLRs-mediate the triggering of specific responses to generate inflammatory cytokines (Akira *et al*., 2001; Janewy and Medzhitov, 2002; Kawai and Akira, 2010), however TLR3, and TLR4 induce both interferon and

inflammatory cytokine responses. The triggering process and proinflammatory cytokine or chemokine production are secured after the recruitment of distinct adaptor molecules to provide biological responses to the pathogens. The TIR domain, including the adaptor molecule myeloid differentiation factor 88, is the first dedicated member of the TIR family, and is generally used by all TLRs types (except TLR3 and TLR4) to induce a biological response to a PAMP (Akira, Uematsu, and Takeuchi 2006). However, TLR3 and TLR4 use TRIF as a TIR-domain to stimulate a substitute pathway to induce type I interferon and inflammatory cytokine response, as well as initiating transcription factors, such as IRF3 and NF-κB (Kawai and Akira 2010; Blasius and Beutler, 2010).

TLRs are the most crucial of the receptors that initiate immune receptors against pathogens. Howvere, not all PAMPs are recognized by TLRs but require membrane-bound C-type lectin receptors (CLRs), RIG-I-like receptors (RLRs) and cytosolic proteins NOD-like receptors (NLRs) as well (Osorio and Reis, 2011). C-type lectin receptors (CLR) are probably the second most important receptors that play a central role in antifungal immune responses (Hardison and Brown, 2013). CLR is one of a large membrane protein family, which contain C- type lectin domains that respond to the activation of inflammatory receptors after recognition by both bacterial and fungal PAMPs. The NLR family includes NALP1 and NALP3, which are expressed intracellularly in macrophages and acts as inflammasomal compartments, mediating the release of IL-1ß. Together, these PRRs recognize distinct pathogens and immediately activate immune response receptor ligands. After this, the exposure of immune cells to these ligands will activate intracellular signalling pathways, which result in the induction of gene expression involved in the immune response (Kawai and Akira 2011).

In a successful immune response, the interplay between the innate host defence and *C. albicans* is finally concluded by killing of the pathogen. Medical intervention use of antifungals can potentially facilitate this outcome.

1.9 Antifungal reagents

There are five major classes of antifungal agents in regular clinical use: polyene agents, derivatives of azoles, the allylamines and thiocarbamates, the fluoropyrimidines and the echinocandins. The first three classes of antifungal agent target sterols or sterol production in the plasma membrane (Dixon and Walsh, 1996; Bartlett *et al.,* 1994). Polyenes are fungicidal compounds produced by *Streptomyces* species. Polyenes, such as amphotericin B have a wide spectrum of activity, targeting ergosterol complexes in the plasma membrane (Zhang *et al*., 2006). They cause cell death by increasing the permeability of the membrane, altering the distribution and leakage of cytoplasmic contents, and inducing oxidative stress (Bolard, 1986). Allylamines (eg. naifitive and terbinafine) and one of the thiocarbamates (eg. tolnaftate) block sterol biosynthesis by direct inhibition of squalene epoxidase. This results in an alteration of membrane structure as a result of both ergosterol depletion and squalene accumulation (Georgopapadakou and Bertasso, 1992; Walsh, 1995; Dixon and Walsh, 1996). Fluoropyrimidines are include 5-fluorocytosine (5-FC) which is a synthetic fluorinated pyrimindine (Mayers, 2009). This antifungal has a wide range of activity against Candida and *Cryptococcus genera* and also active against *Aspergellus* species and protists such as *Leishmania* (Stiller *et al*., 1983; Patrick *et al*., 2012). Fungal cells transport fluoropyramidine via the role of an enzyme cytosine permeases and subsequently convert these to fluorouracil by the action of cytosine deaminase. Fluorouracil is combined into RNA in place of uracil. Additionally, essential thymidylate synthetase is blocked by flucytosine (Mayers, 2009).

Echinocandins are antifungal agents that act by suppression of ß (1,3) glucan synthase which is important for cell wall integrity (Wiederhold and Lewis, 2003). The action of echinocandins results in osmotic instability and cell death. Echinocandins possess good activity against Candida species such as *C. albicans*, C. *parapsilosis* and C. *guilliermandii* and also against *Aspergillus* species (Grover, 2010; Messer *et al.,* 2006).

The azole compounds (eg. fluconazole), discovered in the late 1960s have potent antifungal activity and chemotherapy. Azole antifungals have a broad spectrum of action on both yeast and filamentous fungi – some fungistatic and some fungicidal. Azoles disrupt the plasma membrane and its structure, causing vulnerability to further damage, inhibition of ergosterol synthesis, and cell death in some cases. These activities alter the membrane-bound enzyme activities, involved with processes such as nutrient transport affecting the uptake of amino acids) and synthesis of chitin (Georgopapadakou *et al*., 1987; Dixon and Walsh, 1996). Azole agents are relatively free of serious toxicity issues compared with the other antifungals, often making them the first line of defence in the clinician's armoury (Sheehan *et al.,* 1999). In recent years, fluconazole has been prominent in terms of its spectrum of activity, ease of use via oral or intravenous routes, and potency as a therapeutic agent though there are issues regarding the emergence of resistance (Ghannoum and Rice, 1999; Rogers and Galgiani, 1986).

The fungal cell wall is a unique organelle, which as a potential target fulfils the criteria for selective toxicity. However, the development of specific agents to interfere with different steps in cell wall synthesis has proven difficult and toxicity of potential leads to the host remains a significant hurdle. Finding new models to test antifungal drugs prior to release is therefore imperative if we are to secure a future free from fungal infection.

1.10 Limitation of animal models research for *C. albicans* at 37˚C

Over the last few decades, a plethora of animal models has been developed to understand the fungal disease-host responses mechanisms and investigate various chemical and antifungal compounds (Hohl, 2014). Researchers have developed different models based on vertebrates (e.g. mice, rats, guinea pigs, rabbit, and zebrafish) and others on mini-invertebrate hosts such as fruit flies (*Drosophila melanogaster*) (Lionakis and Kontoyiannis, 2012), nematodes (*Caenorhabditis elegans*) (Muhammed *et al.,* 2012a) and wax moths (*Galleria mellonella*) (Achterman *et al*., 2011; Lionakis, 2011). As it has been reported by earlier studies each

model has some advantages and disadvantages. The rabbit's body size facilitates easy drug administration and repeated fluid sampling. Various genetically defined strains are available in mice and rats; meanwhile the transparency of zebrafish has helped in non-invasive imaging of fungal infections. These common models have therefore been used to study disease syndromes caused by fungi and to gain insight into fungal disease progression, host defence, diagnosis and to examine the effectiveness of vaccination and antifungal treatments (Hohl, 2014).

In case of *C. albicans* infection, *C. elegans* has been used as a model host for *C. albicans* Infection. The advantages of using *C. elegans* model include a direct analysis of *C. albicans* morphogenesis independent of temperature. The gastrointestinal tract of *C. elegans* can easily be infected by feeding *C. albicans* cells to the worms reproducing the commensal colonization of the gastrointestinal tract. This infection mode cannot be readily achieved in fly and waxmoth models due to the difficulty in establishing an infection without animal injection (Pukkila-Worley *et al.,* 2009). Limitations for *C. elegans* include evolutionary distance from us, and lack of organs/tissues such as a blood, brain, internal organs, and defined fat cells. The small length of nematodes (1 mm) leads to difficulty in obtaining material for biochemistry, microarray, and immunoprecipitation studies because these techniques need to be performed by extraction of the whole worms and that may result in a limited understanding of tissue-specific signalling (Tissenbaum, 2015).

Mice have been increasingly used in studies of fungal infection as a result of easy and inexpensive maintainance, handling, and production. Genetically, it has been modified to develop knockout and transgenic models to inoculate with fungi such as oral candidiasis, infection in pulmonary and central nervous system (CNS) (Samaranayake and Samaranayake, 2001; Allen, 1994; Naglik *et al*., 2008; Costa *et al.,* 2013). With regard to the Candida*, albicans*-infection mice have been used to understand host immune response during *Candida* infection and also allow immunosuppressive treatments (Costa *et al.,* 2013). The limitation of using murine models is that mice differ in their indigenous fungal flora from humans. Early studies reported that in natural mice there is no colonization by *C. albicans* (Savage and Dubos, 1967). In setting up murine infections

with Candida no colonization on the murine reproductive tract is observed (Iliev *et al.,* 2012). In the healthy human body*, C. albicans* exhibits an asymptomatic pattern of colonization with respect to mucosal tissues such as the gastrointestinal tract.

1.10.1 Zebrafish in some studies

Due to its optical transparency and similarity to mammals with respect to immune structures, zebrafish have been developed as an important model to examine and visualize pathogen-host interactions. Specifically, in recent years, researchers have developed new transgenic lines of fish (Zebrafish) that express fluorescent proteins in the determined innate immune cells, and developed fluorescent fungal strains for *in vivo* imaging, and modified anti-sense oligonucleotides (i.e. morpholinos). Based on this fact, Zebrafish have become a useful model to examine fungal pathogenicity and help to visualize in real-time the fungal cell-host interaction (Brothers *et al.,* 2011; Brothers *et al.,* 2013). However, it was reported that the optimal temperature is 28°C but it can grow within a range of temperatures between 18°C and 33°C which is considerably lower than human fever condition (39°C) or even at normal human body temperatures (37°C) (Westerfield, 2000). Such studies have demonstrated the infection with C. albicans is affected by temperature. Since high temperatures (37℃) induce a yeast-hyphae transition in *C. albicans*, this model may not reflect efficiently the situation in human disease. In other words, a major problem with the zebrafish as a model for studying Candida infection is their inability to survive at elevated temperatures, promoting a search for alternatives. In this study, we have developed the Arabian killifish embryo as an alternative model for studying infection. We found that Arabian killifish can survive at 37°C (normal human body temperature) or even at 39°C (human fever conditions) which allows us to investigate host-pathogen interactions using *C. albicans* as a model pathogen.

1.10.2 Arabian killifish (*A. dispar*)

The Arabian killifish (*Aphanius dispar*), belongs to the family of Cyprinodontidae fish (Freyhof, 2014). It is widely distributed throughout the Arab Peninsula and in the Middle East countries such as Iraq and Iran and it can be found in East Africa as well (Victor and Menachem, 2000). This species is usually found in estuaries, lakes, and along coastal areas. *A. dispar* can also be seen in streams, shallow water and among vegetation over rocks and sand. It uses plants and rock holes to spawn. The fish is omnivorous, but their diet mostly consists of filamentous algae, diatoms and aquatic insects (Hellyer and Aspinall, 2005).

The species is considered as a euryhaline fish due to its ability to live in the environment tolerating a wide range of salinities from fresh water to the salinities much higher than standard sea water (Plaut, 2000). According to Gholami *et al*., (2011), Arabian killifish are known to live at a wide range of temperatures and can even be acclimated to elevated temperatures (37-40°C). Based on this fact, Arabian killifish is potentially a good mini-vertebrate model to investigate the interaction of pathogens and immune cells at human temperature (37˚C). In addition, it has a good ability to tolerate to low levels of O_2. Currently, there are no data available about its actual population structure, however, according to (Freyhof, 2014), its population tends to be steady. Arabian killifish tend to live in schools (Mehdi *et al.,* 2012).

Arabian killifish can reach 8 cm in total length (Carpenter *et al.,* 1997), and sexual maturity is attained when the length reaches approximately 3 cm in the first year. Usually, females lay their eggs on the river or sea bed. Reproduction occurs throughout the year (peaking in May−July) within areas that have some water flow and plants or algae-covered rocks. Fertility is up to 73 mature eggs, with each egg reaching 2.2 mm in diameter (Keivany, 2012). Eggs subsequently hatch after around two weeks or less (Baensch and Riehl, 2004). The fish body is covered by large cycloid scales and the lateral line is indistinct. There are some differences between the males and females of Arabian killifish. According to Hellyer and Aspinall (2005), reproductive males are greenish-brown to grey in colour with shiny

blue flank spots and brown to light orange, unequal, narrow bars. The anterior belly is blue in colour with pearl spots. The dorsal fin is spotted light blue on a bright orange background and is striped. The caudal fin is striped with 2−3 alternating dark and light blue bars. Males are however less brightly coloured outside the breeding period. In contrast, the females are grey to silver in colour (Hellyer and Aspinall, 2005). The females have a number of narrow bars on their flank and a dark brown stripe on the back. The dorsal and anal fins are shorter in females (Fig. 1.9)

.

Figure 1.9: Arabian killifish (*Aphanius dispar*)

Over the last few decades, *A. dispar* was considered as a biological control agent of mosquito larvae (Victor and Menachem, 2000). In addition, it was recommended to use Arabian killifish as an indicator organism to assess the risk of potential ecotoxicological contamination (Saeed *et al.,* 2015).

Many features make *A. dispar* suitable for experimental use in the laboratory. It is a small fish and it is cheap and easy to maintain. Females have the ability to spawn every day, their spawning is not limited to specific seasons and so it spawns all year round (though our own observations indicate that the rate of spawning increases during the spring). With a short generation period (it takes between 3 to 4 months), they make an appropriate model for research. Compared with other fish, *A. dispar* eggs are large and transparent; the yolk is sequestered into separate cells. Furthermore, fertilization is external, so live embryos are able to be

manipulated and can be monitored through all developmental stages under a dissecting microscope. In addition, since it was observed that its eggs have pigment cells, it makes it an appealing model for research on pigmentation.

The present study investigates *Aphanius dispar,* the Arabian Killifish as a model for studying the interaction of pathogens and immune cells at 37 ˚C. This remarkable fish is resistant to a wide range of salinities and temperature ranges, compared with other commercially grown fish. It is active over from 4-30 ˚C and can tolerate temperatures as high as 40˚C (Victor and Menachem, 2000). Furthermore, Arabian Killifish develop blood vessels and immune cells in the yolk before the muscles and tail develop, allows direct injection of pathogens and drugs into embryos, facilitating live cell imaging without anaesthesia at a physiologically relevant temperature, 37˚C.

The aim of this study is to critically assess *A. dispar*'s suitability as a model to investigate the behaviour of *C. albicans* in a host organism at human body temperatures, and evaluate the immune response against the pathogen in a transparent embryo.

We hypothesised that *A. dispar* could be developed as an alternative model to Zebrafish, for the study of infection processes, with the additional advantage of survival at higher temperatures. The overall objectives of the study are therefore:

- To characterise the normal embryonic development of *A. dispar* as a future model for infection
- To develop protocols for injection of *C. albicans* into *A. dispar* embryos
- To develop tools for monitoring immune cell responses
- To investigate host-pathogen interactions using the *A. dispar* embryo and *C. albicans*
- To investigate the virulence of mutants of *C. albicans* in the *A. dispar* model, potentially revealing mechanisms of infection such as the role of mannan in the cell wall of *C. albicans* and its impact on immune cell recognition and host oxidative stress responses

Chapter 2- Materials and Methods

2.1 Organisms group, strains, plasmids, and primers

2.1.1 *Candida albicans* strains

This study includes strains that are listed in Table 2.1

Table 2.1 *C. albicans* strains used in this study

Strain	Genotype	Origin
SC5314	Wild-type	Exeter University Fonzi and Irwin, (1993)
NGY152	*ura3D::imm434/ura3D:: imm434, RPS1/rps1D::* CIp10	Exeter University Fonzi and Irwin, (1993)
Ca ACT1	*Ca ACT1::GFP* integrated at RP10	Exeter University Walker *et al*., (2009)
Ca TUB1	*Ca TUB1::GFP* integrated at RP10	Exeter University Rida *et al*., (2006)
CAF2-dTomato	*Δura3::imm434/URA3*	Gratacap *et al.,* (2013) Maine University
*och1*Δ+CIp10-*och1*	*ura3*Δ*::imm434/ura3*Δ*::imm434, och1*Δ*::hisG/ och1*Δ*::hisG, RPS1/rps1*Δ*::*CIp10-*OCH1*	Gift from Dr. Steven Bates Hall and Neil, (2013) University of Exeter
*och1*Δ+CIp10	*ura3*Δ*::imm434/ura3*Δ*::imm434, och1*Δ*::hisG/ och1*Δ*::hisG, RPS1/rps1*Δ*::*CIp10	Gift from Dr. Steven Bates Hall and Neil, (2013) University of Exeter
*pmr11*Δ+CIp10-*pmr1*	*ura3*Δ*::imm434/ura3*Δ*::imm434, pmr1*Δ*::hisG/ pmr1*Δ*::hisG, RPS1/rps1*Δ*::*CIp10-*PMR1*	Gift from Dr. Steven Bates Hall and Neil, (2013) University of Exeter
*pmr11*Δ+CIp10	*ura3*Δ*::imm434/ura3*Δ*::imm434,*	Gift from Dr.

	*pmr1Δ::hisG/ pmr1Δ::hisG, RPS1/rps1Δ::*ClP10	Steven Bates Hall and Neil, (2013) University of Exeter
mnt1/mnt2Δ+Clp10-*mnt2*	*ura3Δ::imm434/ura3Δ::imm434, mnt1-mnt2Δ::hisG/ mnt1-mnt2Δ::hisG, RPS1/rps1Δ::*ClP10-*MNT2*	Gift from Dr. Steven Bates Hall and Neil, (2013) University of Exeter
mnt1/mnt2Δ+Clp10	*ura3Δ::imm434/ura3Δ::imm434, mnt1-mnt2Δ::hisG/ mnt1-mnt2Δ::hisG, RPS1/rps1Δ::*ClP10	Gift from Dr. Steven Bate Hall and Gow, (2013) University of Exeter

2.1.2 Bacterial Strain

The bacterial strain used in this study is *E. coli* (JM109).

2.1.3 Fish models

Fish models used in this study are listed in Table 2.2.

Table 2.2 Organism models used in this study

Common name	***Scientific name***	**Origin**
Arabian killifish	*Aphanius dispar*	Exeter University
Medaka killifish	*Oryzias latipes*	Exeter University
Zebrafish (Wild-type)	*Danio rerio*	Exeter University
Zebrafish (Casper)	*Danio rerio*	Exeter University

2.1.4 Plasmids

The plasmids used in this study are listed in Table 2.3.
With regards to features and plasmid maps, see Appendix 1, 2 and 3.

Table 2.3 Plasmids prepared for this study were used to store amplified genes of interest for future use to generate ISH probes.

Plasmids	Gene expression	Origin	Thesis entry
Ol-gch	Leucophore (pigment cells)	Gift received from Dr. Robert Kelsh Nagao *et al.,* 2014 Bath University	Chapter 1
Ad-fms	Pigment cells	Univ. Exeter this study	Data not included
L-plastin	Macrophages (innate immune cells)	Univ. Exeter this study	Data not included
Ad-Ptgst2_PMA-T	Immune response (macrophages)	Univ. Exeter this study	Data not included
Ad-Mfap2_PMK-RQ	Immune response (macrophages)	Univ. Exeter this study	Data not included
Ad-Mpx1_PMA-T	Neutrophils (innate immune cells)	Univ. Exeter this study	Data not included

2.1.5 Primers

The primers used in this study are listed in Table 2.4 With regards to the target gene sequences, see Appendix 2.

Table 2.4 General oligonucleotides used in this study for the qPCR.

Primer name	Sequence	gene expression
Ad_ *Lsm12b*_F	TGAGACCACAAGGAGGAG	Housekeeping gene
Ad_ *Lsm12b*_R	GGCAAGATGAGACAAGTTAGT	Housekeeping gene
Ad_ *Nos2a*_F	TCACAAGACTACGCCAAA	Nitric oxide
Ad_*Nos2a*_R	GCACCAACATCATACTCATC	Nitric oxide
Ad_*Nox1*_F	CTACACAGACAACAAAGAC	NADPH oxidase
Ad_*Nox1*_R	CCATCACGATTCACAATG	NADPH oxidase
Ad_*L-plastin*_F	CTCATCAACCTGTCTGTTC	Macrophages
Ad_*L-plastin*_R	TTCTCCTGCGTAGTGAAG	Macrophages
Ad_*Csf1a*_F	TGGAGTGGAAGTGGATAT	Macrophages
Ad_*Csf1a*_R	ATGGTCATCTGGTATGTG	Macrophages
Ad_*myb*_F	GAAGACCCTGAGAAAGAG	Haematopoietic tissue (lymphocytes and leukocytes)
Ad_*myb*_R	GATAGTGATGGCTGGATT	Haematopoietic tissues (lymphocytes and leukocytes)
Ad_*mpx*_F	AGAATTACTGGATGTGAGGCT	Neutrophils
Ad_*mpx*_R	TGGCTGTGCGATACTTGT	Neutrophils
Ad_cxcr4_F	TCAGCAGCAACTTCAACAA	Chemokines
Ad_*cxcr4*_R	ACAACAACGACCAGTCCA	Chemokines

2.2 Fish Care and Maintenance

2.2.1 Arabian killifish (*Aphanius dispar*)

A. *dispar* fish were kept in a recirculation system in the Aquatic Resource Centre at the University of Exeter. Egg collection was performed once daily by placing egg collection chambers in the tank. The eggs were subjected to incubation under suitable conditions (ASW 35% and 26.0°C) to complete their embryonic development. In the case of the experiments locking at the effect of different temperatures on the embryonic development of *A. dispar*, the water temperature was set at 26.0°C, 30.0°C, 37.0°C, and 38.5°C by using different incubators. Salinity level varied between fresh water, 3 ppt, 10 ppt, 14 ppt, 35 ppt, and 150 ppt. Salt water concentration of 10 ppt, 100 ppt, and 150 ppt were prepared by diluting artificial sea salt (Tropic marine-Germany) while the salinity of fresh water and 35 ppt were set up from recirculation system in the Aquatic Resources Centre of the University of Exeter. Water quality was monitored and changed daily during the experiments days.

For *A. dispar*, the best period for obtaining fertilized eggs with one cell stage was between 8-9 am. Eggs were obtained in the morning with natural spawning by adding a glass chamber to the tanks at 8 am and collecting the eggs after one hour, eggs were then transferred to Petri dishes with 20 ml of ASW at 26°C, with daily water changes. Embryos were kept submerged in “channel gels” made by leaving agarose to set on 1.2 mm diameter glass tubes (Mourabit *et al*., 2011). All photographs were taken using an Olympus, SZX2-ILLKmicroscopes.

2.2.2 Medaka (*Orizias latipes*)

Medaka fish were maintained in RO water with a recirculation system. They spawn eggs at 9-11 am in the morning. The females carry eggs internally. The eggs were manually removed from the fish caught in a fish net. Yolk hair is removed from the collecting eggs with tweezers. Eggs were

incubated with RO water with methylene blue to prevent fungal infection and then incubated at 26°C.

2.2.3 Zebrafish (*Danio rerio*)

Fertilised Zebrafish eggs were obtained from a population (Wild-type and Casper) that were bred and maintained in an A1 recirculating system at temperature of 28°C, pH 7.4, and salinity of fresh water at the aquaria facilities of the University of Exeter. Fish eggs were placed and maintained in the plastic Petri dishes with 20 ml of freshwater and incubated at 28°C in a Heratherm IGS60 (Germany) incubator.

2.3 Microinjection technique

Microinjection of *A. dispar* was performed to deliver directly of injection materials (Candida inocula or oligos) into the developing embryos. Fish embryos were injected at 1 to 4 cell stages to gain transgenic fish and injection with Morpholino oligomer to modify gene expression. In addition, they were injected at the somitogenesis stage (54.5-59.5 hpf) to infect the embryos with the *C. albicans*.

To prepare for microinjection, micro glass needles (capillary tubes) were heated at 52°C using electron puller (NARISHIGE PC-10) to obtain two consistent sizes of pipette needles (short and sharp needle tips in diameter of 10-20 µm which were suitable for the hard chorion of *A. dispar* embryos). The needle tip was cut off under the microscope using forceps to set the volume of solution to be delivered. To visualize the solution during the microinjection, 0.050% phenol red was mixed with the solution to track injection into the embryos successfully. After preparing the needles, they were loaded with a solution and then the microinjector pressure (20 pound per square inch psi) was adjusted. Next, embryos were submerged in “channel gels’’ made by leaving 10% agarose /sea water on setting (1.2 mm diameter glass tubes) (Fig. 2.1). Embryos were rotated using forceps and microinjected with 1 nl of mRNA, morpholino or 5 to 10 nl of *C. albicans* cells using a microinjector (PV820 pneumatic picopump). After microinjection, embryos were transferred to a new Petri dish with seawater

and incubated at 26˚C. To obtain accurate results, embryos were checked, and water changed daily.

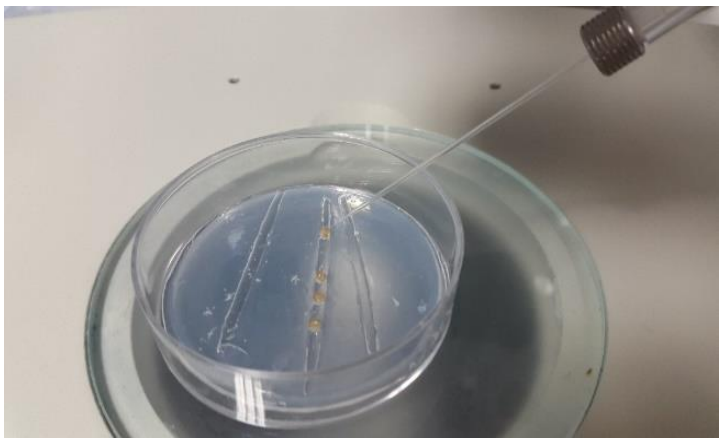

Figure 2.1: Injection of diluted *C. albicans* into *A. dispar* embryos. Agarose bed was made by leaving 10% agarose /sea water on setting (1.2 mm diameter glass tubes, flipped and placed back in same dish and then remove the capillaries tubes. Embryos were held and placed in agarose grooves and rotated for microinjection.

2.4 Media and Culture

2.4.1 Media and culture for *C. albicans*

C. albicans strains were cultured in YPD agar medium plates (1% yeast extract (Difco), 2% glucose, 2% bacteriological peptone, 2% technical agar no. 2) and incubated at 37ºC for 48 hours. To prepare for injection, freshly single colony of *C. albicans* was subcultured onto the 5 ml of YPD broth medium and incubated at 37ºC for 18 hours with 180 rpm shaking. To evaluate and examine the virulence of *C. albicans,* the fungi were cultured in the RPMI1640 1x (Roswell Park memorial institute1640) medium (with L-Glutamine, SIGMA).

2.4.2 Media and culture of Bacteria

Luria broth (LB, Formedium^{TM}) was used to culture *E. coli* at 37°C, 180 rpm. 1 ml of Ampicillin or Kanamycin 50 µg/ml) was added to the 1 litre of LB to

obtain a final concentration of 100 µg/ml, respectively. While LB was supplemented with 2% agar to make a solid medium.

2.4.3 Long-term storage of *C. albicans* strains

Glycerol stocks were prepared with 15% autoclaved glycerol, strains at log phase were suspended in appropriate selective medium supplemented with 15% glycerol. Strains were stored at -80°C.

2.5 Molecular Techniques

2.5.1 *E. coli* preparation

Single colonies of *E. coli* (JM109) were inoculated into 300 ml of LB and Ampicillin broth and incubated at 37°C, 180 rpm overnight. Growth of the *E. coli* was monitored and when cultures were sufficiently dense, culture were transferred into 50 ml tubes x2 (40 ml each), and harvested by centrifugation at 5000 rpm for 10 minutes at 4°C.

2.5.2 Transformation of *E. coli*

E. coli competent cells (JM109) were thawed on ice (3-5 minutes), the plasmid of interest (1 µl) was added to 20 µl competent cells, gently mixed and kept on ice for 20 minutes before incubation at 42°C for 40 seconds (heat shock). Cells were subsequently placed on ice for 5 minutes. 200 µl of the SOB medium was added and then mix was incubated for 1 hour at 37°C with shaking (180 rpm). 100 µl of the culture was then spread on LB Amp or LB Kana plates 100 µg/ml) and then incubated at 37°C for overnight.

2.5.3 Isolation of plasmid DNA

QIAGEN Gene JET plasmid maxiprep kits were used for plasmid extraction. The plasmids were purified according to the manufacturer's instructions. Briefly, bacterial pellets, were resuspended in 4 ml Buffer P1 (Resuspension buffer Tris-Cl, pH 8.0, 10 mM EDTA, 100 µg/ml RNase A). Buffer p2 (lysis buffer; 1200 mM NaOH % SDS); 50mM were added and mixed with gentle version (4-6 times) and incubated at room temperature (15-25°C) for 5 minutes to break the cell wall. Prechilled Buffer 3 (4 ml) (Neutralization buffer) was added to neutralize the solution, mixed

thoroughly inversion and incubated on ice for 15 minutes and centrifuged twice 6000 rpm for 30 minutes at 4°C. 10 ml buffer QBT (Equilibrium 750 mM NaCl, 50 mM MOPS, pH7.0, 15% isopropanol, 0.15% Triton X-100) was added to the column and the column emptied by gravity flow. Then, the supernatant was applied to the column which was then washed with 2x 10 ml Buffer QC (wash buffer; 1.0 mM, NaCl, 50 mM MOPS, pH 7.0, 15% isopropanol). The DNA was eluted with 5 ml Buffer QF (Elution buffer; 1.25 mM, 50 mM Tris-Cl, Ph 8.5, 15% isopropanol). The DNA was precipitated by adding 3.5 ml isopropanol, vortexed and centrifuged (BECKMAN B5437) at 6000 rpm for 30 minutes at 4°C. Supernatants were carefully decanted after washing the pellets (DNA) with 2 ml of 70% ethanol at room temperature with a centrifuge at 15000 rpm for 10 minutes. Pellets were air dried for 5-10 minutes and re-dissolved with the molecular water and stored at -20°C.

2.5.4 Gel electrophoreses to resolve DNA fragments

Agarose gels (2% Agarose in 1x TAE (1.14 ml/L) (glacial acetic acid, 4.84 g/L Tris base, and 0.37 g/L EDTA) was made using a microwave. SYBR safe DNA stain (Invitrogen) was used by adding 0.5 µl to the 50 ml of gel after cooling down to 50° C and then poured into the gel cast. The gel tanks were filled with 1x TAE to cover the agarose gels. 5 µl or 10 µl of DNA sample: (PCR product, digested and purified DNA), 1 or 2 µl of DNA loading buffer (30% (v/v) glycerol, 0.25% (w/v) bromophenol, 0.25% (w/v) xylene cyanol FF) and 0 or 6 µl water were loaded into each well of the gels. 7 µl of DNA ladder (1 Kb or 100 bp) (New England Biolabs) were loaded on the gel and run it for 20 minutes at 120 V. Visualization for the DNA fragments was performed by syngeneic G: Box gel imager.

2.5.5 Generation of transgenic fish

Freshly fertilized eggs were collected in the morning after placing the egg collection chambers in the tanks for 1 hour. Eggs were transferred into the new Petri dish containing ‘’Channel gels’’ made by leaving 10%

agarose/sea water on setting (1.2 mm diameter glass tubes), embryos were rotated using forceps and then using injector (Pneumatic picopump pv820).

To obtain *A. dispar* transgenic, one-cell stage eggs (20 mpf) were microinjected with the following solution: 1 µl of 25 ng/µl (Beta-actin-DsR-LOXP-GFP), 25 ng/µl of Transposase (TPase) mRNA, with 1/20 dilution of phenol red solution (Sigma) for visualization. The solutions were incubated for 10 min at RT prior injection and approximately 1 nl DNA solution was injected into the first cell through the chorion.

After injection, embryos were transferred to a new Petri dish with seawater (35 ppt) and incubated at 26˚C. Embryos then were sorted to check the positive embryos under a fluorescence dissection microscope using RFP filter (Nikon SMZ1500) equipped with a digital camera (Nikon – SIGHT DS-FI2, K20166) and raised for further breeding.

2.6 Gene expression analyses using *in situ* hybridization

2.6.1 Preparation of *in situ* probes

To make *in situ* probes, template DNA was prepared by restriction enzyme digestion (2.6.1.1) of plasmid DNA or by amplifying the DNA using PCR (2.6.1.2):

2.6.1.1 Preparation of template DNA using digestion and purification of plasmid DNA

To make *in situ* probes, Medaka Ol-gch plasmid DNA 10 µg (10 µl) was digested with 4 µl NotI (NEB), 10x NEB Buffer 3 (20 µl), and 170 µl water. Then the reaction was incubated for 2 hours at 37°C. Next, 10 µl of digested DNA was checked using agarose electrophoresis.

Digested DNA was purified using phenol/chloroform extraction; 200 µl of phenol/ chloroform 1:1 was added to the reaction and vortexed to mix the two layers. Around 180 µl of its (Upper phase (aqueous phase) was taken after centrifugation for 2 minutes and moved to a new Eppendorf tube and added 18 µl 3 M sodium acetate pH 5.2 and 450 µl absolute ethanol added mixed and then incubated at -80°C for 1 hour or longer. The samples were centrifuged at 4°C for 20 minutes and 180 µl of 70-75 % ethanol was added

to the pellet after discarding the supernatant. The pellet was dried for 10 minutes and resuspended in 20 µl water and the purified digested DNA was confirmed using agarose gel electrophoresis. Digested and purified DNA was kept at -20°C.

2.6.1.2 Preparation of template DNA using PCR

To prepare DNA template of (ptgs2, mpx, and mfap1), the following were assembled in a PCR tube:

1 µl of forward T3: ATT TAG GTG ACA CTA TAG and reverse SP6: ATT ACC CTC ACT AAA GGG primers, Go Tag PCR master mix (Promega) (10 µl, 1 µl of (Ad_ptgs2, Ad_mpx, and Ad_mfap1) plasmid x1/100 ul, molecular water DEPC (7 µl). The standard conditions of PCR were employed as below:

95°C for 5 min, with replication of denaturation at 95°C for 30 Sec, annealing at 50°C for 1 min, elongation at 72°C for 1 min for 30 cycles and a final extension at 72°C for 10 min. A Thermo Scientific Gene JET PCR Purification Kit was then used to purify the DNA, and the purified DNA was stored at - 20°C. The integrity of DNA was assessed on agarose TAE electrophoretic gel (1%).

2.6.1.3 Probe synthesis using template DNA

The purified DNA samples that were prepared by DNA digestion or PCR, were used to synthesize RNA probes, using 6 µl of template DNA (1 to 2 µg), 2 µL of DIG RNA labelling kit (Roche) and 4 µL of 5x transcription buffer, 1 µL of RNase inhibitor (Roche), 6 µL water and 1 µL of appropriate polymerase (T3 and SP6 20 U/µl) and incubated at 37°C for 5 h. After that, probes were treated with DNase (2 µL) 2500 U/ml at 37°C for 30 min before using 4 M lithium chloride to purify probe. The equal amount of hybridization buffer (50% formamide, 5x SS, 5M EDTA, 0.1% Tween 20, CHAPS 0.1%, 50 µg/ml heparin and 1 mg/ml torula yeast RNA) was added and the probes were stored at -20°C before final use at 1/100 dilution.

2.6.2 Preparation of samples

Fertilised *A. dispar* embryos were kept within embryonic culture water with a salinity of 35 ppt at 26°C. The culture water was replaced daily and monitored. To test the gene expression in *A. dispar*, embryos at somitogenesis stage were collected and photographed before carrying out *in situ* hybridization. Selected embryos were fixed with 4% formaldehyde at 4°C overnight, washed with (PBS) for 10 min before carrying out dechorionation, and stored at -20°C in 100% methanol.

In order to use those embryos in subsequent whole *in situ* hybridization buffer (WISH), a series of methanol dilutions were carried out to rehydrate fixed embryos, using 75%, 50%, and 25% in PBS methanol at a comfortable temperature (20-22°C), and washed for 10 min with PBS and 0.1% Tween20.

2.6.3 *In situ* hybridization

The first step was pre-hybridization; this step was carried out to decrease non-specific binding that might happen between probes and any sites on the tissue. Embryos were placed in 500 µl hybridization buffer (50% formamide, 5x SS, 5M EDTA, 0.1% Tween 20, CHAPS 0.1%, 50 µg/ml heparin and 1 mg/ml torula yeast RNA) for 3 h and then incubated with the suitable probe (diluted 1:100) overnight at 65°C. The appropriate probe was prepared by heating at 80°C for 10 min before shifting quickly on ice for 5 min.

The hybridized samples were subsequently washed with 1 ml of 2xSSC + 50% formamide + 0.1%Tween20 at 65°C for 30 min, and then with 2xSSC 0.1% Tween20 at 65°C for 30 minutes before washing twice with 0.2x SSC 0.1% Tween 20 at 65°C for 30 min.

The blocking reagent (Roche Blocking solution 2%+ HI-BS 5%) was added for 3 h to decrease non-specific binding. After that, the embryos were incubated with the anti-DIG antibody (Roche) (5000x dilution of stock at 150U/200 µl and diluted another 1/100 with blocking solution) for 3 h at

room temperature. Embryos were washed for 4 x 30 min with PBT (0.1% (v/v) Tween 20 in 1x PBS) and then gently placed on a shaker overnight. The next wash was carried out with AP buffer (Tris 0.1 M pH 9.5, NaCl 0.1 M, $MgCl_2$ 50 mM, Tween 20 0.1%) for 10 min.

The AP buffer was changed with 400 µl of BM-Purple AP Substrate (Roche). Then, a top-cut-tip was used to move embryos/ BM-Purple gently to a 24-well plate. In order to prevent light access, the 24-well plate was placed in a box before placing on a shaker 40 rpm for 1-3 h for penetration the BM-Purple through the embryos' tissues and show visible staining.

Staining reactions were achieved at room temperature and continued until signals visible. The process of stopping the reaction was carried out using PBT to wash embryos and drained before fixing them in fresh PFA. Finally, to observe and image stained embryos were visualised using a compound microscope (Nikon SMZ1500) equipped with a digital camera (Nikon – SIGHT DS-FI2, K20166).

2.7 qPCR

2.7.1 *C. albicans* Culture Preparation

Two days prior to the injection of *A. dispar* with *C. albicans*, streak plates from different mutants of Candida (NGY152, *och1*Δ, *pmr1*Δ, and *mnt1-mnt2*Δ) see table 2.1 were prepared on YPD agar to obtain single colonies and incubated at 37°C overnight. One small colony was picked and put into 5 ml of YPD broth and incubated at 37°C at 180 rpm for overnight. In the day of embryo infection, the culture was centrifuged for 2 min at 3500 rpm at 4°C and the pellet was resuspended in 1x of 5 ml phosphate buffer saline and spun down again. This step of washing was repeated twice and then Candida cells were resuspended counted on a Haemocytometer and diluted to $1x10^{8}$ cells/ml.

2.7.2 *A. dispar* embryo infections

A. dispar embryos were collected and incubated at 26°C for 72 hpf. Embryos at somitogenesis stage (54 to 59 hpf) were submerged in "channel

gels'' made by leaving agarose to set under 1.2 mm diameter glass tubes. Embryos were microinjected with 5 to 10 nl of *C. albicans* suspension at $1x10^8$ cell/ml in PBS using microinjector (Pneumatic Picopump PV820) into the yolk and incubated at 37˚C.

2.7.3 Isolation of RNA samples

Total RNA was prepared from control (uninfected) and infected embryos which were microinjected with $1x\ 10^8$ cell/ml of *C. albicans* at somitogenesis stage (54.5-59.5 hpf). Embryos were sacrificed by a plunging; in liquid nitrogen and then transferred to tubes at -80°C until use. RNA extraction was performed by using 1 ml of Trizol reagent (Invitrogen) per 10 embryos; frozen embryos were homogenized to produce a clean pellet in an ice-cold Eppendorf tube by using a hand-held grinder. Samples were incubated for at least 10 min in Trizol to complete dissociation of complexes. To separate the mixture into three phases: 200 µl of chloroform or (1-bromo-3-chloropropane) was added into the 1 ml of homogenized mixture, incubated for 10 min at room temperature RT and then centrifuged at 12000 xg for 15 min at 4°C. The upper aqueous phase was carefully transferred into the fresh tubes. To precipitate RNA, 500 µl isopropanol (ice-cold) was added, incubated 10 min at RT and centrifuged at 12000 xg for 20 min at 4°C. RNA was washed by adding 1 ml of 75% ethanol, centrifuged at 7500 xg for 5 min at 4°C. This step was repeated after removing the supernatant. Finally, the pellets were resuspended in (20 µl water) and RNA concentration was quantified using (Spectrophotometer Nanodrop) with wave length 280 nm and stored at -80°C.

2.7.4 Reverse transcription

cDNA templates were generated using RNase-free DNase (RQ1 – Promega) and M-MLV reverse transcriptase (Promega). For each reaction, the following reagents were added (1 µg/µl of RNA, 1 µl of 1000 U RQ1 DNase, 1 µl RQ1 buffer 400 mM Tris-HCl (pH 8.0), 100 mM MgSO4 and 10 mM CaCl2 with final volume made up to 10 µl with water and then the mixtures in each tube were spun down and incubated for 30 min at 37°C.

The reaction was incubated for 10 min at 60°C, followed by adding 1 µl of the RQ1 stop solution.

Reverse transcription was performed using 1 µl primer (random hexamers) in each reaction and incubated for 5 min at 70°C to melt secondary structures within the template. To prevent secondary structures from reforming, reactions were directly cooled on ice for 2 min. Next, M-MLV 5x reaction buffer (5 µl), 10 mM dNTP mix (2 µl), M-MLV reverse transcriptase (1 µl at 200 Units/µl) and water (5 µl) were added and incubated at 37°C for 60 min. Finally, cDNA was stored at -20°C.

2.8 Protein analysis

2.8.1 Western blotting

Total protein samples from *A. dispar* embryos were prepared from 5 embryos as required. Embryos were kept in 100 µl lysis buffer 150 mM sodium chloride, 1.0% NP-40 (Triton X-100 can be substituted for NP-40, 50 mM Tris pH 8.0 - NP0008, Invitrogen) on ice for lysis and then homogenized by grinding (Greiner Bio-one) using a plastic pestle without removal of the yolk or chorion. Homogenised embryos were heated at 80-90°C for 5 min and centrifuged at 14,000 rpm for 5 min. The supernatants were transferred to new 1.5 ml Eppendorf tubes and used immediately or stored at -20°C until required. The amount of the supernatant which was loaded on an NuPAGE gel (acrylamide 4%~12% Bis-Tris pH7-7.5 - NP 0335BOX, Invitrogen) was set at 30 µl for embryo extracts and 7 µl of pre-stained protein standard ladder (SeeBlue® Plus2 Protein Standard) (Thermo Fisher) in 1x NuPAGE MOPS running buffer at 120 V for 2 hours.

Transfer buffer 1x (144.1 g Glycine, 30.3 g Tris base) was used to transfer the proteins to the polyvinylidene difluoride (PVDF) membrane L16201177 (Bio-RAD) for 1 hour at 30 V, then it membranes were rinsed in ddH_2O. Ponceau red (Sigma-Aldrich): 1 g Ponceau S, 50 ml acetic acid/1000 ml ddH_2O was used to check the efficiency of protein transfer by soaking the membrane for 2-5 minutes. Subsequently, the membrane was incubated in blocking solution (dried skimmed milk powder 5% w/v) in TBS for 2 hours and then probed with primary antibodies (Table 2.5) for overnight at 4°C.

Next day, the membrane was washed three times for 1 hour in 1x TBST (0.1% Tween20, 24.2 g Tris, 84 g NaCl/L pH 7.6) then incubated with the secondary antibodies (Table 2.5) in blocking solution for 2 h at room temperature. To visualize signal development, the membrane was washed for three times for 1 h with 1x TBST and incubated with a mixture of 1 ml luminal solution and 1 ml peroxide solution provided in the Immobilon Western HRP substrate kit (Thermo- Scientific) for 2-5 minutes. The membrane was placed in an autoradiograph cassette with X-ray film for developing. Finally, the membrane was washed twice in Stripping buffer for 10 min, twice in PBS washing for 10 min and twice in 1x TBST washing buffer for 5 min. The membrane was again incubated a positive control antibody (Table 2.5) for overnight at 4°C. At the next day, the membrane had been washed in TBST before incubation with the secondary antibody for 2 hours then washed and visualized the protein bands.

Table 2.5: Primary and secondary antibodies used for Western blots

Antibody	Dilution	Supplier
Primary		
Rabbit anti- mCherry	1/5000	Abcam (ab167453)
Rabbit anti- l- plastin	1/5000	Gift received from Dr. Paul Martin Bristol University
Mouse anti-alpha Tubulin	1/1000	Sigma (T9026)
Mouse anti- Beta-actin	1/1000	Sigma
Secondary		
Goat-Anti-Rabbit immunoglobulin HRP	1/1000	Dako (P0448)
Goat-Anti-Mouse immunoglobulins HRP	1/500	Dako (P0447)

2.8.1.1 Western blot materials

Table 2.6: western blot reagents

Reagents	Component
10x TBS	24.2 g Tris 84 g NaCl/ PH 7.6
1x TBSw	100 ml 10x TBS 900 ml DDW Tween 20 (25%)
10x Running buffer	250 mM Tris 192 mM Glycine 0.5% SDS
10x Transfer buffer	144.1g Glycine 30.3 g Tris base
1x Transfer buffer	100 ml 10x Transfer buffer 100 ml methanol 800 ml molecular DEPC water
Stripping buffer	15 g Glycine 1 g SDS 10 ml Tween 20/ pH 2.2 complete the volume to 1000 ml
Ponceau S staining Solution	1 g Ponceau S 50 ml acetic acid/1000 ml dd H_2O store at 4°C

2.8.2 Immunohistochemistry

2.8.2.1 Paraffin sectioning

A. dispar embryos were fixed in 4 % paraformaldehyde/ Hepes-NaCl, (50 mM Hepes (Sigma), 0.5 M NaCl, pH 7.8) for overnight at 4°C. Labelled embryos carefully transferred from fixation solution and set in the tissue cassette. Dehydration was used by the staging of EtOH treatments (50, 70, 90 and 100%) in order to remove the water contained within the tissue and any residual fixative. To clear the tissue, samples were submerged in the

xylene substitute (Sigma), then gradually dehydrated the samples from (0 to 100%) alcohol. Alcohol was replaced with xylene which is miscible with a medium for embedding. In order to impregnate the tissue, molten paraffin (60°C) was used to embed the tissue after replacing the clearing fluid.

After embedding, a CHANDAN AS325 microtome was used to section the tissue into 5 µm thick sections. The serial ribbon sections were then carefully transferred in a water bath at 45-50°C. Samples were attached to prelabelled slides and the sections were transferred to a hotplate at 60°C until dry. The slides were immersed in a series of ethanol solutions 50% (1 min), 75% (2 min), 90% (3 min) and 100% (5 min) to fix the cells on the slides. Protein detection within tissue sections was achieved by firstly blocking non- specific binding proteins using dried skimmed milk powder 5%(w/v) in TBS (Tris-buffered saline) for 2-3 h then incubated with the primary antibodies overnight at 4°C in a humid box. In a Coplin jar, tissue sections were washed three times with 1x TBS-Tween 20. Secondary antibodies 1:300 were prepared in blocking solution and added to the tissue section for 2-3 h at room temperature (RT), washed three times for 1 h each and incubated with VECTOSTAIN ABC reagent (Vector lab) PK-4000 for 30 min to 1 h and then incubated with peroxidase substrate DAB (Vector lab) SK-4100 for 2-10 min after washing with TBS-Tween. Slides were finally washed with water tap and, hematoxylin and eosin were used to stain the tissue section. Haematoxylin stain binds to DNA complex and nucleus, whereas eosin is a counterstain binding to eosinophilic structures. Tissue sections were rehydrated by immersing in 100% ethanol at 3 min and were finally washed with water for 1 min and mounting on slides.

2.8.3 Immunofluorescence staining of macrophages and Candida cells

Embryos at somitogenesis stage 24 (45.5 hpi) and organogenesis stage 29 (246.5 hpi) were microinjected with 5 to 10 nl of *C. albicans* at $1x10^8$ cell/ml and incubated for 24 hpi at 37°C. Next embryos were fixed in 4 % paraformaldehyde/ Hepes (SIGMA), 0.5 M NaCl (12 g PFA, Hepes 3.57 g, 30 ml NaCl / 300 ml DW and adjust the pH to 7.8) overnight and then washed twice with PBS 0.5% Triton and incubated with 100% methanol

(MeOH) at -20°C. After washing extensively with 70, 50, 25% MeOH and PBS Triton, the embryos were permeabilized with 0.24% w/v trypsin 1x with PBS 0.5% Triton for 2-3 h at room temperature. The trypsin was removed and replaced with blocking solution (1% BSA, 0.5% PBS Triton/ serum FCS-IH) for 3 h at RT. The primary antibody solution was diluted with blocking solution (1:500); dried skimmed milk powder 5% w/v in TBS and then added in the tubes of embryos and incubated for overnight at 4°C. The next day, embryos were washed for 1 h with 1x PBS, 0.5% Triton and incubated with secondary antibodies (1:300) overnight at 4°C. Embryos were then washed three times for 1 h and directly imaged at microscopic magnification of 5x and 10x objective (DIC, GFP and RFP filter) with an inverted Zeiss microscope (Zeiss AxioObserver.Z1-AX10).

Table 2.7 Primary and secondary antibodies used for immunofluorescence

Antibody name	Dilution	Supplier
Primary		
Mouse anti-microglia -4c4 antibody	1:500	Gift received from Dr.Thomas Becker Edinburgh University
Rabbit anti- L-plastin	1:500	Gift received from Dr. Paul Martin Bristol University
Rabbit anti-Candida-R2	1:250	Gift received from Dr. Howard Jenkinson Bristol University
Secondary		
Alexa Fluor 488 goat anti-rabbit	1:300	Life Technologies A11034
Alexa Fluor 594 goat anti-rabbit	1:300	Life Technologies A11012
Hoechst trihydrochloride	1:400	Life Technologies H3570

Chapter 3

Normal Embryonic Development of the Arabian killifish, *Aphanius dispar.*

3.1 Abstract

Arabian Killifish, *Aphanius dispar*, live in the marine coastal areas of the Middle East, as well as in streams. This species is considered as a biological control agent for mosquito larvae. Though the fish live in areas with a variety of salinities and temperatures, it is still not clear how embryonic development is affected by salinity and temperature. In this study, the process of normal embryonic development was analyzed at different temperatures and salinities. Embryogenesis was divided into 32 stages based on diagnostic patterns of development. Embryo development was then examined under different thermal environments at 26.0, 30.0, 37.0 and 38.5°C. Embryos were also reared at seven different levels of salinity; 0.3, 3, 10, 14, 35 and 150 ppt ASW.

Results indicate that temperature has a significant effect on embryonic development; with accelerated development at higher temperatures. In the case of salinity, the data indicate that growth was slightly accelerated by higher levels of salinity. Together, these findings suggest that *A. dispar* can tolerate a wide range of temperatures and salinities including extreme conditions that are 4 times higher in salinity than sea water (150 ppt) and higher than human body temperature (38.5°C). *A. dispar* could therefore be suitable for toxicology and pathogenesis studies at different salinities and temperatures. In particular, fish embryos could provide a relevant biomedical model for analyzing infection by bacterial, fungal and viral pathogens under conditions similar to those found in patients.

During the examination of *A. dispar* embryos, we identified brown pigment cells with a highly fluorescent character under GFP and RFP filter conditions. Various imaging analyses suggest that this is a novel type of

pigment cell possessing some overlapping characters with leucophores from other killifish species (e.g. Medaka). When PTU was used to inhibit melanogenesis, no changes were detected, suggesting that the brown pigment cells in *A. dispar* do not contain melanin. Whole-mount *in situ* hybridization (WISH) for examining gene expression of *gch* (a gene marker of leucophores in Medaka) also supports the suggestion that the fluorescent pigment cells in *A. dispar* are leucophores. We concluded that the fluorescent pigment cell that we have discovered are novel highly fluorescent leucophores that may have developed in *A. dispar* to allow the fish to adapt to live within extreme environmental conditions with strong sunlight and a wide range of temperatures.

3.2 Introduction

The Arabian killifish (*Aphanius dispar*) is a teleost fish and biological control agent of mosquito larvae (Victore *et al*., 2000). It is distributed in coastal areas of the Eastern Mediterranean, Iraq, Iran, Saudi Arabia, Syria, Somalia and East Africa (Gholami *et al*., 2011; Haq and Yadav, 2011). *A. dispar* also lives in streams, shallow lagoons and pond water, among vegetation over rocks and sand (Saeed *et al*., 2015). This omnivore species tends to live in schools (Mehdi, 2012). Arabian killifish can also live at extreme temperatures (37- 40°C) (Arash *et al*., 2014). *A. dispar* is a member of the euryhaline and osmoregulatory teleost fish that are capable of tolerating extreme ranges of salinity, from fresh water to 175 ppt sea water. As a result of having a good ability to withstand wide ranges of salinity through osmoregulation, *A. dispar* can survive in natural saline water, brackish water and fresh water (Haq *et al*., 2013. *A. dispar* can therefore be considered an excellent model fish to study physiological and ecological behaviour and adaptation with respect to the effect of salinity (Lotan,1971; Plaut, 2000). *A. dispar* is also tolerant to a wide range of pesticides and toxins and can tolerate low levels of O_2; therefore, it has been used as a biological model to evaluate eco-toxicity (Saeed *et al*., 2015; Fletcher *et al*., 1992). Hence *A. dispar* might be a suitable model to examine the effects of a wide range of environmental stressors on aquatic species.

Small teleost fish embryos have also been used as models for studying genetic diseases, infection, ecotoxicology, drug testing as well as for assessing mechanisms of normal embryonic development and cell function (Jeng-Wei Lu *et al*., 2015; Hsu *et al*., 1997). Increasingly, over the last decade, zebrafish and medaka have been used as a very popular model animal for these purposes (Arduini *et al*., 2008). These fish lay many eggs in the lab on daily basis throughout the year, with the eggs rapidly developing body and organs within a few days. The process of development can be easily observed due to their small size and the transparency of the embryo. Though zebrafish and Medaka have been very powerful models for a variety of studies, it is still necessary to use other fish models for different purposes. For instance, zebrafish embryos cannot survive at 37°C, therefore, they are not really suitable for infection or drug testing in an environment where human body temperatures would be more appropriate. In addition, zebrafish and medaka are freshwater fish and therefore are not ideal for investigating marine environmental changes and pollution. Here we report that the *A. dispar* embryo can become a very useful model for studying embryonic events at human body temperatures and also at different salinities.

In fish, pigment cells are derived from a provisional group of cells named the neural crest (Kelsh *et al*., 2004). According to Kimura *et al*., (2014), pigment cells in fish can be divided into two types as a result of their interaction with light. The first group, including xanthophores, erythrophores, and melanophores absorb light. Whereas the second group, are light reflecting pigment cells such as iridophores and leucophores (Masazumi, 2002). While melanophores, xanthophores, and iridophores are widely seen in many fish species (including zebrafish), fewer species have leucophores which, uniquely are fluorescent pigment cells (Kimura *et al*., 2014).

Melanophores are particular pigment cells that contain hundreds of melanosomes filled with melanin (Frohnhöfer *et al*., 2013). The key function of melanosomes is melanin dispersion within the cytoplasm or aggregation in the center of pigment cell. This mechanism is essential in changing color and also plays a significant role in protection the body against UV irradiation

(Fujii *et al*., 2002). As mentioned above, leucophores and iridophores have the ability to reflect light using their plates of crystalline of purine and guanine respectively. Though the difference is not always obvious, leucophores are generally considered to reflect light of all wavelengths producing a white colour, whereas iridophores are specific to create iridescent color (Kimura *et al*., 2014). On the other hand, in medaka, it has recently been showed that there is some similarity between leucophores and xanthophores in their developmental process with respect to gene regulation and cell migration (Kimura *et al*., 2014). Although there are many studies examining many of the distinct pigment cell types in killifish, few have characterized the function of leucophores.

Extreme salinity, high water temperature, and strong sunlight may have a dramatic effect on development in some species of fish. We have recently discovered that *A. dispar* has an extraordinarily highly fluorescent pigment cell, suggesting that this fish, living in areas of strong sunlight, may have evolved a novel pigmented cell type as an adaptation to this stress. The present study aims to characterize the *A. dispar* pigment cells using a range of different imaging techniques and whole-mount *in-situ* hybridization to clarify the nature of the fluorescent pigment cells in *A. dispar*.

3.3 Materials and Methods

3.3.1 *Aphanius dispar* care and maintenance

A. *dispar* fish were kept in a recirculation system in the Aquatic Resource Centre at the University of Exeter. *A. dispar* eggs were collected daily (in the morning) in egg collection chambers and then kept in Petri dishes, normally at 26°C, with 35 ppt salinity. The eggs were subjected to incubation to complete their embryonic development. In the case of experiments at different temperatures, water temperature was set to: 26.0˚C, 30.0˚C, 37.0˚C, and 38.5˚C by using different incubators. Salinity level was varied between 0.3 ppt, 3 ppt, 10 ppt, 35 ppt and 150 ppt as required. 10 ppt, 100 ppt, and 150 ppt were prepared by diluting artificial sea salt with distilled water (Tropic Marine - Germany). Water was changed daily during the experiment days. To take photographs, embryos were

submerged in “channel gels” made by leaving agarose to set on 1.2 mm diameter glass tubes (Mourabit *et al*., 2011). All photographs were taken using an Olympus SZX2-ILLK microscope.

3.3.2 Dechorionation

Dechorionation was conducted with some modification according to a method previously used in medaka (Porazinski *et al*., 2010). To prepare hatching enzyme extract (HE extracts) 20 to 30 *A. dispar* embryos at the hatching stages (St.31-32) were homogenized and placed overnight at 4°C with an equal volume of ASW 35 ppt in Eppendorf tubes. The supernatant was collected after centrifugation at 14k rpm for 10 min. The HE extracts were stored at -20°C and were diluted two-fold with ASW for the dechorionation protocol. For dechorionation, eggs were cleaned and transferred to sandpaper then gently rolled (approximately 45-60 s) to make the surface of the chorion slightly softer and scarred. Embryos were then incubated for 1 h with pronase (20 mg/ml) at 28°C. After that, embryos were washed in ASW to remove traces of pronase. HE was added for 2-6 h. Embryos were periodically checked using a stereomicroscope (Prozinski *et al*., 2010). After dechorionation, embryos were transferred gently to another dish of fresh ASW 35 ppt.

3.3.3 PTU

In order to block melanin synthesis, *A. dispar* embryos were treated with 0.005% [w/v] PTU (Sigma) from stage 14 of development (18.5 hpf) as per the method described by (Mourabit *et al.,* 2011) with some modification such as using ASW 35 ppt to prepare the PTU and the treatment started earlier than in medaka. Water was changed, and embryos were checked once daily. The control embryos were incubated with ASW (35 ppt).

3.3.4 *In situ* probe synthesis

The first step used PCR to generate the medaka *gch* DNA template. The following were assembled in a PCR tube: 1 µl of (100 pmol/u) Forward

primer (ATTTAGGTGACACTATAG), 1 µL of (100 pmol/ul) Reverse primer (ATTACCCCTCACTAAAGGG), Go Tag PCR master mix (Promega) (10 µl), 1 µl of Template (cDNA) (plasmid x1/100ul), Molecular water DEPC (4 µL). The standard conditions of PCR were employed as below:
95°C for 5 min with replication of denaturation at 95˚C for 30 s, annealing at 50°C for 1 min, elongation at 72˚C for 1 min for 30 cycles and a final extension at 72°C for 10 min. Thermo Scientific Gene JET PCR Purification Kits were used to purify the DNA. The purified DNA was used to synthesize RNA probes by using 6 µl of template DNA (1 to 2 µg), 1 µl of RNase inhibitor (Roche), 2 µl of DIG RNA labelling kit (Roche) and 4 µl of 5x transcription buffer 6 µl water and 1 µl of (T3 and SP6 20 U/µl) polymerase and incubated at 37°C for 5 h. Before purifying the probe by lithium chloride precipitation, 2 µl DNase was added and then incubated at 37°C for 30 min. An equal amount of hybridization buffer was added and stored at -20°C between final uses at 1/100 dilution.

3.3.5 *In situ* hybridization

In brief, *A. dispar* embryos at stages 19, 22, 24, 25 were chosen and were fixed overnight in 4% formaldehyde at 4°C. Embryos were washed with (PBS) for 10 min before they were manually dechorionated and stored at -20˚C in 100% methanol. Fixed embryos were rehydrated using a gradual series of methanol including; 75%, 50%, and 25% and then washed with PBST (phosphate buffered saline, pH 7.0, containing 0.1% Tween 20) at a room temperature (RT). To stop non-specific binding, the embryos were incubated in 500 µl hybridization buffer at 65°C for 3 h before incubating with the probe overnight at 65°C. The next step was carried out by washing the embryos with 1 ml of 2X SSC, 50% formamide, 0.1% Tween 20, and 2X SSC, 0.1%Tween 20 at 65°C for 30 min, ending with final washes with 0.2X SSC, 0.1%Tween 20 at 65°C for 2x 30 minutes. Before placing embryos in anti-DIG antibody for 3 h, blocking solution was added to reduce non-specific binding for 3 h. After placing in anti-DIG antibody, embryos were washed four times for 30 min in PBT and gently placed on a shaker overnight. The next wash was performed with AP buffer. To stain embryos, AP buffer was replaced with BM-Purple (Sigma) and the embryos/ BM-

Purple were gently moved to a 24-well plate. The 24-well plate was placed in a foil covered box to prevent light access and put on a shaker for 1-3 h to enable BM-Purple to penetrate through the tissues of embryos and to show visible staining. The final step before imaging was conducted using PBTW to wash embryos for 10 min and then draining them before fixing in fresh PFA. Images of stained killifish embryos were acquired using a compound microscope (Nikon SMZ1500) equipped with a digital camera.

3.3.6 Imaging

For imaging purpose, *A. dispar* embryos were supported using the agarose bed technique previously used with mangrove killifish (Mourabit *et al*., 2011). As mentioned above, all images of staging were obtained using a digital Olympus camera interfaced with an Olympus SZX2-ILLK microscope. Other images were captured using a Nikon SMZ1500 microscope or Zeiss microscope with normal incident light and suitable GFP and RFP excitation and emission filters. GFP and RFP filters were used to image fluorescent pigments with different emission spectra - with some green, some red, or some green and red. When assessing the response of cells to light exposure, normal light, GFP and RFP illumination conditions were used, and photographs were taken immediately because of the rapid response of the pigment cells. Then the embryos were incubated in white light for 1 h and photographed again before observing the response of the pigment cells to the light again. Fish embryos were monitored daily over the experimental period. All observations were replicated three times.

3.3.7 Statistical analysis

All treatments were undertaken in triplicate. All the data for the effect of temperature and salinity on embryo size was obtained using ImageJ software. Hence, all the data was transferred to an Excel file. All statistical analyses were conducted in Minitab to examine whether environmental stressors had an effect on embryonic development and hatching time.

3.4 Results

3.4.1 Normal embryonic development in A. killifish (A. dispar)

Staging studies, following fertilized eggs to the late stages of organogenesis, are crucial to understanding development in fish. The following photographs describe and provide accurate morphological descriptions that characterize 32-stages of normal embryonic development in *A. dispar*.

Stage 1 (Fig. 3.1A): Zygote period and one–cell stage (Fig.1)

Following fertilization of the eggs, a hard chorion of rough texture is generated separately from the yolk by a thin blast disc which swells and lifts away from the newly fertilized eggs. The transparent yolk contains many of small oil droplets.

Stage 2 (Fig. 3.1B): Two-cell stage

The first cleavage produces two highly rounded blastomeres of equal size.

Stage 3 (Fig. 3.1C): Four-cell stage

The two-cell blastomere cleavage occurs at a right angle to the first cleavage. It produces four rounded blastomeres of the same size.

Stage 4 (Fig. 3.1D): Eight-cell stage

In this stage cleavages occur in two separate planes; they are parallel to the first one to cut the blastodisc into a 2x4 array of blastomeres forming eight blastomeres.

Stage 5 (Fig. 3.1 E): Sixteen cells stage

The fourth cleavage occurs along two planes to produce a 4x4 array of cells. All of the cells are arranged in two tiers on top of the yolk.

Stage 6 (Fig. 3.1F): 32-cell stage

The 32 blastomeres are present in arrays with more presence in the upper tier. It becomes difficult to distinguish between cells to enumerate them.

Stage 7 (Fig. 3.1G): 64-cell stage

In this stage, the sixth cleavage plane, the blastomeres are dividing and increasing in size producing a mass with less rounded edges.

Stage 8 (Fig. 3.1H): Mid blastula

During the blastula period, and the sixth and later cleavages, cells are difficult to trace with precision. The blastomeres are flattened in shape.

Stage 9 (Fig. 3.1I): End of blastula

The cells of the blastoderm are smaller than in the mid blastula stage and the blastodisc is clearly flattened. The marginal yolk syncytial layer (YSL) becomes clearly visible.

Stage 10 (Fig. 3.1J): Pre-early gastrulation

During gastrulation, the blastoderm begins to flatten and expand over the yolk by epiboly. The thin sheet of cells curves over the yolk and the thickening embryonic shield appears on one side to form the dorsal lip.

Stage 11(Fig. 3.1K): Early gastrula

The blastoderm expands and covers about (1/3 of the yolk sphere). The embryonic shield begins to arise as a thicker end of the dorsal blastoderm.

Stage 12 (Fig. 3.1L): Mid gastrula

Epiboly progressively advances and covers half of the yolk sphere and the embryonic shield projects into the area of the germ ring.

Stage 13 (Fig. 3.1M): Late gastrula

The embryonic shield grows and the blastoderm covers about two-thirds of the yolk sphere.

Stage 14 (Fig. 3.1N): Late gastrula

The blastoderm covers around three-quarters of the yolk sphere and the embryonic shield becomes more longitudinal and clearly defined as a narrow streak.

Stage 15 (Fig. 3.1O): 100% epiboly

Gastrulation ends because the blastoderm covers the entire yolk. In this stage, there is a long bulge on the surface of the egg due to the presence of the embryo.

Stage 16 (Fig. 3.1P): Head and tail regions recognizable

The embryonic body increases in size longitudinally and laterally so that it becomes more distinct.

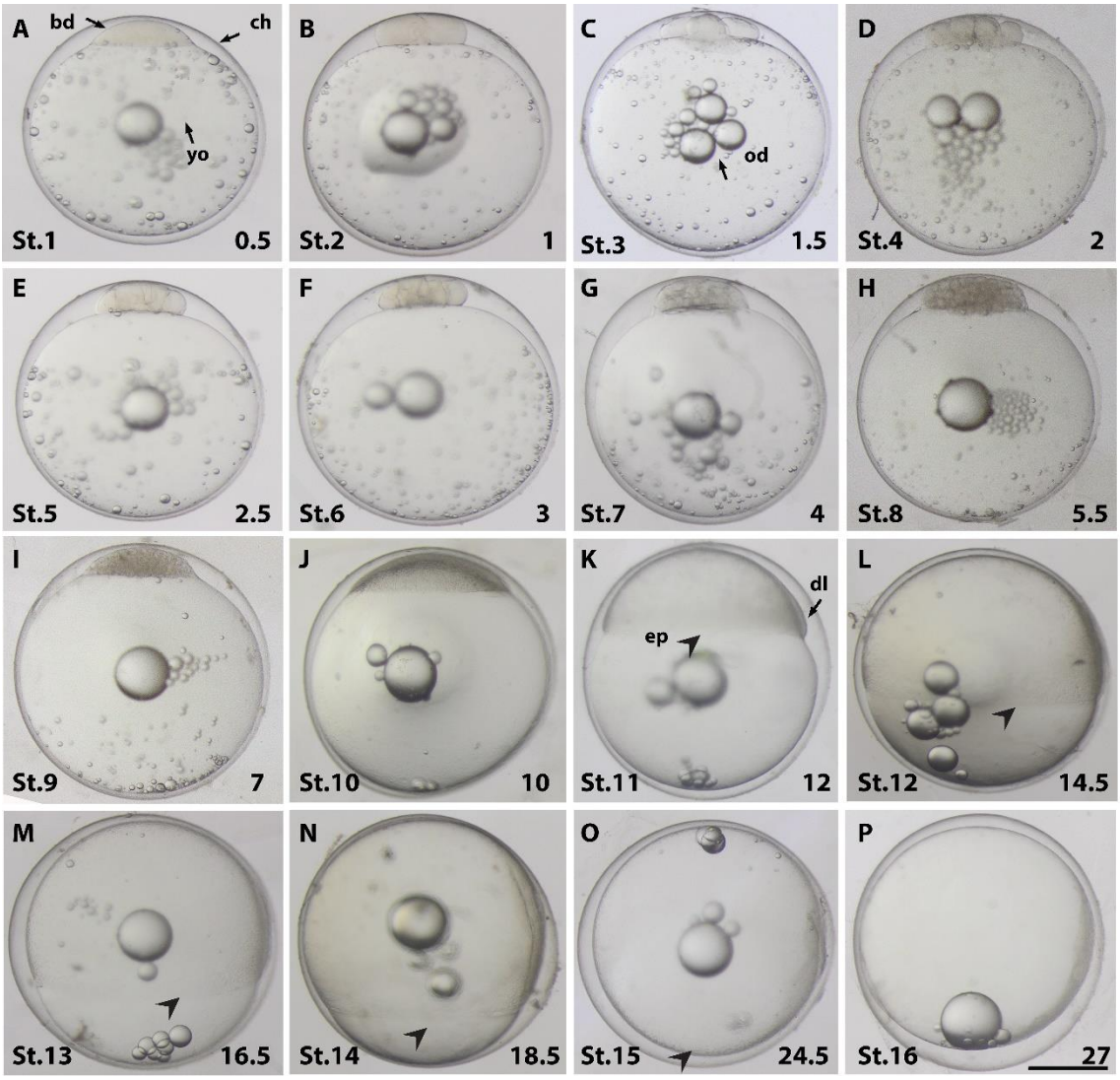

Figure 3.1: **Normal embryonic development in *A. dispar*.** The early (G-I). Gastrula views are shown in (I-P). Stage time (hpf) is shown at the bottom right of each picture. Stage numbers are indicated at the bottom left. bd, blastodisc; ch, chorion; yo, yolk; od, oil droplet; dl, dorsal lip; ep, epiboly and the arrowhead indicated the percentage of epiboly development at 25%, 50%, 75%, 90% and 100% in (K, L, M, N, O) respectively. Scale bar = 500 µm.

Stage 17 (Fig. 3.2A, A'): Optic vesicle and somite recognizable (Fig.2)

At this stage, the optic vesicle can clearly be observed with the forebrain. The four somites can also be distinguished using a 20x Zeiss microscope. In addition, the pigment cells start to form.

Stage18 (Fig. 3.2B, B'): 6 somite stage, pigmentation and brain regionalization

Three regions of the brain are recognizable and pigment cells (leucophores) begin to develop at this stage.

Stage 19 (Fig. 3.2C, C'): Lens formation

The boundaries for the mid and hind brains start to form and the furrow is noticeable in the mid-hindbrain. The lens and retina are distinguishable in the eye.

Stage 20 (Fig. 3.2D, D'): Otic vesicle formation

A pair of otic vesicles form at the posterior part of the head and increases in the number of pigment cells in the embryonic body and in the yolk, occur. The boundaries between mid-brain and hind-brain are very clear.

Stage 21 (Fig. 3.2E, E'): Heart formation

The tubular heart is visible underneath the head but is not beating. The midbrain and hindbrain ventricles expand, and the tail region becomes distinct from the yolk.

Stage 22 (Fig. 3.2F, F'): Heartbeat starts

The blood vessels are formed in the yolk, but no circulation is apparent, although the heart is starting to beat at this stage. Pigment cells are increased in the embryonic body and the yolk and notochord are visible.

Stage 23 (Fig. 3.2G, G'): Circulation and 12 somites

Blood circulation starts within one (vitelline vessel) around the yolk. The three sections of the brain are increased in size and become clearer with 12 somites visible.

Stage 24 (Fig. 3.2H, H'): Increase in circulation

The embryonic body enlarges; otoliths appear within the otic vesicle. The blood vessels are increased in size and circulation is visible in two blood vessels within the embryonic body.

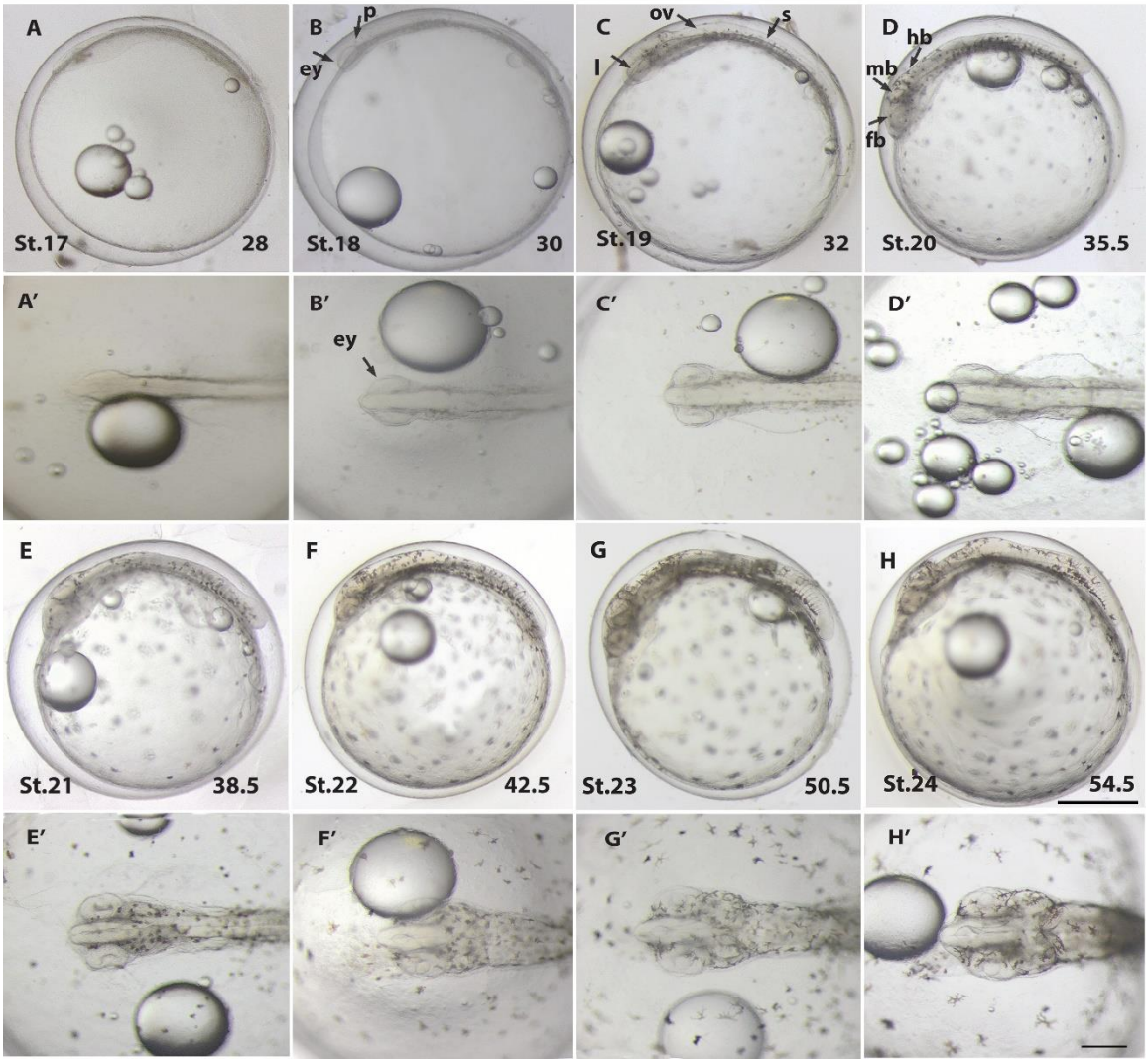

Figure 3.2 Developmental stages in *Aphanius dispar* showing stages from somitogenesis to organogenesis. A-H: Lateral views of developed embryos. A'-H': views of the head. Stage time (hpf) is shown at bottom right of each picture. Stage numbers are indicated at the bottom left. ey, eye; p, pigmentation; l, lens; ov, otic vesicle; s, somite; fb, forebrain; mb, midbrain; hb, hindbrain. Scale bar = 500 µm (A-H), 200 µm (A'-H').

Stage 25 (Fig. 3.3A, A'): Body movement (Fig.3)

The anlage of the liver appears. The tip of the tail is completely free and mobility of the body increases. Pigment cells increase and melanophores appear. The pectoral fin starts to form.

Stage 26 (Fig. 3.3B, B'): Increased pigmentation

Blood circulation increases, and body movement is apparent, especially in the tail. Pigmentation greatly increases in the brown pigment cells, which develop a dendritic shape.

Stage 27 (Fig. 3.3C, C'): Enlarged embryonic body

The body and head increase in size. The heart is clearly observed and there is increased blood circulation in the body. The eyes begin to enlarge, and the retina of the eyes begins to become dark due to melanization.

Stage 28 (Fig. 3.3D, D'): Caudal fin formation

Blood cells clearly are observed in the embryonic body and the yolk through the large vessels. The eyes become dark and the caudal fin forms, but the rays are difficult to recognize. The air bladder starts to form.

Stage 29 (Fig. 3.3E, E'): Anal fin forms

The blood circulates in the caudal and dorsal fins. The air bladder becomes clearer and pigment cells appear in the caudal fin.

Stage 30 (Fig. 3.3F, F'): Pigmentation in the head

The eyes start to move and the pigmentation in it and in the brain regions (especially the midbrain) increases. The dorsal fin lacks movement at this stage.

Stage 31 (Fig. 3.3G, G'): Gut tube and jaws visible

Jaws forms but with no movement. Enlargement of eyes occurs with perfect movement and the caudal fin reaches to the head. There is an increase in the network of pigmentation on the yolk and differences in the shape of these cells compared with early and mid-stages of development become noticeable. Increases occurred in the mobility of the fins and the whole of the body.

Stage32 (Fig. 3.3H, H'): Hatching stage

The whole body is developed, and the swim bladder expands remarkably. Fins rays are observed clearly along with the typical patterns of pigmentation. The mouth moves easily, allowing the fish to tear the chorion and escape by the body and tail movements.

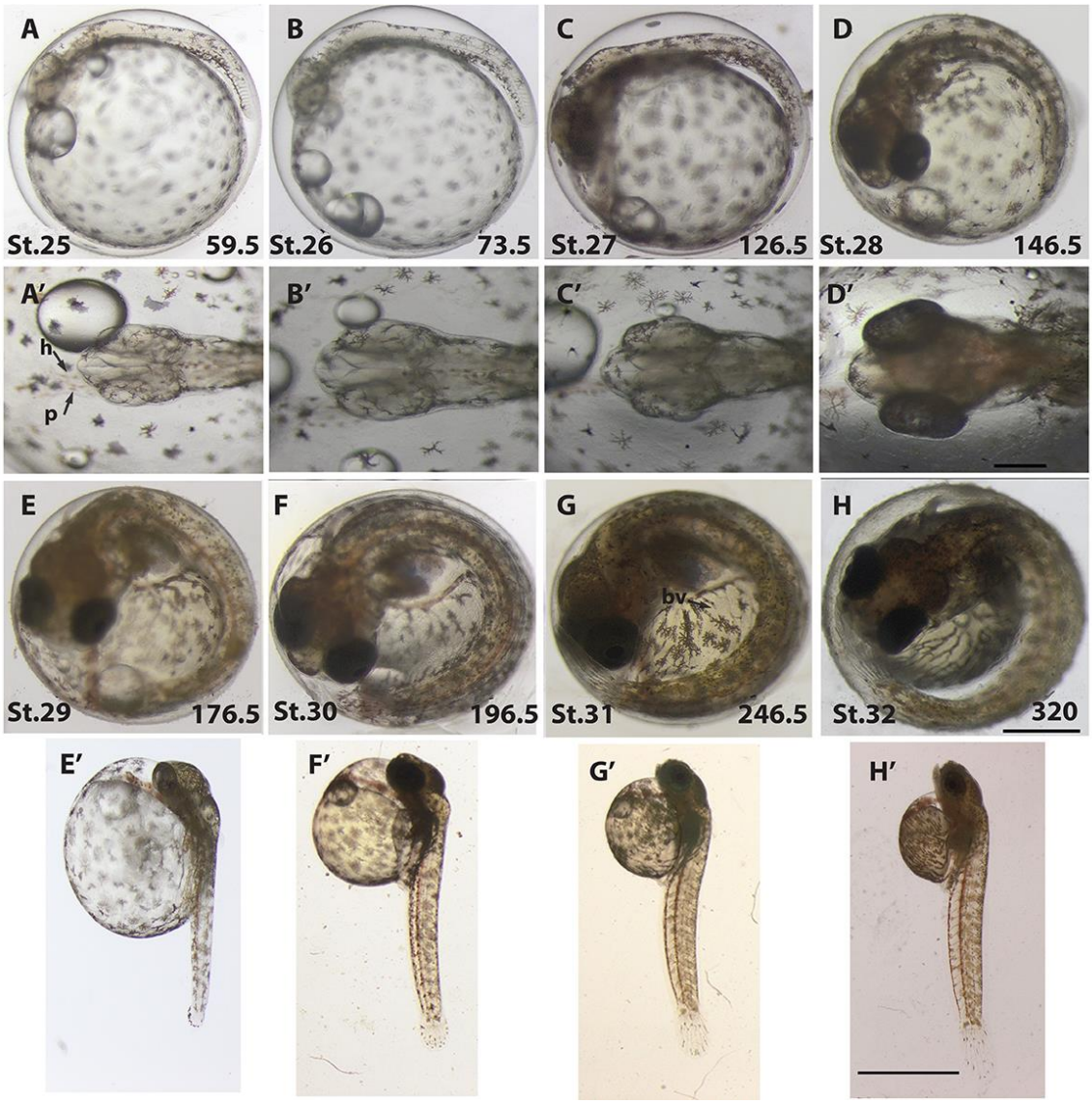

Figure 3.3 Development stages from organogenesis to hatching. A-H: Lateral views of developed embryos at late stages. A'-D': views of the head and E'-H' are dechorionated embryos. Stage time (hpf) is shown at bottom right of each picture. Stage numbers are indicated the bottom left. h, heart; p, pigmentation; bv, blood vesicle. Scale bar = 500 µm (A-H), 2 mm (E'-H').

3.4.2 Influence of water temperature on embryonic development

To examine how *A. dispar* adapted to extreme environments, normal embryonic development was examined under different temperature conditions. Staging curves of embryonic development were examined to the hatching time. *A. dispar* fertilized eggs were incubated at 26.0°C, 30.0°C, 34.0°C, 37.0°C and 38.5°C. The results showed that embryos incubated at higher temperatures had shorter development times, hatching at an average of 168 hpf at 37.0°C compared to 320 hpf at 26.0°C, (Fig. 3.4). As shown in figure 6, the effect of incubation at 30.0°C, 34.0°C resulted in hatching at intermediate times of 208 hpf and 188 hpf respectively.

Our observations also indicated that there was no malformation among the embryos at any of the temperatures that were tested. However, there was a correlation between increasing temperature and an increase in the intensity and the size of pigment cells.

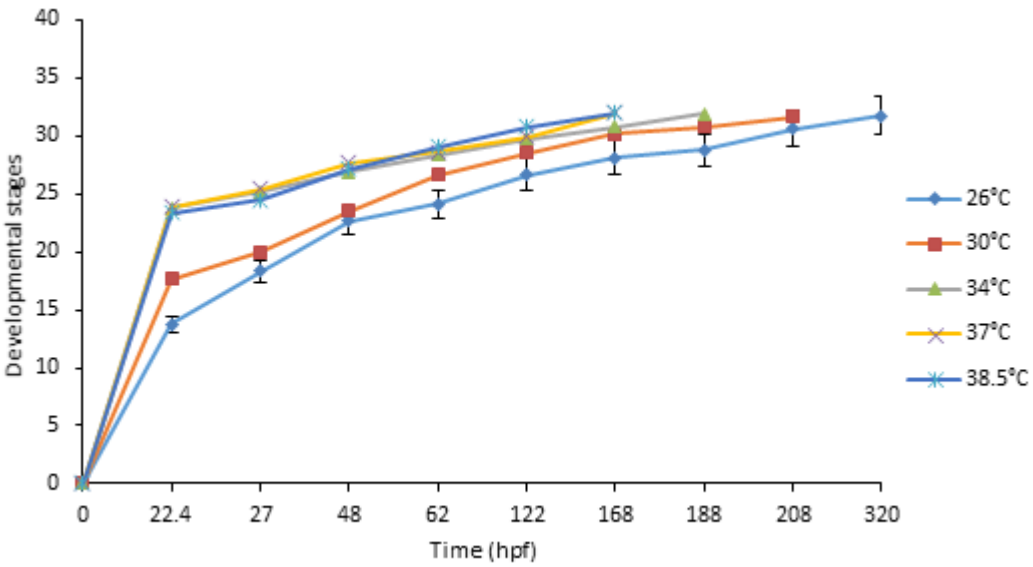

Figure 3.4 Influence of water temperature on the growth of *A. dispar* embryos. Embryonic development was investigated at a range of temperatures (26.0°C, 30.0°C, 37.0°C, 38.5°C). Normal embryonic developmental time monitored from fertilisation. Each point is the mean of three biological replicates ± SE. P-values between 0.05 and 0.001 were considered significant.

3.4.3 Influence of water salinity on the embryonic development

Development and survival were monitored under different water salinity conditions: freshwater, brackish water and artificial seawater (0.3, 3, 10, 14, 35,150 ppt). Embryonic developmental stages were expressed as the length of the period of time from egg fertilization to hatching. When observing the effects of incubation salinity on the hatching rate of *A. dispar* embryos, results showed that there was an inverse relationship between salt concentration and hatching time. In general, fish embryos hatched successfully at all salinities tested (0.3, 3, 10, 14, 35, 150 ppt). However, the effects of salt concentration were more marked at the highest salinity of 150 ppt which resulted in a reduction in the time to hatching (280 hpf at 150 ppt, compared with a normal hatching time (320 hpf) that occurred within salinity of 35 ppt at 26.0°C. On the other hand, when observing the impact of salt concentration of 0.3, 3, 10, 14 ppt, the results reveal that the development rate was slower than at concentrations of 35 and 150 ppt. Generally, a significant reduction in the time of hatching was observed when comparing 35 and 150 ppt to 0.3, 3, 10, and 14 ppt ($p<0.001$) (Fig. 3.5).

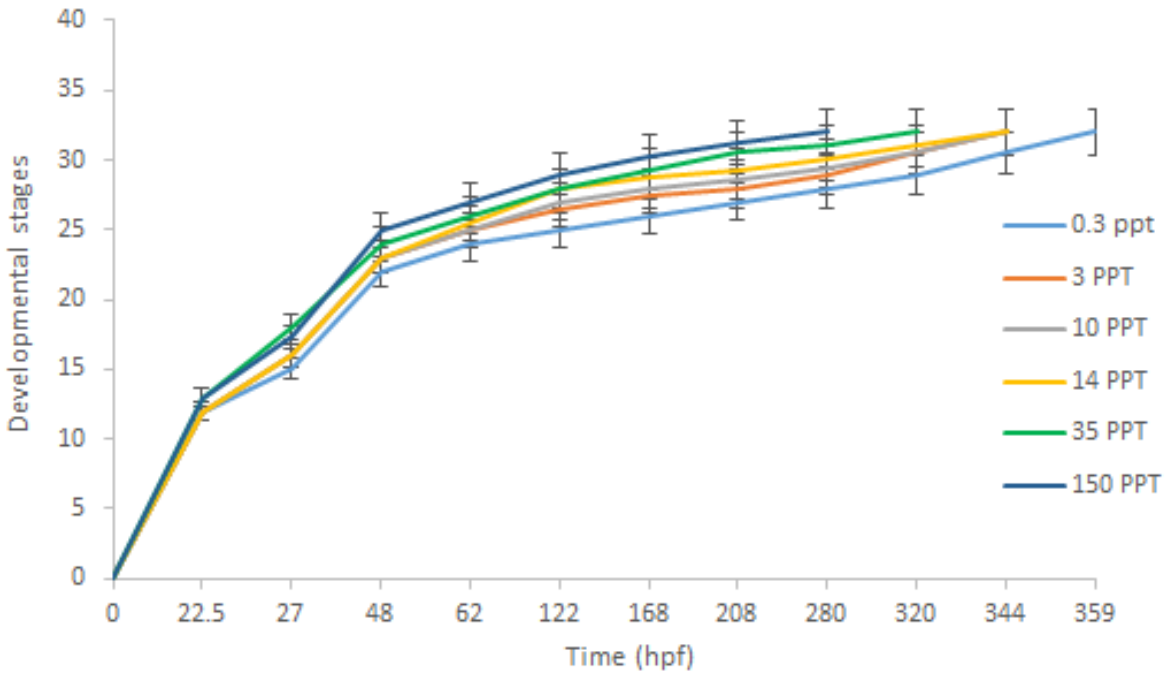

Figure 3.5 Influence of water salinity on the growth of *A. dispar* embryos. Embryonic development was investigated at a different range of salinities (0.3 ppt, 3 ppt, 10 ppt, 14 ppt, 35 ppt, 150 ppt). Normal embryonic development was monitored from fertilisation until hatching time with checking the malformations. Each point is the mean of three biological replicates ± SE. P-values between 0.05 and 0.001 were considered significant.

On the other hand, when observing the effects of changes in salt concentrations including 0.3, 35, 150 ppt on embryonic size, the results were as follows: The optimal length was particularly pronounced within salt concentrations of 35 ppt whereas a one-way ANOVA showed that there was a statistical difference when comparing the influence of salinity of 35, 150 ppt and fresh water on the length of *A. dispar* embryo ($p<0.002$) (Fig. 3.6). Specifically, at the highest and lowest salinities, embryonic body length was shorter. Overall, despite the retardation of developmental growth monitored in freshwater, the result indicated that *A. dispar* can grow and survive in freshwater and higher extremes of salinity.

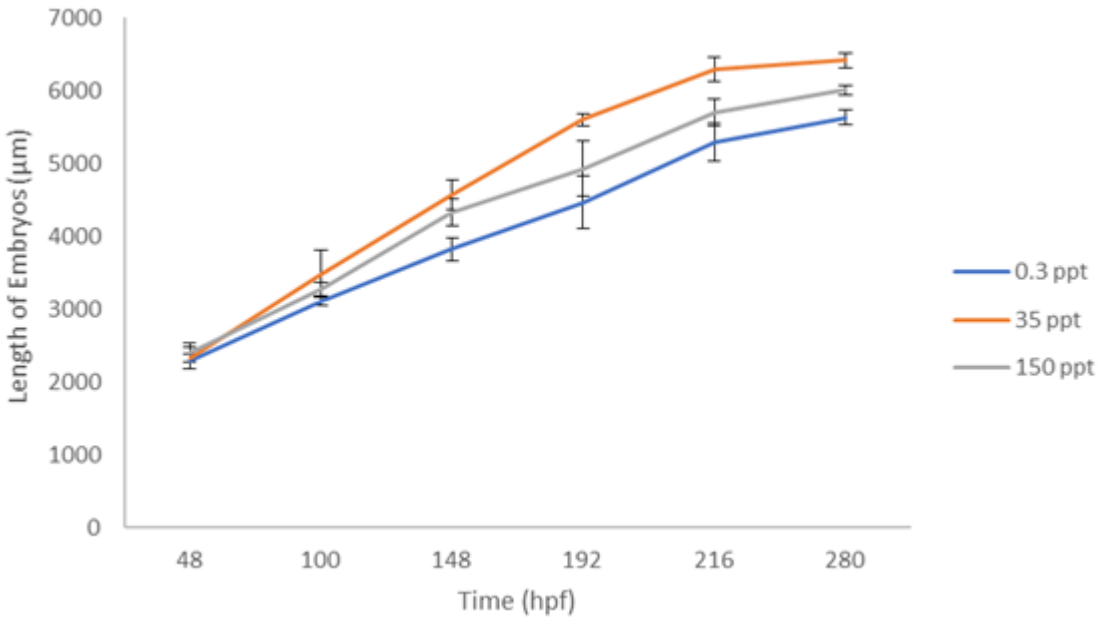

Figure 3.6 Influence of water salinity on the length of *A. dispar* embryos. Embryonic length was measured during the development at 0.3 ppt, 35 ppt, and 150 ppt. Sequence steps of imageJ analysis method was applied to measure the length of embryos at concentrations above. Each point is the mean of three biological replicates ± SE. P-values between 0.05 and 0.001 were considered significant.

3.4.4 The brown pigment in *A. dispar* is highly fluorescent

In this study, it was noted that *A. dispar* has unusual, highly fluorescent pigment cells. Therefore, the appearance, morphology, and development of these cells was characterised. As seen in figure 3.7, the first appearance of the fluorescent pigment cells was detectable in the trunk. Additionally, the pigment size and morphology changed during embryonic development (Fig. 3.7).

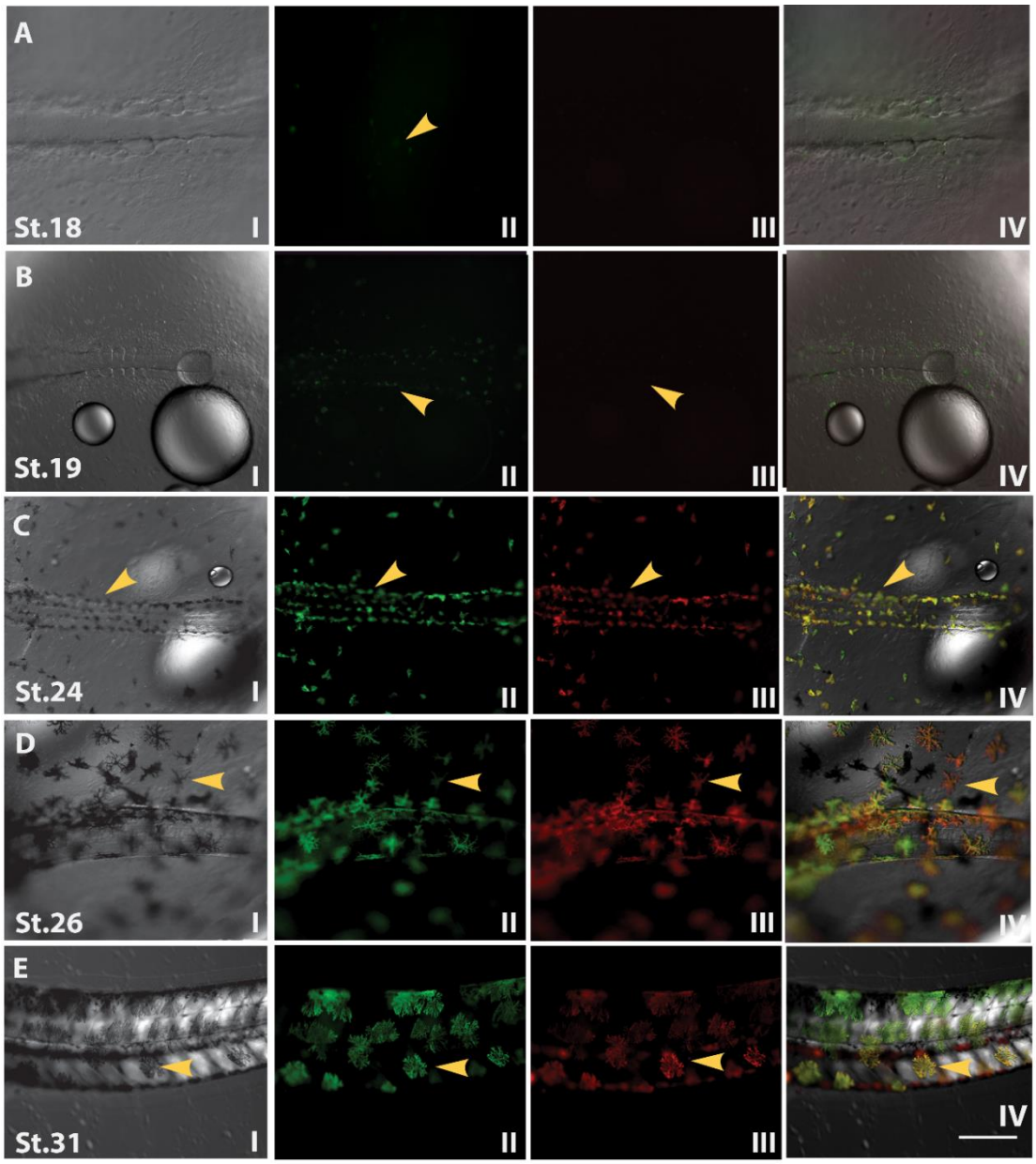

Figure 3.7 Development of fluorescent pigment cells in the trunk. The pigment cell size and morphology changed during embryonic development. First appearance of pigment cells was in the trunk at St.18 and then distributed in the whole of the body and yolk at the following stages. (A-E) Stage numbers are indicated the bottom left. DIC images are shown in (I); GFP filter (II); RFP filter (III); Merge (IV). Arrowheads indicated the developing fluorescent pigment cells. Scale bar (A-B) = 100 µm, (C-E) = 200 µm.

As shown in figure 3.8, which represents views of the head region, the number of pigment cells increases gradually and spread widely over the dorsolateral surface of the embryo head and trunk. In addition, it was observed that pigment cells, especially those with features similar to leucophores, increased markedly in the hindbrain, midbrain and areas surrounding the eyes (Fig.3.8).

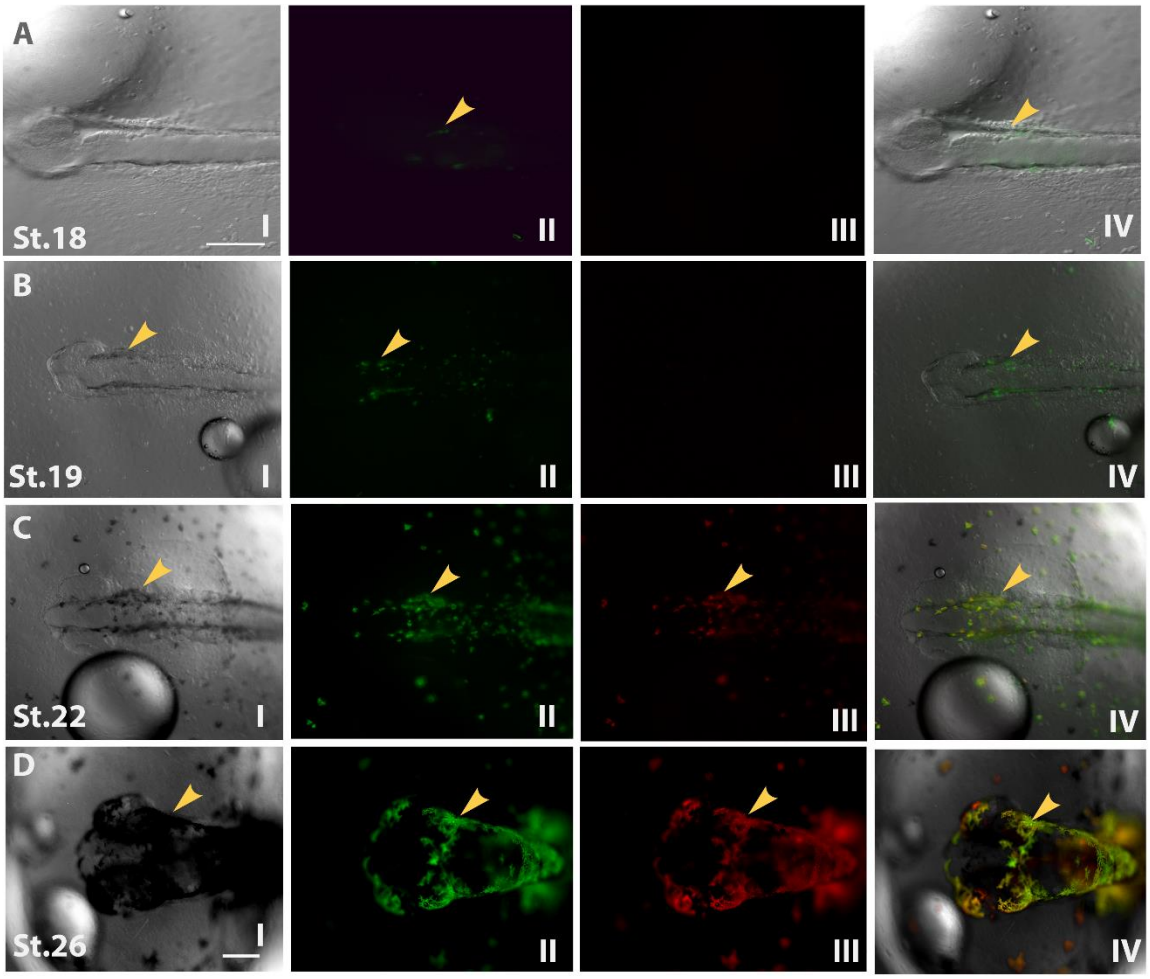

Figure 3.8 Development of fluorescent pigment cells in the head. (A-D) Stage numbers are indicated the bottom left. DIC images are shown in (I); GFP filter (II); RFP filter (III); Merge (IV). The pigment size and morphology change during the embryonic development. Arrowheads indicate the fluorescent pigment cells. Scale bar = 100 µm.

The development of the fluorescent pigment cells in the yolk was also observed and the present observations reveal that leucophore-like pigment cells in *A. dispar* are more branched (dendritic shape) than leucophores in medaka; moreover, the development of the pigment cells occurs much earlier (Fig.3.10 A, Fig. 3.10 B). On the other hand, the observations further support the idea that the brown pigment has different characteristic to melanophores and shows consistent attributes more related to leucophores. The changes in the colour of the brown pigment cells following the exposure to light are shown in figure 3.10.

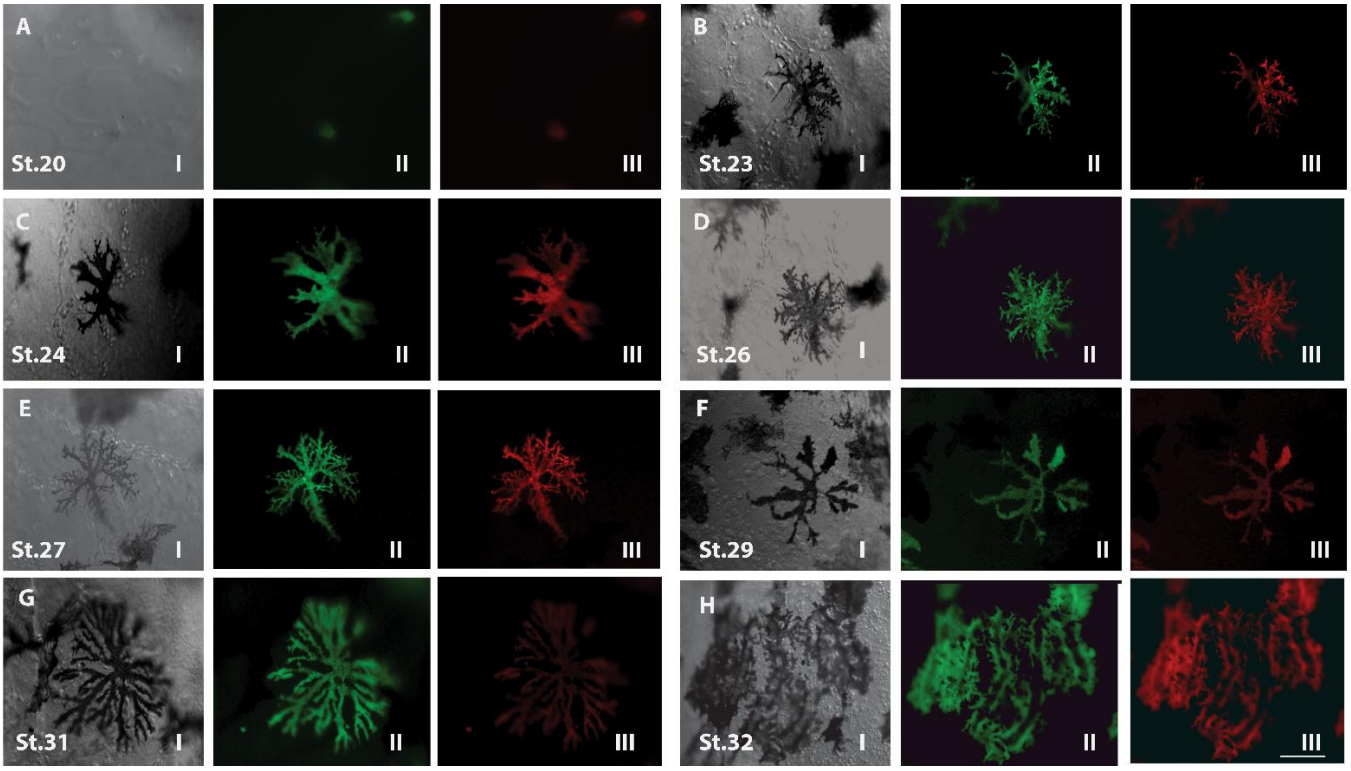

Figure 3.9 Development of fluorescent pigment cells in the yolk. The pigmented cell size and morphology change during embryonic development. (A-H) Stage numbers are indicated at the bottom left. Images shown are (I) DIC; (II) GFP filter; (III) RFP filter. Scale bar (A-H) = 100 µm.

Indeed, it was observed that dramatic changes in the colour of brown pigment cells occurred when the brown pigment cells were exposed to visual light (from above) with the brown pigment cells becoming white. This

pattern is similar to medaka leucophores and iridophore. In addition, the present findings indicate that these pigment cells are highly fluorescent under either GFP or RFP filters. Figure 3.10 A-III and -IV and Fig. 3.10 C reveal the presence of the pigment cells in the heart of *A. dispar* embryos.

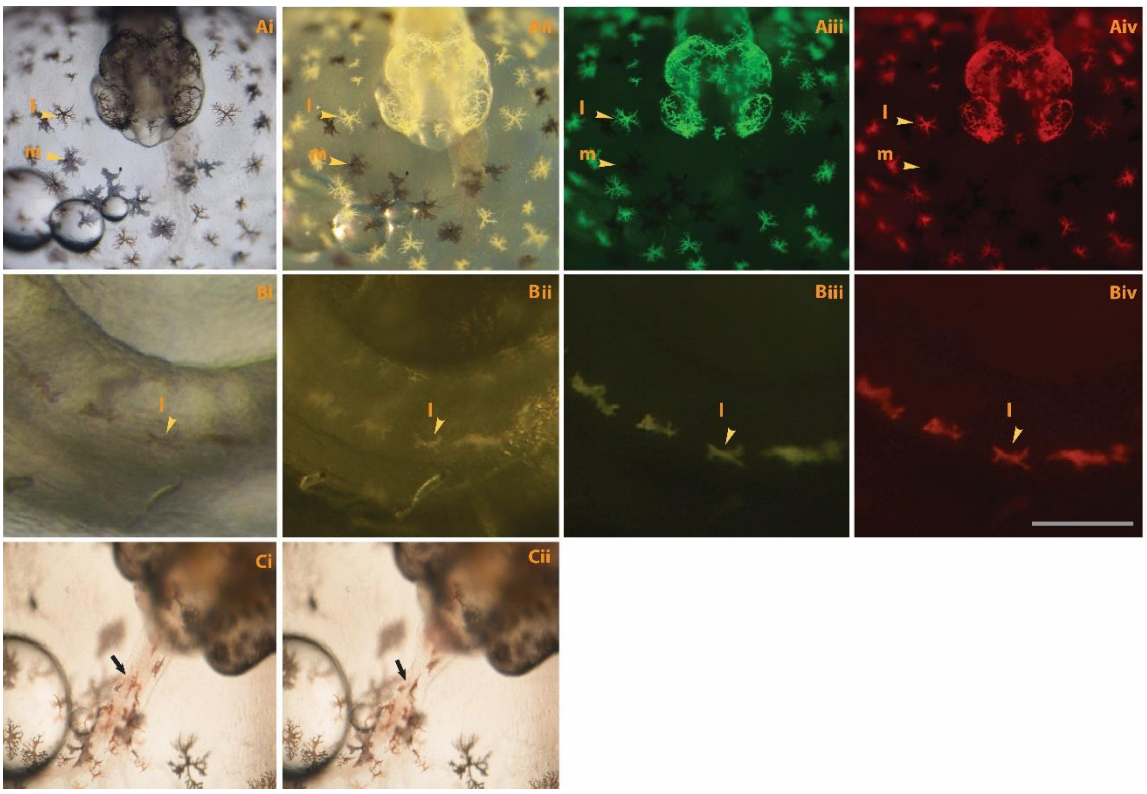

Figure 3.10 Characterisation of fluorescent pigment cells with different filter combinations. (A-i) normal light DIC (brown and black cells). (A-ii) light above (white and black cells). (A-iii) Fluorescent light with GFP filter (green and black cells). (A-iv) RFP filter (red and black cells). Arrowheads indicate (l) leucophores, (m) melanophores. B) Imaging of leucophore in medaka as above. (Ci-ii) normal light DIC, Imaging of the ventral heart through the yolk. The surface of the heart contains leucophores which show vigorous movement with a heartbeat.

A follow-up examination, treating the embryos with PTU, was undertaken to characterize the *A. dispar* pigment cells (black and brown) and examine the effects on pigmentation patterns. The results showed that the PTU inhibited melanogenesis in *A. dispar* black pigment cells whereas the brown pigment

cells were not affected by the drug - suggesting that the brown pigment cells do not contain melanin (Fig. 3.11 A, B). The effect of K+ on the melanophores and leucophores of *A. dispar*, was evaluated using fish embryos that were incubated in 150 mM NaCl and then shifted suddenly to the tested salinity (150 mM KCl). The response of pigment cells was observed after 30 minutes of incubation in the saline concentration. The result showed that 150 mM KCl, caused a marked decrease in melanophores size whereas our observation showed that there was no significant effect on leucophore cell size with KCl. (Fig. 3.11 C).

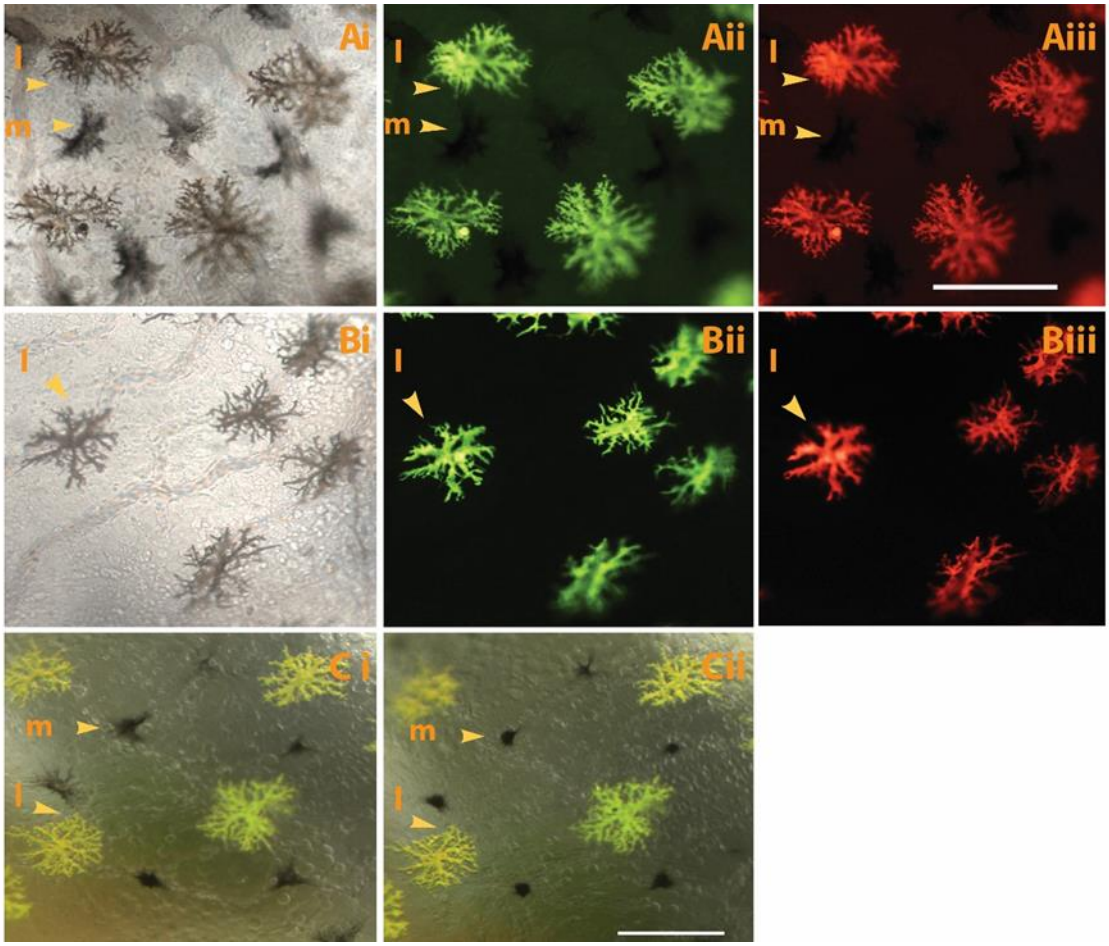

Figure 3.11 Leucophores do not contain melanin. *A. dispar* eggs were treated with PTU (1-phenyl-2-thiourea) at various somitogenesis stage to suppress melanin synthesis. (i) DIC; (ii) GFP filter; (iii) RFP filter. (A) The control embryos show melanophores with black melanin pigment. (B) The PTU-treated embryos show loss of melanin positive cells, whereas the fluorescent cells are still present and show brown pigmentation. Aggregated melanophores after treatment with 150 mM (Ci) NaCl and (Cii) KCl solution at 30 min respectively. Arrowheads indicate (l) leucophore, (m) melanophore. Scale bar = 200 µm.

The amount of fluorescent pigment in *A. dispar* and medaka was examined after different exposure camera times to light (see in figure 3.12). The data demonstrated that the fluorescent pigment cells in *A. dispar* are much brighter than leucophores in medaka (Fig. 3.12 C). In addition, leucophore in *A. dispar* are more branched (dendritic shape) than leucophores in medaka and the development of the pigment occurs much earlier (Fig. 3.12 A, B).

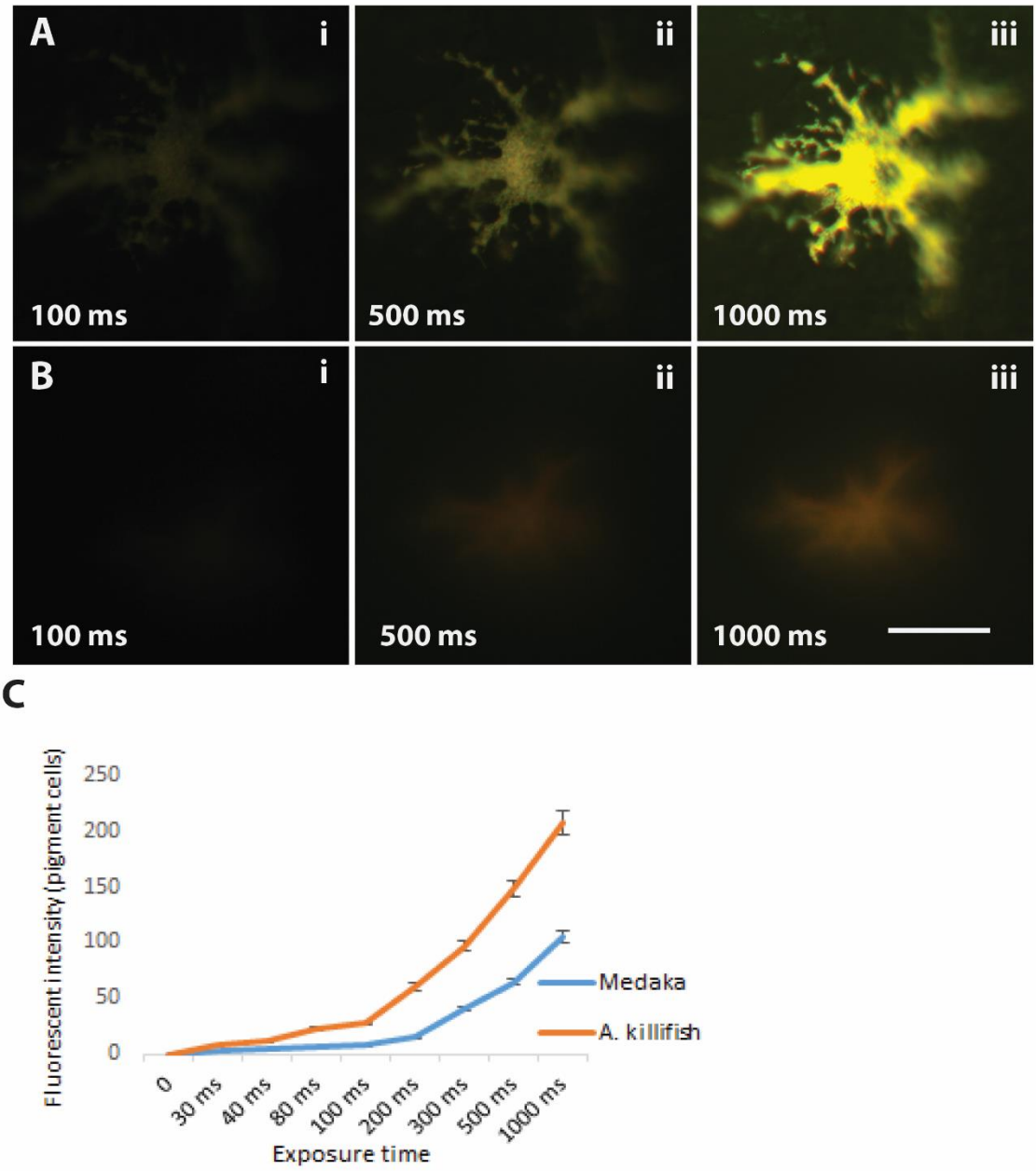

Figure 3.12 Leucophores in *A. dispar* are brighter than in medaka. The fluorescent pigmentation with *A. dispar* (A) and medaka (B) were examined at a range of exposure times (20 ms - 1000 ms); (C) fluorescent intensity of leucophore was measured using imageJ analysis method and each time of exposure was plotted. Each point is the mean of three biological replicates ± SE. are statistically significantly different ($p<0.0001$). Scale bar 100 µm.

To further examine the nature of the pigment cells in *A. dispar*, a molecular characterisation of the expression of a gch marker for medaka leucophores was performed using whole-amount *in situ* hybridization (WISH). As shown in (Fig. 3.13), the gch marker cross-hybridized with *A. dispar* fluorescent pigment cells and could be detected as purple dots on the dorsal trunk of stage 17 embryos. Between stages 19 and 22, gch expressing cells were scattered and increased noticeably in the head and trunk. Other populations of gch expressing cells were detected clearly on the lateral lines, on the dorsal trunk and the yolk at stage 24. At stage 25 the number of purple dots had increased in the head especially in the midbrain and surrounding eyes. These observations provide genetic evidence to support the idea that the fluorescent pigment cells in *A. dispar* are highly related to leucophores.

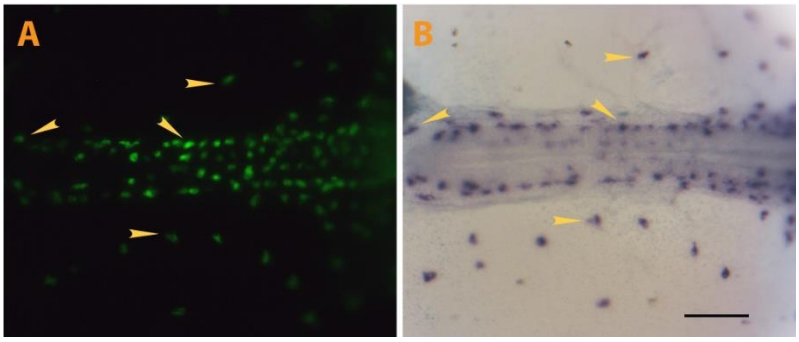

Figure 3.13 Fluorescent pigment cells express gch. A) Embryonic leucophores in *A*. *dispar* at stage 24 was stained with *gch* (purple) using (WISH). The purple dots show *gch* expression in the trunk and head region of *A*. *dispar* hybridised embryos corresponding to *A*. *dispar* leucophores. At this stage the population of *gch* expressing cells were scattered increasingly over the trunk surface and head. B) Pigment cell expressing *gch* in the trunk and yolk surface of the somitogenesis stage 24 embryo. (A) GFP filter; (B) DIC filter. Scale bar = 100 µm. The yellow arrows show that the dotted *gch* signals in the dorsal head and trunk surface coincide with the position of the fluorescent leucophores.

3.5 Discussion

In this chapter, the embryonic development processes in *A. dispar* were examined under “normal’ environmental conditions and at a range of physiologically extreme conditions with respect to both salinity and temperature. The process of development could be divided into 32 stages based on diagnostic patterns of development and morphogenesis. We have clearly demonstrated that *A. dispar* is optically transparent making it a useful model to monitor normal and abnormal embryonic development. The embryonic development of the *A. dispar* is very similar to that seen in other killifish species such as medaka (Iwamatus, 2004) and the mangrove killifish (Mourabit et al., 2011). But unlike medaka, in the *A. dispar* embryo, the chorion does not have hairs. At the early stages of *A. dispar* development, many small oil droplets are also observed in the transparent yolk that become less apparent at the later stages. While in the mangrove killifish, large oil droplets are observed in the yolk and a considerable number of oil droplets are noticeable at the later stages of the fish embryo. Therefore, *A. dispar* is more suitable for imaging analyses with or without the chorion. In addition, *A. dispar* embryos develop intense blood vessel network at the mid-somitogenesis stage (stage 22) which is not seen in the medaka, therefore, it may be highly suitable for studying blood vessel development *per se*, or blood vessel remodelling following interactions with toxicological agents and pathogens.

The data presented reveals that the embryonic developmental time was affected by high-temperatures and that this could result in a reduction of 3-4 days in hatching time as a result of accelerated development rates. Our observations also showed that yolk sac absorption increases with high temperature and supporting earlier findings of Ogira *et al.,* (2014), who had assumed that there is a correlation between increasing temperature and consumption of the yolk sac as a result of increased growth rate in *Oreochromis Niloticus*

Victor *et al*., (2000) reported that *A. dispar* is widely distributed in the coastal areas of Middle East countries. *A. dispar* is therefore normally found in habitats which experience a variety of salinities from freshwater, brackish water, to sea water and even hyper salinine environments (e.g.

rivers from the Dead Sea). Since *A. dispar* usually live in such extreme environmental conditions it is it is considered as a true euryhaline species, Lotan, (1969).

According to our results, an intermediate salinity is most favourable for *A. dispar* growth because the best level of growth and survival was reported at ASW 35 ppt. Preliminary studies such as Toshiaki, (1971) and Reutter, (1986) mentioned that some species of teleost fish possess chemoreceptors that provide information on water condition. Subsequently, adaptation pathways are triggered involving the central nervous system (CNS) including water drinking behaviour, regulation of key hormones (insulin, glucagon and adrenalin) to control growth rate and to activate osmoregulatory events (Gilles *et al*., 2001). A previous study by Swanson, (1998) illustrated that about 50% of the larval yolk is used up within the embryogenesis period and most of it is converted into larval tissue. In addition, both embryonic, larval and yolk absorption are affected by salinity (May, 1975). In the case of *A. dispar*, the present observations showed that the volume of the yolk sac clearly decreased at late stages (St. 31-32) at high salinity levels (150 ppt) at 26.0°C thereby increasing larval size. On the other hand, in *A. dispar* at low salinities, embryo growth was slower than at higher salinity and has a large yolk, similar to the findings of Swanson in milkfish (1998). Salinity clearly influences metabolism and yolk utilization (Ellis *et al.*, 1998). On the other hand, metabolic activities are probably influenced by rates of oxygen consumption which are altered by osmoregulatory costs (Ellis *et al.*, 1998; Swanson, 1996). Naturally, *A. dispar* embryos develop at different rates depending on the temperatures and salinity exposure, therefore, hatching time would be influenced by different treatments. Equilibrium levels of salt and water should be maintained to provide the energy for normal development. In the case of high salinity (150 ppt), embryos developed faster and this might occur due to the decline in the amount of energy which is required by embryos to keep a homeostatic balance, which consequently increases the amount of energy available for embryonic development (Rosemore and Welsh, 2012).

In this study, we also discovered that *A. dispar* produces a variety of pigmented cells including a unique fluorescent cell type. The first

appearance of *A. dispar* leucophore cells is earlier than that described in a previous study by Kimura *et al.,* (2014). In addition, the dendritic morphology observed is similar to that of leucophores and xanthophores. The *A. dispar* fluorescent pigment cells were visible under the fluorescent microscope with both GFP and RFP filters and the light emitted turns the colour to white rather than iridescent, supporting their classification as novel leucophores. The cross-reaction of gch, a marker for medaka leucophores (Kimura *et al*., 2014), with these fluorescent pigment cells provides some additional genetic evidence that these cells are leucophores similar to medaka leucophores (Lynn *et al*., 2005). However, the first detection of leucophores in *A. dispar* occurred at stage 17 (28 hpf) whereas in medaka it was seen at stage 25 (50 hpf) (Lynn *et al.*, 2005). In addition, the present results showed that the fluorescence of *A. dispar* leucophore is higher than that in medaka. The development of both leucophores and melanophores is very early in *A. dispar* (at the beginning of somitogenesis) making it a useful model for further studying the development of pigment cells. Interestingly, it was observed that the heart tube surface contains the fluorescent leucophore and therefore the fluorescent cells move with the heartbeat. This would also be supportive evidence that key issues are possibly protected from strong sunlight during embryonic development. The early appearance and high fluorescence of Arabian killifish may occur as an adaptation to life in an environment of strong sunlight. Since both temperature and salinity appear to influence embryogenesis, the present findings can be used to help manage and coordinate hatching time and create healthy cohorts of fish as well as assisting in understanding the effects of environmental factors on natural populations of *A. dispar*.

As previously mentioned*, A. dispar* tolerates a wide range of salinities from freshwater to hyper salinity environments (Gholami *et al*., 2011). Therefore, it may be suitable for testing and comparing the effects of environmental changes and understanding of the adaptation of some aquatic species to extreme environmental conditions. This study examined the potential effect of K^+ ion on the shape and size of *A. dispar* pigment cells (*A. dispar* melanophores and leucophores). In medaka it was revealed that pigment aggregation in the melanophore and xanthophore can occurre as a result of

increase in extracellular K^+ concentration. In contrast, medaka leucophore showed expansion by K^+ ion (Iga, 1978). Thus, the present results suggest that the activity of K^+ ion in *signal* the melanophores aggregation is similar to that in medaka however the highly fluorescent leucophore in the *A. dispar* did not show expansion with K^+. This is another difference of this leucophore in *A. dispar* to leucophore known from other species. This may suggest complicated diversity of pigment cell development and evolution in different teleost fish species. In general, this kind of study allows us to understand the characteristics of *A. dispar* pigment cells that may play potential role in immune response.

In conclusion, we have characterized the distinct developmental stages of the *A. dispar* embryo. *A. dispar* can survive at different salinities and temperatures including human body temperature. The findings support the idea that *A. dispar* can be explored further as a model to investigate the pathogenicity of infectious agents in a live host, where imaging is directly possible. Such studies cannot be conducted in zebrafish because it cannot survive at temperatures over than 34°C (Avdesh *et al*., 2012). *A. dispar* embryos might therefore serve as the ideal model for *in vivo* immune cell analyses and increase the amenability for deep imaging such as imaging the interaction of pathogen and host cells. Whilst studies of interactions with pathogens might also be possible in other killifish models such as the mangrove killifish, the superior optical transparency of the *A. dispar* cells and yolk would be very helpful in visualizing real time changes. Since we have clearly shown the ability of the *A. dispar* embryos to develop and survive at human body temperatures, our results have demonstrated that *A. dispar* will be useful in the context of studying a variety of cell interactions with human pathogens as well as those of fish.

Chapter 4

The Arabian killifish (*Aphanius dispar*) as a novel model for investigating fungal infections by *C. albicans*

4.1 Abstract

Candida albicans is an opportunistic fungal pathogen of humans. The yeast is present in healthy individuals as a commensal, and can reside harmlessly on the skin and in the oral cavity. However, in immuno-compromised individuals, the fungus can invade tissues, producing superficial infections and, in severe cases, life-threatening systemic disease. Morphogenetic changes from a yeast form to a hyphal growth form are considered essential to this infection process. For the effective control of this debilitating disease, it is important to identify other virulence factors produced by *C. albicans,* since these influences the ability to invade tissues and cause diseases.

In this project, Arabian killifish (*Aphanius dispar)* embryos are utilized as a model to explore the relationship between *C. albicans* and its host. *A. dispar* are useful in this context as they are transparent, making live-cell imaging possible, and they can live at a variety of temperatures (4-40˚C), making them potentially a better model than Zebrafish (which cannot survive at 37˚C).

This study shows that the *A. dispar* embryo can develop at a wider range of temperatures (26.0, 30.0, 34.0, 37.0, 38.5°C) than Zebrafish. Using live cell imaging techniques, the behaviour of *C. albicans* in the fish was examined, both at human body temperature (37°C) and at fever temperature (38.5°C), together with the response of the fish to infection at different doses. Embryos were micro-injected into the yolk with dTomato tagged *C. albicans* cells and different mutants of Candida were characterised to allow counts of viable cells from homogenates after infection. Despite high levels of growth

of *C. albicans*, killifish survived up to 144 hpi. However, Zebrafish died within 72 hpi. Histological analysis revealed dissemination of different fungal forms in the tissue. To quantify the level of infection during time-course in the host embryos, CAF2-d-Tomato expressing Candida was utilised, using western blotting with the mCherry antibody. To evaluate the effect of the mannan of the Candida cell wall on virulence and on the embryo's survival, *C. albicans* mutants with defects in *O*- and *N*-mannosylation were investigated, using CFU and survival rate. The results showed that there was a medium level of growth of Candida mutants compared with the wild-type and their parent controls. Deletion of a major component of the cell wall (mannoprotein) functionally affected the adhesion and the formation of the hyphal form.

Fluconazole (FLC) is widely used as a reliable antifungal medication. To investigate the impact of FLC on *A. dispar* embryos, infected embryos were exposed and injected with FLC at varying doses at 2 and 6 hpi, and then the mortality and fungal burden were examined. The present results showed that high survival was observed with the highest doses of FLC, including a significant reduction of CFU in the embryos. These studies confirm that the *Arabian dispar* embryo can be used as a mini-vertebrate host model to study fungal pathogenesis, and demonstrates the advantages of using this species in future studies of bacterial, fungal and viral pathogens at a physiologically relevant temperature for human infection.

4.2 Introduction

Candida albicans is a commensal organism, present in our gastrointestinal and oral cavity. It is an opportunistic pathogen fungus that colonises different sites in humans *C. albicans* causes considerable morbidity and mortality in immuno-compromised patients (Chao *et al.,* 2010; Torraca *et al*., 2014). Candida requires numerous virulence factors to invade the host, including adhesion, a yeast-hyphae transition and the secretion of hydrolyzes to promote infection of the tissue (Koji *et al.,* 1994).

C. albicans, has four major cellular morphologies, namely yeast cells, pseudohyphae, hyphae, and chlamydospores. These polymorphisms differences between the forms of the growth of *C. albicans* affect the pathogenicity of the fungus. *C. albicans* can sense and adapt to environmental changes and this is essential for their survival (Koji *et al.,* 1994). A range of environmental conditions affects *C. albicans* morphology, such as pH, temperatures and CO_2 levels (Koji *et al.,* 1994). *C. albicans* transformation from yeast cells to hyphal cells forms encourages adhesion and invasion, leading to tissue damage. The cell wall is the prime interaction site between the fungal pathogens and its host because it contains a multitude of proteins which enhance adhesion to the host tissue and bring about immune evasion (Ekkehard *et al.,* 2006). *C. albicans* can invade the tissue by two processes: induced endocytosis and active penetration (Choa *et al.,* 2010). The secretion of hydrolases enzymes contributes to the fungal active penetration into the host cells (Naglik *et al.,* 2014). The secretion of hydrolases occurs after adhesion to host cell surfaces and onset of hyphal growth. Three different classes of secreted hydrolases have been implicated in pathogenesis of *C*. *albicans*: proteases, phospholipases, and lipases. The aspartic proteinases (saps) play an important role in the pathogenicity of Candida by digesting or destroying host cell membranes and causing degradation to the host surface molecules (Schaller *et al.,* 2005). Another important virulence factor is the thigmotropic reaction of Candida*,* which is a special change in the growth of microorganisms in response to touch or contact stimuli. After this contact

with the surface, yeast cells switch to a hyphal form and can proliferate inside the tissue (Francois *et al.,* 2013).

The *C. albicans* cell wall is a robust dynamic organelle important for cell shape and protection against extracellular changes (environment and other organisms). It also plays a critical role in recognition by immune cells (Mora-Montes *et al.,* 2010). The cell wall therefore plays a vital role in the growth and pathogenicity of *C. albicans*. Despite the cell wall being physically robust, for its maintenance it also needs to be flexible to allow expansion and morphogenesis (Whiteway and Bachewich, 2007). It has also to be permeable to permit direct egression of secreted proteins to enhance invasion (Hall and Gow, 2013).

The cell wall is composed of approximately 80 to 90% of carbohydrates, with the major polysaccharides incorporated in three constituents: (i) glucan contains branched polymers of glucan joined via ß-1,3 and ß-1,6 linkages; (ii) chitin, unbranched polymers of N- acetyl-D-glucosamine or GlcNAc; and(iii) mannan, polymers of mannose, which are covalently linked to proteins. Mannoproteins with α and ß-linked mannose chains have a key role in the cell wall, and are also important as secreted proteins, as the cell wall is decorated with these carbohydrate structures. Mannoproteins are modified to three structures: highly branched *N*- linked mannan, linear *O*-linked mannan, and phospholipomannan (Hall and Gow, 2013).

The growth rate and morphology of *C. albicans* is affected by the cell wall components. Deletion of mannose from the cell wall results in a reduction in growth rate, a tendency to aggregate, and reduction of cell wall adherence (Hall and Gow, 2013). Deletion of mannan from the cell wall also results in a reduction of the capacity for adhesion and biofilm formation, suggesting that *O*-and *N*- mannosylation are fundamental for cell wall integrity and interaction with the host (Munro *et al.,* 2005; Timpel *et al.*,1998;Timpel *et al.,* 2005).

Treatment of fungal infections is notoriously difficult within a human host because of the drug-resistant strains that have emerged and the limited effectiveness of antifungal drugs (Cowen *et al*., 2008). Several antifungal agents target ergosterol biosynthesis the main sterol of the fungal membrane (Onishi *et al.,* 2000). The antifungal drugs such as triazole

agents (fluconazole and itraconazole) intercalate into the ergosterol-containing membranes and cause leakage of cellular components and cell death by forming membrane–spanning channels. One of the most commonly used groups of antifungal agents is triazoles, which have been used for approximately two decades. Triazoles bind to a haem group in the target protein through a nitrogen group in the azole ring and blocks the demethylation of C-14 in lanosterol, leading to the accumulation of toxic sterol intermediates that disrupt membrane integrity (Cowen and Steinbach, 2008).

Due to the high resistance of fungi to the recently used antifungal reagents and scarcity or toxicity of drugs (Ostrosky-Zeichner *et al.,* 2010), zebrafish have been an excellent model for infection studies; testing many alternative strategies and clinical approaches to improve the function of drugs against pathogens such as Candida (Chin *et al.,* 2016). In addition, Zebrafish have been used because of the transparency of their embryos and availability of transgenic lines. However, there is a limitation in utilising zebrafish as a model because the fish embryos have a physiological optimum temperature of 28.5°C, which means there is no possibility of them being used to test the function of drugs against pathogens with an optimum temperature of 37°C. Therefore, recently, we have developed Arabian killifish, that can survive at 37°C or even at human fever temperatures (39°C) as an alternative model for testing the efficiency of an antifungal drug (Fluconazole, FLC) against *C. albicans.*

The overall aim of the study is to compare and contrast the feasibility of using *A. dispar* and Zebrafish as a model to understand *C. albicans* pathogenicity. More specifically the work sets out to investigate the survival of *A. dispar* embryos with Candida infections established at different inoculum doses. To investigate the suitability of this model to test antifungal agents (Fluconazole) at a range of doses. Finally, to test the suitability of this model to screen mutants with defects in key virulence traits; including the yeast-to-hyphae transition and cell wall architecture.

4.3 Experimental procedures

4.3.1 *C. albicans* strains and growth conditions

The *C. albicans* strains used in this study were wild-type SC5314 and NGY152; CAF2-dtomato, and the double mutants *mnt1-mnt2*Δ, and *mnt1-mnt2*Δ with URA3 reintegrated at RPS10 using the Clp10 vector, *pmr1*Δ, *pmr1* with URA3 reintegrated at RPS10 with Clp10, *och1*Δ *and och1*Δ with URA3 reintegrated at RPS10 using Clp10, *Ca ACT1::GFP* integrated at RPS10, and Ca *TUB1*::GFP integrated at RPS10.

A single colony from fresh YPD agar was inoculated in 5 ml of YPD broth and incubated at 30°C overnight. *C. albicans* cells were then washed three times with 1x sterile phosphate- buffered saline (PBS), the cells were counted using a haemocytometer and suspended in sterile PBS before adjusting to final concentrations for colony assays and injection assays.

4.3.2 Maintenance of Arabian killifish and embryo collection

Arabian killifish (*A*. *dispar*) and Zebrafish (*D. rerio)* were kept with ASW and fresh water respectively in a recirculation system in the Aquatic Resource Centre at the University of Exeter. *Aphanius dispar* fertilized eggs were obtained 1-hour post fertilization (hpf) from the breeding tanks at the University of Exeter using spawning mops. They were washed with water and checked using a stereomicroscope to choose the only fertilized eggs for following procedures. Fish embryos were moved and distributed into groups of plastic Petri dishes with 20 ml seawater (35 ppt) at a density of 10-15 embryos per dish and maintained at 26 ± 1°C for 3 dpf in an incubator (model Heratherm IGS60, Germany).

4.3.3 Microinjection

A. dispar or *D. rerio* embryos were microinjected with different doses of *C. albicans* mutant cells at comparable somitogenesis stages - 54 to 59 h post fertilization for *A. dispar* and 24 hpf for *D. rerio.* Embryos were submerged in “channel gels’’ made by leaving 10% agarose /sea water to setting with 1.2 mm diameter glass tubes as moulds (Mourabit, *et al.,* 2011). Embryos

were rotated using forceps before microinjected a 5 to 10 nl of *C. albicans* cell suspension at $3x10^7$, $6x10^7$, $1x10^8$ or $3x10^8$ cells/ml in PBS. Cells were microinjected into the yolk using the microinjector (WPI) and micromanipulator (Narishige).

4.3.4 Enumeration of fungal burdens

Embryos at somitogenesis stages (54-59 hpf) microinjected with 5 nl of *C. albicans* at $3x10^7$, $6X10^7$,$1x10^8$, $3X10^8$ cells/ml were incubated at different temperatures (26.0°C, 30.0°C, 34.0°C 37.0°C and 38.5°C) during infection. Colonies were counted after incubation for 24-72 hpi for Zebrafish and 24-120 hpi for *A. dispar* at (30.0°C, 37.0°C). Two living embryos were then collected in 100 µl of 35‰ artificial sea water, homogenized and added to 400 µl of 1/100 penicillin-streptomycin stock solution 100 mg/ml P4458 (Sigma) to give a final volume of 500 µl. Finally, 100 µl of the suspension was plated in triplicate onto YPD agar (Vylkova, *et al.,* 2011).

4.3.5 Calcofluor staining

Calcofluor white dye was a gift from Dr Isabelle Jourdain (University of Exeter). *C. albicans* cell walls (chitin) were stained using 4 µg/ml fluorescent calcofluor. Embryos were microinjected with $1x10^8$ cell/ml of Candida into the yolk and incubated at 37°C for 24 h. After preparing the agarose (0.7 g agarose and 40 ml water), embryos were collected in 100 µl 1x PBS, homogenized and then glass slid was coated with agarose after its cooling down, then 5 µl of the sample was added along with 0.4 µl Calcofluor dye (4 µg/ml). Finally, the slide left to semidry and put the coverslip before imaging.

4.3.6 Histological analysis of *C. albicans* colonization in *A. dispar*

Embryos were microinjected with $1x10^8$ cells/ml of SC5314 *C. albicans* and incubated for 24 h. The embryos were fixed in 4 % paraformaldehyde (SIGMA) 500 mM NaCl, 50 mM Hepes, pH of 7.8 for four days, followed by sequential dehydration. Paraffin sections (5 µm thickness) were incubated

with serum-free protein block for 2 h at room temperature. Sections were incubated at 4°C overnight with an anti-GFP antibody (to reveal *C. albicans*) at 1:300 dilution with blocking buffer then washed three times for 5 min each. Secondary antibody, anti-Rabbit IgG BA-1000 IVD (1:300 in blocking buffer) was applied to sections for 1 h at room temperature. Sections were incubated with VECTOSTAIN ABC reagent (Vector lab) PK-4000 for 30 mins to 1 h, washed three times for 5 min each and incubated with peroxidase substrate DAB (Vector lab) SK-4100 for 2-10 min, then washed for 5 min with tap water. Finally, the sections were immersed in haematoxylin and eosin for 1 sec each and then washed before rehydration and mounting on slides.

4.3.7 Immunofluorescence staining

For whole-embryo immunofluorescence studies, 11-12 dpf embryos were microinjected with $1x10^8$ cell/wall Wild-type SC5314 of *C. albicans*. At 24 hpi, embryos were fixed in 4 % paraformaldehyde (SIGMA) 500 mM NaCl, 50 mM Hepes, pH o 7.8 for four days. Embryos were then washed with PBST before being permeabilized in 0.24% trypsin solution for 2 h. Embryos were incubated with blocking solution (1% BSA in 0.5% PBSTx and FSC-Hl) for 2 h at room temperature. Embryos were placed with R2-Rabbit primary antibody was a Gift received from Dr. Howard Jenkinson Bristol University 1:250 diluted in blocking solution and incubated for overnight at 4°C. Alexa 594-conjugated goat anti-rabbit secondary antibody (1:300 dilution), followed by three times washing by PBSTx20 min each, and then imaged.

4.3.8 Western blotting

Five embryos with no removal of the yolk or chorion (uninfected and infected embryos at 24-120 hpi) were placed in 100 µl of cell dissociation buffer NP0008 (Invitrogen) in Eppendorf tubes on ice and then homogenized by grinding (Greiner Bio-one) using plastic pestles. Homogenised embryos were then heated at 80-90°C for 5 min and centrifuged for 5 min at 2,000 rpm. Supernatants were loaded on to

NP0335BOX gels (Invitrogen) 15 µl for yeast and 30 µl for embryo's extracts. After blotting, membranes were incubated with the anti-mCherry rabbit antibody (1:5000 in blocking buffer) (Abcam) or anti-GFP antibody overnight at 4°C and then washed for 20 min x3. Blots were then incubated with secondary antibody (polyclonal Goat Anti-Rabbit immunoglobulin HRP P0448, DAKO) 1:5000 for 2 h at room temperature with shaking and then washed with PBST for 1 h. Signals were visualized by using a mixture of 1 ml luminol solution and 1 ml peroxide solution from the Immobilon Western HRP substrate kit (Thermo Fisher Scientific) kit according to the manufacturer's instructions. Blue film was exposed to the blots for 30 mins in the dark room. After developing the film, membranes were washed and incubated with an anti-alpha-Tubulin antibody (a mouse monoclonal antibody clone DM1A (Sigma) with 1:1000 dilution overnight at 4°C). Secondary antibody was applied (Polyclonal Goat Anti-Mouse immunoglobulins HRP, DAKO, P0447) at 1:500 for 2 h.

4.3.9 *A.* Direct *dispar* egg infections

To investigate the optimal conditions for direct egg infection, embryos were washed with sterilized egg water three times and then embryos were placed in 6-well plates with either 4 ml sterilized sea water, or RPMI/17ppt, or RPMI 35 ppt, or RPMI/SERUM 17 ppt, or RPMI/ SERUM 35 ppt. Egg water and RPMI/SERUM containing 10% Heat Inactivated Fetal Calf Serum (FSC-HI). Embryos were co-incubated with $5x10^5$ cell/ml *CAF2-dTomato C. albicans* and different mutants: Wild-type (*NGY152*), *mnt1-mnt2*Δ*, pmr1*Δ*, och1*Δ*,* all with shaking at 80 rpm and 37°C for 4 h. Embryos were incubated in Artificial water 35 ppt after removing non-adhered *C. albicans* cells for an additional two days at 37°C. In each treatment, 10 embryos were used. Survival rate of embryos was determined after two days incubation. The Zeiss inverted microscope (Zeiss Axio-Observer.Z1-AX10) was used for imaging to identify interactions with different *C. albicans* mutants.

4.3.10 *A. dispar* survival and killing assay **(**Fluconazole serial dilution)

A. dispar embryos in the somitogenesis and organogenesis stages (59.5-73.5) hpf were selected to evaluate the antifungal agent (Fluconazole) F8929_100 MG at different concentrations. *C. albicans* strain Wild-type (NGY152) cells were collected, washed and prepared as a suspension at $1x10^8$ cells/ml. After preparing the Candida suspension, Candida cells were microinjected directly into the yolk of *A. dispar* with $1x\ 10^8$ cells/ml. Control embryos received 5 to 10 nl Phosphate Buffered Saline (PBS). Fluconazole was applied at different doses by directly exposing the embryos to artificial seawater containing the drug. A series of doses were used for the Flucanazole agent. FLC was administrated 0, 2, 4, 8, 16, 32, 64, 128 mg/l, respectively at 2 and 6 h post-infection at 37°C. Survival rates of embryos were determined and plotted at different concentration of drug. The fungal burden was assessed to evaluate the therapeutic efficiency of Fluconazole against different *C. albicans* strains.

4.3.11 Growth analysis of *C. albicans* strains

Candida cells (*NGY152*, *mnt1-mnt2*Δ*, mnt1*Δ and *mnt2* Δ integrated at clp10*, pmr1*Δ*, pmr1*Δ integrated at clp10, *och1*Δ, *och1* integrated at clp10) were diluted into YPD broth to $3x10^7$, $6x10^7$, $1x10^8$ and $3x10^8$ cells/ml for *NGY152*; and $1x10^8$ cells/ml for other strains. Flat bottomed 96-well plates were inoculated with 100 µl of the cells and covered with transparent sterile film, then the VersaMax™ Absorbance Microplate Reader pre-warmed to 37°C, 40°C and placed the plate. Optical density (OD_{600}) readings were measured every 10 minutes intervals over a 22 hours period, with shaking between reads.

4.4 Results

4.4.1 *A. dispar* embryos infected with *C. albicans* show dose dependent lethality

To examine the effect of *C. albicans* on *A. dispar* embryos, embryos at the somitogenesis stage were microinjected into the yolk with a range of inocula covering $3x10^7$, $6x10^7$, $1x10^8$ and $3x10^8$ cells/ml). Infected embryos were incubated at 37°C for 120 hpi (hours post infection). It was found that 100% of embryos survived with a low dose of *C. albicans* ($3x10^7$ cells/ml). Embryos continued to survive until 120 hpi and their fungal burden precipitously dropped until the infection was cleared. When the dose of *C. albicans* inocula was increased to $6x10^7$ cells/ml, at 96 hpi, the rate of mortality was 100%. There was still some evidence of clearing, the fungal burden decreased, compared to the high fungal burden at 24 and 48 hpi (Fig. 4.1) At the two highest concentrations ($1x10^8$ and $3x10^8$ cells/ml) illustrate that the number of surviving embryos quickly decreased evidenced by the high mortality at 24, 48, and 72 hpi. The highest level of inoculation ($3x10^8$ cells/ml) resulted in 100% mortality at 72 hpi, depending on the fungal burden, whereas, the fungal burden declined significantly at ($1x10^8$ cells/ml) and at 72 hpi caused 50% mortality. Subsequently, the inoculum of $1x10^8$ cells/ml colony forming unit (CFU)/embryo was reliable to optimize the *A. dispar-C. albicans* infection model.

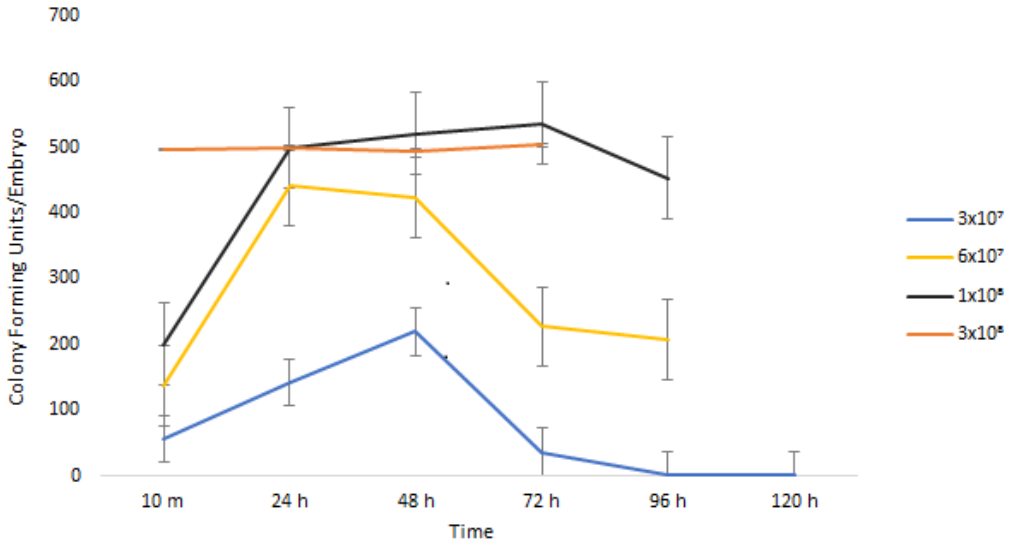

Figure 4.1 *A. dispar* killing assays by *C. albicans*. The CFU of *A. dispar* embryos at St. 24 (54.5 hpf) microinjected with different doses of *C. albicans*. Candida infection can kill *A. dispar* embryos at dose dependent manner. Each experiment was performed in triplicate.

4.4.2 Injection of *A. dispar* with *C. albicans* at different temperatures

To examine the effect of temperature on infection outcomes, *A. dispar* embryos at the somitogenesis stages were microinjected with $1x10^8$ cells/ml of *C. albicans* and incubated at different temperatures (26.0, 30.0, 34.0, 37.0 and 38.5°C). Fig. 4.2 shows that *A. dispar* embryos can remain alive even at a *C. albicans* infection dose of $1x10^8$ cells/ml at 24 and 48 hpi at 38.5°C. Assessment of the fungal burden at different temperatures within *A. dispar* yolk, indicated that the highest Candida burden was at 30.0°C at 24 and 48 hpi and 37°C at 48 hpi. The optimal temperature for growth was found to be between 26-30°C. However, when we elevated the incubation temperature to 37.0°C, the growth of Candida decreased at 24 hpi more than in 30.0°C. The cell burdens at 26.0°C and 30.0°C were higher than at 34.0°C, and much higher than at 37°C.

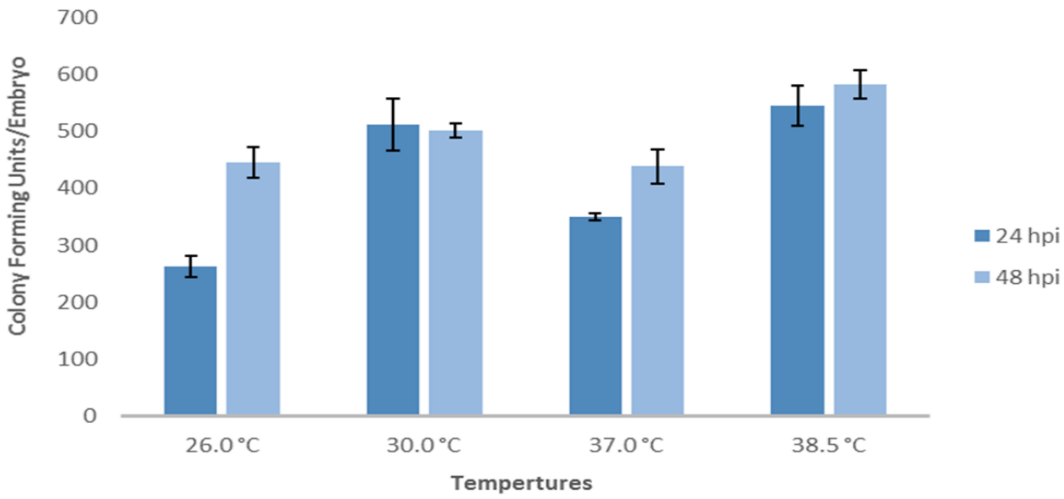

Figure 4.2 Injection into the *A. dispar* at (26°C, 30°C, 37°C and 38.5°C). *A. dispar* embryos were injected with of 1x10 ^{8} cells/ml. *Ca TUB1::GFP* in *RP10* into the yolk, and incubated for 24 and 48 hpi at different temperatures (26.0, 30.0, 37.0 and 38.5°C). Embryos were homoginized and determinate fungal burden by serial dilution to grow the Candida on YPD plates. Each bar is the mean of three biological replicates ± SE. Bars that do not share a common letter are statistically significantly different ($p<0.05$).

4.4.3 The *A. dispar* embryo shows greater tolerance to Candida infection than zebrafish

In order to assess the suitability of using *A. dispar* as a model host for Candida infections, survival rates of infected *A. dispar* and zebrafish embryos were compared. As demonstrated in Fig. 4.3, Zebrafish embryos died significantly faster than *A. dispar* embryos after being injected with 1x 10^{8} cells/ml. However, *A. dispar* displayed a resistance to the infection (with reduced CFUs after 24 hpi until the end of experiment) compared to zebrafish that showed a sustained increase and survived at 144 hpi. Although both demonstrated a high growth of Candida at 24, 48 hpi. The present data showed that the mortality of zebrafish embryos increased at 48 hpi to 95%, whereas when *A. dispar* survival was monitored after 4, 24, 48, 72, 144 hpi and the infection time was detected at 24, 48 hpi, the cells of Candida reduced gradually, especially at 144 hpi.

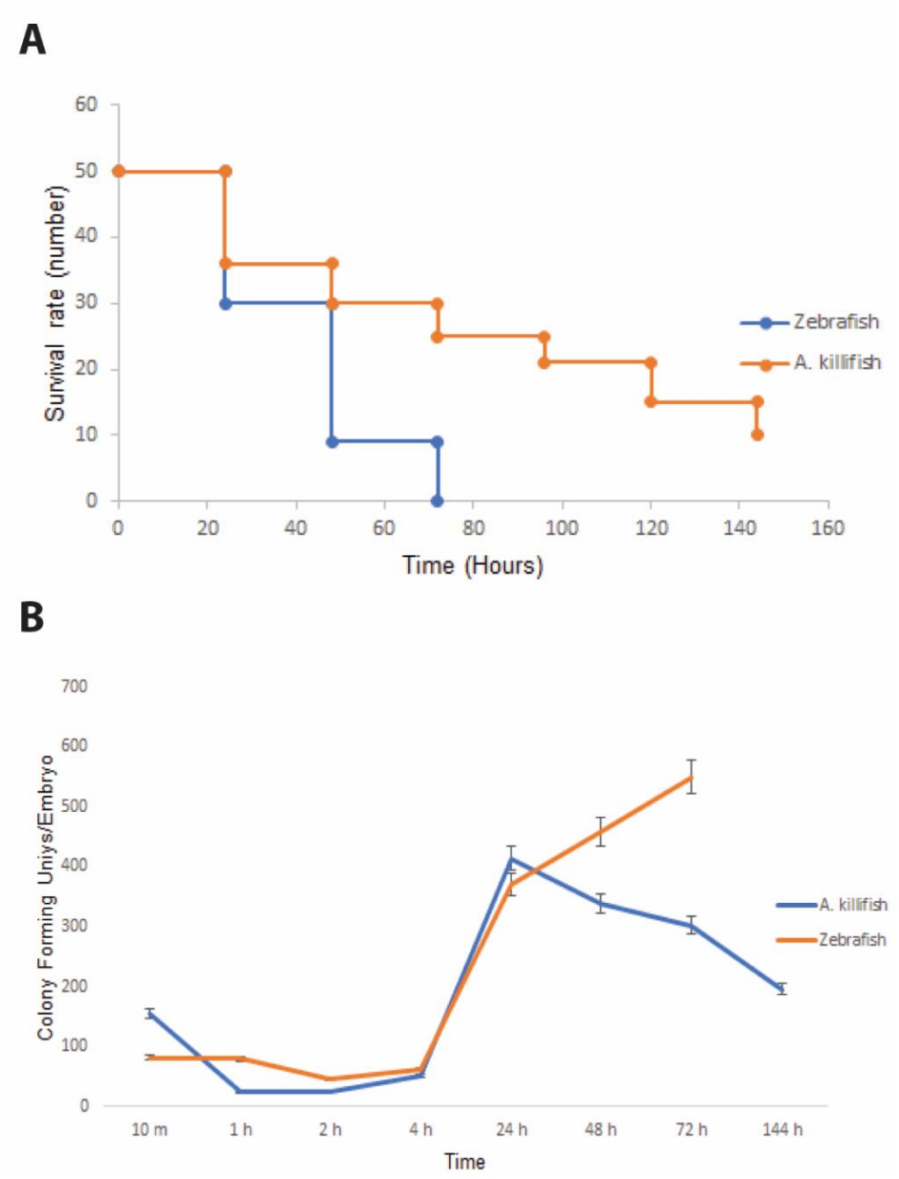

Figure 4.3 Fungal burdens in the yolk of *A. dispar* and zebrafish at 30°C. The rate of Candida growth in *A. dispar* and zebrafish were checked at different time points (10 min and 1, 2, 4, 24, 48, 72, 144 hpi). Embryos were injected with 1x 10^8 cells/ml into the yolk and incubated at 28.0°C. (A) Survival rate: (B) fungal burden of *C. albicans*. Each point is the mean of three biological replicates ± SE. P-values between 0.05 and 0.001 were considered: significant.

4.4.4 Dynamics of fungal burden of the *C. albicans* infected in the *A. dispar* embryos at 37°C

A. dispar embryos can develop "normally" at 37°C (as shown in chapter 3). Since *C. albicans* infection occur at 37°C in their natural host, the development of *C. albicans* in embryos at 37°C was followed. Figure 4.4 shows the CFU burden in *A. dispar* embryos injected in the yolk with 1x 10^8 cells/ml CAF2-dTomato *C. albicans* cells at 37°C. Significant growth of Candida was observed at 24, 48 hpi (increase of CFU from 343 to 355 and this was related to the transition of the yeast to hyphal phase at 37.0°C. Despite this high growth of *C. albicans*, killifish stayed alive at 72 hpi. The embryo survived even up to 144 hpi. These results suggest that *A. dispar* is a suitable model for studying virulence factor at 37.0°C., because the timing of hyphal formation is related to the physiologically relevant temperature and *C. albicans* virulence.

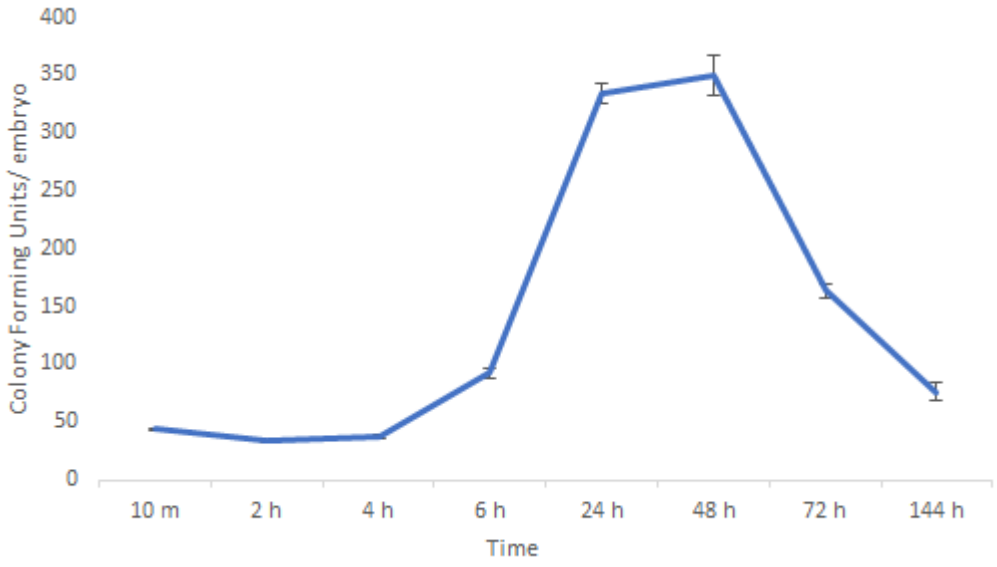

Figure 4.4 Human body temperature is required to evaluate the infection in *A. dispar*. Embryos were injected with CAF2-dTomato Candida into the yolk of *A. dispar* and cultured at 37°C. The fungal burden was determined at 0, 10 min, 2, 4, 6, 24, 48, 72, and 144 hpi. Each point is the mean of three biological replicates ± SE are statistically significantly different ($p<0.05$).

4.4.5 *C. albicans* can infect both brain and yolk tissues in *A. dispar* embryos

To examine the tissue preference of the *C. albicans* cells, *A. dispar* embryos were injected into the yolk and hindbrain ventricles and the fungal burden was then compared. Initially, we attempted to infect the embryos with up to 10^8 cells/ml. These cells were examined and little lethality was observed during infection at 24, 48, 144 hpi in the yolk and brain. As shown in Figure 4.5, the burden of infection of Candida in the yolk was higher than in the brain at all of the infection times (24, 48, 120 hpi). On the other hand, both a progressive reduction in the burden of Candida in the brain was observed at both 48 hpi and 120 hpi. In contrast, the fungal burden in the yolks significantly increased at 48 hpi and then slightly decreased at 120 hpi in the yolk.

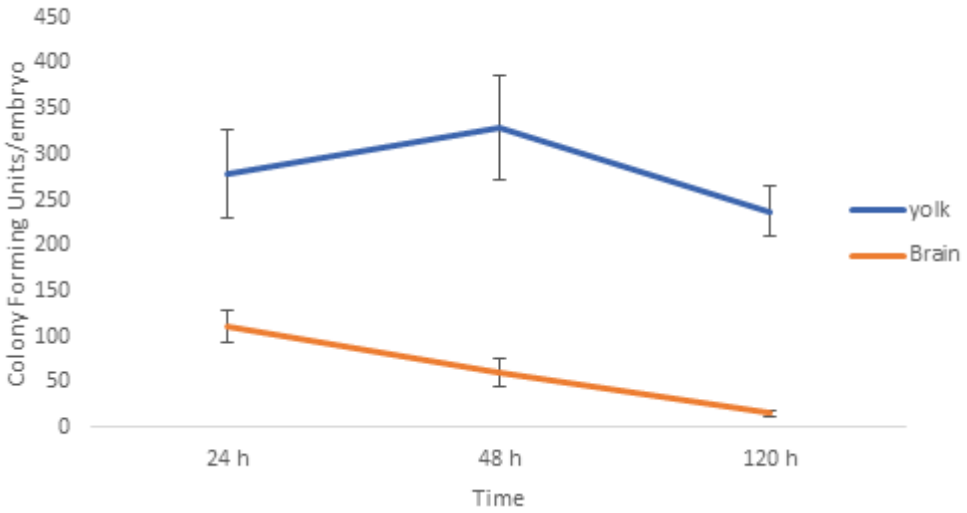

Figure 4.5 Injection *A. dispar* embryos into the hindbrain and yolk with 1X10^8 cells/ml *C. albicans*. Embryos were injected into the hindbrain and yolk and incubated at 37°C. Fungal burdens were assessed after the homogenization at 24, 48, and 120 hpi. There are significant differences ($p>0.05$).

4.4.6 *C. albicans* can develop as hyphae in the *A. dispar* embryo

To visualize Candida cell types in the yolk of infected embryos without the interference from melanophores and internal organs, crushed embryos were used. *A. dispar* embryos at 37°C were therefor injected with $1x10^8$ cells/ml colony forming unit (CFU)/embryo *C. albicans* strains. Embryos were then homogenised with the method described for the fungal burden assay at 24, 48 hpi and 8 dpi. Embryos were stained with calcofluor and observed with DIC and with DAPI fluorescent filters (Fig. 4.6). These studies revealed that *C. albicans* cells proliferated rapidly, and by 24 hpi they had colonized and invaded the tissue with a heavy growth of cells in the filamentous form (Fig. 4.6 B, F). The images collected also showed that Candida can revert *in vivo* to a yeast form at 8 dpi (Fig. 4.6 C, F).

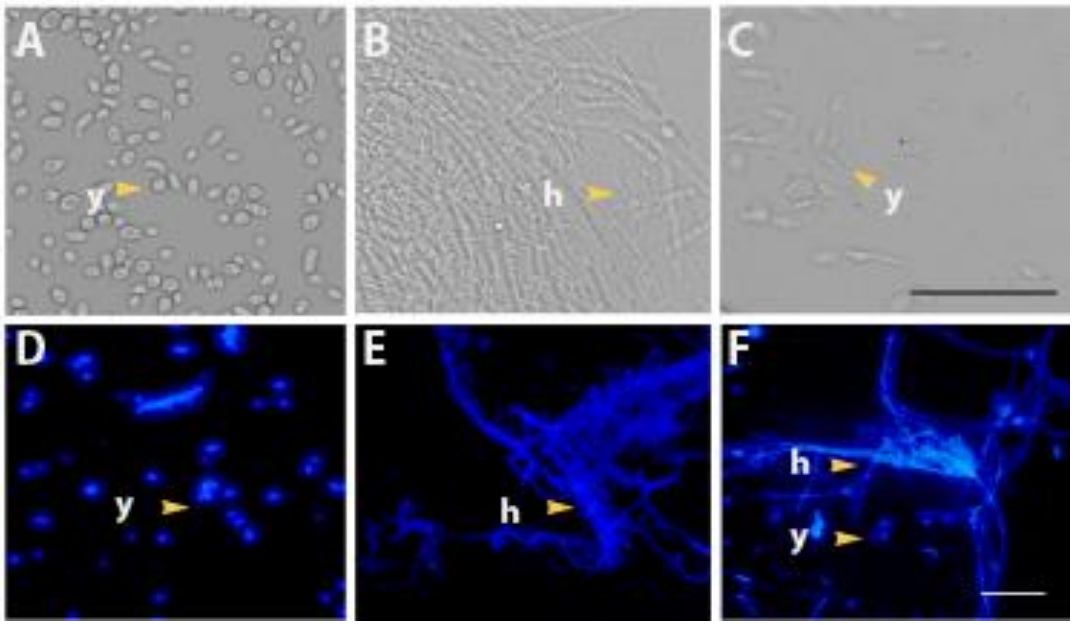

Figure 4.6 Morphogenesis of *C. albicans* in crushed embryos. Embryos at somitogenesis were injected into the yolk with $1x10^8$cells/ml and incubated at 37°C. Candida cells were imaged after crushing the embryos at 24, 48 hpi and 6 dpi. (A) Candida yeast. (B), Hyphae within crushed embryos at 48 hpi, (C) re-switched Candida yeast form at 6 dpi. (D) Stained Candida yeast with 4 µg/ml of fluorescent Calcofluor. (E) Hyphae cell wall stained with Calcofuor at 24 hpi. (F) Hyphae-h and yeast-y stained with Calcofluor at 6 dpi. Arrows indicate labelling of *C. albicans* cell wall by Calcofluor. Scale bar, A-B=50 µm; C=20 µm.

4.4.7 Examination of *C. albicans* invasion in *A. dispar*

C. albicans can colonize and damage tissue by invading the host tissue (Gow *et al.,* 2011). Histological analysis was therefore used to examine colonization of *C. albicans* within the yolk and brain of infected fish. Figure 4.7 shows clear evidence of *C. albicans* invasion of the yolk at 24 hpi. There was proliferation of cells, and Candida switching to a filamentous form within the sits of infection. In the case of brain infection, *A. dispar* embryos were injected with $1x10^{8}$ cells/ml *C. albicans*, and immunohistochemistry (IHC) was used to detect the target proteins in Candida, indicating that *C. albicans* grew in the brain as both yeast and hyphae (Fig. 4.7 A'). Similar observations indicate *C. albicans* proliferation and filamentous forms were observed in the yolk (Fig. 4.7 B'). Taken together these results suggest that *A. dispar* can be used as a simple model for studying Candida morphogenesis in real time at a physiological relevant temperature.

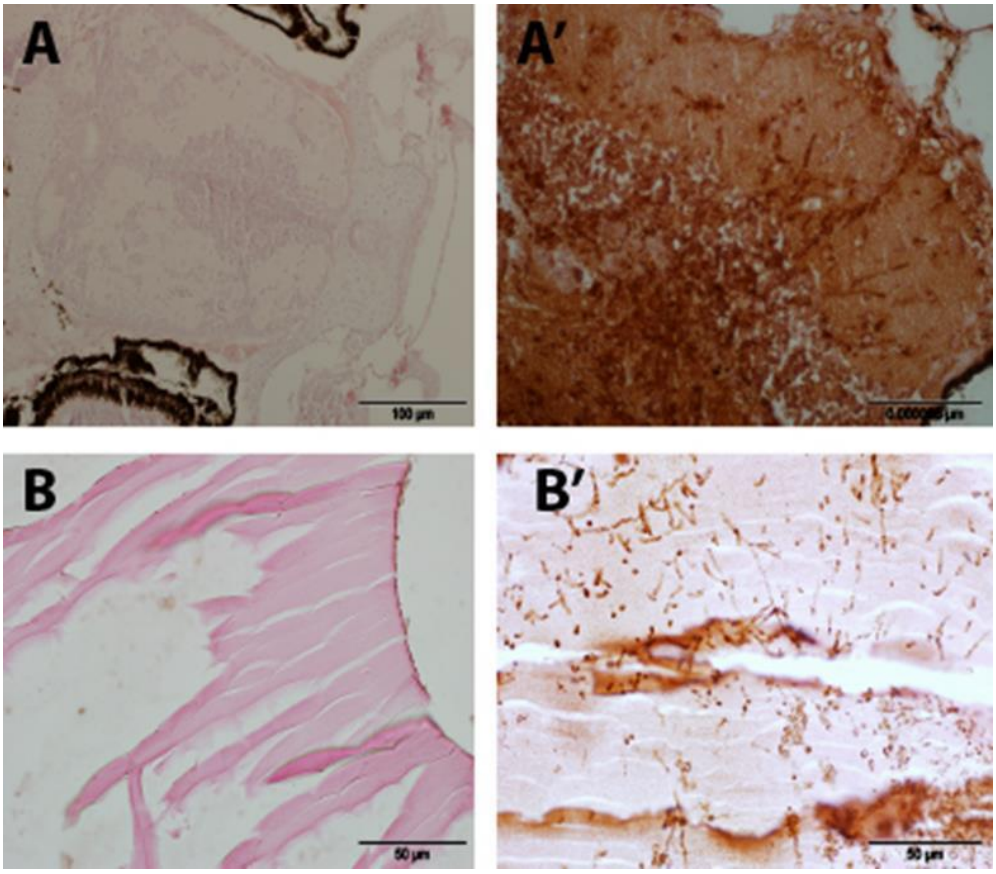

Figure 4.7 Morphological transition of *C. albicans* (CAF2-dTomato) cells attached to *A. dispar*. Filamentous form of *C. albicans* was found in the infected brain and yolk of embryos at 24 hpi**.** The embryos were injected with 1x10 ^{8} cells/ml and sacrificed for histological analysis. (A) Brain control, (A') infected brain. (B) Yolk control, (B') infected yolk.

4.4.8 Visualization of *C. albicans* infection using red-fluorescent *C. albicans* line infected in the live *A. dispar* embryos

To examine the suitability of *A. dispar* embryos for live cell imaging of *C. albicans* in the host, two routes of infection were compared yolk and trunk infections at St. 24 (54.5-59 hpi). *A. dispar* embryos at St. 32 (320 hpi) were micro-injected with 5 nl of 5x10^{8} cell/ml of WT of *C. albicans* into the yolk and trunk and then incubated at 37.0°C for 24 h. At 24 hpi, the hyphal form of *C. albicans* can be easily observed in the live embryo (Fig. 4.8). It was also observed that the hyphae spread and ultimately extended from the sites of inocula of yolk and trunk (Fig. 4.8). To detect the dissemination into

other sites within the embryo, whole mount immunofluorescence WHIF was used, and this revealed that there was no obvious dissemination of *C. albicans* observed except at the infection site. This finding suggests that the *A. dispar* embryo model may be useful model to study Candida infections in live embryos.

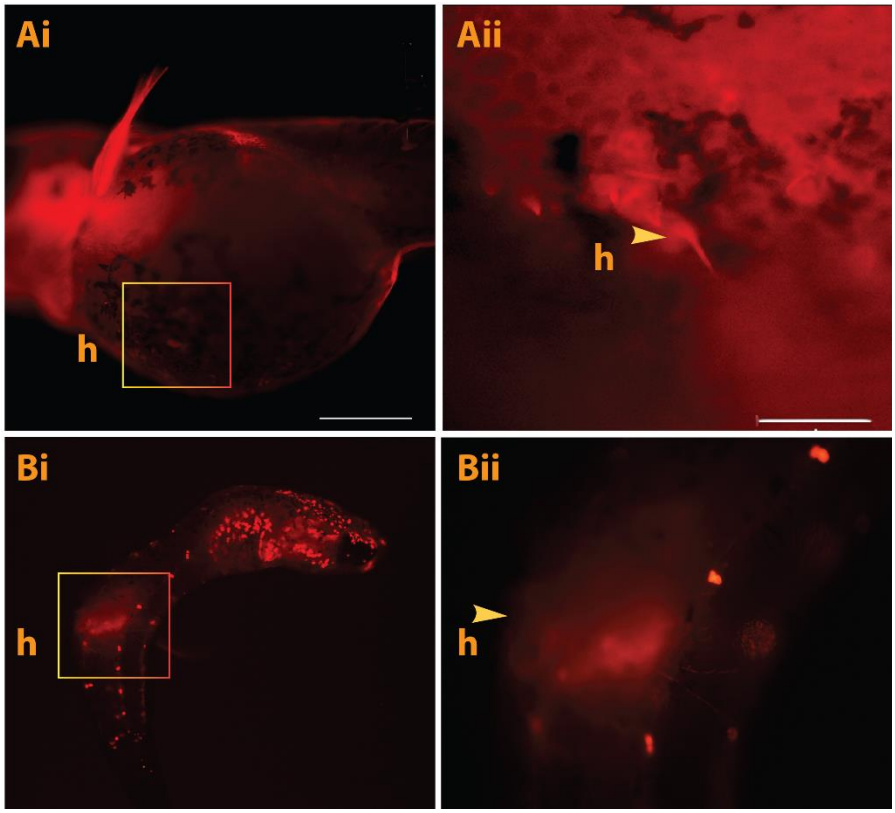

Figure 4.8 Whole mount immunofluorescence of hyphal growth of *C. albicans* in life embryos stained with anti-rabbit-R2 antibody. Fish embryos were injected with $5x10^8$ cell/ml of WT of *C. albicans* into the yolk and trunk. (Ai-ii) yolk, (Bi-ii) trunk were shown an overgrowth of filamentous form at infection sites. (h) indicates hyphae that were emerging from infected sites. Scale bar (Ai and Bi= 500 µm, Aii and Bii= 200 µm respectively.

4.4.9 Time-course of infection in *A. dispar* embryos

Colony assays revealed an initial increase in fungal burden followed by decrease of Candida during infection in the *A. dispar* embryos. However, it is likely that multi-cellular hyphae could easily generate single colonies in the assay even though a larger number of cells may have developed. To quantitatively assess the amount of Candida infection in the infected host embryos using western blotting, the levels of dTomato and GFP protein (Fig. 4.9 A, B, C) expressed in Candida in infected *A. dispar* and zebrafish embryos were assessed after 24 h and during a time-course of infection at 24, 48, 72, 96, and 120 hpi (Fig. 4.9 D and E). The western blot in figure 4.9 D shows that the dTomato protein increased both at 24 and 48 hpi and slightly reduced at 72 hpi. However, the expression significantly decreased at 96 and 120 hpi. The specificity of the assay was confirmed, as no band in the uninfected embryos was detected (control sample). The histogram displays the relative signal intensity of CAF2-dTomato protein in quantitative units (Fig. 4.9 E) that are normalized with the signal intensity of α- tubulin control for each treatment. These data suggest that not only the colony forming ability, the amount of Candida itself was dynamically increased at the initial phase (0-48hpi) and gradually decreased in the following hours (48 h to 120 hpi).

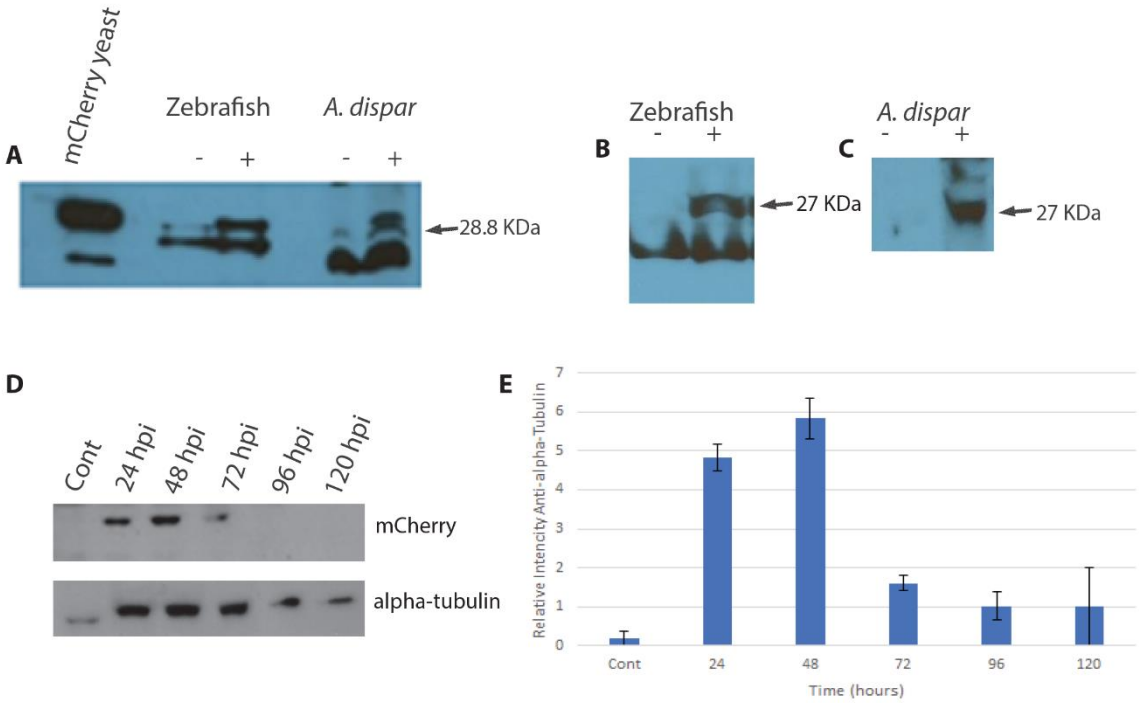

Figure 4.9 Candida CAF-dTomato and GFP proteins in the yolk of *A. dispar* and Zebrafish embryos. At 24 hpi, whole 5 killifish embryos lysate and 10 for Zebrafish per 100 µl SDS were prepared and applied to immunoblot analysis with antibodies mCherry and polyclonal. Proteins were detected after improving the experiment by increasing exposure time of film developing into 2 h. Using GFP-rabbit antibodies and polyclonal to detect GFP Candida proteins within injected Zebrafish and *A. dispar* at 24 hpi. Yeast extract (Wt, GFP and CAF-dTomato) with 1/300 Cell/ml. (A), mCherry and wild type of Candida yeast, uninfected Zebrafish and *A. dispar* and infected at 24 hpi. (B) Uninfected and infected Zebrafish at 24 hpi with GFP Candida. (C) Uninfected and injected, killifish at 24 hpi with (GFP Candida). (D) Time-course of fungal infection using the *A. dispar* embryos model. Embryos were injected with the $1x10^8$ cell/ml of CAF-dTomato *C. albicans* and incubated for 120 dpi. (E) The histogram displays the signal intensity of CAF-dTomato protein band in *A. dispar* embryos after normalization with the α-Tubulin signal intensity for each sample. Molecular weight of GFP= 27 KDa, mCherry= 28.8 KDa.

4.4.10 Attenuation of virulence in the *C. albicans* mannosylation mutants

Mutants of *C. albicans* have been shown to have reduced or attenuated virulence in a number of models (Paulovicova *et al.,* 2015). To determine if *A. dispar* embryos can used to screen mutants with defects in virulence traits, strains with defects in cell wall architecture were tested. Specifically, the role of mannosylation in the cell wall of *C. albicans* for infection and growth of the cell was assessed, using three mutants with loss of cell wall mannosylation (*pmr1*Δ*, mnt1-mnt2,* and *och1*Δ) (Hall *et al*., 2013), and copies of the same strains that were reintegrated with the wild type gene to assay the fungal burden with infected *A. dispar* embryos.

Before starting the infection assay, growth curves of the mutant lines were analysed in the YPD broth (Fig. 4.10 and 4.11) showing that all these mutants show slightly slower growth rate with slightly decreased final growth yield concentrations. Subsequently, embryos were micro-injected into the yolk with 5 nl of $1x10^8$ cells/ml of either the mutants or the parental strain and incubated at 37.0°C for 72 hpi. The fungal CFU burden assay was used to assess the effect of loss of glycosylation on virulence. The data revealed that *pmr1*Δ and *mnt1-mnt2*Δ mutants showed slower increases in fungal burden compared to the reintegrated control strains. The lower levels of fungal burden seem consistent with the slightly decreased growth rate of these mutants in YPD broth (Fig. 4.12 A, B and C). On the other hand, loss of *N*-mannan (*och1*Δ) drastically reduced the fungal burden of the infected embryos for 24, 48 and 72 hpi, while at the same time there was an increase in the fungal burden within the reintegrated control (Fig. 4.12 D). These observations are consistent with the finding that *och1*Δ mutants cannot separate and therefore even if cell growth and nuclear division occurred, the fungal burden (CFU) would not increase (Csonka *et al*., 2017). The overall data suggest that *pmr1*Δ and *mnt1-mnt2*Δ have slightly reduced growth rate but can still proliferate in the host embryo.

Host embryo survival following infection with the mutant strains was then examined. Surprisingly the data (Fig. 4.12 E-H) shows that *pmr1*Δ and *mnt1-mnt2*Δ mutant Candida cells killed the host embryos more rapidly than the reintegrated control strains (Fig. 4.12 E, F and G). This is a very

interesting observation, since these mutant cells proliferate with lower rates but can display greater virulence in the host embryo. In contrast, the *och1*Δ mutant which did not show a high fungal burden was completely avirulent in the host (Fig. 4.12 H). Reintegration of *och1*Δ restored full virulence.

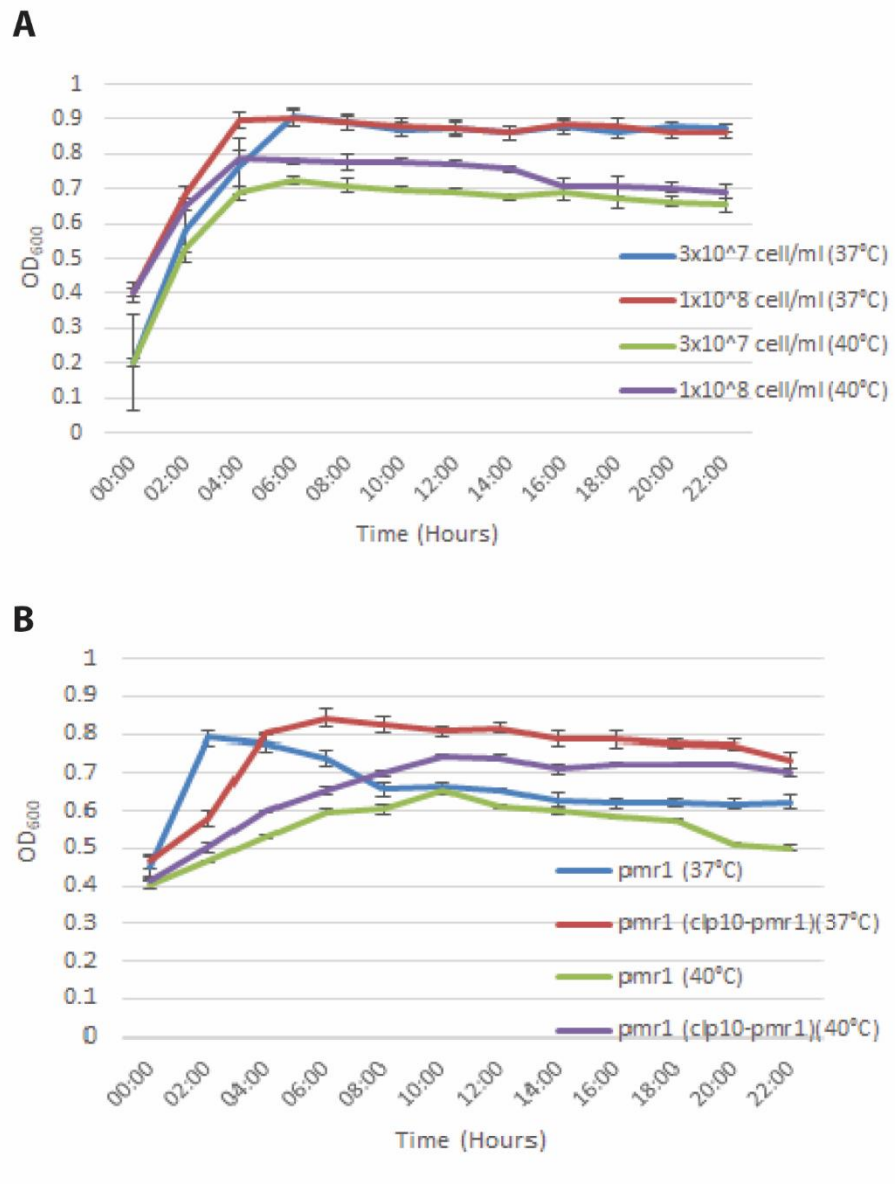

Figure 4.10 Growth curves of *C. albicans* mutant's cells from culture growing in YPD for 22 hours. *C. albicans* cells were incubated at 37°C and 40°C for 22 hours in (a VersaMax^{TM} absorbance microplate reader). The reading of OD_{600} was measured every 10 min intervals with 550 Sec shaking between reads. (A) Growth profile of Wild-type of *C. albicans* at 37°C and 40°C. (B) Growth profile of *pmr1*and parental strain of *C. albicans* at 37°C and 40°C.

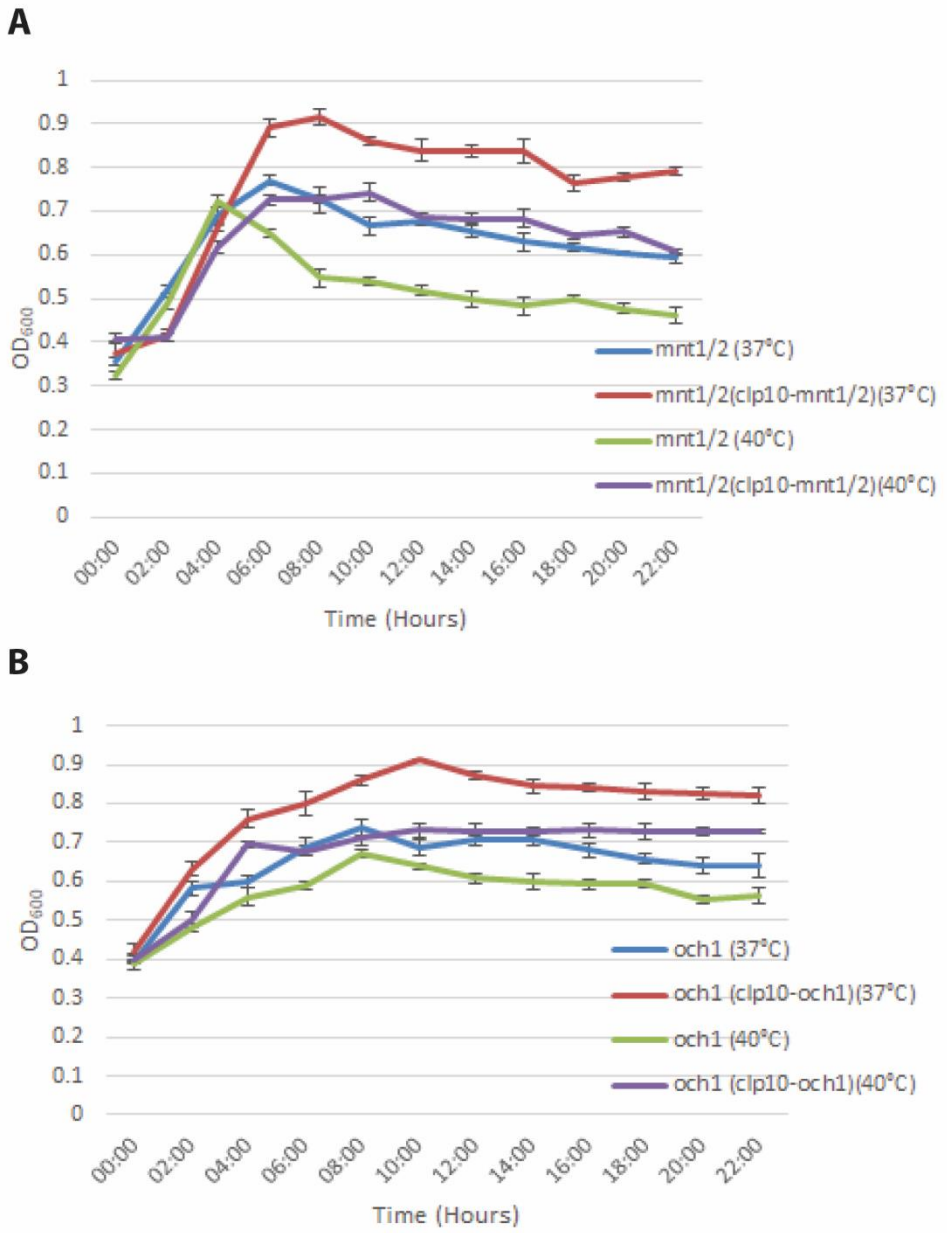

Figure 4.11 Growth curves of *C. albicans* mutant and parental strain at 37°C and 40°C. *C. albicans* cells were incubated at 37°C and 40°C for 22 hours in (a VersaMax^{TM} absorbance microplate reader). The reading of OD_{600} was measured every 10 min intervals with 550 Sec shaking between reads. (A) *mnt1-mnt2*Δ and parental strain, (B) *och1*Δ and parental strains.

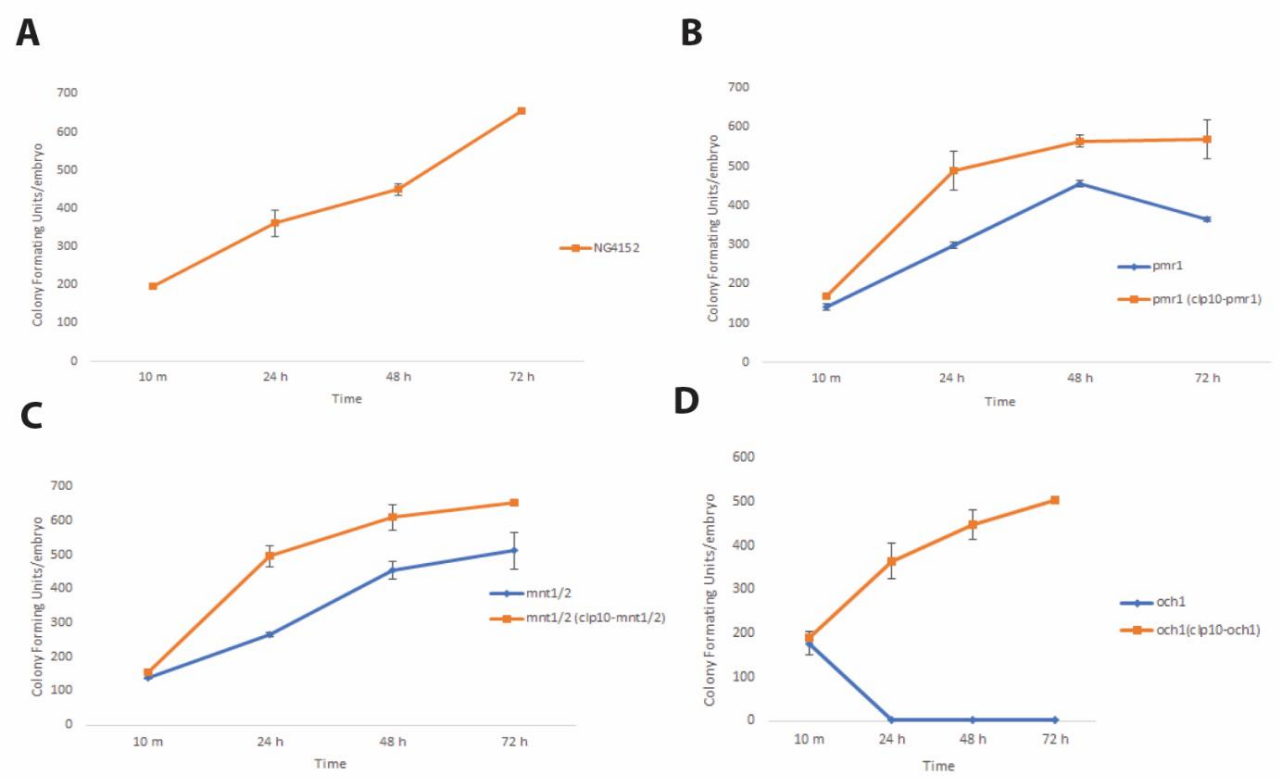
A
Colony Formating Units/embryo
700
600
500
400
300
200
100
0
10 m
24 h
48 h
72 h
Time
NG4152
B
Colony Formating Units/embryo
700
600
500
400
300
200
100
0
10 m
24 h
48 h
72 h
Time
pmr1
pmr1 (clp10-pmr1)
C
Colony Forming Units/embryo
700
600
500
400
300
200
100
0
10 m
24 h
48 h
72 h
Time
mnt1/2
mnt1/2 (clp10-mnt1/2)
D
Colony Formating Units/embryo
600
500
400
300
200
100
0
10 m
24 h
48 h
72 h
Time
och1
och1(clp10-och1)

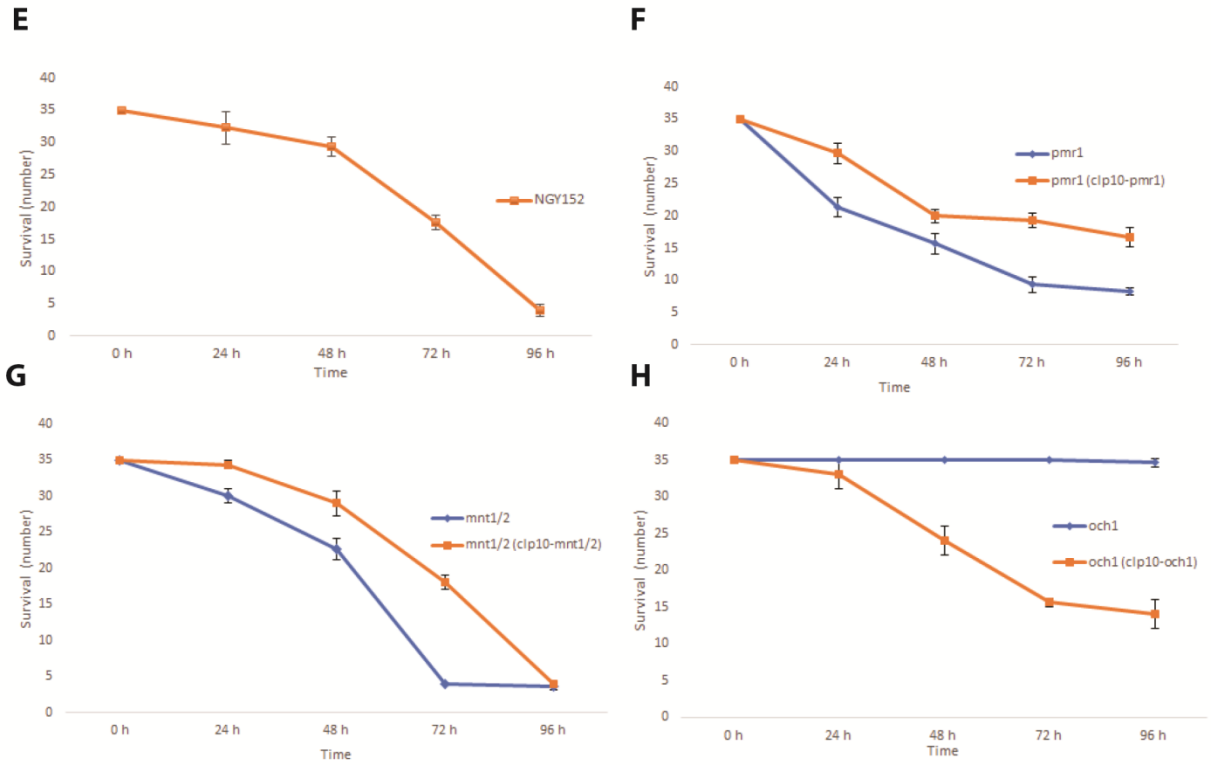

Figure 4.12 Human body temperature is required to evaluate the infection in *A. dispar*. Embryos were injected with different strains of Candida (A) NGY152 (B) *mnt1-mnt2*Δ (C) *och1*Δ (D) *pmr1*Δ into the yolk of *A. dispar* and cultured at 37°C. The fungal burden was determined at 24, 48, 72 hpi. Survival rate of *A. dispar* model during the infection (E) *NGY152*, (F) *pmr1*Δ, (G) *mnt1-mnt2*Δ, (H) *och1*Δ. Each group consists 35 embryos. The survival rate of *och1*Δ was significantly higher than in the WT, *pmr1*Δ and *mnt1-mnt2*Δ of *C. albicans*.

4.4.11 *C. albicans* can infect the chorion of the *A. dispar* eggs

C. albicans cells were cultured on the *A. dispar* eggs (chorion) under different conditions of salinity and nutrition. Fig. 4.13 shows the effect of salinity and medium with and without serum on the transition from yeast to the hyphal form of *C. albicans* on the *A. dispar* eggs. Infected eggs were co-incubated with the wild-type CAF2-dTomato and mutants of *C. albicans* (*och1*Δ*, mnt1-mnt2*Δ *and pmr1*Δ) for 4 h at 37.0°C, with shaking at 80 rpm. Eggs were then washed with sterilized sea water and incubated for 24 h at

37.0°C. In the presence of ASW 35 ppt *C. albicans* showed a low level of growth after 24 hpi (Fig. 4.13 A), with the majority of the cells remaining in the yeast form. In the same conditions but with serum added to the egg water, the growth rate was increased and hyphal growth was detected (Fig. 4.13 B). Addition of RPMI medium to infected eggs at 17 ppt ASW also induced a transition from yeast to hyphal forms (Fig. 4.13 C). Also, higher salinity of 35 ppt the growth rate was lower (Fig. 4.13 D). Subsequently, adding serum into the both salinities/RPMI produced an overgrowth of *C. albicans* (Fig. 4.13 E); whereas the growing intensity of *C. albicans* at higher salinity was slightly lower than at RPMI 17 ppt/serum (Fig. 4.13 F).

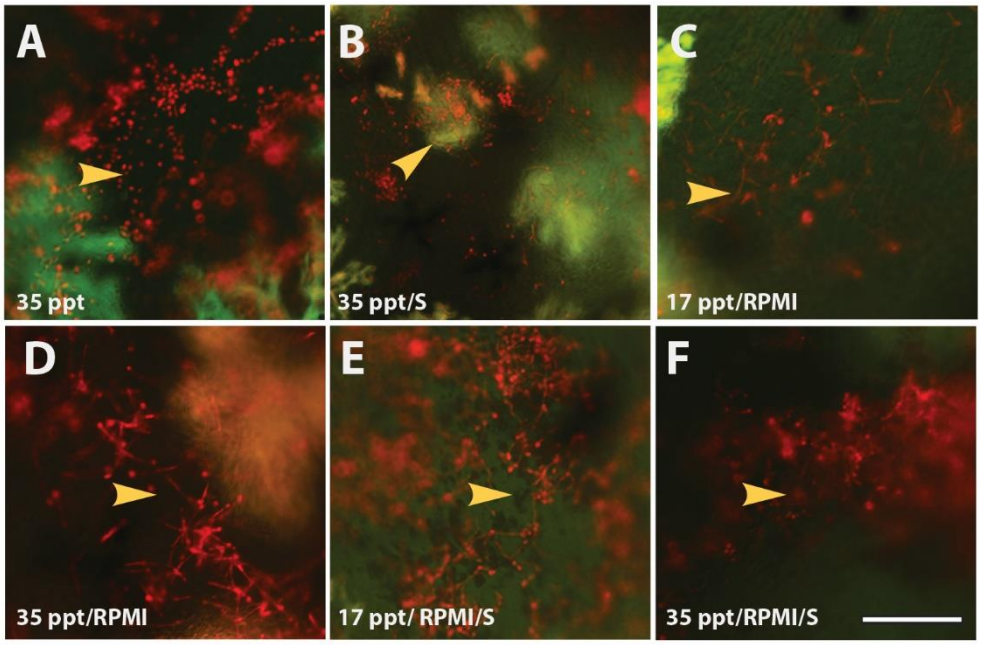

Figure 4.13 Infection of *A. dispar* eggs with different condition. Fish embryos were co-incubated with $5x10^5$ cell/ml of CAF-dTomato *C. albicans* for 4 h at 37.0°C, with shaking at 80 rpm in different nutrition conditions (A) embryos were incubated with Candida in seawater. (B) Candida in presence of serum. (C) Candida cells in 17 ppt/RPMI. (D) Candida cells in 35 ppt/RPMI. (E) Candida in 17 ppt/RPMI/S. (F) Candida cells in 35 ppt/RPMI/S. The images were shown the overgrowth of *C. albicans* (adhesion) after washing the embryos with sterilized sea water and incubation for 24 h at 37.0°C.

Despite the intense growth by *C. albicans*, the survival rate of embryos was rated at 100% possibly because the CAF2-dTomato *C. albicans* cells did not penetrate the chorion and could not reach the embryos themselves. Subsequently, to determine the CAF2-dTomato *C. albicans* burden treated eggs, the western blot technique was performed utilising the mCherry antibody (Abcam). Protein samples were extracted from *C. albicans* cells maintained under different conditions of salinity and nutrition. A single band of 28 kDa representing dTomato in the incubated embryo samples with ASW showed less intense bands compared with the extracts obtained from RPMI/serum. These 3 nutritional conditions supported much higher growth compared to ASW alone. Extracts from 35 ppt/serum generated higher expression levels - 4-fold greater than the ASW sample and lower than a sample of 17 ppt/ RPMI (7.6-fold) and 35 ppt/RPMI (5.9-fold). Overall, the amount of Candida growth was increased in both nutritional supplements (RPMI and serum) by 1.6- fold compared with the 35 ppt/ RPMI. In contrast, the expression was slightly reduced in the 17 RPMI/ serum compared with RPMI alone by 0.8-fold (Fig. 4.14). These results suggest that Candida can grow in (ASW 35 ppt) conditions when nutrition supplemental is provided.

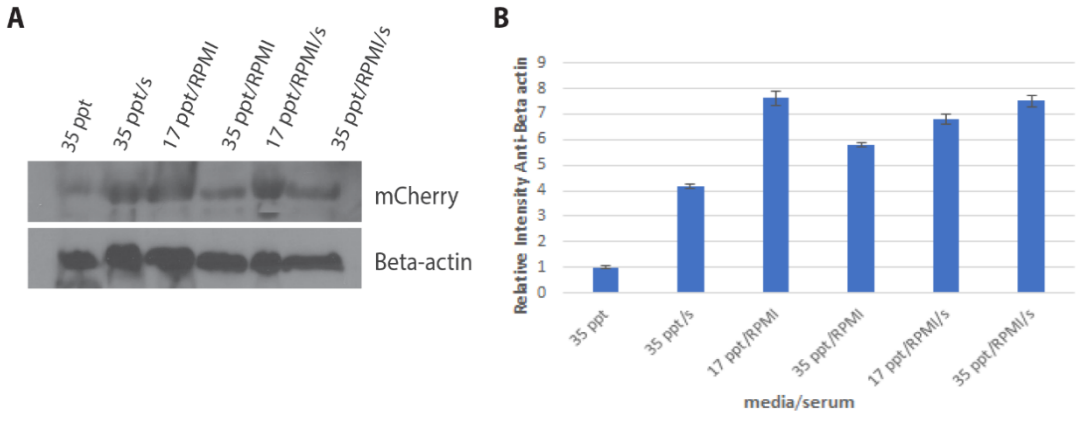

Figure 4.14 Evaluation of CAF2-dTomato *C. albicans* protein within infected embryos under different condition of media/serum and salinity. Western blot analysis of CAF2-dTomato Candida extracted form infected embryos. At 24 hpi, whole 5 killifish embryos lysate per 100 µl SDS were prepared and applied to immunoblot analysis with antibodies mCherry and polyclonal. The mCherry antibody was used to determine the amounts of protein were expressed. The expression was increased with samples that RPMI/serum was used. (E) The histogram displays the signal intensity of CAF-dTomato protein band in *A. dispar* embryos after normalization with the Beta-actin signal intensity for each sample. Molecular weight of mCherry= 28.8 KDa.

Adhesion of wild-type and mutants of *C. albicans* (*mnt1-mnt2*Δ, *och1*Δ *and pmr1*Δ) to eggs was also examined. Eggs incubated in sea water and Candida showed relatively little growth. Eggs co-incubated with the mutants in 17 ppt / RPMI or 35 ppt/serum at 37.0°C with shaking at 80 rpm for 4 h supported growth. Figure 4.15 shows that the deletion of *O*-and *N*-mannosylation from the cell wall of *C. albicans* lead to a decrease in the adhesion of *mnt1-mnt2*Δ and *och1*Δ, while the *pmr1*Δ mutant was relatively similar to the wild-type. In all cases, there was considerable growth of *C. albicans* on the surface of the chorion 24 h after inoculation.

These data indicate that *C. albicans* cells can infect *A. dispar* embryo at the surface of chorion and grow to a greater or lesser extent depending on the nutritional conditions and the salinity of the seawater.

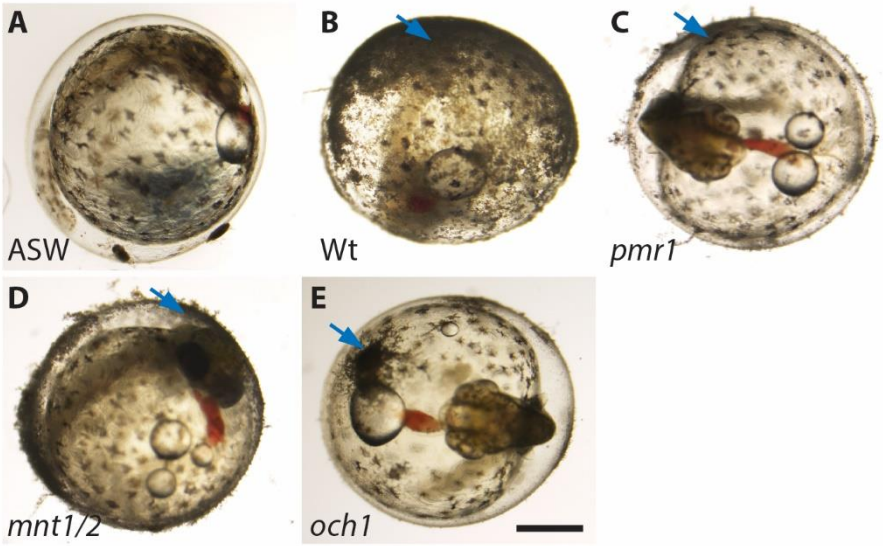

Figure 4.15 Localization of *NGY152*, *och1*Δ, *mnt1-mnt2*Δ and *pmr1*Δ of *C. albicans* cells in the infected *A. dispar* embryos model. Fish embryos were infected with 5x10^5 cells/ml of *C. albicans* mutants and co-incubated at 37.0°C with shaking at 80 rpm for 4 h. Infected eggs were washed and photographed after additional 24 hp incubation. Arrows indicate adhesion of *C. albicans* cells. Scale bar=500 µm.

4.4.12 *C. albicans* infections in the *A. dispar* are suppressed by fluconazole in a dose and time dependent manner.

The *A. dispar- C. albicans* embryo infection a model was examined after treatment with various doses of Fluconazole (FLC) at 2 and 6 hpi. For the experiments, a series of doses of FLC were used, including 4, 8, 16, 32 and 64 mg/l to establish the optimal concentration for clearing infection from embryos. Drugs were administered by treatment at either 2 or 6 hpi. The *A. dispar* embryo survival data showed that different therapeutic effects occurred at the two-administration times examined (2 hpi and 6 hpi). The greatest reduction of *C. albicans* infection was noticed at the earlier drug delivery time of 2 hpi. As shown in Fig. 4.16 A, the dose applied influenced the survival rate. The lowest levels of embryo survival were obtained at 4 and 8 mg/l of FLC. In contrast, at the highest doses of FLC, including 32 and 64 mg/l, the highest levels of protection in the infected embryos was

seen. A concentration of 16 mg/l also showed a good level of embryo survival.

When comparing the effect of drug doses on survival at 50 hpi (Fig. 4.16), it was found that approximately 40% of infected embryos survived with a concentration of 4 mg/l, whereas more than 60% of the embryos survived with a concentration of 16 mg/l at the same time of observation. It was notable that with the administration of 32 mg/l of FLC,～ 75% survival of embryos was observed at 50 hpi. In the case of the highest doses of 32 and 64 mg/l, the results demonstrated that the FLC protected the embryos from Candida infection, starting from 24 by 90% and 95% respectively. As shown in Figure 4.16, between the time of 100 hpi and the end of the observation period there was stability in the survival rate of treated embryos within most of the concentrations of FLC. A control group (uninfected embryos) and the other control group that received 5 nl phosphate buffer saline (PBS) showed 100% and 98% survival respectively.

Further evaluations were made to evaluate the effect of diluted concentrations of FLC on survival rate at 6 hpi. As seen in Fig. 4.16 B, the results demonstrated that the survival rate could be influenced by dosages for all doses with drug delivery time of 6 hours post infection. With both low concentrations of 4 and 8 mg/l, the survival rate continued to decrease until reaching the lowest level at hatching time, whereas, when the influence of a dose-effect of 16 mg/l of FLC at 50 hpi and 100 hpi, was observed, it was found that the survival rate increased by 58% and 35% respectively.

The effect of high doses of FLC on the survival rate was examined at 32 and 64 mg/l. At 50 hpi it was found that a concentration of 64 mg/l of FLC the rate of survived embryos was about 75% whereas about 67% of infected embryos were survived at 32 mg/l of FLC. At 100 hpi and it was observed that the survival rate of embryos was around 43% within dose of 32 mg/l FLC whereas around 43% of survived embryos was recorded within dose of 64 mg/l of FLC. These rates then continued until the end of observation time. Our observations indicated that approximately 27.5% of infected embryos that were untreated (control) could survive at 50 hpi while by 100 hpi they have decreased to 0% survival. Moreover, to exclude the possibility of mortality arising from injury associated with injection, embryos

were microinjected with PBS and the result showed that embryos continued to survive until hatching day.

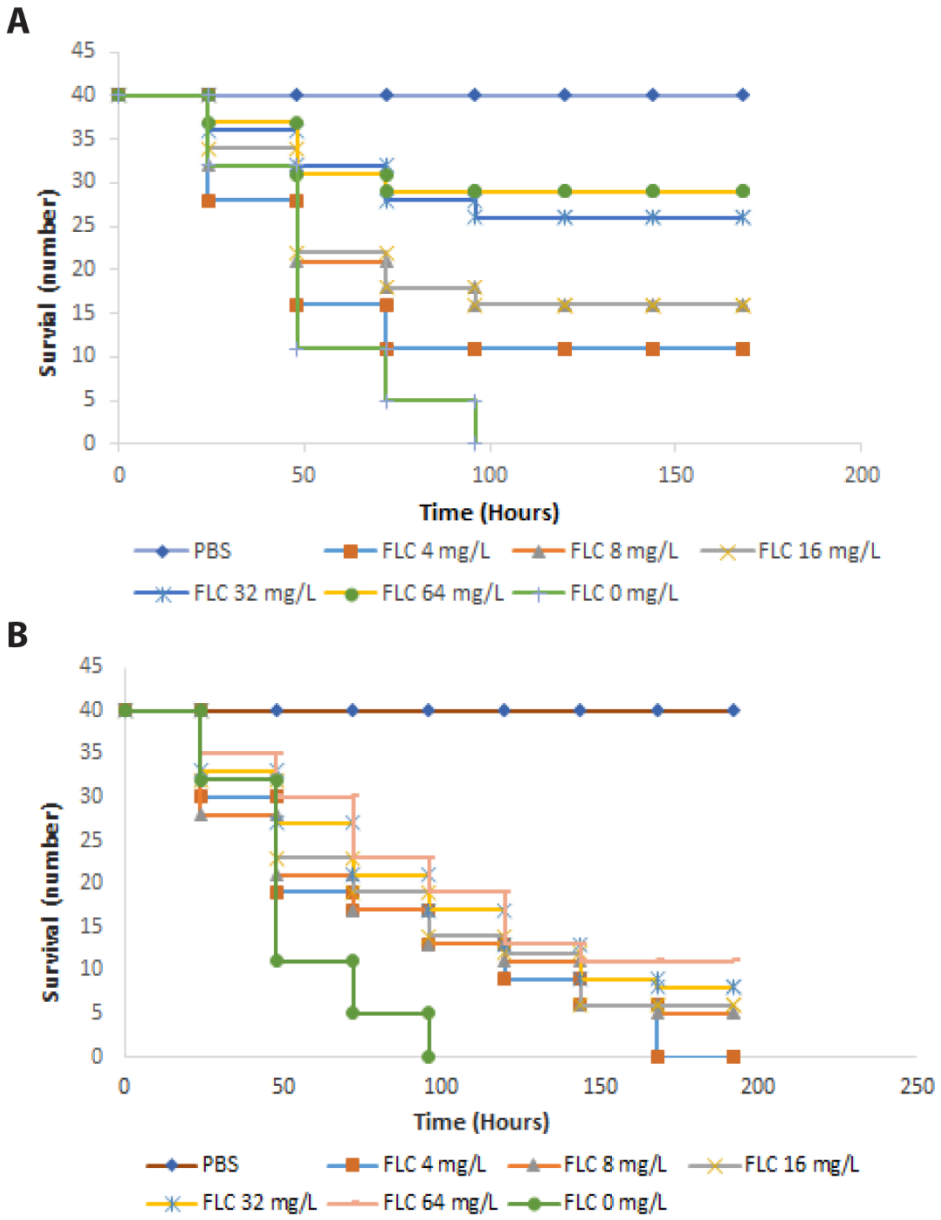

Figure 4.16 The Protective Role of FLC with different doses against *C. albicans* Strains in the *A. dispar* Infection Model. Fish embryos were infected with $1x10^8$ cells/ml of Candida. Forty embryos in each group were monitored; embryos injected with PBS remained alive. The antifungal drug was delivered to the embryos (A) 2 hpi, (B) 6 hpi with different doses.

4.4.13 Effect of fluconazole on the number of CFU of *C. albicans* within *A. dispar* embryos

On the basis of the above experiments, two doses of FLC were chosen as suitable concentrations for evaluation of the fungal burden within *A. dispar* embryos. Fluconazole at 16 and 32 mg/l significantly protected the embryos from the Candida infection ($p<0.001$). In the range of the doses of FLC tested the FLC protected the embryos in a dose-dependent manner. The effect of the FLC on the diminution of fungal burdens was evaluated in the *A. dispar* embryos (Fig 4.17 A) with results showing that the CFU obtained from the infected embryos at 2 hpi was suppressed in accordance with the data for the survival rates. After 48 hpi, embryos infected with *C. albicans* demonstrated a reduction in Candida CFU. In addition, the results indicated a significant decrease ($p<0.05$) in the fungal burden at both FLC doses of 16 and 32 mg/l until hatching at 168 hpi. In the case of a later antifungal administration time (6 hpi), Fig. 4.17 B the result for CFU obtained from the infected embryos both concentrations suppressed *C. albicans* growth within *A. dispar,* resulting in a reduction of fungal growth, especially at 96-168 hpi. CFU numbers were highest at 24 hpi after infection, except for the infected embryos at 32 mg/l at 2 hpi. The data for administration of drug treatments at 6 hpi demonstrated the highest fungal burden at 48 hpi and the number of CFU in the control at 72 hpi.

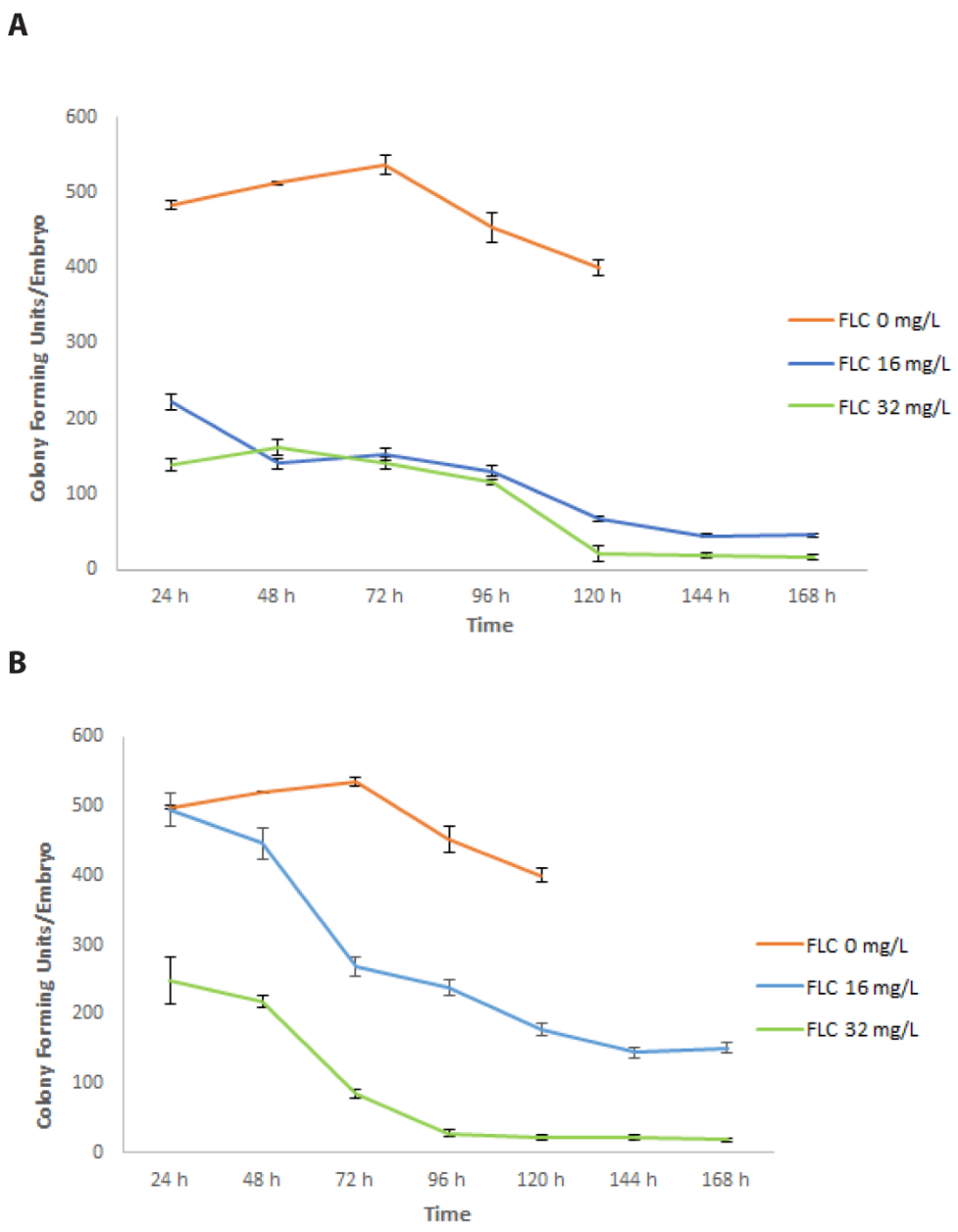

Figure 4.17 Fungal burden during *A. dispar* infected with *C. albicans*. CFUs of fish embryos were infected with $1x10^8$ cells/ml of *C. albicans*, embryos were treated with 16 mg/l, 32 mg/L of fluconazole at different times (A) 2 hpi, (B) at 6 hpi.

4.5 Discussion

4.5.1 Utility of *A. dispar* as a model

During the last twenty years, Zebrafish have been used as an excellent model for infection studies (Sohnle and Hahn, 2002). However, there are limitations in using zebrafish as a model because the fish embryos cannot survive at 37°C. Recently, it has been discovered that *A. dispar* is able to live within a wide range of temperatures, including 37°C. In this study, *A. dispar* embryos were exploited as a novel model for the investigation of the pathogenicity of *C. albicans* in a live host at human body temperature. Secondly, since *A. dispar* has a good optical transparency, this makes it an excellent vertebrate model for *in vivo* imaging which allows us to monitor *C. albicans* infection.

The data presented in this chapter demonstrated that *A. dispar* embryos can be infected via injection at different stages of embryonic development and via direct exposure to inoculum in egg water. After testing a range of inocula, *C. albicans* was found to kill *A. dispar* embryos in a dose-dependent manner. After being infected within *Candida* ($1x10^8$ cells/ml) *A dispar* embryos survived for 120 hpi at 37.0°C, whereas other species, such as *G. mellonella* larvae, all die at $1x10^6$ cells/ml (5 µl volume) within 48 hpi; and none of the Zebrafish survived for >50 hpi at $1x10^8$ cells/ml at 30.0°C (Chao *et al*., 2010; Li *et al.,* 2013). Furthermore, after injection, the data in this study indicated that at low concentrations of *Candida* ($3x10^7$ and $6x10^7$ cells/ml), the fungal burden in the surviving embryos dropped precipitously. Indeed, the fungal burden of the surviving embryos demonstrated that they were clear of infection, with embryos continuing to survive for 96 hpi and 120 hpi.

Adherence is the first step taken by a pathogen to invade host tissue. In this study, *A. dispar* eggs were examined in different conditions (co-incubation with wild-type and mutants of *C. albicans* at $5x10^5$ cells/ml in 4 ml 17 ppt ASW and 35 ppt ASW/RPMI, and 17 or 35 ppt ASW/serum at 37°C for 4 h) to evaluate the localization of *C. albicans* grown at 37°C. To mimic the condition of bloodstream infections in the human, RPMI/serum and shaking at 80 rpm was conducted (Gratacap *et al.,* 2013). The *C. albicans* visible

growth and growth rate on infected eggs was evaluated in the *A. dispar* model with various mutants of Candida*,* defective in key virulence determinants.

Avoidance of the immune system by a pathogen may lead to its dissemination to new sites in the body (Yang, 2003). Observations in this study showed that deletion of *O*-and *N*-mannan of the *C. albicans* cell wall (key virulence factors) affected both adhesion and hypha formation, so that there was no lethality detected among the embryos. This result leads to the proposal that the capabilities of Candida to adhere and to form biofilms are critical during co-incubation (Chen *et al*., 2015).

In general, the induction of morphological changes (yeast to hyphae) at 37°C is fundamental for virulence. Stimuli, such as serum, can be essential to causing full virulence (Chen *et al.,* 2015). The current data showed that the hyphal form of *C. albicans* was observed on the chorion of the eggs within the co-incubated egg water and serum, and it increased with RPMI/serum at 37.0°C. This result seems to be in agreement with many previous findings, such as those of Weerasekera *et al.* (2016) and Kucharrkova *et al.*, (2011) who have reported that the RPMI 1640 enhanced biofilm formation by heightening the yeast-to-hypha transition in *C. albicans.* Chen *et al.,* (2015) also showed that the incubation of Zebrafish eggs with RPMI/serum and *C. albicans* enhanced formation of hyphae.

When growth of *C. albicans* was evaluated in different media (17, 35 ppt ASW/RPMI and 17, 35 ppt ASW/RPMI serum) the results showed that *C. albicans* can grow in both of these media and that under these conditions *C. albicans* is tolerant to the salt. This observation is supported by the results of Krauke and Sychrova (2010) who reported that *C. albicans* is more tolerant of salt than other species, such as *C. glabrata.* However, images of *C. albicans* on the chorion and levels of marker proteins (dTomato detecting by western blotting) showed that there was some delay in the growth of *C. albicans*, even at 35 ppt ASW, and this result agrees with the findings of Krauke and Sychrova (2010), who found that using 500 mM NaCl resulted in a 20% delay to the beginning of the exponential phase of *C. albicans* growth.

Further experiments were designed to evaluate the suitability of using *A. dispar* as a model host for Candida infections in comparison to other models. Our results showed that zebrafish embryos started to die at 48 hpi, but all died by 72 hpi following CAF2-dTomato Candida infection. This result agrees with the study of Chao *et al,* (2010), which found that the zebrafish embryos survived for 48 hpi, but none of the zebrafish infected with same Candida concentration we tested survived for >50 hpi. In contrast, *A. dispar* embryos survived to 144 hpi at 30.0°C. It is possible that temperature not only affects the transition of Candida forms in the host, but also the physiology of *A. dispar* influencing infection outcomes.

Endothermy is a characteristic of the mammalian host (36.8 ±4°C) and mice (36.0 to 37.0°C), while the ideal temperature for growth of a ectotherm such as Zebrafish is only 28.0°C (Chao *et al.,* 2010). However, we have shown that *A. dispar* is a satisfactory model for evaluating Candida growth at 37.0°C and higher temperatures. This study was designed to exploit *A. dispar* embryos and eggs to provide non-invasive imaging of Candida morphological transitions at human body temperature its natural host.

Previous studies reveal that temperature is an essential determinant of Candida growth and pathogenicity (Mayer *et al*., 2013). In terms of environmental temperatures, a high temperature of 37°C induces Candida to transit to the hyphal form but at the lower temperature of 30°C to stays in the yeast form (Chao *et al.,* 2010; Lee *et al*., 1975). Such transition cannot be studied in zebrafish since the embryos cannot survive at this high temperature. Therefore, in the present study we have developed *A. dispar*, that can survive well at 37°C, as an alternative model to investigate host pathogen interaction at human body temperature. When *A. dispar* embryos were infected with *C. albicans* and incubated at 26.0, 30.0, 34.0, 37.0 and 38.5°C the highest Candida burden was observed at 30.0°C, this result suggests that Candida growth at 30.0°C is probably greater than the growth rate at 37.0°C (Antley and Hazen, 1988), however mortality of embryos was greatest at 37°C. Importantly, higher temperatures enhanced yeast-hyphae switching. The influence of higher temperatures on fish immunity is connected to resistance to fungal infection (Avtalin and Clem, 2009; Brothers *et al.,* 2011; Fuchs and Mylonakis, 2006).

In the case of higher temperatures, normally associated with fever, wild-type *C. albicans* growth was lower at 40°C compared to 37°C. This finding agrees with earlier results of Lowman *et al.,* (2012). The reduction of growth rate at 40.0°C may be attributable to the influence of temperature on the structural complexity of the cell wall (eg. mannan) on cultures at a higher temperature.

Histological and immunofluorescence analyses revealed that *C. albicans* disseminated from the infected site of the embryo, producing filamentous cells within the infected tissues at both 30°C and 37°C, but much higher levels at 37°C.

Use of western blots to detect pathogen specific proteins in homogenized tissues or extracts allows the monitoring of the progression of an infection. The levels of GFP and CAF2 dTomato Candida protein were easily assessed using western blotting experiments, revealing protein expression at 24 hpi in the yolk of both *D. rerio* and *A. dispar.*

It is notable that the use of *Zebrafish* for the study of human diseases, such as infection with *C. albicans,* is rapidly increasing. (Brothers *et al.,* 2011; Teresa *et al.,* 2010; Ingham, 2009) however zebrafish cannot be used at 37°C. Compared to other vertebrate models, *A. dispar* can therefore be recommended as a novel alternative to mammals in the study of fungal infections of *C. albicans* at 37°C. At 37.0˚C *A. dispar* embryos develop blood vessels and immune cells in the yolk before the muscles and tail develop.

4.5.2 Utility of *A. dispar* as a model to screen mutants

The *C. albicans* cell wall plays an important role in the maintenance of the cells, their division, and expansion, as well as being essential for its virulence (Hall and Gow, 2013). Many studies have argued that the *C. albicans* cell wall is an important dynamic structure for the protection and maintenance of fungal cells. It has a physically robust structure, and it is also sufficiently flexible to allow expansion and morphogenesis (Mora-Montes *et al.*, 2010). Glycosylated proteins are located in the outer layer of the fungal cell wall. Deletion of mannan from the cell wall results in different

phenotypic characteristics, such as diminished growth rate, an increased sensitivity to temperature, flocculation and morphological change; and a decreased capacity to activate immune cells and (Hall and Gow, 2013). Deletion of *och1*Δ results in the absence of outer chain alpha-1-6 mannose backbone elongation (Bates *et al.,* 2006; Netea *et al.,* 2006). In the present study, in terms of an *N*-mannosylation defect (*och1*Δ*)*, our results demonstrated that there was a clear attenuation of virulence as a result of a reduction in adherence. Previous studies have suggested that mannan behaves as a ligand on the host surface (Bates *et al.,* 2006; Munro *et al.,* 2005; Hall and Gow, 2013). The fungal burden of *och1*Δ in *A. dispar* reduced dramatically at 24, 48 and 72 hpi and all embryos survived until the end of experiment. The results indicate that there was no tissue colonization, suggesting that clearance occurred because of the alteration of the host-fungal interaction (adhesion), and also because the cellular aggregation phenotype of *och1*Δ resulted in a defective growth rate (Bates *et al.,* 2006).

Disruption of mannosylated proteins, through a deletion of *PMR1* (*pmr1*Δ), results in an abnormal cell shape, reduced mannan content of the cell wall and increased duplication rates (Bates *et al.,* 2006; Navarro-Arias *et al.,* 2016; Hall and Gow, 2013). The resulting defect in *O*-linked and *N*-linked mannans significantly affects the immunostimulatory response and recognition of fungal cells and thus their uptake by immune cells (McKenzie *et al*., 2010). In the case of the *pmr1*Δ mutant in the *A. dispar* model, there was a significant reduction of the fungal burden within infected embryos at 72 hpi compared with the fungal burden of the wild-type strain. This result is partially supported by a previous study, where a high attenuation of the virulence of *pmr1*Δ was seen in a mouse model (Bates *et al.,* 2005). However, the survival of *A. dispar* embryos was decreased; therefore, we hypothesize that as the *O*-and *N*-mannan were deleted from the cell wall of *C. albicans,* its ability to cause disease in the host would be altered. To further test this hypothesis, *A. dispar* embryos were injected into the yolk with *pmr1*Δ and *mnt1-mnt2*Δ mutants of Candida to examine the differences in the host-pathogen interaction compared with the control. Looking at CFU numbers in infected embryos we observed that *pmr1*Δ and *mnt1-mnt2*Δ

showed slower increases in fungal burden compared to the reintegrated control strains (*pmr1* with URA3 reintegrated at RPS10 with Clp10). The present data indicated that it would be easy to use *A. dispar* to identify the differences between glycosylation mutants in response to the host. The morphological change and delay in the growth rate resulted from truncation of the cell wall *O*-and *N* -linked mannan (Castillo *et al.,* 2011; Munro *et al.*, 2005) could also be investigated.

Our data also demonstrated that the *C. albicans pmr1*Δ and *mnt1-mnt2*Δ mutants displayed an increase in the rate of mortality of infected embryos at 48-96 hpi. It is possible that the defect in *N*- and *O*-mannosylation influences the rate of uptake of Candida cells by phagocytic cells. This suggestion can be supported by a previous study of McKenzie *et al.* (2010) who mentioned that a lack of cell wall mannan decreases phagocytosis in mice. In addition, studies of *C. albicans* and *C. guilliermondii*, in a different model (*Galleria mellonella* larvae) by Bates *et al.,* (2005), indicated that the defect in *N*- and *O*-mannosylation had the same effect. Moreover, Murciano *et al.* (2011) indicated that the mannan-deficiency in the cell wall of *C. albicans* affects the induction of proinflammatory cytokines in epithelial cells due to the absence of mannose residues on hyphae activating a MAPK or MKP1 mediated immune response. Both the outer and inner layer of the cell wall are required to stimulate high levels of pro-inflammatory cytokines, and thus, macrophage behaviour and phagocytosis (Netea *et al.,* 2006; Cambi *et al.*, 2008; McKenzie *et al.,* 2010). In the next chapter the interaction of Candida cells with the immune system of *A. dispar* will be examined in further detail.

4.5.3 *A. dispar* as a model to investigate antifungal drug therapy

A. dispar was tested as a model to evaluate antifungal efficacy and potential to be used in drug screens. Treatment with fluconazole (FLC) had a positive effect on the survival of infected embryos. Furthermore, the data demonstrated that the effect of FLC on the numbers of CFU and the mortality of the embryos was dependent upon the time of inoculation and the dose of fluconazole applied. *A. dispar* therefore seems to be useful

model for studying the effects of FLC, and potentially other antifungal drugs on the viability of *C. albicans* cells *in vivo*.

It should be considered that some mortality and increased numbers of CFU were observed between the 24 and 100 hpi at doses of 16 and 32 mg/l. The present study clearly demonstrated that FLC displayed a greater activity against *C. albicans* in infected embryos at the highest concentrations of FLC tested (32 mg/l and 64 mg/l) even at 6 hpi, showing both a reduced number of CFUs and the continued survival of embryos at subsequent times.

Survival rates of embryos at all concentrations of drug were evaluated at two different times of drug administration – 2 hpi and 6 hpi. In spite of a high fungal burden at 24 hpi within embryos treated at 6 hpi, FLC was also efficient.

A possible explanation for the significant reduction in the fungal burden under both conditions (2 hpi and 6 hpi) after 24 h incubation is that after a few hours of treatment with FLC, the drug begins to diffuse all over the body, thus causing a decrease in the fungal burden. At 96 hpi there was a significant difference between the fungal burden of *C. albicans* within embryos that were treated with fluconazole at 6 hpi and those that were treated at 2 hpi.

Apart from monitoring survival *per se*, *A. dispar* has the advantage that it can also be used to study the effect of FLC treatment on the dissemination of *C. albicans* throughout a host as the embryos are transparent and the recruitment of immune cells during treatment could also be assessed.

In conclusion, many animal models have been used in fungal infection studies as test beds for antifungal efficiency / susceptibility (mice, zebrafish, *G. mellonella*, *Drosophila* and *C.elegans* - Cacciapuoti *et al*., 1992; Li *et al.,* 2013; Sohnle and Hahn, 2002). Whilst zebrafish have recently been considered as an excellent model for infection studies because of the transparency of their embryos and the availability of many transgenic and mutant lines, there are limitations since the fish embryos cannot survive at 37°C. *A. dispar* therefore stands out, as it allows studies to be conducted at a wide range of temperatures (normal and pyrexic) and the transparency of the embryos facilitates direct monitoring of both the pathogen and host

immune cells as infections develop. In addition, *A. dispar* seems to be more resistant to *C. albicans* than zebrafish.

Based on these results, further work was therefore undertaken to investigate host-pathogen interactions and analyse innate immune responses following invasive Candida infections using the *A. dispar* embryo whole animal model system – see Chapter 5.

Chapter 5

Infection and the immune response of *A. dispar* embryos

5.1 Abstract

In this chapter we explore the immune response of *A. dispar* embryos towards *Candida albicans* infections. In *A. dispar*, embryo movement is only initiated at the late organogenesis stage (45.5-57.5 hpf) which allows direct injection of pathogens into the embryo without anaesthesia at early stage of development when the innate immune system is active. The transparent nature of the embryos allows visualisation of immune cells in real time. Macrophages and microglia were visualised by whole-mount immunofluorescence staining with L-plastin and 4C4 antibodies. Neutrophils were visualised by Sudan Black staining. Following infection of *A. dispar,* dissemination of the pathogen is observed, accompanied by a yeast-hyphae transition. Phagocytosed yeast cells were observed within macrophages. Loss of macrophages induced by MO injection for *irf8* or *cxcr4* was accompanied by an increase in virulence of *C. albicans* suggesting a crucial role of the macrophage in protecting the host from the Candida infection.

In the immune system, Reactive Oxygen Species (ROS) play a protective role against pathogens. In the present study, ROS were assessed in the *A. dispar* embryo using a redox indicator 2', 7'- dichlorofluorescein (H_2DCFDA)/ DCFDA. The accumulated fluorescent probe indicative of ROS was observed at the site of infection (trunk) and in the tail fin at 30 mpi.

Quantitative and qualitative analyses of the immune response were accomplished within *A. dispar* embryos after infection with the WT and mutant strains of *C. albicans* (WT, *pmr1*Δ*, mnt1-mnt2*Δ*, and och1*Δ). After infection with the WT, ROS levels increased at the site of infection. Moreover, ROS levels increased as the infection progressed. Mutants of *C. albicans* had lower levels of induction of ROS, suggesting that mannan in the cell wall plays a key role in the immune response.

To monitor host-pathogen interaction, a new transgenic fish line of *A. dispar* was developed using a transgenic plasmid vector, beta-actin-DsRed-LoxP-GFP. This would be the first transgenic fish generated in this fish species. Using this novel fish line, it is possible to visualise behaviour of immune cells and to examine host-pathogen interaction at human body temperature in live embryos. It is therefore expected that these species should be utilised as a novel model in future studies in a range of applications. The outcomes of this study will help us to investigate and assess the role of macrophages and neutrophils during infection.

5.2 Introduction

The immune response is a robust line of defence that is required to protect tissues against superficial and systemic candidiasis (Jacobsen *et al*., 2008). A slight alteration in the host's physiology can turn the morphology of *C. albicans* from harmless to a more aggressive pathogenicity (Naglik *et al.,* 2004).

The common fungal pathogen, *C. albicans,* is a human commensal, and grows in both yeast and hyphal forms during infection. Whilst it can invade tissues by inducing endocytosis and by active penetration, dissemination of candidiasis is limited by innate immunity (Chao *et al.,* 2010). The immune system, responds rapidly to combat infections by altering populations of key phagocytic cells. Macrophages and neutrophils are the major effector cells that reside in host tissues and organs and attempt to damage or kill invading fungi by phagocytosis. The antifungal effector cells release antimicrobials, such as ROS, or secrete inflammatory signals, such as cytokines and chemokines, which are required to recruit additional immune response cells to the site of infection. Macrophages and neutrophils are in many ways the first line of defence, and they kill the fungus with a variety of potent chemicals, such as ROS, which are produced by means of an NADPH oxidase complex (Torraca *et al.,* 2014).

Three essential mechanisms mediate immune defence: an antimicrobial peptide; recognition of foreign microbes by the component system; and immune response to microbes (Duhring *et al*., 2015; Peter *et al*., 2011).

Immune recognition of fungi is achieved by phagocytosis through detection of the cell wall constituents, such as carbohydrate polymers and proteins.

The *C. albicans* cell wall is the first point of contact with the innate immune cells, and therefore plays an important role in the pathogen's interaction with the host immune system. The polysaccharide core of the fungal cell wall is highly immunogenic, resulting in rapid recognition by cells of the innate immune system, especially neutrophils and macrophages (McKenzie *et al.,* 2010). Carbohydrates in the cell wall form a rigid framework, which provides shape and protection. ß-glucan and chitin are the inner meshwork, which is masked by an outer layer of mannosylated proteins. These constituents vary between fungal species, conferring different immunological properties.

The process of immune recognition is important in controlling both the dissemination of the pathogen and reducing tissue damage. Recognition of fungi occurs via several mechanisms requiring both innate and adaptive immunity, such as pathogen-associated molecular patterns (PAMPs), recognized by host pattern recognition receptors (PRRs) (Shoham and Levitz 2005; Naglik, 2014; Duhring *et al*., 2015; Qin *et al*., 2016; da Silva Dantas *et al.,* 2016). PRRs that recognize different cell wall polysaccharides of *C. albicans* (alpha- and beta-glucans) are expressed on the surface of the host cell or in the cytoplasm of macrophages, neutrophils, and dendritic cells. These receptors trigger a variety of intracellular signalling cascades, leading to the production of chemokines, cytokines and inflammatory mediators (Naglik, 2014).

Different groups of PRRs have been shown to contribute to the sensing of microbes, including toll-like receptors (TLRs), C-type lectin receptors (CLRs), nucleotide-binding domain leucine-rich repeat containing receptors (NLRs), and retinoic acid-inducible gene (RlG-I) receptors (RLRs). Among these receptors, TLR1 and CLRs play a fundamental role in the antifungal immune response (Qin *et al*., 2016).

The active detectors of PAMPs reside on and in monocytes and macrophages, contributing to the recognition of Candida by phagocyte receptors. The efficiency of phagocytosis depends on the composition of the cell wall, cell morphology, and the host cell type. To kill extracellular and

intracellular microbes, oxidative and non-oxidative activities are utilized during phagocytosis. These activities are controlled largely by cytokines and different soluble mediators (Selders *et al.,* 2017; Brown, 2011) and they subsequently enhance anti-fungal mechanisms. The mechanism of respiratory burst is one of the important oxidative-anti-fungal processes, in which ROS are produced and act as the most important antifungal defence of phagocytes. This mechanism is mediated by a complex of multi-component proteins, such as NOX expression (phagocyte NADPH oxidase, Phox). ROS production occurs by transferring an electron from cytoplasmic NADPH to O_2^-, leading to the production of a superoxide (Vázquez-Torres and Balish, 1997). Human myeloperoxidase (MPO) is an enzyme that acts as an effective fungicidal oxidant. Antimicrobial oxidants can be produced by generation of hydrogen peroxide during the oxidative burst of neutrophils (Paumann-Page *et al*., 2013). The fungicidal activity of the respiratory burst is generally caused by the toxic effects of ROS. In neutrophils, potassium influxes induced by the respiratory burst and increase in the pH of phagolysosomes, are important for the release of antifungal proteases from neutrophil granules (Emer *et al*., 2002; Brown, 2012).

Reactive nitrogen intermediates (RNI) in phagocytes are induced by nitric oxide synthases (*NOS2*). RNI production is induced via TLRs and cytokine production, which is essential for the control of pathogens (Aguirre and Gibson, 2000). Dynamic changes in neutrophils and macrophage population sizes and the establishment of an appropriate activation state are fundamental to the regulation of the immune response and an effective immune system (Metcalf, 1985). To contain the threat of pathogens during an infection, specific subsets of the population are activated to proliferate robustly and differentiate into populations of effector cells (Fontana *et al.*, 2016). Leukocyte specific proteins that regulate and recruit innate immune cells during infection include csf1r, L-plastin, and cxcr4 (Bennett *et al.,* 2001; Garcia *et al.,* 2016; Angsana *et al.,* 2016). Colony stimulating factor1 (Csf1R) is essential to regulate macrophage defence against microbes (Guleria and Pollard, 2001). Studies, confirmed more than three decades ago, that colony-stimulating factor 1 (Csf1) regulates phagocyte cells via the CSF1 receptor (Csf1R), which is a type III receptor tyrosine kinase. Csf1R

deficiency leads to a failure to recruit monocytes to the sites of infection, resulting in insufficient control of an infection (Guleria and Pollard 2001).

The actin-bundling protein L-plastin is essential for the regulation of cellular polarization, and the function of integrins in both leukocytes and lymphocytes (Freeley *et al.,* 2012; Morley 2012). L-plastin binds to macrophage-specific proteins that may regulate the functional roles of macrophages (Bennett *et al.,* 2001). Chemokines were first linked to the immune system, influencing the accumulation of immune cells (lymphocytes) at inflammatory sites (Raz and Mahabaleshwar, 2009; Baggiolini, 1998). During development and infection, chemokines are considered to play the role of guides in cell migration as mediators of monocyte/macrophage traffic. They are vital to the immune response, as the interaction between chemokines/stromal cell-drived-1 CXCR4/SDF-1 is indispensable to immune defence (Raz and Mahabaleshwar, 2009; Schimd *et al.,* 2004). Chemokines also play a key role in the activation of leukocyte circulation. In this respect, there is therefore a homeostatic balance between monocyte egression into the peripheral blood and the control of retention of monocytes in the bone marrow by *cxcr4* (Wang *et al.,* 2009).

A number of models of infection for studying the immune response to *C. albicans* have been developed. Pathogenicity has been tested in a range of invertebrate models, such as *Galleria mellonella*, *Drosophila melanogaster*, and *Caenorhabditis elegans*. These model organisms are used in large-scale studies because of their low cost and the availability of well-developed molecular tools. However, these mini-hosts have simple immune systems which differ from those in mammals.

On the other hand, mice have been extensively used in fungal research. For instance, genetically modified knockout and transgenic murine models have been used to establish infections of *C. albicans* at a range of sites including the oral cavity, pulmonary system and central nervous systems (CNS) (Samaranayake and Samaranayake, 2001; Allen, 1994; Naglik *et al.,* 2008; Costa *et al*., 2013). Mice have been used to understand host immune responses during Candida infections and to monitor the efficacy of immunosuppressive treaments and antifungal therapies (Costa *et al*., 2013). However, one of the factors limiting the using murine models is that mice

differ in their indigenous fungal flora from humans. Such studies also raise ethical dilemmas and issues of cost.

Recently, the zebrafish has become a powerful model for understanding the interaction of the pathogens and the host immune system. The zebrafish has many similarities to a mammal in terms of its genetics, anatomical structures, and organs. Importantly, it has both innate and adaptive immune systems, (comparable to that of humans) which allows us to study the role of components of the immune defence system against *C. albicans* in real-time (Choa *et al.,* 2010; Brothers *et al.,* 2011). However, a significant problem with the zebrafish model is its inability to survive at the elevated temperatures that are more typical of those encountered by *C. albicans* in a mammalian host.

In this study, I set out to identify normal patterns of immune system development in *A. dispar* embryos, contrasting it with zebrafish to establish its suitability as a model to monitor immune system pathogen interactions in embryos infected with *C. albicans*; and to develop techniques to investigate the interaction of the pathogen with its host. The overall aim of this chapter is therefore to test the feasibility of using Arabian killifish (*A. dispar*) as a model to understand the host-pathogen interaction; to characterize the ability of *A. dispar* to mount an immune defence against *C. albicans*; to test the suitability of this model to detect and trace the immune response and follow the immune function-related gene expression during infections. Finally, we aimed to develop a new line of transgenic fish which is an important step towards performing real-time investigations of the interaction between pathogens and immune cells.

5.3 Experimental procedures

5.3.1 RNA-sequence of *A. dispar* to reveal immune function

Fertilised eggs of *A. dispar* were collected, cleaned and kept in a Petridish with ASW at 26°C. Developmental stages were observed and samples were collected at different stages: St.9 (7 hpf), St. 11 (12 hpf), St.14 (18.5 hpf), St.18-19 (30-32 hpf), St.25-26 (59.5-73.5 hpf) and St.28 (146.5 hpf). Around 10 embryos at each stage were collected in Eppendorf tubes, water was removed and embryos were frozen at -20°C. Total RNA was extracted from fish embryos using Trizol. Next, equal amounts of each RNA samples were mixed and sequenced by the Exeter sequence service (http://sequencing.exeter.ac.uk) with Illumina HiSeq2500 100 bp paired-end reading. The sequencing data was trimmed to remove sequencing adaptors and the low-quality terminal ends (<Q20) and then short sequences were excluded using fastq-mcf v1.1.2-537 26. *De-novo* transcriptome assembly was performed for each of the groups using Trinity v v2.2.0. Immune system related genes: Ad*_ptgs2, mpx, irf8, cxcr4*, *nos1a, L-plastin, mpo, csf1r, nox1* were sought using blastx with the medaka genes as query sequences to identify *A. dispar* orthologs. From the identified *A. dispar* cDNA sequence, qPCR primers were designed using Beacon designer (list of primers supplied in Table 2.4).

5.3.2 Removing the chorion

A. dispar embryos were dechorionated by transferring the eggs to the lid of a Petri dish covered with sandpaper; eggs were rolled for 60 seconds within a sufficient a mount of water to prevent drying. Eggs were then incubated for 1 h with pronase (20 mg/ml) at 28°C. Before washing with ASW to remove traces of the Pronase 5 times, hatching enzyme was added to an equal volume of ASW containing the embryos were incubated for 2-5 h. Embryos were periodically checked to assess the progress of hatching (Porazinski, 2010). After dechorionation, embryos were transferred gently to a fresh dish of ASW (35 ppt).

5.3.3 Survival rates in infected zebrafish embryos

Wild-type and Casper zebrafish (pigment free, White *et al*., 2008) were microinjected with *C. albicans* (NGY152) with $1x10^8$ cells/ml into the yolk and kept at 28°C for 72 hpi; this experiment was performed in triplicate. The mortality rates were observed by monitoring live and dead embryos at constant time points between 6 and 72 hours post-infection.

5.3.4 Sudan Black and tyramide-FITC staining of embryos to reveal neutrophils

A. dispar embryos were dechorionated and injected with CAF2-dTomato *C. albicans* into the brain and trunk and after 24 hpi embryos were fixed in 4 % paraformaldehyde/ HEPES-NaCl, for 2 h at room temperature. Embryos were rinsed in PBS, incubated in Sudan black B (Sigma,199664) (0.03% in 70% ethanol with 0.1% phenol) for 30 min and then washed extensively in 70% ethanol and rehydrated progressively to PBST 0.1% Tween 20. To visualize individual neutrophils, embryos were incubated with 1% KOH and 1% H_2O_2 solution for 15 min at room temperature (Le Guyader et al. 2008). Casper zebrafish and *A. dispar* embryos were fixed at 35 hpf and 5-6 dpf respectively with PFA 4% for overnight and finally fixed with methanol at -20'C. Embryos were washed with PBTx and incubated with tyramide-FITC (1 µl/50 µl) for 30 min. After three washes for 10 min each, the embryos were imaged using a Leica fluorescent microscope (x20 lens).

5.3.5 Immunofluorescence staining

Fish embryos were microinjected with 5 to 10 nl ($1x10^8$ cells/ml) of CAF2-dTomato *C. albicans* either into the yolk of zebrafish (*D. rerio*) and or the yolk, brain, and trunk of *A. dispar*. Phagocytic cells (macrophages) were stained with a rabbit anti-L-plastin primary antibody. (It was a gift from Paul Martin-Bristol University, UK). Infected embryos were rehydrated and rinsed with PBSTx (0.5% Triton in PBS) after fixation with PFA and HEBES. Embryos were permeabilized with proteinase K (2.7 µl/ml) for 15 min at RT and then with 0.24% trypsin in PBS, blocking buffer (1% BSH in 0.5%

PBSTx and 10% Heat Inactivated Fetal Calf Serum (FCS-HI) to minimize nonspecific binding of the antibodies. Embryos were washed again and then incubated with the polyclonal primary antibody (anti L-plastin antibody) 1:500 *v/v* dilution in blocking buffer (10% HI-BS and 1% (*w/v*) bovine serum albumin (BSA) in 0.5% PBSTx) for overnight at room temperature. Next embryos were washed and blocked for 1 h and then incubated with secondary the antibody (Alexa 488 goat-anti-rabbit (Life Technologies A11034) 1:300 *v/v* dilution overnight at 4°C (Jim *et al.,* 2016).

5.3.6 Morpholino knockdown

Morpholino oligonucleotides (Gene Tools) were diluted to 2 ng/nl with water. *A. dispar* eggs were microinjected with 1 nl of the morpholino into the 1 cell stages. For knockdown of macrophages, macrophages and neutrophils, and chemokines respectively; Three morpholinos each were used (*Ad_irf8* Mo: 5' CCCGAGTTTGACATCTTAACAGCGC 3'; *Ad_Cebpa* Mo: 5' CATGGAGAACCTAAAGCCGGGCAT 3' and *Ad_CXCR4* Mo: 5' AAGTCCATCTCTCCCATGTTTAGCT 3').

5.3.7 Western blot analysis of L-plastin expression in infected embryos

A time course of total protein samples was extracted from infected embryos following infection. This protein was used to measure the concentration of L-plastin protein as marker for macrophages (Bennett *et al.,* 2001). 30 µl of protein was loaded on an NuPAGE gel (acrylamide 4%~12% Bis-Tris pH 7-7.5 - NP 0335BOX, Invitrogen) along with 7 µl of pre-stained protein standard ladder (SeeBlue® Plus2 Protein Standard) (Thermo Fisher). The gel was run and the protein was transferred to the PVDF (Bio-RAD) cellulose membrane at 120 V for 2 hours. Membranes were blocked with 10% skim- milk for 2 hours, probed with 2:5000 rabbit polyclonal anti-L-plastin antibody for overnight at 4°C. After that 10 min washes with PBSTw, polyclonal goat anti-rabbit immunoglobulin HRS DAKO) was used to hybridize to the primary antibody (1:5000) for 2 hours at room temperature. After that 10 min washes with PBSTw, the membrane was treated with ECL

western blotting substrate (Thermo Scientific) reagent and then exposed to the auto radiography film (Thermo Scientific).

5.3.8 Time-lapse fluorescent imaging of *A. dispar* embryos

Time-lapse fluorescent images were obtained with an inverted Zeiss fluorescent microscope (Zeiss AxioObserver.Z1-AX10) and Leica confocal laser microscope (LSM 510). Videos were recorded for 1 h at 1 frame/min. *A. dispar* embryos were imaged for 30 minutes post-infection in the yolk after infection with *C. albicans* CAF2-dTomato. Embryos were embedded in 1% low melting agarose which has been dissolved in ASW in a glass bottom Petri dish. Images were acquired at 1 min intervals for 1 h immediately after microinjection. To process the Time-lapse image (brightness/ contrast and enhancement), image j and Photoshop were used.

5.3.9 RT-PCR

5.3.9.1 RNA isolation, cDNA synthesis, and expression assay

Total RNA was extracted from infected and uninfected *A. dispar* embryos using 1 ml of Trizol reagent (TRI, Sigma T9424) per 10 embryos. Isolated RNA was purified. A cDNA library was synthesized using 1 µl random hexamer primers (Promega C118A) for each reaction and incubated for 5 min at 70°C. Reactions were directly cooled on ice for 2 min to prevent secondary structures from reforming. Next, M-MLV 5x reaction buffer (5 µl), 10 mM dNTP mix (2 µl) Promega U151A. M-MLV reverse transcriptase (1 µl at 200 units/µl) Promega M170A and water (5 µl) were added and then incubated 37°C for 60 min. Finally, cDNA samples were stored at -20°C.

5.3.9.2 Primer design

Primers were designed manually using Beacon designer software (http://www.premierbiosoft.com/molecular_beacons/hrm.html).

The parameters to design the primers for use in the SYBR green qPCR system are:

Table 5.3.9.2 Parameters for primer design

Parameter name	Parameter ratio
Primer length	18-25 bp
Amplicon length	80-150 bp
GC content	45-55%
Max self-complementary	3
Primer Tm	59-62°C
Self-complementary	1

5.3.9.3 Primer optimisation

After designing the primers and selecting reference genes, cDNA was diluted 1:10 and added to the PCR reaction (2x SYBR green mix 7.5 µl, 0.375 µl of sense and antisense primer (10 µM), 0.75 µl of cDNA (1:10) and 6.0 µl water were added). The reaction was pipetted (15 µl) in to each well of a PCR plate, then the plate was tightly sealed and spun to remove any air bubbles and collect the liquid. The PCR cycling conditions comprised 15 min polymerase activation at 95°C, and 40 cycles of 95°C for 10 sec, annealing temperatures Ta for 20 sec.

Post amplification, Ct values for different Ta on the gradient were compared and then the highest Ta with the longest threshold cycle Ct (stable and consistent amplification) for each assay was selected.

5.3.9.4 Amplification efficacy and primers specificity

When the linearity and efficiency of the qPCR reaction were optimised, cDNA from infected embryos with different mutants of *C. albicans* and uninfected samples were tested. To test the PCRs, a 5-fold serial dilution of a cDNA sample mixture was used and total of 5 dilutions (5, 25, 50, 125, 625 x) were assessed. PCR reactions were performed by mixing 2x SYBR green mix (7.5 µl), 0.375 µl of each sense and antisense primer (10 µM) and 6.0 µl water. A total of 14.3 µl of the mixture was added to the required wells and then 0.75 µl of cDNA was added. The PCR plate was sealed spun, and then set up under the following PCR condition:

95°C for 15 min, 40 cycles of 95°C for 10 sec, Ta for 20 sec, melt curve 95°C for 1 min, 55°C for 1 min (100 cycles for 10 sec beginning at 50°C). Post amplification, the software plotted a standard curve mean threshold cycle (Ct) against log cDNA dilution.

The ideal range for the qPCR slope on the standard curve and Ct (R^2> 0.99) along with single peak in melt curve analysis was selected depending on the strength of the relationship between the primers and concentration of target cDNA.

5.3.9.5 qPCR quantification of *A. dispar* samples

Samples were assayed in triplicate, firstly, cDNA was diluted 1:2 by reducing the volume of water that was added to the master mix and double volume of cDNA. PCR amplification was carried using 2x SYBR green mix (7.5 µl), 0.375 µl of each sense and antisense primer (10 µM) and water 5.25. The volume of mixture 13.5 µl was added to the wells and then 1.5 µl of cDNA (1: 5) and NTC (water).

The PCR conditions were 95°C for 15 min, 40 cycles of 95°C for 10 sec,Ta for 10 sec, melt curve conditions were; 95°C for 1 min, 55°C for 1 min, 100 cycles each for 10 Sec starting at 50°C.

5.3.9.6 Data analysis

Efficiency-corrected relative gene expression levels were calculated using the ΔΔ Ct method (Livak and Schmittgen, 2001).

5.3.9.7 ROS detection

A. dispar embryos were microinjected with the PBS, WT or mutants of *C. albicans (pmr1Δ, mnt1-mnt2*Δ and *och1Δ)*. After injection, embryos were collected and 6 embryos were combined in each tube were and rinsed with 1x HBSS buffer. ROS detecting solution was prepared by adding 10 µl of 20 mM H_2DCFDA (abcam113851) to 10 ml of 1x HBSS buffer then 500 µl of the reagent was added to the embryo samples which were then and incubated in the dark for 30 min at 37°C. Immediately, after the end of the

incubation time, embryos were washed twice with 1x HBSS buffer. Embryos were imaged using Leica microscope SE37213. To quantitatively analyse the ROS levels after infection, a microplate reader assay was used by adding treated embryos to wells of a 96 well-plate and cover it by 100 µl of 1x HBSS buffer. The fluorescence intensity was read at (Ex/Em=485/535 nm) and ROS levels expressed as a percentage of the control after background subtraction.

5.3.10 Production of transgenic *A. dispar*

Freshly fertilized *A. dispar* eggs at the one cell stage were collected for microinjection. Eggs were placed in a Petri plate containing ''Channel gels'' made by leaving 10% agarose/sea water set with imprints of 1.2 mm diameter glass tubes. Eggs were rotated using forceps and then using an injector (Pneumatic picopump pv820). Eggs were microinjected with 1 -2 nl of 25 ng/µl a Beta-actin-DsR-LoxP-GFP plasmid (Yoshinari *et al*., 2012), 25 ng/µl of transposase (TPase) mRNA, with a 1/20 dilution of a phenol red solution 10% (Sigma) for visualization. Embryos were then transferred to a new Petri dish with ASW (35 ppt) and incubated at 26˚C. The embryos showing some red-fluorescence (as a mosaic) were selected at around stage 24 (54.5 hpf) to stage 32 (320 hpf) and raised for further breeding.

5.4 Results:

5.4.1 Analysis of total RNA of *A. dispar*

Neither a reference genome sequence nor cDNA sequence for *A. dispar* were available at the start of this project. Therefore, to obtain cDNA sequence information to identify genes linked with immune functions; total RNA from *A. dispar* embryos was prepared and sent to the Exeter sequencing service. Total RNA of *A. dispar* at different stages (St. 9, 10-11, 14, 18-19, 25-26 and 28) was isolated (Fig. 5.1 A). All samples showed high integrity (RIN>8.0), suggesting that the quality of the RNAs was good for RNA-Seq analyses and samples were therefore analysed using the next generation sequencer, illumina Hiseq 2500 (Fig. 5.1 B and C).

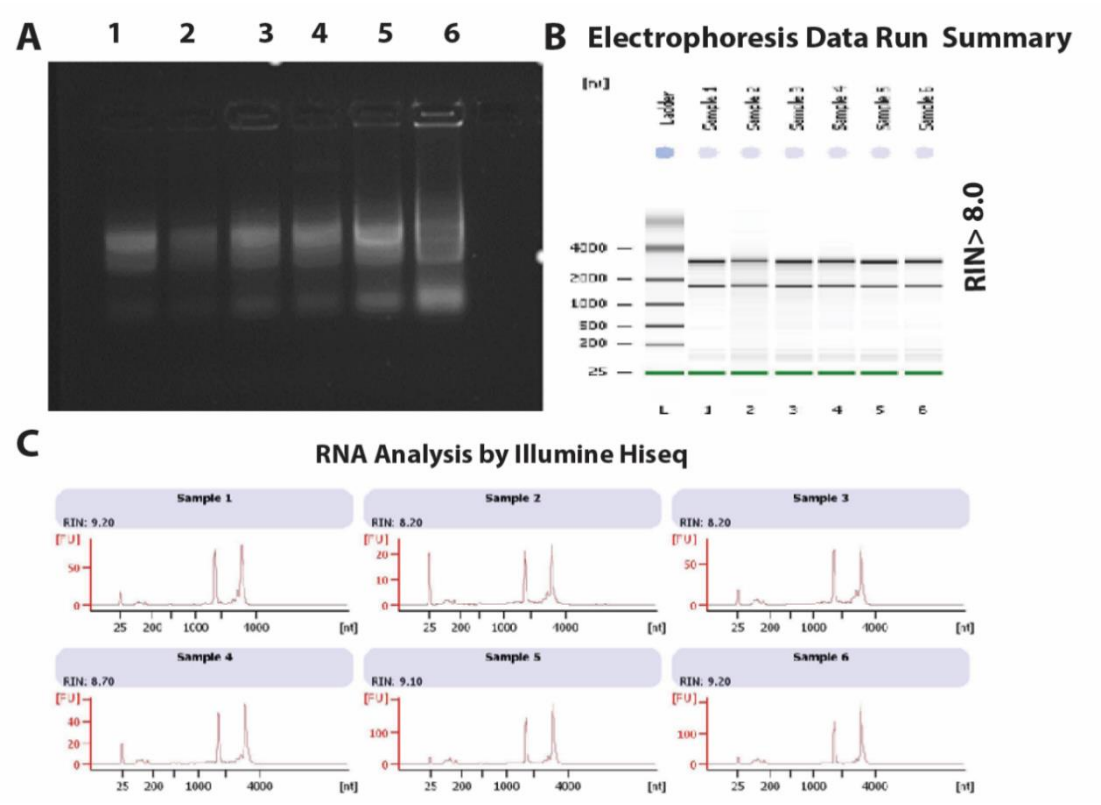

Figure 5.1 Assessment of RNA integrity and quantification of RNA from *A. dispar*. (A) Agarose gel showing total RNA of Arabian killifish embryos at different stages (1. St. 9, 2. St. 11, 3. St. 14, 4. St.18-19, 5. St. 25-26, 6. St. 28). Concentrations of RNA (nanodrop) (A) 248, 159, 264, 182, 357, 484 ng/µl respectively. (B) Electropherogram files of RNA extracted from different stages of *A. dispar*. (C) RNA quantity on the same samples. RIN (RNA integrity number) > 8.0 for all samples.

5.4.2 Assays of wild-type and Casper zebrafish killing by *C. albicans*

To analyse immune cell-pathogen interactions in live fish embryos, we used transparent embryos in which development of pigments are suppressed and therefore microscopic observation of the immune cells and pathogens are easier. To create transparent embryos, development of pigment cells or pigment synthesis can be supressed using genetic mutations such as Casper with combined loss of melanocytes and iridophores or chemical treatments such as PTU (White *et al.,* 2008; Mourabit *et al*., 2011). However, it is not clear if the presence or absence of pigment cells may affect immune cell activity. To examine the function of pigmentation in the

immune response of wild-type and Casper zebrafish embryos, *C. albicans* NGY152 was used to infect the yolk of these embryos at 24 hpf. In these infection models, survival of 100 embryos was monitored daily at constant time points between 6-72 hpi. As shown in Fig. 5.2, the highest rate of lethality was recorded within infected Casper zebrafish at 24 and 48 hpi. Infected wild-type zebrafish embryos survive the infection one day longer than the Casper group. This result suggests that, it is possible that pigment cells play a potential role in protecting body from the effect of pathogens possibly by enhancing the immune cell activity. Therefore, to investigate natural response of immune system against pathogens, we decided to mainly use the pigmented wild-type fish lines for further analyses.

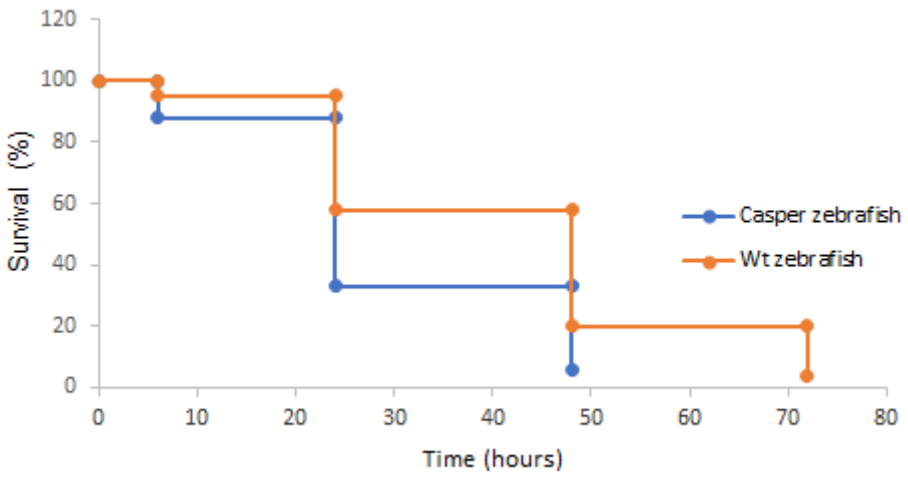

Figure 5.2 Pigment free mutants of zebrafish (Caspar) are less resistant to *C. albicans* infection than the WT embryo. 100 embryos for each group of Casper zebrafish and WT zebrafish were injected within $1X10^8$ cells/ml of *C. albicans* and survival rate was monitored for 72 hours post infection (hpi). The experiment was performed in triplicate, with values plotted representing the mean at each time point.

5.4.3 Sudan Black (SB) stained granulocytes in *A. dispar* embryos

We investigated the distribution of granulocytes (neutrophils) in *A. dispar* and Casper zebrafish by using Sudan black and a FITC-tyramide specific staining method that can detect the strong peroxidase activity which can be assessed with these cell types. In this experiment, the transparent Casper zebrafish strain was used as an initial testing platform for the staining techniques. Sudan black (SB) was staining was limited in uninfected embryos (Fig. 5.3 A) but resulted in positive staining of neutrophils in infected zebrafish at 48 hpf and *A. dispar* embryos at st.27 (Fig. 5.3 B and D) respectively. These results demonstrated that this method works efficiently with fixed embryos. In *A. dispar embryos*, the stained granules of neutrophils were also noticeable during DIC-microscopy. By 1 hpi, slight staining by SB was present in the trunk and tail fin of Casper zebrafish and in *A. dispar* (Fig. 5.3 Di-ii). The highly detectable SB stain appeared in the entire trunk and tail fin of zebrafish. Notably, by St.30 in *A. dispar*, heavy staining was observed in the tail fin (Fig. 5.3 D iii), in contrast to the uninfected control embryos. To detect granulocytes, FITC-tyramide (green) staining was also used with Casper zebrafish and *A. dispar* embryos, (Fig. 5.3 E, F respectively). Green dots indicate peroxidase-positive granulocytes in the trunk of the embryo. From these results, we clarified the distribution of neutrophils throughout both *A. dispar* and Zebrafish embryos after infection using SB staining and FITC-tyramide.

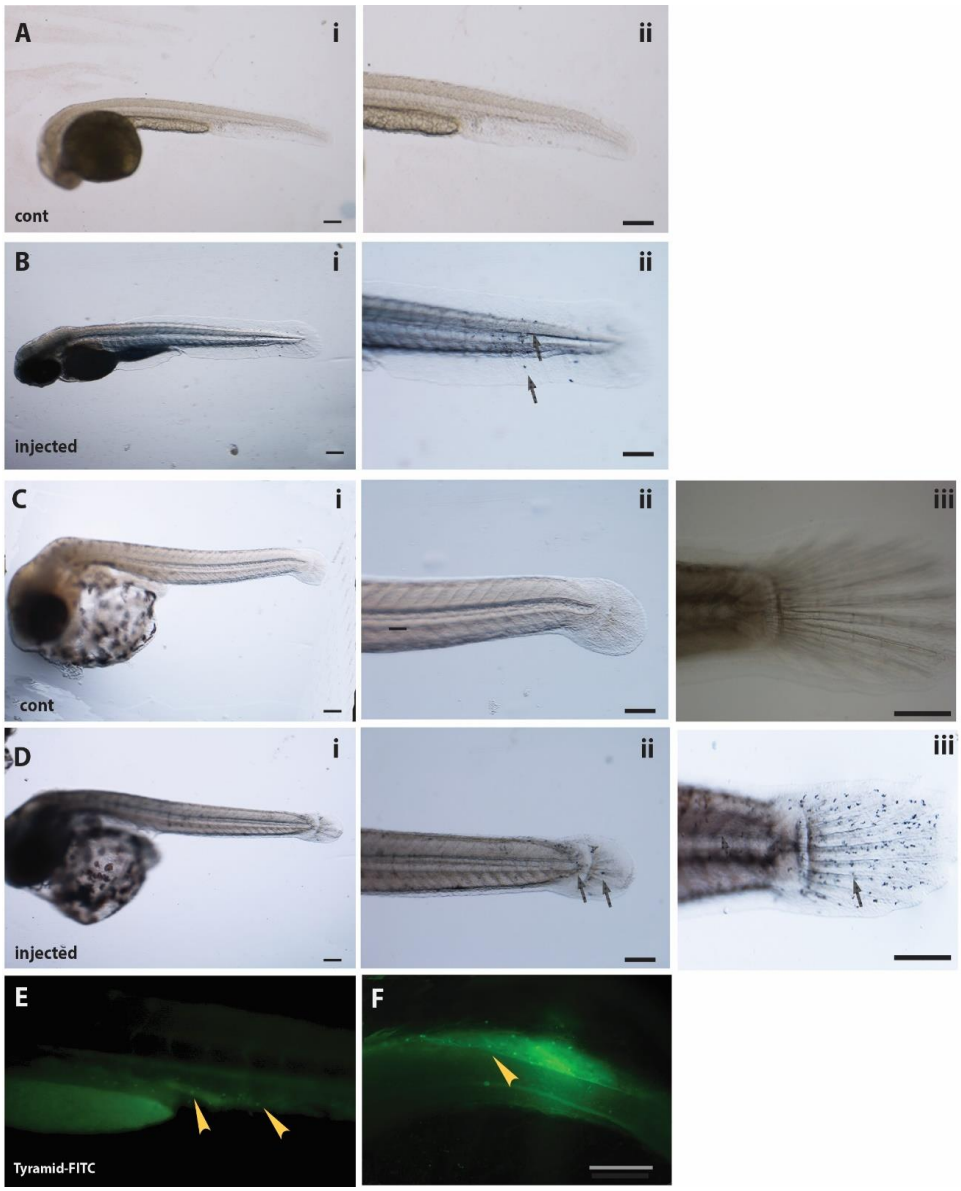

Figure 5.3 Sudan Black (SB)-stained neutrophils in *A. dispar* embryos. Lateral view of embryos shows the distribution of granulocytes. The accumulation of stained granulocytes was appeared in the trunk and tail fin (superficial) in the infected embryos. (Ai-ii) Control uninfected zebrafish embryo 35 hpf, (Bi-ii) SB staining of neutrophils in infected zebrafish embryo 48 hpf; (Ci-ii) control *A. dispar* embryo at st.27; (Ciii) SB staining in injected embryos at st.30 in the tail. (Di-iii) SB staining of neutrophils in injected *A. dispar* embryo at st.27. (E-F) FITC-tyramide detection of endogenous peroxidase activity within zebrafish and *A. dispar*. Scale bar = 100 µm (A-C) and 200 µm (D-E). Arrows indicate neutrophils.

5.4.4 Rapid and specific dissemination of macrophages in response to Candida infection

Macrophages are essential for protecting embryos from infection. To examine the response of macrophages to *C. albicans* infection, a preliminary experiment was conducted to test L-plastin antibody labelling of macrophages (Antonio *et al*., 2015), within *A. dispar* embryos and zebrafish embryos. *L-plastin*-positive macrophages were detected within both the control and the infected embryos at 24 hpi. Increased macrophage infiltration was observed within infected embryos at 24 hpi in both zebrafish and *A. dispar* embryos (Fig. 5.4 B and D) but not in the uninfected embryos (Fig. 5.4 A and C). Due to this finding, in subsequent experiments we focused on the L-plastin antibody to detect the macrophages during fungal infections.

To further investigate the necessity for macrophages during fungal infection, infected embryos were incubated for 1 to 48 hpi and fixed. Immunofluorescence staining for *L-plastin* activity was performed to determine the presence of macrophages in the embryos at these times. At 1 hpi, a difference between control and infected embryos was clearly observed and there was evidence of macrophage infiltration within 1 hpi embryos (Fig. 5.5 A, B). However, by 24 hpi, L-plastin showed significantly increased expression, indicating the efficacy of macrophages in challenging the pathogens (Fig. 5.5 C). Staining at 48 hpi showed that labelling of macrophages by *L-plastin* antibody was similar to the expression at 24 hpi (Fig. 5.5 D). The time course is summarised graphically in figure 6.

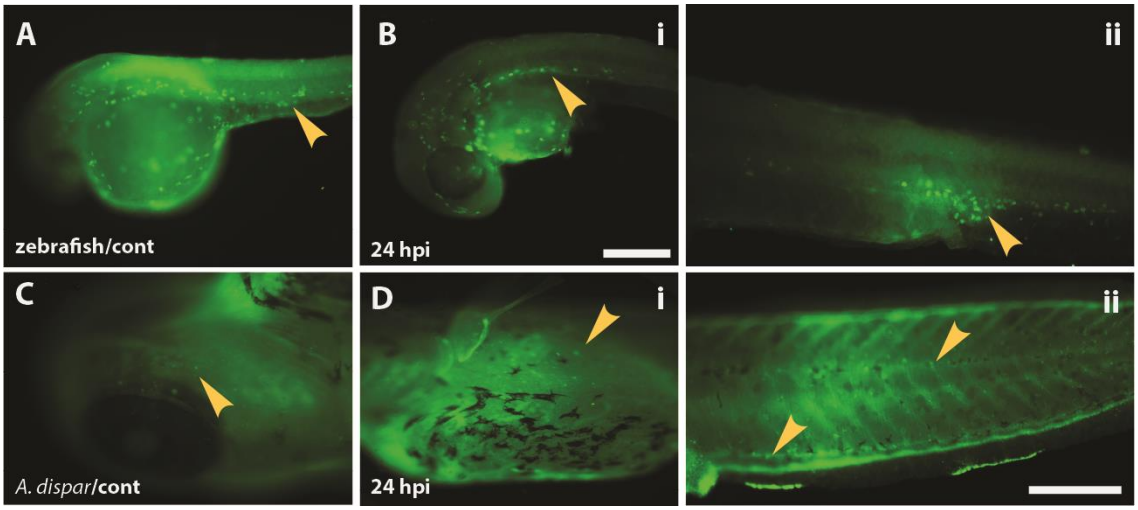

Figure 5.4 Macrophages revealed by *L-plastin* marker within zebrafish and Arabian killifish embryos. Embryos were microinjected with *C. albicans* and stained with an L-plastin primary antibody and detected via Alexa 488 fluorescence after 24 hpi. (Bi, Bii) Fluorescence imaging showing Alexa 488/L-plastin signal of macrophages within uninfected and infected zebrafish at 24 hpi. (C-Dii) L-plastin expression within *A. dispar* embryos at 24 hpi. Imaging was show lateral view, Bii shows the trunk of a zebrafish; C-Dii show brain, yolk and trunk of *A. dispar* embryos. Arrow head indicates macrophages. Scale bar (A and Bi) = 200 µm; (Bii-Dii) = 500 µm.

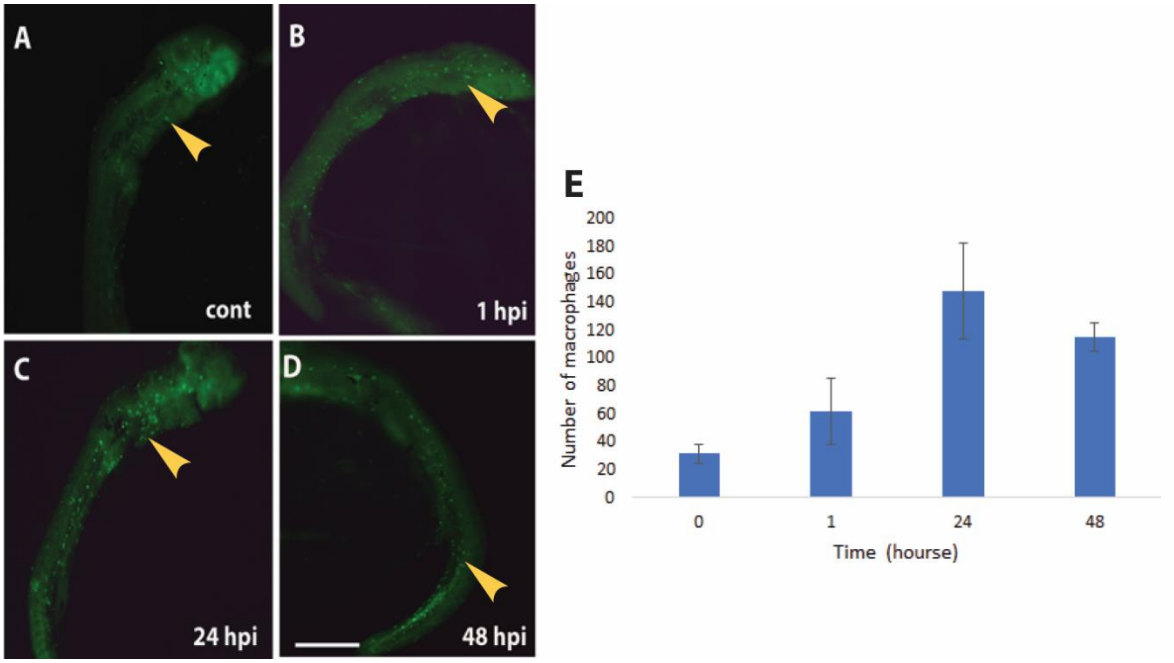

Figure 5.5 *L-plastin* labelled macrophages are significantly recruited during fungal infection in *A. dispar* embryos. Embryos at somitogenesis St.25 were microinjected with *C. albicans* and incubated for 48 hpi. Images show L-plastin labelled macrophages at different times of infection. (A) uninfected embryos (control), (B) infected embryos at 1 hpi, (C) infected embryos at 24 hpi, (D) infected embryos at 48 hpi, (E) number of macrophages at each time points. Scale bar = 200 µm. The experiment was performed in triplicate (N=9; values shown are means ± SEM). Arrows indicate macrophages.

5.4.5 Suppression of *irf8* and *cxcr4* expression blocks the development of macrophages

irf8 expression is generally associated with macrophage (Holtschke *et al.*, 1996). Therefore, we hypothesised that macrophages are crucial in the defence of *A. dispar* against *C. albicans* infection. To test this hypothesis, we tried to reduce macrophage involvement in embryos using a morpholino. To investigate the role and effect of irf8 knockdown on the development of macrophages, the L-plastin antibody was used to examine macrophage development within infected embryos and to stain them. The data clearly shows that *irf8*-MO-injected embryos lacked macrophages (Fig. 5.6 B), in contrast to the uninfected control irf8-MØ embryos (Fig. 5.6 A). The depletion of L-plastin expression in macrophages by irf8-MO was clearly specific.

To assess the distribution of immune cells (macrophages) within infected embryos for 24 h, cxcr4-MO was injected into the 1 cell stage of *A. dispar* embryos, and at the somitogenesis stage. These mutant embryos were microinjected with $1x10^8$ cells/ml of *C. albicans*. The cell-type specific marker L-plastin was used to examine the impact of *cxcr4* knockdown a macrophage distributions post infection. The data demonstrated that there was a lack of detectable *cxcr4* staining and the macrophages cells were restricted to a small region (Fig. 5.6 Ci). In contrast, *cxcr4*-uninjected control embryos (Fig. 5.6 A) showed *L-plastin* -expression macrophages in the whole embryo.

We then investigated whether knockdown of macrophages by *irf8*-MO and *cxcr4*-MO could influence *A. dispar* survival at 24 to 72 hours post infection. 93% of embryos died within 24 hpi when treated with *irf8*-MO. *A. dispar* embryos that were injected with *irf8*-MO and *cxr4*-MO died by 48 hpi and 24 hpi respectively (Fig. 5.7). In contrast, 73.3% of the control group were a live at 24 hpi, 60% survived at 48 hpi and 13.3% survived until the end of the experiment at 72 hpi.

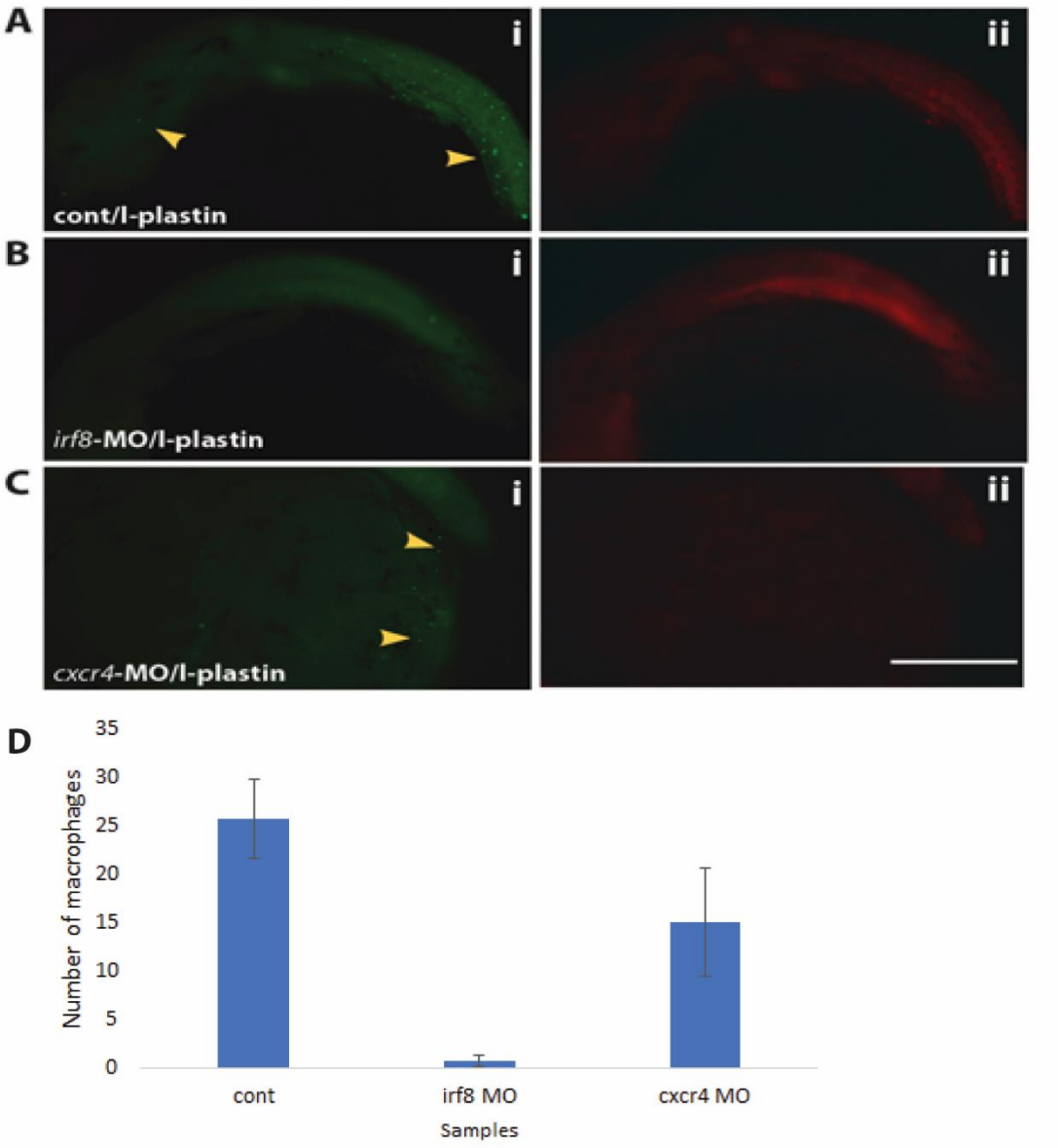

Figure 5.6 *irf8* and *cxcr4*-MO injected embryos have no macrophages and randomly expression of macrophages with *cxcr4*-MO. *Irf8*-Mo and *cxcr4*-MO were injected into the one cell stage and then at stage 24, embryos were injected with *C. albicans*. Images show clearly disruption of macrophages with irf8 mutants and restriction of macrophages in a small region with cxcr4 mutants. (A) control/L-plastin (uninfected embryos), (B) *irf8*-MO/*L-plastin* expression at 24 hpi shows a complete defect of macrophages, (C) *cxcr4*-MO/ *L-plastin* expression at 24 hpi shows a restriction of macrophage cells to a small region (arrowed), (D) number of macrophages. The experiment was performed in triplicate (N=9; values shown are means ± SEM).

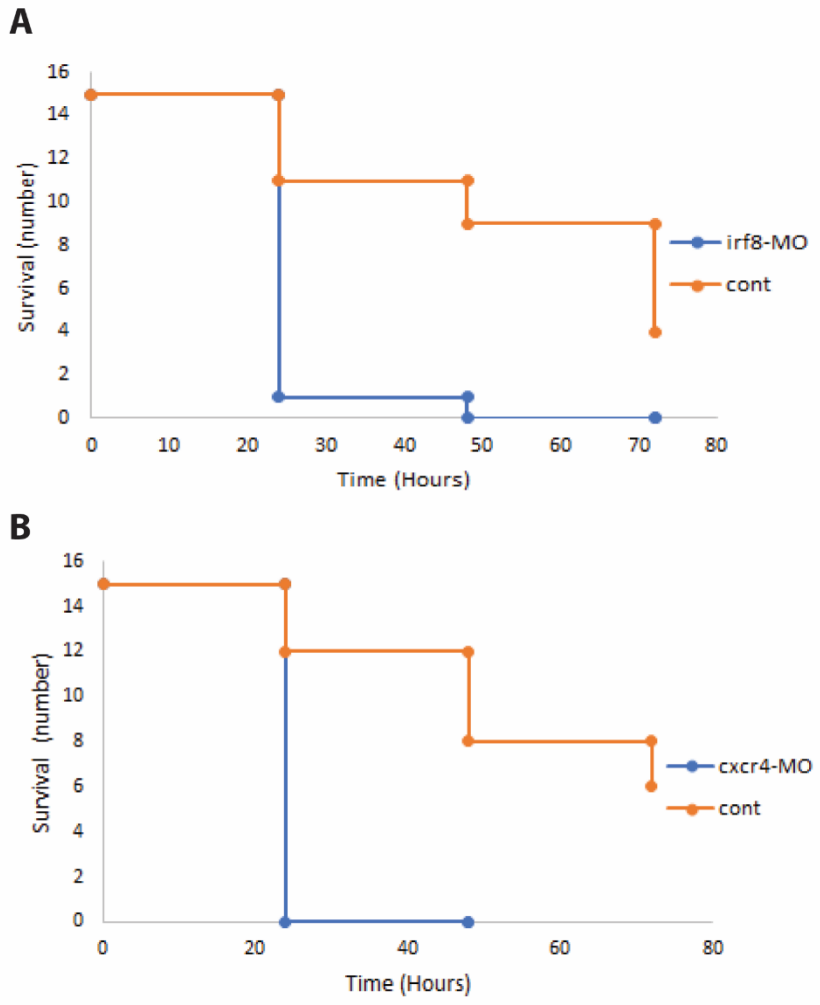

Figure 5.7 Survival curve of *A. dispar irf8*-MO after *C. albicans* infection. Embryos for each group (N=15) for (A) *irf8*-MO and control; (B) *cxcr4*-MO and control were monitored after infection within *C. albicans* at $1X10^8$ cells/ml Observations on survival were made for 72 hours post infection.

5.4.6 Immunofluorescence analysis of microglial cell distribution

The distribution of microglia in different regions of the *A. dispar* brain was studied, using immunofluorescent techniques. A 4C4 antibody was used to detect microglial cells (Beker and Beker, 2001). To assess the infiltration of microglia in the brain of *A. dispar* embryos at 24 hpi, embryos were microinjected with $1x10^8$ cells/ml of *C. albicans* and incubated at 37°C for 24 h. The results indicate that microglia proliferate at 24 hpi in both the brain (Fig. 5.8 Aii) and the spinal cord (Fig. 5.8 B) suggesting the activation

of autophagic responses to protect the brain from the infection (Olson, 2010). Generally, the density of microglia was higher in the midbrain and lower in the hindbrain. The microglia in the uninfected embryos (control) showed smaller numbers in the brain and spinal cord (Fig. 5.8 Ai-Bi).

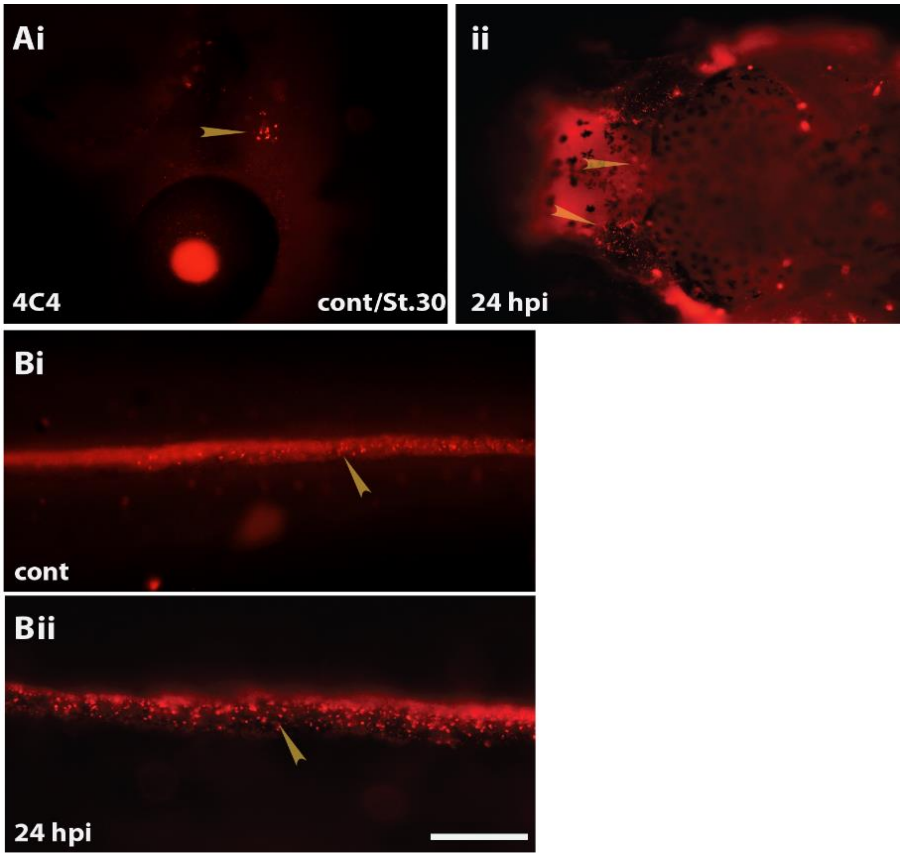

Figure 5.8 Visualization of microglia in the brain and spinal cord of *A. dispar* embryos. Embryos were injected into the hindbrain with $1x10^8$ cells/ml of *C. albicans* and incubated at 37°C for 24 h. *A. dispar* show activated microglia in both brain and spinal cord, in contrst to the uninfected embryos. (Ai) brain, control/4C4; (ii) dorsal view of infected brain at 24 hpi; (Bi-ii) lateral view of the spinal cord (control) and infected embryos at 24 hpi. Arrow head indicated staining microglia by 4C4 antibody. Scale bar = 200 µm.

5.4.7 Time-course of phagocytosis in *A. dispar* embryos

Since the ability of *A. dispar* to manage *C. albicans* infection is dependent on macrophages, the time-course of macrophage proliferation was examined in more detail. Infected *A. dispar* embryos were homogenized at somitogenesis stages St. 24 and 25 (54.5-59.5 hpf), and the time-course of the macrophage marker protein L-plastin was analysed, using western blotting (Fig. 5.9 A). The result demonstrated that the macrophage population changed over time in a complex manner. Measurement of L-plastin after 24 hpi showed high expression and significant differences compared to the first 10 min of infection ($p<0.005$) Infected embryos at 48, 72 and 120 hpi displayed significant down-expression of L-plastin, compared with 96 hpi which showed a higher expression than at other incubation times.

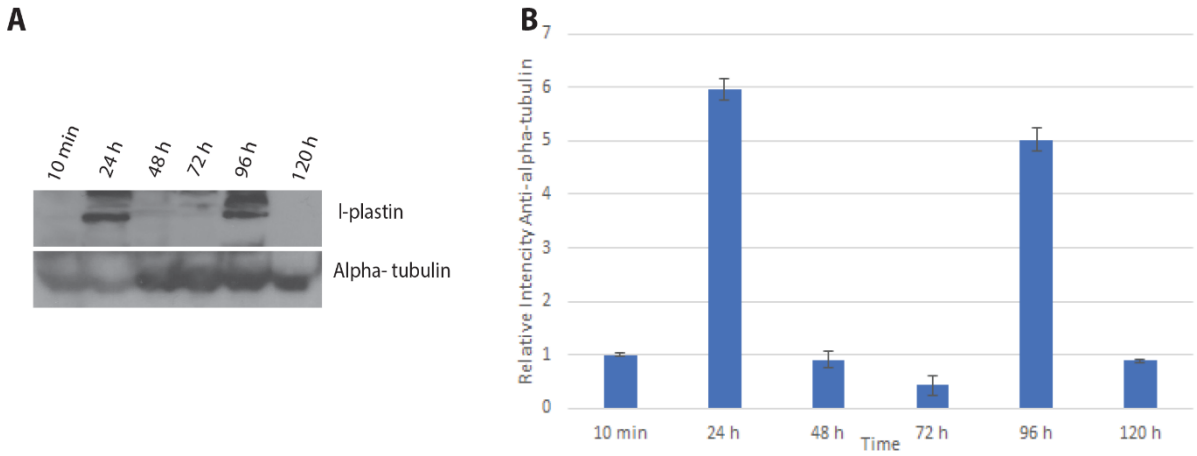

Figure 5.9 Time-course of L-plastin expression within activated macrophages following *C. albicans* infection. *A. dispar* embryos were microinjected with *C. albicans* and incubated for 120 hpi. Six whole fish embryos were lysed in100 µl SDS and subjected to immunoblot analysis with poluclonal antibodies to L-plastin and tubulin. The histogram displays the signal intensity of the lower 67 kDa L-plastin protein band in *A. dispar* embryos after normalization with the α-tubulin signal intensity for each sample. N = 3. Values plotted are means ± SEM.

5.4.8 Deletion of mannan from the *C. albicans* cell wall affected macrophages-L-plastin levels

To determine the effect of impaired cell wall biosynthesis outer layer on the immune response of the host, mutants of *C. albicans* with defection cell wall mannasylation were compared alongside the WT. L-plastin levels in infected embryos were assessed by western blot analysis. The WT levels steadily increased showing increased macrophages production over 24 hpi. Deletion of *mnt1-mnt2Δ* resulted in a significant increase of *L-plastin*. Whereas, then *pmr1Δ, och1Δ* showed a similar response to the wild-type. (Fig.5.10). Statistical analyses of WT and mutant responses were compared using one-way ANOVA.

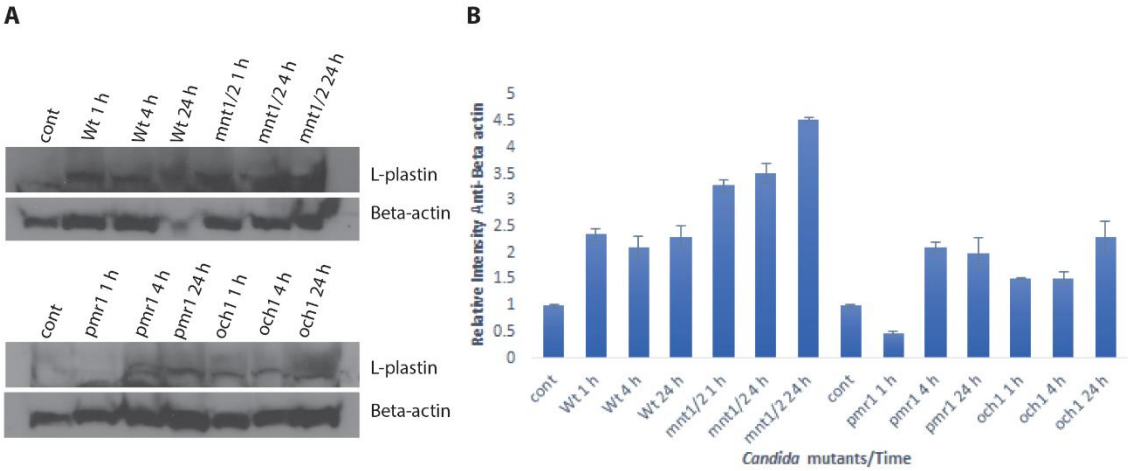

Figure 5.10 Activation of L-plastin level by different *C. albicans* mutants. (A) Levels of L-plastin expression following infection with different strains of Candida cell wall mutants, *pmr1Δ, och1Δ, mnt1-mnt2Δ* or the WT NGY152 were examined using western blotting. Uninfected controls were included for comparison. Total proteins were isolated from infected embryos at different times of infection. Relative intensities are measured with respect to the ß-actin control signal. N = 3. Values plotted are means ± SEM.

5.4.9 Direct real-time visualisation of Candida-host immune cell interactions *in vivo*

To assess the interaction of immune defence cells against *C. albicans*, *A. dispar* embryos were injected with 1 to 2 nl of CAF2-dTomato C*. albicans* ($5x10^{10}$ cells/ml). Fungal cells and the immune response was visualised

between 5 mpi and 24 mpi (Fig.5.11). Macrophages can be seen phagocytosing the yeast form of the pathogen. As expected, macrophages swiftly engulfed Candida cells present in the infected yolk. After their phagocytosis of the Candida cells, macrophages acquired different shapes and their movement accelerated.

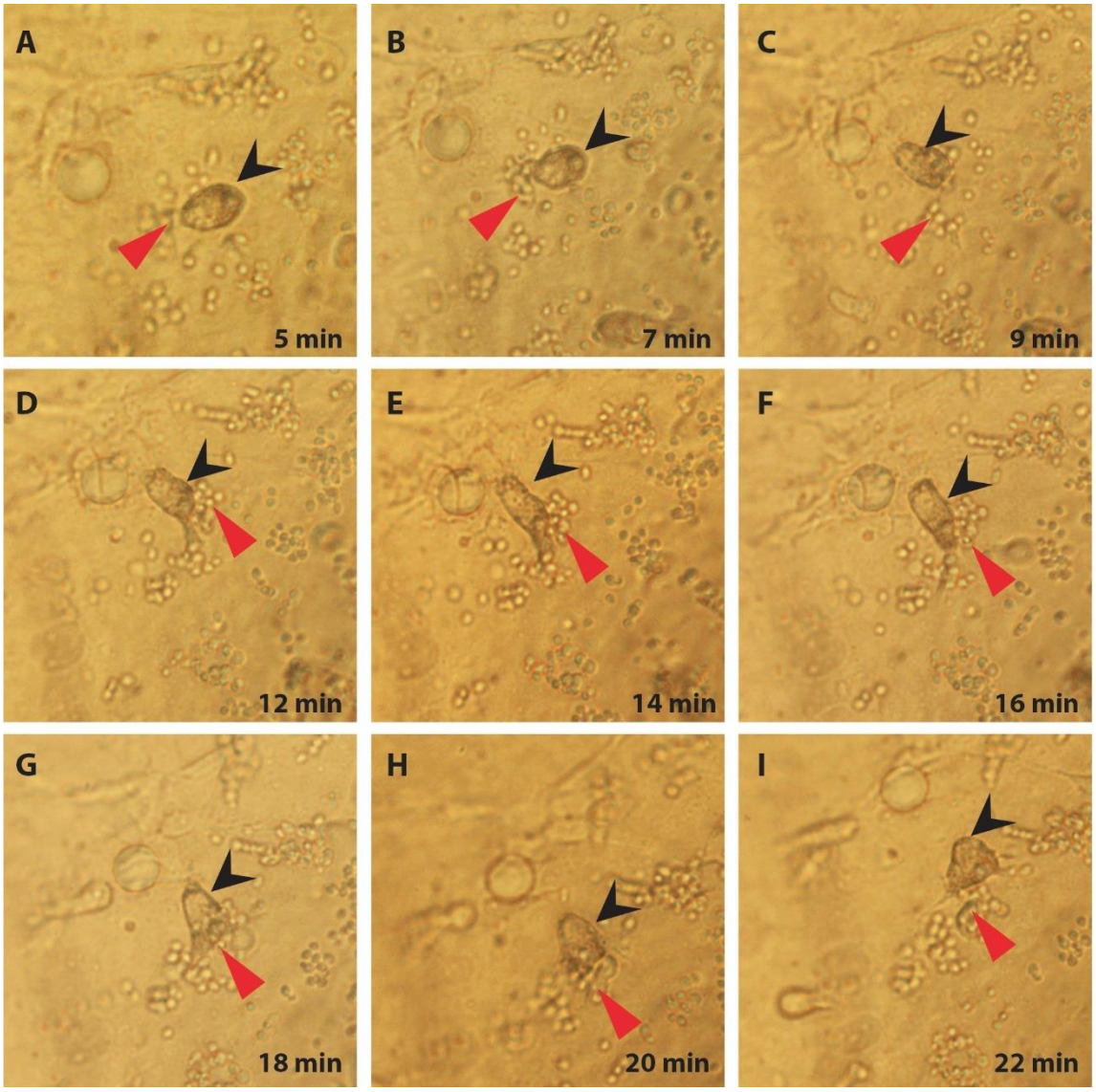

Figure 5.11 Direct real-time visualization of the Interaction between Candida and immune cells of *A. dispar*. Time lapse images were obtained from injected embryos with ($5x10^{10}$ cells/ml) of Candida cells at (A) 5, (B) 7, (C) 9, (D) 12, (E) 14, (F) 16, (G) 18, (H) 20, (I) 22. The black arrows indicate macrophages and red arrows indicate Candida cells in the yolk. Movie time, minutes post infection (mpi) is shown at the bottom right of each image.

5.4.10 Macrophages show tissue specific response in relation to interact with *C. albicans*.

Analysis of the real-time of interaction between macrophages and *C. albicans* in embryos, allows a consideration of the impact of anatomical location on the immune response. The results shown in Figure 5.12 displayed the interaction between CAF2-dTomato Candida and macrophages at 1 hpi. This time of infection revealed clear differences in the immune response when comparing different infected niches. Macrophages were immediately attracted by fungal pathogens at all sites. Interestingly, macrophages deeply infiltrated the Candida cells at the yolk of *A. dispar* embryos (Fig. 5.12 Bi-ii). In the brain, an obvious interaction occurs between microglia and *C. albicans* cells, (Fig. 5.12 C). The trunk also showed a clear interaction (Fig.5.12 D). In comparison with the uninfected embryos, macrophages displayed less individual distribution than in the injected embryos (Fig. 5.12 A).

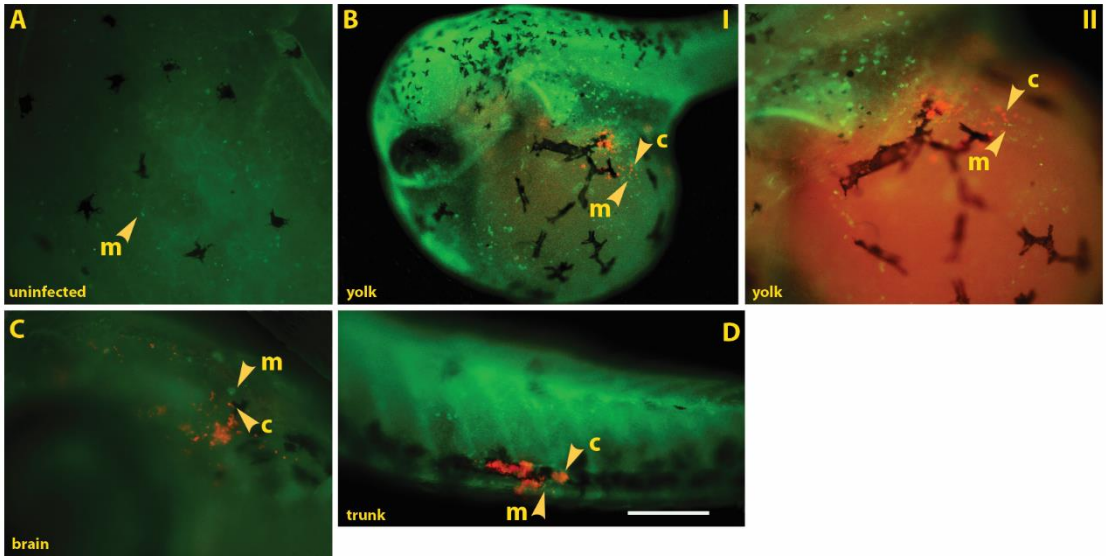

Figure 5.12 Fluorescence imaging of *C. albicans* and macrophages (L-plastin) within *A. dispar* embryos. Embryos at somitogenesis stage were injected with CAF2-dTomato *C. albicans* into the different sites (Brain, trunk and yolk) and incubated for 1 hpi. Whole mount immunofluorescence was performed using an L-plastin primary antibody and secondary Alexa 488 labelling and CAF2-dTomato *C. albicans* in the *A. dispar* embryos. (A) Uninfected; (Bi-ii) infected yolk; (C) Brain. Arrows indicate; m, macrophage. c, *C. albicans*.

5.4.11 Reactive Oxygen Species (ROS) detection within *A. dispar* embryos

To evaluate the production of ROS within infected embryos, 2',7'-dichlorofluorescein (H_2DCFDA) was used to assess the distribution of ROS (Fig. 5.13) and quantify ROS production (Fig. 5.14). After the trunks of embryos were microinjected with 1-2 nl of *C. albicans* at $1x10^8$ cells/ml for 30 minutes (Figure .5.13) ROS production was detected at the site of the microinjection itself and at a distal site such as the tail fin (Fig. 5.13 B). Notably, the accumulation of fluorescent probes was discernible even at the short observation time chosen in this experiment. The uninfected control embryo, however, showed negative signal for the probe (Fig.5.13 A).

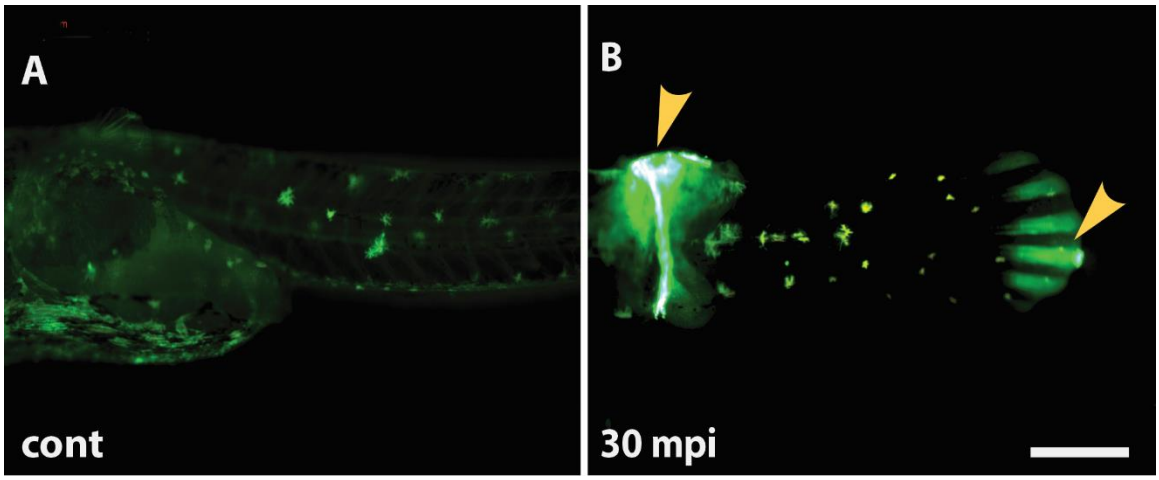

Figure 5.13 Whole mount ROS-detection in *A. dispar* embryos. *A. dispar* embryos at mid-somitogenesis stage (St.24-25) were microinjected with *C. albicans* at 1x 10^8 cells/ml. Image show ROS accumulation at the infected site (trunk) and an induced signal in the fin tail. ROS production was detected with H_2DCFDA. (A) Representative image showing uninfected control and (B) induction of ROS in *A. dispar* at 30 min after infection. Arrows indicate infection site (trunk) and induced site (tail fin). Scale bar=500 µm.

To quantify the fluorescence of labelled ROS using (H_2DCFDA) kit, real-time analysis of fluorescence intensities was applied to measure ROS, using a microplate reader (Fig. 5.14). The data reveal that there was an increase in of ROS levels during the infection. Moreover, depending on the effectiveness of *C. albicans* mutants of causing disease, the immune response altered. Embryos infected with WT *C. abicans* showed higher fluorescent intensity than all mutants. The *mnt1-mnt2*Δ mutant likewise demonstrated a fairly high level of fluorescence (Fig. 5.14 A) a result consistent with the real-time imaging. In the cases of the *pmr1*Δ and *och1*Δ mutants, a lower intensity level of ROS production was measured. (Fig. 5.14 B, C).

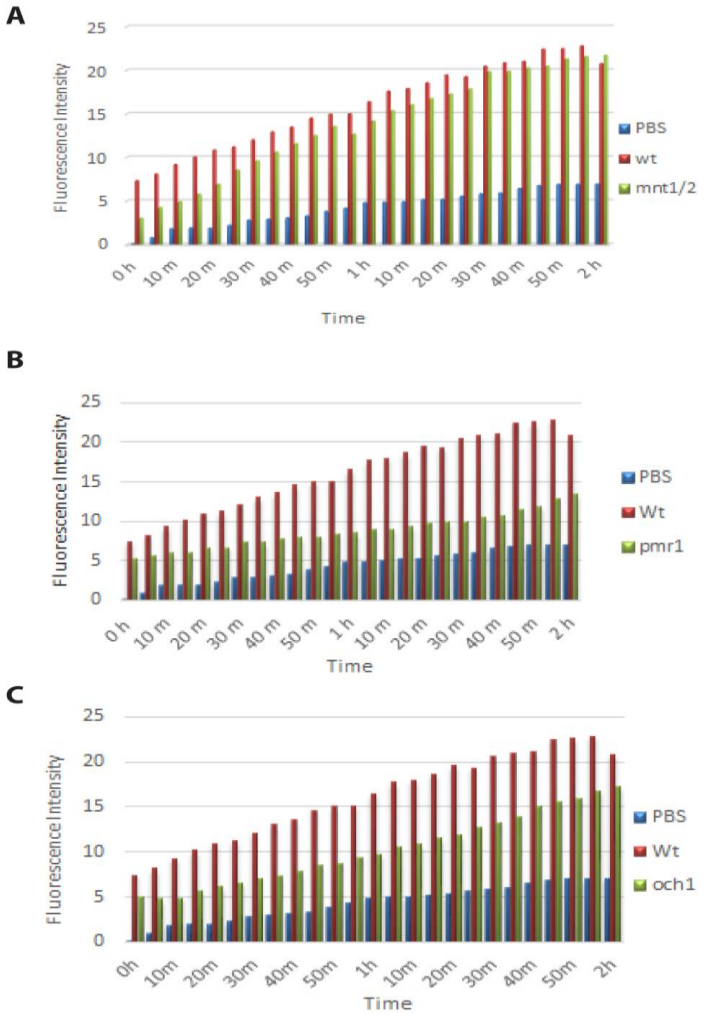

Figure 5.14 Quantification of ROS in *A. dispar* embryos using H2CFDA fluorescence intensity measurements in a microplate reader. Fluorescence of 2',7'-dichlorofluorescein (DCF) formed when H_2DCFDA is oxidised by ROS in embryos was monitored (Ex/Em: 485/535 nm) from 30 mpi until 2 hpi. Fluorescence intensities of embryos following infection with different mutants of Candida were measured. ROS levels in infected embryos were compared with the uninfected embryos (control). Fish embryos were microinjected with (A) *mnt1-mnt2*Δ mutants of Candida, (B) *pmr1*Δ mutants of Candida, and (C) *och1*Δ mutants of Candida.

5.4.12 Induction of the immune response and gene expression is required for elimination of the fungal Infection

To elucidate the molecular mechanisms of the innate immune response of the *A. dispar* embryos against fungal infections, we first examined the expression of immune response genes during embryo infection using qPCR analysis. Embryos were microinjected into the yolk with WT strain and different mutants of *C. albicans (mnt1-mnt*Δ*2, pmr1*Δ and *och1*Δ*)* and incubated for 24 hpi. Total RNA was then extracted from homogenized *A. dispar* embryos, cDNA was synthesized, and the gene expression level was then determined for *L-plastin, cxcr4, csf1-r, nox1* and *nos1a.* Clear differences in expression level were detected following infection. Overall high expression levels were detected for all genes following infection of the embryo infected by the wild type *C. albicans* shown (Fig. 5.15). Whereas embryos with mutant *C. albicans* showed a lower level of expression. Some mutants elicited a down-regulation of gene expression in some case. With *och1*Δ produces significantly ($P<0.005$) of all genes tested. *L-plastin* and *csf1r* are used as markers for macrophage, suggesting that wt *C. albicans* increased macrophage by 2.5-fold and 1.8-fold respectively whereas in the three mutants, *L-plasin* was suppressed (Fig.16 A, C). *Nox1* is expressed in neutrophils (Balázs Rada, 2008) and the expression was increased in the WT *C. albicans* infected embryos by 9-fold (Fig.5.15 D). However, the *nos1a* which is also expressed in the neutrophil only showed 1.2 folds increase (Fig. 5.15 E). *Cxcr4* is expressed in both macrophage and neutrophil and also showed increase of expression in the WT *C. albicans* infected embryos (Fig. 5.15 B). In all mutants tested, mutant-infected embryos showed lower gene expression compared to WT (Fig. 5.15 A- E) suggesting importance of mannosylation for detection of Candida and activation of immune response.

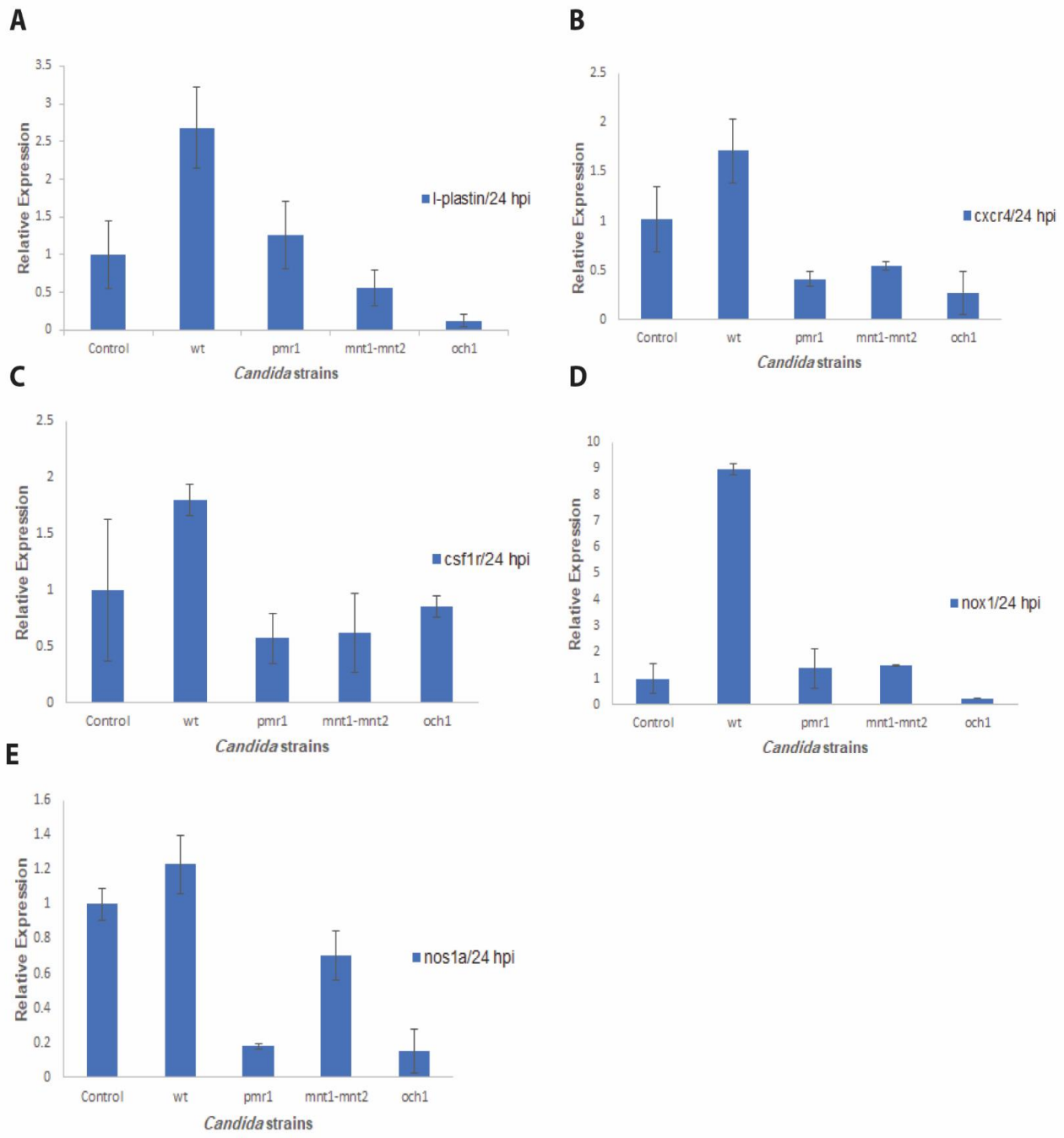

Figure 5.15 qPCR monitoring of immune response in *A. dispar* embryos after Candida infection. *A. dispar* embryos were microinjection with WT or mutants of *C. albicans* (*pmr1*Δ*, mnt1-mnt2*Δ and *och1*Δ) into the yolk and incubated for 1 and 24 hpi. Gene expression levels were determined using qPCR and the relative fold change for each marker gene was plotted and normalised against a housekeeping gene (Ad_ Lsm12b) ± SEM. (A) *L-plastin*, (B) *cxcr4*, (C) *csf1a*, (D) *nox1* and (E) *nos1a* expression levels at 24 hpi. N= 3 (with 10 embryos per replicate). Values plotted are means ± SEM.

5.4.13 Development of a transgenic *A. dispar* fish

To demonstrate that *A. dispar* can be genetically labelled and modified, a transgenic *A. dispar* line was produced by microinjection of the pBeta-actin-DsR-LoxP-GFP plasmid into the one-cell stage of eggs. At 24 hpf, embryos were checked, using fluorescent microscopy, and classified into positive (with mosaic fluorescence) and negative (no fluorescence) batches. Nine positive transgenic embryos were raised to adult fish (F0 fish). Each adult F0 fish was crossed with a wild-type fish in pairwise mating. When fluorescent embryos were obtained (Fig. 5.16), the parent F0 fish was designated as a career. We crossed 9 F0 fish and identified 3 career fish. Among these career fish, one female which lays eggs most was selected and 30 fluorescent embryos were raised to adult (F1) to establish the transgenic fish line.

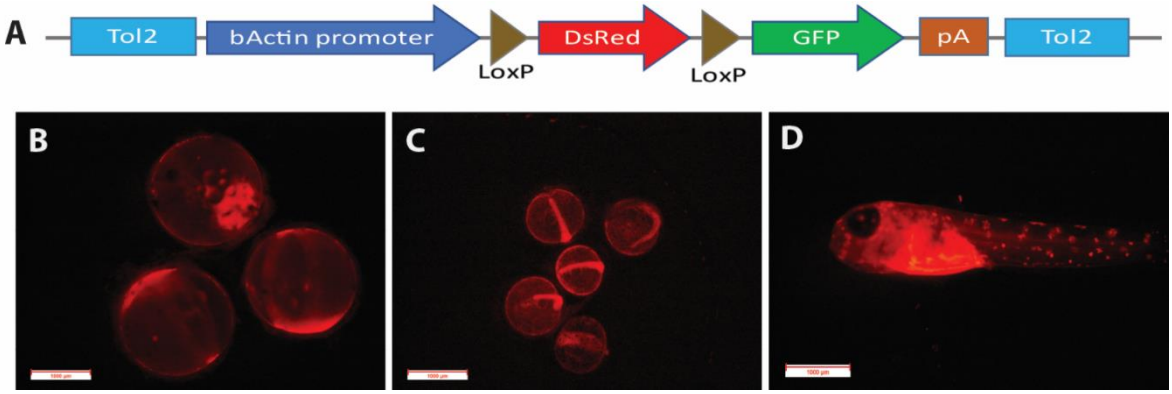

Figure 5.16 Generation of transgenic Arabian killifish. Arabian killifish were genetically engineered to express red fluorescent protein (RFP) to evaluate the potential to generate transgenic lines for future studies. Figures show *A. dispar* embryos at different stages of development. Red signal indicates expression of Beta-actin-DsR-LOXP-GFP. (A) Map of the transgenic DNA. The DNA contains, Tol2 transposon sequence, medaka beta-actin (bActin) promoter, LoxP sequence, DsRed and GFP fluorescent protein genes, poly A signal (pA). (B-D) Red fluorescent signals at epiboly stages (B), somitogenesis stages (C) and larval stage (D). Scale bar = 1000 µm.

5.5 Discussion

In this work, *A. dispar* was used for the first time as a model to investigate the host-immune response to infection. This is significant as *A. dispar* can survive at 37°C, enabling us to study the fungal infection at human body temperatures and the immune system is similar to that in other vertebrates. Fish embryos are transparent, so that the Candida-immune response can be directly investigated using non-invasive approaches as well as permitting biochemical assays to follow the progression of infection at a molecular level.

Before this study was undertaken, gene sequence information for the Arabian killifish (*Aphanius dispar*) was not available. The RNA-seq analysis of killifish embryos provided the foundation for identifying immune response genes and the critical information for the design of PCR primers and morpholinos.

The fundamental immune system is similar in both fish and mammals. Fish models have become very important and attractive for the study of functional immunity responses to infection (Rauta *et al.,* 2012). Interestingly, a previous study by Levesque *et al.,* (2013) suggested that the zebrafish is a novel model for examining the assumption that pigment cells are capable of playing an important role in combatting microbes by providing evidence of the migration of melanocyte and melanoblasts to the wounds or infection sites. Furthermore, the early induction of innate immune cells is induced by direct signals (attractants) to guide the movement of melanocytes (Levesque *et al.,* 2013). The results presented in this chapter show that there was a decrease in the ability of the Casper zebrafish mutant to survive, compared to the wild-type zebrafish. For example, only 2% of Casper zebrafish survived after 48 hpi, while 20% of wild-type zebrafish were alive at that time (Fig. 2). The present data therefore suggests that a higher rate of mortality was observed within Casper zebrafish because of the deficiency of pigmentation, including a possible role for pigment cells in antimicrobial activity and regulation of inflammatory responses. This idea is supported by Mackintosh (2001), who reported that the melanisation of skin has a crucial role in innate immune defence, due to the functional role melanocytes play as inhibitors of the

proliferation of microorganisms. Lévesque *et al. (*2013) suggested that in the wound response, hyperpigmentation might occur as a result of this potential antimicrobial role. Such as mechanism might have a role during tissue damage caused by fungal infection. Clinical studies have also mentioned that within an inflammatory environment, melanocytes can be stimulated by leukocytes and keratinocytes to become more dendritic (Levesque *et al.,* 2013). These literature findings and our results suggest that if we are to investigate fully the effects of a pathogen in live animal, we should use wild-type pigmented lines rather than transparent animals.

To investigate the distribution of granulocytes (neutrophils) in *A*. *dispar* and Casper zebrafish embryos, Sudan Black and FITC-Tyramide were used. These stains were found to be suitable techniques for defining and tracing the origin of neutrophils and their distribution and allowing clear visualisation of functional granule trails (Le Guyader *et al.*, 2008). The distribution of neutrophils seen in Casper zebrafish at 35-48 hpf during infection agreed with findings of the previous study, which had shown the simultaneous appearance of neutrophils at 48 hpf in whole embryos (Le Guyader *et al.*, 2008). Within *A. dispar* embryos, we found that the appearance of granulocytes over the whole trunk and tail fin of *A. dispar* increased during the infection time at a late stage (St. 30) while only a few granulocytes were observed at st.27 in these locations. SB staining suggested the appearance of a small number of these cells referred to still immature neutrophils (Le Guyader *et al.*, 2008). Additionally, no cells were stained in the head of *A. dispar* embryos. It is possible likely that this technique stained neutrophils in the tail very well but could not stain the neutrophils in the head because of the large and deep extent of these tissue at the late embryonic stages. In addition, the existence of pigmentation in the head and yolk of model may have disturbed the view and reduced the clarity of the staining. However, *A. dispar* as a model still provides a platform for future studies that will facilitate new insights into the immune interaction during fungal infections.

Immunofluorescence was used to detect the distribution of immune function proteins within infected embryos. We stained macrophages positively with an L-plastin antibody. The data collected showed that *Candida* infection

leads to an increasing incidence of inflammation associated cell types, which can significantly induce immune cell interactions at the site of infection. Our observations showed the highest number of labelled macrophages was detected at 24 and 48 hpi.

It is well known that *irf8* is a factor involved in diverse aspects of innate immune system function and developmental (Holtschke *et al.*, 1996). In this study, we knocked down the *irf8* gene using a Morpholino in *A. dispar* embryos, and found that *irf8* deficiency resulted in a failure to form a macrophage population. Similarly, in zebrafish there was a failure to establish macrophages in to *irf8* MO knockdown, but the neutrophil population exhibited an expansion that was not attributable to the acceleration of prolonged cell survival (Li *et al.,* 2010). In the *irf8* MO injected *A. dispar* embryos, survival of the embryo by Candida infection was strongly decreased (e.g. more than 50% in control whereas 0% in irf8 MO at 48 hpi) (Fig. 8). These data suggest that macrophages have a crucial role in protecting embryos from Candida infections. In macrophage, it is known that *cxcr4* is expressed as it plays an important role in regulating cell migration to the sites of inflammation (Angsana *et al.,* 2016). In this study, microinjection of *cxcr4* MO blocked the function of *cxcr4* in the infected *A. dispar* embryos as there was lack of detectable *cxcr4* expression and macrophages cells were restricted to a small region, confirming earlier findings that reveal the involvement of *cxcr4* signaling in controlling and directing movement of macrophages cells (Richard *et al.*, 2008).

Many Morpholino work very well to block translation through targeting the start codon of mRNAs as well as, targeting splice sites in the pre-messenger RNA to knock down gene expression. However, some side effects have been noticed using MOs including the non-specific binding to unintended RNAs or even other macromolecules (Eisen and Smith, 2008). In addition, recently, it was observed that the efficiency of some morpholinos may be decreased over time (Chow *et al*., 2017). Therefore, further work should also be conducted using a CRISPR/Cas9 mediated gene knock out of *irf8*.

Microglia are activated immune cells that play a key role in the immunological characteristics of the Central Nervous System (CNS)

(Ginhoux *et al.*, 2013). A previous study by Olson (2010), suggested that a possible difference in immune reactivity may be found between microglia in the spinal cord and those in the brain. It has also been suggested that the immune response in the spinal cord could be higher than that in the brain due to the high immune reactivity of microglia in the spinal cord compared to those in the brain (Olson, 2010; Jin *et al.,* 2016).

In this study, an immunofluorescent technique using a 4C4 antibody was used to examine the distribution and the infiltration of microglia in the brain of *A. dispar* embryos infected with *C. albicans.* At 24 hpi, the results illustrated that *C. albicans* infection triggered increased number of microglial cells at the site of infection in the brain and also in distal domains in the spinal cord. The present findings therefore confirm earlier studies that reported the important role of microglia in immune response in the brain and the spinal cord (Olson, 2010).

In general, the proliferation of macrophages is accompanied by rapid changes in gene expression (Davis *et al*., 2013). Our study suggested that there is a balance between two macrophage populations activated at different timing during infection: activated macrophages (proinflammatory) and alternative macrophages (anti-inflammatory) (Martinez and Gordon, 2014). The time course of macrophage development in *A. dispar* embryos was assessed using western blotting technique, depending on the macrophage population. The data showed that high levels of L-plastin expression were observed at 24 hpi and 96 hpi, compared with other inoculation times. The data indicated a bi-phasic activation of macrophages at different time point after infection. Previous studies by Mounier *et al*., (2013); Wang *et al*., (2014) have illustrated that after injury, activated M1 macrophages release pro-inflammatory cytokines and chemokines, which 24 to 72 hours later, leads to the M1 macrophages being sequentially replaced by anti-inflammatory macrophages M2, which in turn are responsible for stimulating myogenic precursor cells to differentiate and form new regenerating myofibres.

In zebrafish, Nguyen-Chi *et al*., (2015) demonstrated that M1 macrophages were induced in a caudal fin wound at 6 hours post amputation (hpa), and that there was upregulated expression at 16 h post inoculation with *E. coli*.

In addition, it was found that macrophages were recruited to the fin wound from 1 hpa. Similarly, infection with *E. coli* in the muscle induced the expression of macrophages a few hours post-infection. The same study reported that, in both conditions, *E. coli* infection and fin amputation, a steady increase in the macrophage population from 6 to 20 h was followed by a dramatic decrease at 26 hpa and 26 hours post-infection. Overall, these findings support our results, which showed an increase in macrophages expression at 24 hpi. it was proposed that the recruitment of macrophages was observed at the inflammation site as a response to the wounding of the zebrafish. Based on our results which show that *A. dispar* can still survive for more than 96 hpi, following *C. albicans* infection it would be appropriate to investigate M1 and M2 sub-populations in future studies.

In this work, *A. dispar* embryos were evaluated as a potentially advantageous *in vivo* model for carrying out studies to measure oxidative stress following infection. ROS levels in *A. dispar* embryos were measured using two distinct procedures. Firstly, whole mount ROS detection by fluorescence microscopy was found to be an easy way to detect oxidative stress in living embryos, and it has the advantage of allowing a rapid qualitative assay. The results indicate that ROS was increased during the infection by WT *C. albicans* indicating that release of ROS is a part of key immune response of the host cells. On the other hand, infection by mutant *C. albicans* cells showed different responses. All three mutants tested showed lower ROS levels compared to WT infection; however, the mutant *mnt1-mnt2*Δ show relatively higher responses than the other two mutants (*pmr1*Δ and *och1*Δ*).* This suggests, specific mannosylation events mediated by *Pmr1* might be particularly important for immune cell recognition. The *och1*Δ is a mutant which does not proliferate well and therefore it was predictable that it did not induce a strong ROS reaction. Our findings are in consistent with previous study of Wellington *et al.,* (2008) who found that ROS production was suppressed in mice as a result of increasing exposure β-1,3 glucan of *Candida*.

Immune responses require the specific expression of key regulators following invasion by different foreign pathogens. In this study, qPCR was

used to follow changes in immune system gene expression after infection (Lionakis *et al*., 2011).

L-plastin belongs to a family of actin-binding proteins (Freeley *et al.,* 2012; Morley 2012). During fungal infection, cells expressing *L-plastin* increased within infected embryos demonstrating the role of upregulated L-plastin in the clearance of Candida cells at 24 hpi. The highest expression was seen when embryos were exposed to the WT.

L-plastin is expressed at a high level in zebrafish at 18 h: It is evident in the both posterior intermediate cell mass (ICM) and throughout the body at 28 hpi, but expression diminishes drastically at 5 dpf (Bennett *et al.,* 2001). Chemokines play a central role in the activation and regulation of leukocyte trafficking to the inflammatory sites (Shi *et al.,* 1998). Colony-stimulating factors (CSF) regulate myeloid cell differentiation, and the development and proliferation of many cells, such as monocytes and macrophages (Garcia *et al.,* 2016). High level expression of *csf-1r*, which is known as macrophage colony-stimulating factor M-csf, can play an essential part in the survival and promotion of macrophages in both steady state conditions and during infection (Hamilton and Achuthan, 2013). In the present study, *csf-1r* gene expression within *A*. *dispar* embryos infected with *C*. *albicans* was examined, using qPCR. Our results showed that, during an infection, there was an increase in *csf-1r* gene expression correlated with a recruitment of macrophages at 24 hpi. It can be suggested that *csf-1r* gene expression increases, due to its important role in inducing phagocytosis and driving the amplification of pro-inflammatory macrophages (Cao *et al*., 2014). The present result is also supported by earlier findings of Guleria and Pollard (2001), who found that after mice were infected with *Listeria monocytogenes*, macrophage density increased dramatically within 24 hpi. Our results are in agreement with the recent study of Al-Zaidan (2017), who reported that exposure of zebrafish to toxic ammonia, resulted in an up-regulation of *csf-1r* at 24 h.

NOX is an important family of NADPH oxidases, and has the ability to produce ROS in the host cells, especially within immune response. NOX -mediated oxidative innate immune defence against bacteria and fungi operates by deriving ROS to react against pathogens and regulate the

adaptive immune response (Balázs Rada, 2008; Segal *et al.,* 2000). In addition, according to Simona-Adriana *et al.,* (2015), during microbial infection, NOX is rapidly regulated and expressed against invading microbes (Simona-Adriana *et al.,* 2015). Moreover, in their study, Selemids *et al., (*2013) illustrated that *nox1* modulates the inflammation state at 3-7 hours post influenza infection and subsequently clears the viruses.

Prior to this study, the expression levels of *nox1* oxidase in the *A. dispar* embryos within fungal infection had not been examined. Our results showed that the expression was significantly higher (9 fold) in embryos infected by WT *C. albicans* after 24 hpi. On the other hand, with the cell wall mutants, (*pmr1*Δ*, mnt1-mnt2*Δ*,* and *och1*Δ), expression levels were not up-regulated compared to the uninfected control. This result can be explained by findings reported by Selemidis *et al.,* (2013) who reported that *nox1* expression plays an important and effective role in the pro-inflammatory response that protect host tissues. The present results also seem to be in agreement with many previous findings, such as those of Panday *et al., (*2015), and Silva (2007), who had suggested that the over-expression of *nox1* during infection probably participates in increasing the production of H_2O_2, which is one of the ROS required for antimicrobial activity.

NOS (nitric oxide) is an important inducible component of the immune response, required to control infection (Li *et al.,* 2006). According to Korhonen *et al*., (2005), nitric oxide itself plays a significant role in combatting pathogenic microbes by means of its cytotoxic properties. NO can produce reactive nitrogen species as a result of its interaction with molecular oxygen and superoxide anion (Chauvin *et al.,* 2017). The nitric oxide synthesis (NOS) gene can eliminate and prevent infections through its involvement in mediating the signals by NOS enzymes (Li *et al.,* 2006).

Earlier studies have revealed that NOS plays a fundamental role in the immune response (Tripathi *et al*., 2007; Jun *et al*., 2014). Jun *et al*., (2014) found that NOS gene expression was elevated after bacterial infection, and was dependant on the time of migration of innate immune cells in catfish. It was observed that the NOS gene was highly expressed in the brain of catfish after bacterial infection (Holmqvist *et al.,* 2000).

As mentioned previously, mannan is an essential element in the recognition of fungi by pattern recognition receptors. Disruption of a1, 2-mannan can have a significant influence on monocyte recognition of *C. albicans* (Hall *et al.,* 2013). The present study suggested that loss of mannan in *C. albicans* is likely to influence recognition of *Candida* by macrophages in *A. dispar*, and that it is likely to have an impact on production of nos. This idea was assessed using qPCR and the results showed higher NOS expression within embryos infected with WT Candida compared to those were infected with mutants. A possible explanation for the differences in NOS expression is that with WT condition, mannan increases recognition and migration of macrophage to the infection sites which leads to upregulate production of nos as a key aspect of the antifungal response (Tripathi *et al.,* 2007; Jun *et al.,* 2014). The present results agree with those of Wu-Hsieh *et al.,* (1998) and Shen *et al.,* (2015) who demonstrated a correlation between NOS expression and severity of disease: NOS was highly expressed in splenocytes after *C. sinesis* infection. However, further investigations will be required to determine the exact relationship between the presence of α1, 2-mannan and increases in nitrogen species production.

Although differential gene expression was detected in the qPCR data, it is still not clear how this relates to the number of active immune cells in the WT and mutant infected embryos. For instance, if *pmr1*Δ infection did not induce proliferation of the macrophage, *L-plastin* would not be increased, but if *pmr1*Δ infection induced proliferation of macrophage but did not induce transcription of *L-plastin*, the level of *L-plastin* would also be low. Therefore, more detailed examination of response of immune cells and genes would be needed.

Polysaccharide analysis within the *C. albicans* cell wall has shown that hyphal cell walls contain a lower amount of mannan and a higher amount of chitin and glucan compared to those of yeast cell walls (Mukaremera *et al*., 2017). Further it has been demonstrated that the *C. albicans* yeast cell wall stimulated more chemokines than hyphal cell walls (Torosantucci *et al.,* 2000). Our study assessed the expression of the immune response within WT and *N*- and *O*-mannanosylation mutants of *Candida*. The mutants showed lower induction of immune response genes at 24 hpi than the WT.

This might be resulted from a reduced stimulation of the immune response in the host that is normally effected by glycosylated mannoproteins (Bates *et al.,* 2006). Elicitors of mannans and glucans in the cell wall may induce phagocytosis as a result of increased recognition by a range of immune receptors, such as C-type lectin and toll-like receptors (Erwig and Gow, 2016; Netea *et al*., 2006).

ß-glucan which is mostly buried beneath the outer layer of mannan (Levitz, 2010), can be considered as an essential layer for immune response by immune receptors such as dectin-1 (Wheeler and Fink, 2006; Torosantucci *et al.*, 2005). Overall, the immune response to Candida mutants can be explained as follows: the deletion of *O*- and *N*- mannan permits increased glucan exposure and therefore altered immune cell recognition (Mukaremera *et al.,* 2017; Wheeler and Fink, 2006).

Finally, transgenic *A. dispar* fish were generated in this study. The new line of *A. dispar* express a red fluorescent protein can be a useful model for Candida research. By using this fish, it may be possible to track the *C. albicans* dissemination inside the tissue after infection with contrasting GFP Candida strains.

In conclusion, the current study has shown the utility of the *A. dispar* model to monitor the evolution of the immune response following infection by fungal pathogens such as *C. albicans.*

Chapter 6-General discussion

6. 1 Normal embryonic development of *A. dispar* embryos

Over the last twenty years, the zebrafish, *Danio rerio*, has emerged as an excellent model for fungal infection studies due to its transparency, small size, high reproductive rate and extensive tool-kit for molecular analyses. However, there are limitations in using zebrafish as a model because the fish embryos cannot survive at 37°C. Recently, it has been discovered that the Arabian killifish (*A. dispar*) is able to live at a wide range of temperatures, including 37°C. In this study, *A. dispar* embryos were therefore exploited as a novel model for the investigation of the pathogenicity of *Candida albicans* in a live host at human body temperature.

As reported, the Arabian killifish is found in waters around the eastern Mediterranean, Iraq, Iran, Saudi Arabia, Syria, and north-east Africa, including Somalia. *A. dispar* tolerates a wide range of ambient temperatures and salinities and, as such, is unique among common laboratory models (Gholami *et al.,* 2011; Haq and Yadav, 2011). This species is known as a biological control agent for mosquito larvae. *A. dispar* is also tolerant of a wide range of pesticides and toxins and can tolerate low levels of O_2; therefore, it has been used as a biological model to evaluate ecotoxicity (Saeed *et al.*, 2015; Fletcher *et al*., 1992). Hence *A. dispar* can be considered as a suitable model to examine the effects of a wide range of environmental and pathogen mediated stressors on aquatic species.

Before this study, a detailed description of the stages of normal development in *A. dispar* was not available. Therefore, one of the main objectives of the study was to present accurate descriptions of embryonic development of *A. dispar*. In this study, fertilized eggs of *A. dispar* were incubated at 26 ± 1 °C to analyse the process of normal embryonic development. Embryogenesis was divided into 32 stages based on diagnostic features of development such as the number and size of blastomeres, formation of the blastoderm, range of epiboly and development of optic, otic, notochord, heart tissue and blood circulation

systems. In addition, embryonic development of *A. dispar* was examined under different thermal environments including 26.0, 30.0, 37.0 and 38.5°C ± 0.1°C. Moreover, *A. dispar* fertilised eggs were incubated in salinities of 0.3, 3, 10, 14, 35 and 150 ppt of NaCl at a temperature of 26°C to assess the effect of variation in salinity and temperature on the developmental process in *A. dispar*. The observations revealed that *A. dispar* eggs and embryos are optically transparent and so can be a novel model to investigate and monitor normal and abnormal fish embryogenesis with high quality imaging. Generally, our results show that the features of embryonic development in *A. dispar* are similar to those of the related medaka (Iwamatus, 2004) and mangrove killifishes (Mourabit *et al.*, 2011). However, some differences can be noticed between *A. dispar* and these better established models. For instance, as it was reported by Iwamatus (2004), that short hairs are distributed on the surface of the medaka chorion, whereas in *A. dispar* embryos, the chorion is smooth and does not have villi.

Compared with the Mangrove killifishes, that have a number of oil droplets in their yolk which remain in the later stages of development and disturb the quality of live imaging, the oil droplets in *A. dispar* yolk are rarer and smaller and they become less apparent at the later stages fish embryogenesis. Therefore, this study suggests that *A. dispar* is highly suitable for imaging analyses with or without the removal of the chorion. Contrary to the previous findings by Iwamatus (2004) who reported in medaka that the onset of blood circulation occurred at the late somite stage (stage 25) within a single blood vessel in the yolk, *A. dispar* embryos develop an intense blood vessel network earlier at the mid-somitogenesis stage (stage 22). Consequently, we propose that *A. dispar* is an excellent model for future studies to understand and study blood vessel development *per se*, or blood vessel reactions and remodelling following physical damage or interactions with toxicological agents and pathogens.

Various conditions including temperature and salinity might affect normal embryonic development of *A. dispar*. We therefore characterized the influence of both these conditions on *A. dispar* to provide detailed information on the relationship between increasing temperature and salinity

upon embryonic developmental rates. Our data are consistent with earlier studies that recorded accelerated embryonic development of fish in response to increased incubation temperatures (Hamel *et al*., 1997). *A. dispar* embryos incubated at higher temperatures had shorter development times, hatching on average at 168 hpf at 37.0°C compared to 320 hpf at 26.0°C. We also observed that the yolk sac size at higher temperatures was smaller than at low temperatures. It can be suggested that the increase in temperature may increase the rate of yolk absorption required for building tissue. This result supports previous studies of Ogira *et al*, (2014) and Fukuhara (1990) who reported that there is a correlation between increasing temperature and consumption of the yolk sac in *Oreochromis niloticus*, *Paralichthys olivaceu*, *Acanthopagrus schlegeli*, *Engraulis japonica* and *Pagrus major*. Moreover, the effect of temperature on embryogenesis of *A. dispar* presented in this study resembles the findings reported by Jun *et al.* (2015) who demonstrated that the incubation time of the obscure puffer, *Takifugu obscurus*, was significantly reduced as a response to increases in temperature.

Though the effect of temperature on developmental rates in *A. dispar* was of primary interest, salinity as a factor was also examined to assess its influence on embryonic development. It was hypothesized that successful growth and hatching can occur at extremes of salinity, to reflect its natural habitat range. To test this hypothesis, groups of embryos were incubated at a range of salinities and the survival, hatching time and morphologies of the embryos were assessed. An inverse relationship between salt concentration and hatching time was observed. In addition, at high salinity (150 ppt), the yolk sac at the later stages of development was clearly diminished. A result in agreement with Swanson (1998) who showed that milkfish growth rates tend to be higher at high salinities.

6. 2 *A. dispar* as a model to investigate fungal infections

Candida albicans is an opportunistic fungal pathogen. The yeast is present in healthy individuals as a commensal and can reside harmlessly on the skin and in the oral cavity (Naglik, 2014). However, it can cause morbidity

and mortality in both healthy and immunocompromised individuals, highlighting the key role of host defence mechanisms (Richardson *et al.,* 2015). *C. albicans* has numerous virulence factors that contribute to its potential survival and ability to become pathogenic at different infection sites (Mayer *et al.,* 2013). Fungal infections caused by *C. albicans* involve a variety of phenotypes and host-Candida interactions, often making it difficult to treat patients. *In vitro* studies of fungal infections have been attempted but are somewhat naïve, however *in vivo* (live-host) studies need more extensive evaluation of their validity (Vanherp *et al.,* 2018), particularly with respect to immunopathogenic characterizations and their dependance on context. A summary of the differences between *A. dispar* and other model organism are indicated in Table 6.1.

Table 6.1 *C. albicans* kills host organisms in a dose-dependent manner. Data shown in the table below are derived from the following publications or calculated from values given within them.

1 Chao *et al*., 2010
2 Loyola *et al*., 2002
3 Li *et al*., 2013
4 Davis *et al.,* 2011
5 Pukkila-Worley *et al*., 2011

Factors	*A. Dispar*	*D. rerio*	Mice	*G. mellonella*	*D. melanogaster*	*C.elegans*
Volume of the host organisms	0.4 µl	0.134 µl [1]	20g (20ml = 20,000 µl)[2]	134.6 µl[3]	3.14 µl[4]	0.006 µl[5]
Lethal dose: Cells/host	50,000	500[1]	200,000[2]	10,000[3]	500[4]	Unknown
Lethal dose: Cells/µl	125,000	3,730	10	74	160	Unknown
Tolerated dose: Cells/host	500	<5[1]	10000[2]	1250[3]	3[4]	Unknown
Tolerated dose: Cells/µl	1.25	37.30	0.50	9.28	0.95	Unknown
Commensal	✓	×	✓	×	×	×
Live imaging	✓	✓	×	×	✓	✓
Immune system	Innate/ Adaptive	Innate/ adaptive	Innate/ adaptive	Innate	Innate	Innate
Gastrointestinal infection/ no-injection	?	×	✓	×	✓	✓

To study infection in animal models, survival rates and fungal burdens are commonly used as parameters for assessing virulence. Initial results establishing *A. dispar* as a model for investigating the virulence of *C. albicans* indicated higher levels of tolerance, as seen by persistence of *C. albicans* in the host compared with other models (Table 6.1).

Lethal dose for an infectious agent is generally defined as the initial dose which is required to kill 50% or more of infected animals (Haschek *et al*., 2013). The method and site of inoculation and species of animal model under study may affect the dose required. Tolerance relates to the maximal dose of a pathogen that a host can withstand without causing overt disease. Tolerance reflects the ability of a host to clear an infection and is therefore a proxy for the effectiveness of the immune response.

In this study, we detected the ability of *A. dispar* to grow and survive and develop as a commensal at the lower Candida concentrations. This contrasts with zebrafish and *Drosophila melanogaster* that both show high mortality at relatively low doses (Chao *et al*., 2010; Li *et al*., 2013; Ames *et al*., 2017).

Table 6.1 shows the similarity in the high lethal dose: cells/ *A. dispar* and mice compared with other models even though the size of the host is very different. This is a remarkable feature of *A. dispar* as a model. It is possible that such behaviour may depend on its capacity to adapt to the harsh environment it commonly encounters.

Our hypothesis was partly correct and partly wrong: *A. dispar* embryos and eggs were suitable for investigating infection at 37°C; however, *A. dispar* embryos were much more tolerant to Candida infection than Zebrafish potentially making these fish a very useful model for the future.

To evaluate *A. dispar* as a novel model for infection studies, we compared the effects of Candida infection in zebrafish and *A. dispar* at 26°C. The results showed that Candida inocula at $1x10^8$ cells/ml killed all zebrafish embryos within 72 hpi but *A. dispar* embryos survived more than 120 hpi. We still do not know the mechanisms by which a stronger antifungal immune system is acquired in *A. dispar* so it would be beneficial to quantitatively compare numbers of macrophages and neutrophils in the

two-species using more stage specific analyses such as western blotting or qPCR.

Numerous *in vivo* observations have revealed that the immune system response against pathogens is bi-directional and complex (Nguyen-Chi *et al.,* 2015). Although fungal infections have been extensively studied in mammals and zebrafish, and we have an extensive understanding of the Candida-induced cellular responses in zebrafish at 28°C and mice at 37°C, we have limited understanding of fungal infection-innate immune responses at 37°C in a model animal that is amenable to live imaging techniques. Therefore, one of the main objectives of the present project was to address the ability of the *A. dispar* embryos to develop and survive at human body temperatures. Further investigations of *C. albicans* interactions with *A. dispar* embryos were therefore conducted at physiologically relevant temperatures of 30°C and 37°C. Generally, our results support the proposition that *A. dispar* will be useful for studying cellular and tissue interactions with human pathogens as well as those of fish.

This study also focused on an investigation of the survival of *A. dispar* embryos with Candida infections, examining the impact on virulence and host mortality of the fish following the deletion of mannose residues from the cell wall of *C. albicans*. We also investigated the survival of infected *A. dispar* embryos with an antifungal agent (Fluconazole). Finally, we investigated and assessed the role of innate immune cells such as macrophages and neutrophils and quantitatively analysed their responses during infection.

It was found that after testing a range of inocula, that *C. albicans* killed *A. dispar* embryos in a dose-dependent manner. After infection with *C. albicans* ($1x10^8$ cells/ml), *A dispar* embryos survived for 120 hpi at 37.0°C, contrasting with other models. *Galleria mellonella* larvae die at $1x10^6$ cells/ml; and none of the zebrafish embryos survive for about 50 hpi at of $1x10^8$ cells/ml at 30.0°C (Chao *et al*., 2010; Li *et al.,* 2013).

To test if Candida can infect *A. dispar* embryos in different ways, we incubated the *A. dispar* embryos with Candida under different culture

conditions. We found that if the culture is enriched with RPMI and serum, both WT and mutant Candida strains can proliferate. However, cells introduced via media did not show any penetration through the chorion and therefore could not infect the embryo itself. This result contrasts with the previous data relating to zebrafish, in which Candida could penetrate the chorion and infect embryos (Chen *et al*., 2015). This difference is possibly due to the harder and thicker chorion of *A. dispar.* Pathogens often use a variety of hydrolytic enzymes and proteases to break down and penetrate the surface structures of the host (e.g. chorion, epidermal skin). During this study, we found that very intense protease treatment is required to break down the chorion of *A. dispar* (1 hour of 20 mg/ml pronase + 3 hours of crude hatching enzyme extract - see methods chapter for details). In contrast, zebrafish, only require 10 min of 1 mg/ml pronase treatment to break down the chorion (Mandrell *et al*., 2012).

Our egg infection system was mainly used for demonstrating the adhesion activity of Candida to the host permitting the examination of growth and germ tube formation in culture conditions.

As a next step of study, it would be interesting to remove the chorion of the embryo and set up infections via Candida in water. This would allow us to investigate the interaction of Candida with the host skin at human body temperatures. Feeding adult *A. dispar* fish with *C. albicans* would be of interest to see if a gut commensal relationship could be established – however current licensing and facilities preclude this.

Candida showed adherent behaviour and proliferation on the surface of eggs (chorion). If we want to further improve this assay to examine adhesion and growth of Candida, it should be possible to isolate the chorion itself and use it as a substrate for adhesion. This would allow better imaging due to the smaller size and flatter architecture of the surface. Zebrafish chorion might possibly be a better substrate because it would also allow us to monitor event of adhesion and penetration due to its softer nature.

A. dispar is potentially a suitable model to study Candida infection under conditions that mimic the bloodstream in humans. Previously it was found

that media additives such as serum, can be essential to causing full virulence in *C. albicans* infecting zebrafish (Chen *et al*., 2015). This study addressed the requirement for serum for induction of morphological changes (yeast to hypha switches) at 37.0°C. The current data showed that the hyphal form of *C. albicans* was observed on the chorion of embryos within the co-incubated egg water and serum, and it increased further when supplemented with RPMI/serum. Kucharrkova *et al.*, (2011) have reported that the RPMI 1640 enhanced biofilm formation by heightening the yeast to hyphal transition in *C. albicans.* Use of eggs rather than embryos may facilitate high-throughput screening of mutants or antifungal drugs.

We observed also that *C. albicans* can grow in RPMI media supplemented with 17 and 35 ppt/ indicates that it becomes tolerant to salt. Krauke and Sychrova (2010) also argues that *C. albicans* is more tolerant of salt than other species, such as *C. glabrata*-allowing comparison to be made between these species in our model. There was some delay in the growth of *C. albicans* with 35 ppt/ASW, a result that agrees with the findings of Krauke and Sychrova (2010) who found that 500 mM NaCl (equivalent to 35 ppt/ASW) resulted in a 20% delay in the onset of the exponential phase of *C. albicans* growth.

Temperature is a vital factor for controlling *C. albicans* morphology (Nadeem *et al.,* 2013). *C. albicans* growth can be affected by a wide range of temperatures, the morphogenetic transition to a hyphal form is regulated by elevation of temperature to 37.0°C (Shapiro *et al.,* 2009). Studies of the impact of temperature on the outcome of *C. albicans* and *C. tropicalis* infections revealed that faster killing of *G. mellonella* occurs at 37.0°C compared with 30.0°C (Mesa-Arango *et al.,* 2013; Ames *et al*., 2017).

Nadeem *et al.,* (2013) reported that Candida can develop germ tubes in culture media containing serum. When infections of *C. albicans* were set up in *A. dispar* incubated at different temperatures, the highest Candida burdens were observed at 30.0°C at 24, 48 hpi and 37.0°C at 48 hpi, a result supporting previous studies by Hazen and Hazen (1987) and Antley and Hazen, (1988), who suggested that the virulence of *C. albicans* increased at 26.0°C compared to 37.0°C in mice. Virulence characteristics

can be influenced by growth temperature. For example, Candida cells appear to form germ tubes and are able to adhere to the tissue which is a crucial initial step in causing infections at RT (Antley and Hazen, 1988). In addition, temperature can influence the conjugation and engulfment of nonopsonic phagocytosis due to the cells of *C. albicans* at RT being more hydrophobic than at 37.0°C (Saito *et al.,* 1986). Antley and Hazen (1988), also showed that incubation at RT appears to positively influence the increase in *C. albicans* growth. When challenged by phagocytes, at RT *C. albicans* produce abundant germ tubes preventing the polymorphonuclear leukocytes (PMNs) from killing the pathogen, which are not active at lower temperatures.

Comparisons of the burden of Candida in the brain and yolk of embryos reveal a progressive reduction in the burden of Candida in the brain at 48 hpi and 120 hpi compared with the infected yolk. A possible explanation is that the brain infection results in increased activation of microglial cells and astrocytes. Microglial cells are known to develop an activated state, following injurious stimuli where they migrate, proliferate and phagocytose follow a morphological transition at the injured sites. In addition to the secretion of molecules for repairing the tissue (Maneu *et al*., 2014), microglial cells have the ability to invade targeted tissue to provide protection by promoting regeneration and supporting neuronal survival (Langmann, 2007). The possibility that dissemination of Candida away from infection sites might be linked to increases of temperature was explored. In the present study, three methods were used to analyse the dissemination of Candida inside the embryos; a histological and immunofluorescence analysis. Live-imaging revealed that whilst *C. albicans* disseminated away from the infected site within the embryos at 37°C, cells were only observed to undergo a morphological transition at the site of infection. *A. dispar* is therefore a valuable model for studying the progression of *C. albicans* at different temperatures.

The quantitative assessment of *C. albicans* proteins were used in this study to highlight the time-course of infection in *A. dispar* embryos. The level of Candida proteins expressed in infected *A. dispar* embryos increased at 24 hpi and 48 hpi and slightly reduced at 72 hpi, with the expression dramati-

cally decreasing at 96 hpi. A previous study in zebrafish showed that higher proliferation of *C. albicans* was observed in surviving fish at 24 hpi (Brothers *et al.*, 2011). This contrasts somewhat with our result demonstrating that *A. dispar* survived longer and the quantity of Candida detected by GFP/mCherry protein significantly dropped whilst we did not assess the protein level beyond 120 hpi. This result suggests that the lower level of Candida protein at 120 hpi probably occurred as a result of cleared infections or it is also possible that small numbers of Candida cells remained having established a commensal relationship without causing further disease. This should be an interesting focus for future research with detailed imaging and quantification of Candida cells in long-term infection.

Our work clearly demonstrates the utility of *A. dispar* to understand virulence of mutants in *C. albicans*. Differences between glycosylation mutants in in *A. dispar* were compare with published data. Glycosylation deficient mutants have been extensively studied and both *pmr1*Δ and *och1*Δ show similarities in their phenotypes as a result of a reduction of the 1,6-mannosyltransferase and therefore the α-1,6-linked polymannose core (Bates *et al.,* 2006). Whereas *O*-and *N*- glycosylation mutants lack an α-1,2-linked polymannose core, leading to an increased sensitivity to cell wall perturbing agents (Munro *et al.,* 2005). The present result demonstrated that the fungal burden with the three mutants of *C. albicans (mnt1-mnt2*Δ*, pmr1*Δ and *och1*Δ) seemed to be clearly lower than that observed with the reintegrant control. A possible explanation for the decrease in fungal burden with *och1*Δ is that the cells tend to aggregate due to cell separation defect infectious influencing growth rates *per se* and the ability to form multiple colony forming units. However, *pmr1*Δ exhibits a delayed morphological transition, while *mnt1-mnt2*Δ*,* mutant showing defects in cell separation (Hall *et al.,* 2013). The observed decline in growth rate, seems to be in agreement with previous findings, which showed a decreased virulence of *mnt1-mnt2*Δ in *G. mellonella* (Navarro-Arias *et al.,* 2016). Moreover, our studies can indicate a change in adherence to eggs suggesting that the outer layer of the *C. albicans* cell wall (mannosylated proteins) is important for cell adhesion and biofilm formation (Chaffin *et al.,* 1998). The present study also explored the possibility that a deficiency of

mannan on the Candida cell wall might influence the rate of mortality of infected embryos. Despite the attenuation of fungal burden with all three mutants, we found that the rate of mortality was increased, especially with *pmr1*Δ and *mnt1-mnt2*Δ mutants at 48-96 hpi. This result suggests that the defect in *N*- and *O*-mannan may affect the recognition of fungal cells and subsequent immunostimulatory response and thus their uptake by immune cells.

A. dispar can be utilized to address the efficacy of antifungal drug agents. *C. albicans* infections were suppressed in *A. dispar* by fluconazole (FLC) in a dose and time dependent manner. The present study demonstrated that FLC displayed a strong activity against *C. albicans* in infected embryos, resulting in both a reduced number of CFUs of *C. albicans* and continued survival of embryos, especially at the highest concentrations of FLC at 32 mg/l and 64 mg/l at 6 hpi. Such a finding is corroborated by Richardson *et al.,* (1985) and Trok *et al.,* (1985), who demonstrated the high efficiency with which FLC can clear fungal infections in mice. However, it is not possible to directly compare dose response effects between *A. dispar* and mice as we added the FLC in the culture water and cannot determine precisely the actual concentration incorporated into the embryo without further tissue analysis. Overall, the results of the current study demonstrate that fluconazole was able to promote the clearance of infections of *C. albicans*; howevere, we do not know if this was a result of fungistatic or fungicidal activity. *A. dispar* therefore represents a valid model for screening antifungal compounds against *C. albicans* and potentially other pathogenic fungi.

6.3 Immune response against *C. albicans*

A complex relationship exists between *C. albicans* and the host immune system that must recognise distinct pathogen-associated molecular patterns (PAMPs) (Duhring *et al*., 2015; Qin *et al*., 2016; da Silva Dantas *et al.,* 2016). Several major types of PAMPs are associated with the fungal cell wall including *O*- and *N*-linked mannans, ß-glucans and phospholipomannans (Netea *et al.,* 2008). The majority of PAMPs are recognised by host PRRs leading to activation of both innate and adaptive

immune cells. The outcome of these interactions is an induction of a wide range of cytokines, and chemokines and other inflammatory mediators (Naglik, 2014). The sequence information we have obtained from *A. dispar* allows gene expression to be studied and cellular changes to be quantified following external stimuli in both the healthy and diseased states.

During microbial infections, innate immune cells play a key role in protecting the host from Candida infection through activation of an inflammatory response (Gratacap *et al*., 2017). Pigment cells may act as a guide to the site of injury following immune cell responses (Levesque_*et al*., 2013). Our data support this view, as killing assay show that there was a decrease in the ability of the Casper zebrafish mutant (lacking pigment cells) to survive, compared to the wild-type zebrafish embryos. Casper mutants lack melanophores, xanthophores and iridophores. Our data indicate the importance of these pigment cells in the immune response against *C. albicans*. Makosh (2001) suggested that melanisation plays an important role as an inhibitor of microorganisms, recruiting melanocytes to the infection sites. Indeed, there is a strong correlation between melanocytes and the inhibition of infection through an inducition of hypo- or hyperpigmentation that results in activation of Toll-like receptors (TLRs) (Tapia *et al.*, 2014). Even though we may want to remove pigmentation for improving imaging capabilities, it is not ideal to do so when we need to examine the natural immune response of the host organism.

Neutrophils are the hallmark of inflammation and can migrate towards infected sites in Zebrafish (Chen *et al*., 2013), and it is possible to stain and monitor their activity (numbers and migration) as an accurate and efficient way to assess acute inflammatory responses.

Sudan black was found to be suitable stain to define neutrophil granules in *A. dispar*. This technique can easily be used to trace neutrophils and assess their distribution and functional lineages during development (Le Guyader, 2008). We found that in infected embryos neutrophils were mostly distributed in the entire trunk and tail fin of zebrafish, whereas almost no neutrophils were observed in the uninfected controls suggesting an increase of the numbers of immune cells during infection. This result suggests the requirement for granulocytes in the immune response against

Candida infections. Previous studies have revealed the utility of zebrafish as a suitable host for tracing neutrophils and shown that these coincide with the distribution of endogenous peroxide (Guyade *et al*., 2008). Therefore, the use of another transparent host such as *A. dispar* will help the understanding of granulocytes at physiologically relevant temperatures. In addition, another neutrophil specific stain, FITC-tyramide, was tested to reveal endogenous peroxide in both zebrafish and *A. dispar* embryos. The results indicated the accumulation of peroxidase-positive granulocytes in the trunk. It is therefore possible to analyse the interactions of Candida and neutrophils using a range of tools.

The response of macrophages to Candida infection in *A. dispar* was assessed using a variety of approaches. We examined host-Candida interactions by spatial detection of macrophages using whole mount immunohistochemistry and a macrophage marker (L-plastin). We tested *L-plastin* expression within both the control and the infected zebrafish and then investigated *L-plastin* expression within *A. dispar.* Increased macrophage was detected within infected embryo at 24 hpi in both zebrafish and *A. dispar,* and our detection of the macrophages was greatest at 48 hpi. *L-plastin* dramatically increased in expression after 1 hpi, indicating the rapidity of the macrophage response when challenging the pathogens. The peak induction of macrophages to Candida infection was much later however at 24 and 48 hpi. Giulian *et al*., (1989) illustrated that the peak of the phagocyte cell response occurs 2 d after injury, supporting our result.

Previous work has shown that the knockdown of *irf8* function in zebrafish results in a depletion of macrophages and increase of the neutrophil population (Li *et al*., 2011; Jin *et al*., 2012). To investigate the suppression of *irf8* in our model *A. dispar,* we designed and injected *irf8*-MO into the one-cell stage. We found that after infection with Candida at the somitogenesis stages, macrophages were not observed, in contrast to those that appeared in the untreated embryos. The reduction of *L-plastin* expression following *irf8*-MO treatment was clearly specific. When the *ifr8* gene was knocked down in *A. dispar*, the survival rate following infection by *C. albicans* was reduced, and all of the embryos died by 48 hpi compared with the control

which survived until 96 hpi. Our analyses therefore strongly suggest that blocking macrophage development caused the lethality of embryos upon Candida infection, and that macrophages have a crucial role in protecting the host from infection. However, further research is needed to clarify and assess the role of neutrophils in protection of the embryos alongside the study of macrophage in *A. dispar*.

In this study, we also investigated the role of *cxcr4* in regulating macrophage differentiation. Richard *et al.,* (2008) mentioned that *cxcr4*, which belongs to the chemokine family, has been known as a director of precursor cells and plays a signalling role in regulating movement of macrophages. The suppression of *cxcr4* in *A. dispar* embryos resulted in an irregular distribution of monocytes with reduce numbers after infection. The survival rate was lower and all the embryos died by 24 hpi. Knockdown of *cxcr4* function may lead to an inhibition of the receptors which are responsible for regulating monocyte migration and differentiation (Sánchez *et al*., 2011). This suggestion is supported by previous finding of Gupta *et al*., (1999) who illustrated the essential role of *cxcr4* in guiding and regulating the movement of monocytes during the inflammatory response in zebrafish. The expression of *cxcr4* has an essential role in the differentiation of monocytes to a distinct type of macrophage (Sánchez *et al.,* 2011); monocyte development is therefore reduced as a result of interruption in *cxcr4* expression, potentially explaining why lethality is higher than *irf8* MO treatment.

Microglia have immune defence functions to maintain the central nervous system CNS (Kettenmann *et al.*, 2011). Many researchers have referred to the sentinel function of microglia as an immune cell in detecting the first sign of foreign pathogens and preventing tissue damage in the delicate sites of the CNS such as the brain (Kettenmann *et al.*, 2011; Perry *et al.,* 2010; Lull and Block 2012). Previously, systematic infections have been studied in mice and results show significant activation and distribution of microglia in infected sites (Maneu *et al*., 2014). It was therefore hypothesized that brain tissue infected with Candida might trigger microglial cell proliferation (Thompson *et al.,* 2017). This hypothesis was mainly supported: Immunofluorescence experiments detecting microglia in *A. dispar* em-

bryos using a 4C4 antibody showed the proliferation of microglia in both the brain and spinal cord. Interestingly, even though the Candida was injected into the midbrain, massive increases of microglia were also observed in the spinal cord. This implies that Candida cells can spread along the neural tube, or damage in the brain may trigge a massive expansion of the microglia which may repair the CNS tissues in the spinal cord connected to the brain. To test these possibilities, we would need to examine the distribution of Candida using fluorescently labelled cells, and simultaneously assess microglial/inflammatory markers in CNS tissues, the brain and spinal cord.

In the current study, despite the clear pathogenicity of *C. albicans*, the *A. dispar* model showed an ability to survive infection doses better than zebrafish demonstrating an adaptation of the immune system. Time-course studies of the immune response (the amount of *L-plastin*/macrophages) assessed using western blotting, demonstrated that the macrophage population changed. In response to the infection, we observed the highest expression of *L-plastin* at 24 and 96 hpi, but a significant down-regulation at 48 and 120 hpi suggesting a bi-phasic activation of activated (M1) and alternative (M2) macrophages (Wang, Liang, and Zen 2014). Previous studies have indicated that M1, the activated macrophages, have an important role secreting proinflammatory cytokines and chemokines to protect the tissues from surrounding cells, whereas alternative macrophages (M2) play a key part in wound healing and reduce the expression of pro-inflammatory cytokines to promote tissue repair (Wang, Liang, and Zen 2014; Kapellos et al 2016; Collins and Carmody, 2015; Biswas and Mantovani, 2010).

The excellent live cell imaging achieved with *A. dispar* allows direct viewing of the

phagocytosis of yeast cells at infection sites. By building on this new model fish, it is clear that macrophages seem to be effective actors in clearing *Candida* infections, however, this may be dependent on the site and state (chronic *versus* acute) of infection. Herbomel *et al*., (1999), also implied that microbe elimination by phagocyte cells depends on anatomical sites of infection and the nature of the pathogens.

Reactive Oxygen Species (ROS) play a protective role in the immune system (McCallum *et al.,* 2016). 2',7'- dichlorofluorescein (H_2DCFDA / DCFDA)

is the most frequently used method for measuring redox state of the cells as an accurate sensor for ROS (Eruslanov and Kusmartsev, 2009). The advantages of this technique are that it is easy to use, inexpensive, highly sensitive to redox state changes and can be used to trace ROS changes in the cells over time (Eruslanov and Kusmartsev, 2009). In this work, we examined the Candida induced ROS immune response within *A. dispar* because this may help to better understand immune interactions at the sites of infection. The fluorescent probe was observed to accumulate at the site of infection (trunk) and in the tail fin at 30 mpi. A possible explanation for the detection of ROS in the tail fin site is that Candida cells may be transported to the tail by blood circulation.

Comparison of WT and mannosylation mutants revealed the importance of the cell wall in bringing about a ROS response. Compared with the *pmr1*Δ mutant, a high level of ROS was detected within WT and *mnt1-mnt2*Δ, while lower expression was observed within PBS control samples. Release of ROS after infection with a mutant can occur as a result of subsequent detection of β-glucans by immune cells. Since the innate immune response is required to control foreign pathogens, we hypothesized that different immune response requirements determine the specific patterns of gene expression. A range of gene markers related to the macrophages, neutrophils and NADPH oxidase were examined by qPCR and they were found to be expressed at different ratios following infection, providing important details regarding the effect of Candida infection and the impact of deleting mannans.

Finally, in this work, we have generated a new transgenic line of *A. dispar* by microinjection of plasmid DNA (Beta-actin-DsR-LoxP-GFP) at the one cell embryo stage indicating the clear potential to provide to manipulate aspects of the pathogen and immune interaction in *A. dispar*. In addition, we believe that the generation of transgenic *A. dispar* can provide a useful tool for future developmental, embryological infection studies with *C. albicans* and other pathogens.

6.4 Future scope

The use of *A. dispar* as a model for studying fungal infections in a live host has emerged as a new powerful tool for research. Imaging is directly possible because of its transparency. The fish can survive at a wide range of temperatures. In contrast to zebrafish and mice, the transparency *A. dispar* embryos and its ability to survive at different temperatures (4 to 40°C) will allow a range of human infectious diseases to be examined (not just *C. albicans*) in real-time revealing in greater detail the interaction between the pathogen and immune cells. A summary comparison of *A. dispar* and *D. rerio* as models is provided in Table 6.2

Table 6.2 Summary comparison of *A. dispar* and *D. rerio* as models

	A. dispar	*D. rerio*
Candida infection	Survive longer	Quicker mortality
Temperature range	Up to 40˚C	Up to 32˚C
Muscle movement	3 dpf	15 hpf
Fluorescent pigments	Highly fluorescent leucophore	Weakly fluorescent iridophore
Genome and transcriptome	Only in house RNA-seq data	Rich in both information
Fecundity	- 20 eggs/day	- 200 eggs/day
Hatching	12 days	2 days
TG fish lines	bAct_DsR_LoxP_GFP	Many immune specific lines and other lines

A reference genome for *A. dispar* was not available at the time of the analysis. This limitation can be solved by undertaking a systematic genome sequencing project. The quantitative analysis of immune responses conducted in *A. dispar* embryos used some specific primers of immune response genes such as *L-plastin, cxcr4, csf1r, nox1,* and *nos1a*. However, sequences of other immune response markers for *A. dispar* were not fully

available from our database - including markers for activated and alternative macrophages, granulocytes and pigment cells. We tested knockdowns of *irf8* and *cxcr4* in *A. dispar* embryos using morpholino, this approach showed that macrophages functions could be suppressed. The limitation of this approach is that testing of immune function can only occur for a few days after infection as the morpholino may be degraded over time. To confirm the results and conduct further analyses of the long-term effects of manipulating genes during infection, it would be interesting to create gene knock out using CRISPR/Cas9 mediated genome editing approaches (Ota *et al.,* 2014).

Interestingly, a new line of transgenic *A. dispar* fish with red fluorescence colour was generated in this work but there was not enough time to use this line for additional research. Therefore, in the future, we would like to simultaneously track *C. albicans* dissemination and host interactions using these fluorescence fish alongside GFP, RFP or CFP labelled macrophages and neutrophils in the live embryo. Nevertheless, we conclude that *A. dispar* has the capability to be developed further and potentially play a key role as a model in different areas of host-pathogen research.

The work presented in this thesis has raised several questions and our new model has given an insight into fungal infections and immune responses. The ability of *A. dispar* to withstand a range of host temperatures should allow the Candida response to be examined under low, normal and pyrexic / inflammatory conditions – something that is unique to this model.

References

Achterman, R. R., Smith, A. R., Oliver, B. G., White, T. C. (2011). Sequenced dermatophyte strains: growth rate, conidiation, drug susceptibilities, and virulence in an invertebrate model. Fungal Genetics and Biology, 48(3), 335–341.

Aguirre, K. M., Gibson, G. W. (2000). Differing requirement for inducible nitric oxide synthase activity in clearance of primary and secondary *Cryptococcus neoformans* infection, Medical Mycology, 38(5), 343–353.

Ahmad, I., Owais, M., Shahid, M. and Aqil, F. (2010). Combating fungal infections: Problems and remedy, Combating Fungal Infections: Problems and Remedy, 1–539.

Akira, S., Takeda, K., Kaisho T. (2001). Toll-like receptors: critical proteins linking innate and acquired immunity. Nature Immunology, (2), 675-680.

Al-Zaidan, A. S. (2017). The Acute Effects of Un-ionized Ammonia on Zebrafish (*Danio rerio*). Fisheries and Aquaculture Journal, 8(3), 2150-3508

Ames, L., Duxbury, S., Pawlowska, B., Ho, H. L., Haynes, K., Bates, S. (2017). *Galleria mellonella* as a host model to study *Candida glabrata* virulence and antifungal efficacy. Virulence. 8(8), 1909-1917.

Antley, P. P., Hazen, K. C. (1988). Role of yeast cell growth temperature on *Candida albicans* virulence in mice. Infection and Immunity, 56(11), 2884–2890.

Antonio, N., Bonnelykke-Behrndtz, M. L., Ward, L. C., Collin, J., Christensen, I. J., Steiniche, T., Schmidt, H., Feng, Y. and Martin, P. (2015). The wound inflammatory response exacerbates growth of pre-neoplastic cells and progression to cancer. The EMBO Journal, 34(17), 2219–2236.

Arash, A., Azam, N. M., Ahmad, N., Paria, P., Mohammad, A., Morteza, Y., Hadi, D., Ehsan, K. (2014). Responses of the killifish (*Aphanius dispar*) to long-term exposure to elevated temperatures: growth, survival, and microstructure of gill and heart tissues. Marine and Freshwater Behaviour and Physiology, 47(6), 429-434.

Arduini, B.L., Gallagher, G.R., Henion, P.D. (2008). Zebrafish endzone regulates neural crest-derived chromatophore differentiation and morphology. PLoS ONE 3(7), e2845.

Arias, M. J., Defosse, T. A., Dementhon, K., Csonka, K., Mellado-Mojica, Erika., Dias Valério, A., González-Hernández, R, J., Courdavault, V., Clastre, Marc., Hernández, N, V., Pérez-García, L, A., Singh, D, K., Vizler, C., Gácser, A., Almeida, R, S., Noel, T., Lopez, M, G., Papon, N., Mora-Montes, H. M. (2016) Disruption of Protein Mannosylation Affects *Candida guilliermondii* Cell Wall, Immune Sensing, and Virulence. Frontiers in Microbiology, 7, 1951.

Avdesh, A., Chen, M., Martin-Iverson, M. T., Mondal, A., Ong, D., Rainey-Smith, S., Taddei, K., Lardelli, M., Groth, D M., Verdile, G., and Martins, RN. (2012). Regular care and maintenance of a Zebrafish (*Danio rerio*) laboratory: An introduction. Journal of Visualized Experiments: JoVE, 69, 4196.

Avtalin, R. R. And Clem, L., W. (2009). Environmental control of the immune response in fish. CRC Review in environment control, 11(2), 163-188.

Bader, O., Naglik, J., Albrecht, A., Bader, O. and Hube, B. (2004). *Candida albicans* proteinases and host / pathogen interactions. Cell microbiology, 6(10), 915-926.

Bae, Y. S., Oh, H., Rhee, S. G. and Yoo, Y. Do (2011). Regulation of reactive oxygen species generation in cell signaling, Molecules and Cells, 32(6), 491–509.

Baensch, H. A. and Riehl, R. (2004) Aquarium Atlas. Volume 4. Mergus Verlag, Melle, Germany.

Baggiolini, M. (1998). Chemokines and leukocyte traffic. Nature 392, 565 - 568.

Balázs Rada, and T., L., L. (2008). Oxidative innate immune defenses by Nox/Duox family NADPH Oxidases. Defense, 15,164–187.

Bañuelos, S., Saraste, M., Carugo, K. D. (1998) Structural comparisons of calponin homology domains: implications for actin binding. Structure, 6(11), 1419–1431

Bates, S., Bleddyn Hughes, H. B., Munro, C. A., Thomas, W. P. H., MacCallum, D. M., Bertram, G., Atrih, A., Ferguson, M. A. J., Brown, A. J. P., Odds, F. C., Gow, N. A. R. (2006). Outer Chain N-Glycans Are Required for Cell Wall Integrity and Virulence of *Candida albicans*. The journal of biological chemistry, 281(1), 90 –98.

Bates, S., MacCallum, D. M., Bertram, G., Munro, C. A., Hughes, H. B., Buurman, E. T., Brown, A. J., Odds, F. C., Gow, N.A. (2005). *Candida albicans* Pmr1p, a secretory pathway P-type Ca2+/Mn2+-ATPase, is required for glycosylation and virulence. Journal of Biological Chemistry, 280(24), 23408-23415.

Bates, S., Hughes, H. B., Munro, C. A., Thomas, W. P. H., MacCallum, D. M., Bertram, G., A., Ferguson, M. A. J., Brown, A. J. P., Odds, F. C., Gow, N. A. R. (2006). Outer chain N-Glycans are required for cell wall integrity and virulence of *Candida albicans*. Biological Chemistry, 28(1), 90-98.

Becker, T., Becker, C., G. (2001). Regenerating descending axons preferentially reroute to the gray matter in the presence of a general macrophage/microglial reaction caudal to a spinal transection in adult zebrafish. The journal of comparative neurology, 433(1), 131-14.

Benard, E. L., van der Sar, A. M., Ellett, F., Lieschke, G. J., Spaink, H. P., & Meijer, A. H. (2012). Infection of zebrafish embryos with intracellular bacterial pathogens. Journal of visualized experiments, 61. e3781.

Bennett, C. M., Kanki, J. P., Rhodes, J., Liu, T. X., Paw, B. H., Kieran, M. W., Langenau, D. M., Delahaye-Brown, A., Zon, L. I., Fleming, M. D. and Look, A T. (2001). Myelopoiesis in the zebrafish, *Danio rerio.* Blood, 98(3), 643–651.

Biswas, S. K., Mantovani, A. (2010) Macrophage plasticity and interaction with lymphocyte subsets: cancer as a paradigm. Nature Immunology, 11(10), 889–896.

Blasius, A. L., and Beutler, B. (2010). Review intracellular Toll-like receptors, Immunity, 32(3), 305–315.

Bolard, J. (1986). How do the polyene macrolide antibiotics affect the cellular membrane properties? Biochim Biophys Acta, 864 (3-4), 257-304.

Bony, M., Thines-Sempoux, D., Barre, P., Blondin, B. (1997). Localization and cell surface anchoring of the *Saccharomyces cerevisiae* flocculation protein Flo1p. Journal of Bacteriology, 179(15), 4929–4936.

Brand, A. (2012). Hyphal growth in human fungal pathogens and its role in virulence, International Journal of Microbiology, 2012.

Brothers, K. M., Newman, Z. R., Wheeler, R. T. (2011). Live imaging of disseminated candidiasis in zebrafish reveals role of phagocyte oxidase in Limiting Filamentous Growth. Eukaryotic cell, 10(7), 932–944.

Brothers, K. M., Gratacap, R. L., Barker, S. E., Newman, Z. R., Norum, A., Wheeler, R. T. (2013). NADPH oxidase-driven phagocyte recruitment controls *Candida albicans* filamentous growth and prevents mortality. PLoS pathogens, 9, e1003634.

Brown, G. D. (2012). Innate antifungal immunity: the key role of phagocytes. Annual Review of Immunology, 29, 1–21.

Brown, G.D., Taylor, P. R., Reid, D. M., Willment, J.A., Williams, D.L., Martinez-Pomares, L. (2002). Dectin-1 is a major beta-glucan receptor on macrophages. Journal of experimental. Medicice, 196, 407–412.

Butler, G. (2010). Fungal sex and pathogenesis. Clinical Microbiology Reviews, 23(1), 140-159.

Buurman, E. T., Westwater, C., Hube, B., Brown, A. J., Odds, F. C., Gow, N. A. R. (1998). Molecular analysis of CaMnt1p, a mannosyl transferase important for adhesion and virulence of *Candida albicans*. Microbiology, 95, 7670–7675.

Cacciapuoti, A., Loebenberg, D., Parmegiani, R., Antonacci, B., Norris, C., Moss, E. L., Menzel, F., Yarosh-Tomaine, T., Hare, R. S. and Miller, G. H. (1992). Comparison of SCH 39304, fluconazole, and ketoconazole for treatment of systemic infections in mice, Antimicrobial Agents and Chemotherapy, 36(1), 64–67.

Calderone RA, Clancy C. J. (2012). Candida and candidiasis, Second Edition, 524.

Calderone, R. A., Fonzi, W. A. (2001). Virulence factors of *Candida albicans*. Trends Microbiology, 9(7), 327-35.

Cambi, A., Gijzen, K., de Vries, l. J., Torensma, R., Joosten, B., Adema, G. J., Netea, M. G., Kullberg, B. J., Romani, L., Figdor, C. G. (2003). The C-type lectin DC-SIGN (CD209) is an antigen-uptake receptor for *Candida albicans* on dendritic cells. Immunology, 33(2), 532–538.

Cao, Q., Wang, Y., Harris, D. C. H. (2014). Macrophage heterogeneity, phenotypes, and roles in renal fibrosis. Kidney International Supplements, 4(1), 16–19.

Castillo, L., Calvo, E., Martínez, A. I., Ruiz-Herrera, J., Valentín, E., Lopez, J. A., Sentandreu, R. (2008). A study of the *Candida albicans* cell wall proteome. Proteomics, 8, 3871–3881.

Castillo, L., MacCallum, D. M., Brown, A. J. P., Gow, N.A. R., Odds, F. C. (2011). Differential regulation of kidney and spleen cytokine responses in mice challenged with pathology-standardized doses of *Candida albicans* Mannosylation Mutants. Infectious Immunology, 79(1), 146-152.

Chaffin, W. L., López-Ribot, J. L., Casanova, M., Gozalbo, D., Martínez, J. P. (1998). Cell wall and secreted proteins of *Candida albicans*: identification, function, and expression. Microbiology and Molecular Biology Reviews, 62(1), 130–180.

Chaffin, W. L. (2008). *Candida albicans* cell wall proteins. Microbiology and Molecular Biology Review, 72(3), 495–544.

Chande, M. S., Schieber, N. S. (2014). ROS function in redox signaling and oxidative stress michael', Current Biology, 24(10), 1–25.

Chandra, J., Kuhn, D. M., Mukherjee, P. K., Hoyer, L. L., McCormick, T., Ghannoum, M. A. (2001). Biofilm Formation by the Fungal Pathogen *Candida albicans*: Development, Architecture, and Drug Resistance. Journal of Bacteriology, 183(18), 5385–5394.

Chao, C. C., Hsu, P. C., Jen, C. F., Chen, I. H., Wang, C. H., Chan, H.-C., Chuang, Y. J. (2010). Zebrafish as a Model Host for *Candida albicans* Infection. Infection and immunity, 78(6), 2512–2521.

Chaplin, D. D. (2010). Overview of the Immune Response. The Journal of Allergy and Clinical Immunology, 125 (2), 3–23.

Chaplin, D. D., (2006). Overview of the human immune response. Journal of allergy and clinical immunology, 117(2), 430 - 435.

Charles, J. S., Martine F. R., Carl W. R. (1988). Colony-stimulating factor-1 receptor (c-fms). Cellular biochemistry, 38 (3), 179-187.

Chauvin, J., Judée, F., Yousfi, M., Vicendo, P., Merbahi, N. (2017). Analysis of reactive oxygen and nitrogen species generated in three liquid media by low temperature helium plasma jet. Scientific Reports, 7, 4562.

Chen Y. Z, Yang Y. L, Chu W. L, You M. S, Lo H. J. (2015). Zebrafish egg infection model for studying *Candida albicans* adhesion Factors. PLoS ONE, 10(11), e0143048.

Chen, Y. Y., Chao, C. C., Liu, F. C., Hsu, P. C., Chen, H. F, Peng, S. C., Chuang, Y. J., Lan, C. Y., Hsieh, W. P., Wong, D. S. (2013). Dynamic transcript profiling of *Candida albicans* infection in zebrafish: a pathogen-host interaction study. PLoS One, 8, e72483.

Chin, V. K., Lee, T. Y., Rusliza, B., Chong, P. P. (2016). Dissecting *Candida albicans* Infection from the perspective of *C. albicans* virulence and omics approaches on host–pathogen interaction: A Review. International Journal of Molecular Sciences, 17(10), 1643.

Christ, A., Bekkering, S., Latz, E., Riksen, N. P. (2016) Long-term activation of the innate immune system in atherosclerosis. Seminars in Immunology, 28(4), 384-393.

Cikos, Š., Bukovská, A., Koppel, J. (2007). Relative quantification of mRNA: comparison of methods currently used for real-time PCR data analysis. BMC Molecular Biology, 8, 113.

Collins, P. E., Carmody, R. J. (2015). The Regulation of Endotoxin Tolerance and its Impact on Macrophage Activation, 35(4), 293-323.

Cooper, M. D. and Alder, M. N. (2006). The evolution of adaptive immune systems. Cell, 124(4), 815 – 822.

Costa, A. C., Pereira, C. A., Junqueira, J. C., Jorge, A. O. (2013). Recent mouse and rat methods for the study of experimental oral candidiasis. Virulence, 4(5), 391–399.

Cowen, L.E., and Steinbach, W.J. (2008). Stress, Drugs, and Evolution: the role of cellular signalling in fungal Drug resistance. Eukaryotic cell, 7(5), 747–764.

Crowhurst, M. O., Layton, J. E., Lieschke, J. G. (2002). Developmental biology of zebrafish myeloid cells, 46, 483 – 492.

Csank, C., Makris, C., Meloche, S., Schroppel, K., Rollinghoff, M., Dignard, D., Thomas, D.Y., and Whiteway, M. (1997). Derepressed hyphal growth and reduced virulence in a VH1 family-related protein phosphatase mutant of the human pathogen *Candida albicans*. Molecular Biology Cell, 8(12), 2539–2551.

Csonka, K., Vadovics, M., Marton, A., Vágvölgyi, C., Zajta, E., Tóth, A., Gácser, A. (2017). Investigation of OCH1 in the virulence of *Candida parapsilosis* using a new neonatal mouse model. Frontiers in microbiology, 8, 1197.

Da Silva Dantas, A., Lee, K. K., Raziunaite, I., Schaefer, K., Wagener, J., Yadav, B., Gow, N. A. R. (2016). Cell biology of *Candida albicans*–host interactions. Current Opinion in Microbiology, 34, 111–118.

Dalle, F., Wachtler, B., L'Ollivier, C., Holland, G., Bannert, N., Wilson, D., Labruère, C., Bonnin, A. Hube, B. (2010). Cellular interactions of *Candida albicans* with human oral epithelial cells and enterocytes. Cellular Microbiology, 12(2), 248-271.

Dana, A. D. (2009). How human pathogenic fungi sense and adapt to pH: the link to virulence. Current Opinion in Microbiology, 12 (4), 365-370.

Daniel, R., Luciane, M., Michael, G. (2004). The PA14 domain, a conserved all-β domain in bacterial toxins, enzymes, adhesins and signalling molecules. Trends in biochemical sciences, 29 (7), 335-339.

Das, I., Krzyzosiak, A., Schneider, K., Wrabetz, L., D'Antonio, M., Barry, N., Bertolotti, A. (2015). Preventing proteostasis diseases by selective inhibition of a phosphatase regulatory subunit. Science, 348(6231), 239–242.

David, D., and Chaplin (2010). Overview of the immune response, 125(2), 3–23.

Davis, M. J., Tsang, T. M., Qiu, Y., Dayrit, J. K., Freij, J. B., Huffnagle, G. B., Olszewski, M. A. (2013). Macrophage M1/M2 polarization dynamically adapts to changes in cytokine microenvironments in *Cryptococcus neoformans* Infection. mBio, 4(3), e00264-13.

Davis, M. M., Alvarez, F. J., Ryman, K., Holm, Å. A., Ljungdahl, P. O., and Engström, Y. (2011). Wild-Type *Drosophila melanogaster* as a model host to analyze nitrogen source dependent virulence of *Candida albicans*. PLoS ONE, 6(11), e27434.

De Viragh, P. A., Sanglard, D., Togni, G., Falchetto, R., Monod, M. (1993). Cloning and sequencing of two *Candida parapsilosis* genes encoding acid proteases. General Microbiology, 139, 335–342.

Deady, L. E., Todd, E. M., Davis, C. G., Zhou, J. Y., Topcagic, N., Edelson, B. T., Morley, S. C. (2014). L-Plastin Is essential for alveolar macrophage production and control of pulmonary pneumococcal infection. Infection and Immunity, 82(5), 1982–1993.

Dixon, D. M. and Walsh, T. J. (1996) Chapter 76 Antifungal agents. Medical microbiology. 4th edition.

Dixon, R. E., Ramsey, K. H., Schripsema, J. H., Sanders, K. M. and Ward, S. M. (2010). Time-dependent disruption of oviduct pacemaker cells by Chlamydia infection in mice. Biology of reproduction, 83, 244–253.

Donlan, R. M., and Costerton, J. W. (2002). Biofilms: survivalmechanisms of clinically relevant microorganisms. Clin.Microbiol. Rev., 15(2), 167–19.

Pujol, C., Daniels, K. J., Lockhart, S. R., Srikantha, T., Radke, J. B., Geiger, J., Soll, D. R. (2004). The Closely Related Species *Candida albicans* and *Candida dubliniensis* can Mate, Eukaryotic Cell, 3(4), 1015–1027.

Duhring S., Germerodt S., Skerka C., Zipfel P. F., Dandekar T., Schuster S. (2015). Host-pathogen interactions between the human innate immune system and *Candida albicans* understanding and modeling defense and evasion strategies. Front. Microbiology, 6, 625.

Ebert, R. H., Florey, H. W. (1939). The extravascular development of the monocyte observed In vivo. British Journal of Experimental Pathology, 20(4), 342–356.

Eisenman, H. C., Nosanchuk,J. D., Webber, J. B. W., Emerson, R. J., Camesano, T. A., and Casadevall, A. (2005). Microstructure of cell wall-associated melanin in the human pathogenic fungus *Cryptococcus neoformans*. Biochemistry, 44 (10), 3683–3693.

Ekkehard, H., Martin, Z., Nicole, H., Kai, S., Anke, B-Kentischer, K.L., Steffen, R. (2006). Adaptation, adhesion and invasion during interaction of *C. albicans* with host-focus in the function of cell wall proteins. Medical Microbiology, 301(5), 384-389.

Elhelu, M. A. (1983). The role of macrophages in immunology. Journal of the National Medical Association, 75(3), 314–317.

Eligini, S., Brioschi, M., Fiorelli, S., Tremoli, E., Banfi, C. and Colli, S. (2015). Human monocyte-derived macrophages are heterogenous: Proteomic profile of different phenotypes. Proteomics, 124, 112-123

Ellis, E. P. (1998). Light intensity and salinity effects on eggs and yolk sac larvae of the summer flounder. The Progressive Fish-culturist, 60 (1), 9-19.

Emer, P. R., Hui, L., Hugues L. J., Carlo, G. M. M., Steve, B., Giorgio G., Eric, O. P., Alice, w., Jurgen, R., Anthony, W. S. (2002). Killing activity of neutrophils is mediated through activation of proteases by K+ flux. Nature, 416 (6878), 291-297.

Epelman, S., Lavine, K. J., Randolph, G. J. (2014). Origin and functions of Tissue-Macrophages. Immunity, 41(1), 21–35.

Eruslanov, E., Kusmartsev, S. (2009). Identification of ROS Using Oxidized DCFDA and flow-cytometry. Methods in Molecular Biology, 594, 57-72.

Erwig, L. P and Gow, N. A. R. (2016). Interactions of fungal pathogens with phagocytes. Nature Reviews Microbiology, 14(3), 163–176.

Feng, J., Zhao, J., Li, J., Zhang, L and Jiang, L. (2010). Functional characterization of the PP2C phosphatase CaPtc2p in the human fungal pathogen *Candida albicans*. Yeast, 27(9), 753–764.

Fletcher, M., Teklehaimanot, A., Yamane. (1992). Control of mosquito larvae in the port city of Assab by an indigenous larvivorous fish, *Aphanius dispar*. Acta Tropica, 52(2-3) 155-166.

Fontana, M. F., de Melo, G. L., Anidi, C., Hamburger, R., Kim, C. Y., Lee, S. Y., Pham, J., Kim, C. C. (2016). Macrophage colony stimulating factor derived from CD4+ T cellscContributes to control of a blood-borne infection. PLOS Pathogens, 12(12), e1006046.

Fonzi, W. A., Irwin, M. Y. (1993). Isogenic strain construction and gene mapping in *Candida albicans*. Genetics, 134(3), 717–728.

Francois, L.M., Duncan, W. and Bernhard, H. (2013). *Candida albicans* pathogenicity mechanisms. Virulence, 4(2), 119-128.

Freeley, M., O'Dowd, F., Paul, T., Kashanin, D., Davies, A., Kelleher, D. and Long, A. (2012). L-Plastin regulates polarization and migration in chemokine-stimulated human T lymphocytes. The Journal of Immunology, 188(12), 6357–6370.

Freeman, J., Lovegrove, A., Wilkinson, M. D., Saulnier, L., Shewry, P. R., Mitchell, R. A. C. (2016). Effect of suppression of arabinoxylan synthetic genes in wheat endosperm on chain length of arabinoxylan and extract viscosity, Plant Biotechnology Journal, 14(1), 109–116.

Freeman, S. A., Grinstein, S. (2014) Phagocytosis: receptors, signal integra-tion, and the cytoskeleton. Immunological review, 262(1), 193-215.

Freyhof, J. (2014). *Aphanius dispar*. The IUCN Red List of Threatened Species.

Frohnhofer, H., Krauss, J., Maischein, H., Nüsslein, C. (2013). Iridophores and their interactions with other chromatophores are required for stripe formation in zebrafish. Development, 140(14), 2997–3007.

Fuchs, B., and Mylonakis, E. (2006). Using non-mammalian hosts to study fungal virulence and host defense. Current. Opinion. Microbiology, 9(4), 346–351.

Fujii, R., Goda, M., Oshima, N. (2002). The mechanism by which an elevation of extracellular glucose concentration induces pigment aggregation in medaka melanophores. Microscopy Research and technique, 58(6), 514–522.

Fukuhara, O. (1990). Effects of temperature on yolk utilization, initial growth, and behaviour of unfed marine fish-larvae. Marine Biology, 106(2), 169–174.

Furze, R. C. and Rankin, S. M. (2008). Neutrophil mobilization and clearance in the bone marrow', Immunology, 125(3), 281–288.

Garcia, S., Hartkamp, L. M., Malvar-Fernandez, B., van Es, I. E., Lin, H., Wong, J., Long, L., Zanghi, J. A., Rankin, A. L., Masteller, E. L., Wong, B. R., Radstake, T. R. D. J., Tak, P. P. and Reedquist, K. A. (2016). Colony-stimulating factor (CSF) 1 receptor blockade reduces inflammation in

human and murine models of rheumatoid arthritis, Arthritis Research and Therapy. Arthritis research and therapy, 18(1), 75.

Geoffrey C, Huntting W. (1981). Embryology and influence of temperature and salinity on early development and survival of Yellowtail Flounder *Limanda ferruginea*. Marine Eecology, 6, 11-18.

Georgopapadakou, N. H., and Bertasso, A. (1992). Effects of squalene epoxidase inhibitors on *Candida albicans*. Antimicrobial agents and chemotherapy, 36(8), 1779–1781.

Ghannoum, M. A., Rice, L. B. (1999). Antifungal Agents: Mode of action, mechanisms of resistance, and correlation of these mechanisms with bacterial resistance. Clinical microbiology reviews, 12(4), 501–517.

Gholami, Z., Mobedi, I., Esmaeili. H., R., Kia, E., B. (2011). The occurrence of *Clinostomum complanatum* in *Aphanius dispar* (Actinopterygii: Cyprinodontidae) collected from mehran river, hormuzgan province, south of Iran. Asian pacific journal of tropical biomedicine, 1(3), 189-192.

Gilles, B., Payan, P. (2001). How should salinity influence fish growth? – Review. Comparative biochemistry and physiology. Comp Biochemistry Physiology Toxicology Pharmacology, 130(4), 411-23.

Ginhoux, F., Lim, S., Hoeffel, G., Low, D., Huber, T. (2013). Origin and differentiation of microglia. Frontiers in Cellular Neuroscience, 7(45), 1–14.

Giulian, D., Chen, J., lngeman, J. E., George, J. K., Noponen, M. (1989) The Role of Mononuclear Phagocytes in Wound Healing After Traumatic Injury to Adult Mammalian Brain. Neuroscience, 9(12), 4418-4429.

Gordon, S. (2007). The macrophage: Past, present and future, European Journal of Immunology, 37(1), 9–17.

Gordon, S. and Pluddemann, A. (2017). Tissue macrophages: Heterogeneity and functions, BMC Biology. BMC Biology, 15(1), 1–18.

Gordon, S., and Taylor, P. R. (2005). Monocyte and macrophage heterogeneity. Nature reviews immunology. 5 (12), 953-64.

Gow, N. A. R., Hube, B. (2012). Importance of the *Candida albicans* cell wall during com-mensalism and infection, Current Opinion in Microbiology, 15(4), 406-412.

Gow, N. A. R., van de Veerdonk, F. L., Brown, A. J. P., Netea, M. G. (2011). *Candida albicans* morphogenesis and host defence: discriminating invasion from colonization. Nature Reviews. Microbiology, 10(2), 112–122.

Gratacap, R. L., Rawls, J. F., Wheeler, R. T. (2013). Mucosal candidiasis elicits NF-κB activation, proinflammatory gene expression and localized neutrophilia in zebrafish. Disease Models and Mechanisms, 6(5), 1260–1270.

Grover, N. D. (2010). Echinocandins: A ray of hope in antifungal drug therapy. Indian Journal of Pharmacology, 42(1), 9–11.

Guleria, I., Pollard, J. P. (2001). Aberrant macrophage and neutrophil population dynamics and impaired the response to *listeria monocytogenes* in colony-stimulating factor 1-deficient mice. Infection and Immunity, 69(3), 1795–1807.

Guo, B., Styles, C. A., Feng, Q., Fink, G. R. (2000). A *Saccharomyces* gene family involved in invasive growth, cell–cell adhesion, and mating. Proceedings of the National Academy of Sciences of the United States of America, 97(22), 12158–12163.

Gupta, M., Shin, D., Ramakrishna, L., Goussetis, D. J., Platanias, L. C., Xiong, H., Morse, H. C., Ozato, K. (2015). IRF8 directs stress-induced autophagy in macrophages and promotes clearance of *Listeria monocytogenes*. Nature communications, 6, 6379.

Gupta, S. K., Pillarisetti, K., Lysko, P. G. (1999). Modulation of *CXCR4* expression and SDF-1a functional activity during differentiation of human monocytes and macrophages. Journal of leukocyte biology, 66(1), 135-143.

Hag, S., Yadav, RS. (2011). Geographical distribution and evaluation of mosquito larvivorous potential of *Aphanius dispar* (Rüppell), a native fish of Gujarat, India. J Vector Borne Dis, 48, 236–240.

Hajjeh, R. A., Sofair, A. N., Harrison, L. H., Lyon, G. M., Arthington-Skaggs, B. A., Mirza, S. A., Warnock, D. W. (2004). Incidence of Bloodstream Infections Due to *Candida* Species and In Vitro Susceptibilities of Isolates Collected from 1998 to 2000 in a Population-Based Active Surveillance Program. Journal of Clinical Microbiology, 42(4), 1519–1527.

Hall, C. J., Flores, M. V., Oehlers, S. H., Sanderson, L. E., Lam, E. Y., Crosier, K. E., and Crosier, P. S. (2012). Infection-Responsive Expansion of the Hematopoietic Stem and Progenitor Cell Compartment in Zebrafish Is Dependent upon Inducible Nitric Oxide. Cell Stem Cell, 10(2), 198-209.

Hall, R. A., Gow, N. A. R. (2013). Mannosylation in *Candida albicans*: role in cell wall function and immune recognition. Molecular Microbiology, 90(6), 1147–1161.

Hamel, P., Magnan, P., East, P., Lapointe, M., Laurendeau, P. (1997). Comparison of different models to predict the in situ embryonic developmental rate of fish: with special reference to white sucker (Catostomus commersoni). Canadian Journal of Fisheries and Aquatic Sciences, 54(1), 190-197.

Hamilton, J. A., Achuthan, A. (2013). Colony stimulating factors and myeloid cell biology in health and disease. Trends Immunology, 34(2), 81–89.

Haq, S., Srivastava, H. C. (2013). Efficacy of *Aphanius dispar* (Rüppell) an indigenous larvivorous fish for vector control in domestic tanks under the Sardar Sarovar Narmada project command area in District Kheda, Gujarat. J Vector Borne Dis, 50(2), 137-40.

Hardison, S. E., Brown, G. D. (2013). Europe PMC funders group C-type lectin receptors orchestrate anti-fungal immunity, 13(9), 817–822.

Hawksworth, D. L. (2001). The magnitude of fungal diversity: the 1 .5 million species estimate revisited. Mycological Res, 105(12), 1422–1432.

Hawser, S. P., Douglas, L. J. (1994). Biofilm formation by *Candida* species on the surface of catheter materials in vitro. Infection and Immunity, 62(3), 915–921.

Hazen, K. C., and B. W., Hazen. 1987. Temperature-modulated physiological characteristics of *Candida albicans*. MicrobiolImmunology. 31(6), 497-508.

Hellyer, P. Aspinall, S. (2005) The Emirates: A natural history. Trident Press Limited, London.

Herbomel, P., Thisse, B. and Thisse, C. (1999). Ontogeny and behaviour of early macrophages in the zebrafish embryo. Development, 126(17), 3735–45.

Hohl, T. M. (2014). Overview of vertebrate animal Models of fungal infection. Journal of Immunological Methods, 0, 100–112.

Holmqvist, B., Ellingsen, B., Alm, P., Forsell, J., Anne-Margrete Øyan, Goksøyr, A., Fjose, A., Seo, HC. (2000). Identification and distribution of nitric oxide synthase in the brain of adult zebrafish. Neuroscience Letters, 292(2), 119-122.

Holtschke, T., Kanno, Y., Fehr, T., Giese, N., Rosenbauer, F., Lou, J., Knobeloch, K., Gabriele, L., Waring, J. F., Bachmann, M. F., Zinkernagel, R. M., Iii, H. C. M., Ozato, K. and Horak, I. (1996). Immunodeficiency and Chronic Myelogenous Leukemia-like Syndrome in Mice with a Targeted Mutation of the ICSBP Gene, 87, 307–317.

Hong, Y., Song, B., Chen, H. D. and Gao, X. H. (2015). Melanocytes and skin immunity. Journal of Investigative Dermatology Symposium Proceedings. Elsevier Masson SAS, 17(1), 37–39.

Hsu, C. H., Wen, Z. H., Lin, C. S., Chakraborty, C. (2007). The zebrafish model: use in studying cellular mechanisms for a spectrum of clinical disease entities. Current Neurovascular Research, 4(2), 111-20.

Iliev, I. D., Funari, V. A., Taylor, K. D., Nguyen, Q., Reyes, C. N., Strom, S. P., Brown, J., Becker, C. A., Fleshner, P. R., Dubinsky, M., Rotter, J. I., Wang, H. L., McGovern, D. P., Brown, G. D., Underhill, D. M. (2012) Interactions be-tween commensal fungi and the C-type lectin receptor Dectin-1 influence coli-tis. Science, 336(6086), 1314–1317.

Ingham, P. W. (2009). The power of the zebrafish for disease analysis, Human Molecular Genetics, 18(1), 107–112.

Iwamatus, T. (2004). Stages of normal development in the Medaka *Oryzias latipes* Mechanisms of development, 121(7-8), 605-618.

Jacobsen, M. D., Duncan, A. D., Bain, J., Johnson, E. M., Naglik, J. R., Shaw, D. J., Gow, N. A.R., Odds, F. C. (2008). Mixed *Candida albicans* strain populations in colonized and infected mucosal tissues. FEMS Yeast Research, 8(8), 1334–1338.

Jakubzick, C., Bogunovic, M., Bonito, A. J., Kuan, E. L., Merad, M., Randolph, G. J. (2008). Lymph-migrating, tissue-derived dendritic cells are minor constituents within steady-state lymph nodes. The Journal of Experimental Medicine, 205(12), 2839–2850.

Janeway, C.A. Jr. and Medzhitov, R. (2002). Innate immune recognition. Annual Review Immunology, 20, 197–216.

Jim, K. K., Engelen-Lee, J. Y., van der Sar, A. M., Bitter, W., Brouwer, M. C., Ende, A., Veening, J., Beek, D., Christina M. J. E. Vandenbroucke-Grauls. (2016). Infection of zebrafish embryos with live fluorescent *Streptococcus pneumoniae* as a real-time pneumococcal meningitis model. Journal of Neuroinflammation, 13(1), 188.

Jin Xu., Tienan Wang., Yi Wu., Wan Jin, Zilong Wen. (2016). Microglia Colonization of Developing Zebrafish Midbrain Is Promoted by Apoptotic Neuron and Lysophosphatidylcholine, 38(2), 214-222.

Jin, H., Li, L., Xu, J., Zhen, F., Zhu, L., Liu, P. P., Wen, Z. (2012). Runx1 regulates embryonic myeloid fate choice in zebrafish through a negative feedback loop inhibiting Pu.1 expression. Blood, 119(22), 5239–5249.

Jin, S., Kim, J. G., Park, J. W., Koch, M., Horvath, T. L., Lee, B. J. (2016). Hypothalamic TLR2 triggers sickness behavior via a microglia-neuronal axis. Scientific Reports, 6, 29424.

Jones, S. L., Wang, J., Turck, C. W., Brown, E. J. (1998). A role for the actin-bundling protein l-plastin in the regulation of leukocyte integrin function. Proceedings of the National Academy of Sciences of the United States of America, 95(16), 9331–9336.

Joseph, T., Zalenskaya, I. A., Sawyer, L. C., Chandra, N. and Doncel, G. F. (2013). Seminal plasma induces prostaglandin-endoperoxide synthase (PTGS) 2 expression in immortalized human vaginal cells: involvement of Semen Prostaglandin E2 in PTGS2 Upregulation1', Biology of Reproduction, 88(1), 1–10.

Jun Yao, Chao Li, Jiaren Zhang, Shikai Liu, Jianbin Feng, Ruijia Wang, Yun Li, Chen Jiang, Lin Song, Ailu Chen, Zhanjiang Liu. (2014). Expression of nitric oxide synthase (NOS) genes in channel catfish is highly regulated and

time dependent after bacterial challenges. Developmental and Comparative Immunology, 45(1), 74-86.

Kanayama, A. and Miyamoto, Y. (2007). Apoptosis triggered by phagocytosis-related oxidative stress through FLIPS down-regulation and JNK activation. J. Leucocyte biology, 82(5), 1344-1352.

Kapellos, T. S., Taylor, L., Lee, H., Cowley, S. A., James, W. S., Iqbal, A. J., Greaves, D. R. (2016). A novel real-time imaging platform to quantify macrophage phagocytosis. Biochemical Pharmacology, *116*, 107–119.

Karkowska-Kuleta, J., Kozik A. (2014). Moonlighting proteins as virulence factors of pathogenic fungi, parasitic protozoa and multicellular parasites. Molecular Oral Microbiology, 29(6), 270–283.

Kawai, T., Akira, K. (2010). The role of pattern-recognition receptors in innate immunity: update on Toll-like receptors. Nature Immunology. 11(5), 373-384.

Kawai, T., Akira, S. (2011). Toll-like receptors and their crosstalk with other innate receptors in infection and immunity. Immunity, 34(5), 637-650.

Kelsh R, Inoue C, Momoi A, Kondoh H, Furutani M, Ozato K, Wakamatsu Y. (2004). The Tomita collection of medaka pigmentation mutants as a resource for understanding neural crest cell development. Mechanisms of development. 121, 841–859.

Keivany, Y. (2012). Distribution of *Aphanius dispar dispar* (Ruppell,1829) populatios in Iran, with a new record from western Iran (*Actinopterygii: Cyprinodontidae*). Turkish Journal of Zoology, 36, 824-827.

Keppler-Ross, S., Douglas, D., Konopka, J. B., Dean, N. (2010) Recognition of yeast by murine macrophages requires mannan but not glucan. eukaryotic cell, 9(11), 1776–1787.

Kettenmann, H., Hanisch, U.-K., Noda, M. and Verkhratsky, A. (2011) Physiology of Microglia, Physiological Reviews, 91(2), 461–553.

Khan, M. S. A., Ahmad, I., Aqil, F., Owais, M., Shahid, M., Musarrat, J. (2010). Virulence and pathogenicity of fungal pathogens with special reference to *Candida albicans*. Combating Fungal Infections, 21-45

Khorshidi, F., Haghighi, M. M., Nazemalhosseini Mojarad, E., Azimzadeh, P., Damavand, B., Vahedi, M., Almasi, S., Aghdaei, H. A. and Zali, M. R.

(2014). The Prostaglandin Synthase 2/cyclooxygenase 2 (PTGS2/ COX2) rs5277 Polymorphism does not influence risk of colorectal cancer in an iranian population. Asian Pacific journal of cancer prevention, 15(8), 3507–11.

Kimura, T., Nagao, Y., Hashimoto, H., Yamamoto-Shiraishi, Y., Yamamoto, S., Yabe, T., Naruse, K. (2014). Leucophores are similar to xanthophores in their specification and differentiation processes in medaka. Proceedings of the National Academy of Sciences of the United States of America, 111(20), 7343–7348.

Klis, F. M., Boorsma, A., De Groot, P. W. J. (2006). Cell wall construction in *Saccha-romyces cerevisiae*. Yeast, 23(3), 185-202.

Kobayashi, S. D., Cutler, J. D. (1998). *Candida albicans* hyphal formation and virulence: is there a clearly defined role? Trends in Microbiology, Volume 6(3), 92 – 94.

Koji, Y., Haruokaji, K. N., Makoto, M. (1994). The role of microfilaments and microtubules during pH-regulated morphological transition in *Candida albicans.* Microbiology. 140(2), 128-287.

Kojic, E. M., and Darouiche, R. O. (2004). Candida Infections of Medical Devices. Clinical Microbiology Reviews, 17(2), 255–267.

Kokare, C. R. Chakraborty, S., Khopade, N. A., Mahadik, K. R. (2009). Biofilm, Importance, and application. Indian journal of biotechnology, 8, 159-168.

Kollar, R., Reinhold, B. B., Petrakova, E., Yeh, H. J. C., Ashwell, G., Drgono-va, J., Kapteyn, J. C., Klis, F. M., Cabib, E. (1997). Architecture of the yeast cell wall β (1→6) glucan interconnects mannoprotein, β (1→3)-glucan, and chitin. The Journal of Biological Chemistry, 272(28), 17762-17775.

Korhonen, R., Lahti, A., Kankaanranta, H., Moilanen, E. (2005). Nitric Oxide Production and Signaling in Inflammation. Current Drug Targets - Inflammation and Allergy. 4 (4), 471-479.

Krauke, Y., Sychrova, H. (2010). Four pathogenic Candida Species differ in salt tolerance. Current Microbiology, 61(4), 335-339.

Kruppa, M., Rachel, G. R., Noss, I., Lowman, D., David L. W., (2011). *C. albicans* increases cell wall mannoprotein, but not mannan, in response to blood, serum and cultivation at physiological temperature. Glycobiology, 21(9), 1173-80.

Kurotaki, D., Osato, N., Nishiyama, A., Yamamoto, M., Ban, T., Sato, H., Tamura, T. (2013). Essential role of the IRF8-KLF4 transcription factor cascade in murine monocyte differentiation. Blood, 121(10), 1839–1849.

Langmann, T. (2007). Microglia activation in retinal degeneration. Journal of Leukocyte Biology, 81(6)1345-1351.

Le Guyader, D., Redd, M. J., Colucci-Guyon, E., Murayama, E., Kissa, K., Briolat, V., Mordelet, E., Zapata, A., Shinomiya, H., Herbomel, P. (2008). Origins and unconventional behaviour of neutrophils in developing zebrafish. Blood, 111(1), 132–141.

Lévesque, M., Feng, Y., Jones, R. A., Martin, P. (2013). Inflammation drives wound hyperpigmentation in zebrafish by recruiting pigment cells to sites of tissue damage. Disease Models Mechanisms, 6(2), 508–515.

Levitz, S. M. (2010). Innate Recognition of Fungal Cell Walls, 6(4), 4–6.

Lewis, K. L., and Reizis, B. (2012). Dendritic cells: arbiters of immunity and immunological tolerance. Cold Spring Harb Perspect Biol; 4(8), a007401.

Li, Y, Wang, L, Jing, J. X, Li, Z. Q, Lin, F., Huang, L.F., Pan, Q.H. (2007). The pikm gene, conferring stable resistance to isolates of *Magnaporthe oryzae,* was finely mapped in a crossover-cold region on rice chromosome 11. Molecular Breeding, 20(2) 179–188.

Li, D. D., Deng, L., Hu, G. H., Zhao, L. X., Hu, D. D., Jiang, Y. Y., Wang, Y. (2013). Using *Galleria mellonella–Candida albicans* Infection Model to Evaluate Antifungal Agents, Biological and Pharmaceutical Bulletin 36(369), 1482–1487.

Li, E., Zhou, P., Singer, S.M. (2006). Neuronal nitric oxide synthase is necessary for elimination of *Giardia lamblia* infections in mice. Journal of Immunology, 176(1), 516-21.

Li, L., Jin, H., Xu, J., Shi, Y. and Wen, Z. (2017). Irf8 regulates macrophage versus neutrophil fate during zebrafish primitive myelopoiesis, 117(4), 1359–1370.

Li, T., Li, H., Zhang, Y. X., Liu, J. Y. (2011). Identification and analysis of seven H_2O_2-responsive miRNAs and 32 new miRNAs in the seedlings of rice (Oryza sativa L. ssp. indica). Nucleic Acids Research, 39(7), 2821–2833.

Li, Y., Zhang, Q., Zhang, J., Wu L., Qi, Y., Zhou, J. M. (2010). Identification of microRNAs involved in pathogen-associated molecular pattern-triggered plant innate immunity. Plant Physiology, 152(4), 2222–2231

Li, Z., Xu, X., Leng, X., H. M., Wang, J., Cheng, S., Wu, H. (2017). Roles of reactive oxygen species in cell signalling pathways and immune responses to viral infections. Archives of Virology, 162(3), 603-610.

Lin, s., Lin, C. R., Gukovsky, I., Lusis, A. J., Sawchenko, P.E., Rosenfeld, M. G. (1993). Molecular basis of the little mouse phenotype and Implications for cell type-specific growth. Nature, 364, 208–213.

Lionakis, M. S. (2011). *Drosophila* and *Galleria* insect model hosts new tools for the study of fungal virulence. Pharmacology and Immunology, Virulence, 2(6), 521-527.

Lionakis, M. S., Lim, J. K., Lee, C. C., Murphy, P. M. (2010). Organ-specific innate immune responses in a mouse model of invasive candidiasis. Journal of Innate Immunity, 3(2), 180–199.

Lo, Y. M., Tein, M. S., Lau, T. K., Haines, C. J., Leung, T. N., Poon, P. M., Hjelm, N. M. (1998). Quantitative analysis of fetal DNA in maternal plasma and serum: implications for noninvasive prenatal diagnosis. American Journal of Human Genetics, 62(4), 768–775.

Loria, V., Dato, I., Graziani, F., Biasucci, L. M. (2008). Myeloperoxidase: A New Biomarker of Inflammation in Ischemic Heart Disease and Acute Coronary Syndromes. Mediators of Inflammation, 135625.

Lotan, R. (1971). Osmotic adjustment in the euryhaline teleost *Aphanius dispar* (Cyprinodontidae). Comparative Physiology, 75(4), 383–387.

Lowman, M., Trott, P., Hoecht, A. H., and Sellam, Z. (2012). Innovation risks in outsourcing within pharmaceutical new product development. Technovation, 32(2), 99-109

Loynes, C. A., Martin, J. S., Robertson, A., Trushell, D. M. I., Ingham, P. W., Whyte, M. K. B., Renshaw, S. A. (2010). Pivotal Advance:

Pharmacological manipulation of inflammation resolution during spontaneously resolving tissue neutrophilia in the zebrafish. Journal of Leukocyte Biology, 87(2), 203–212.

Lu, J. W., Ho, Y. J., Yang, Y. J., Liao, H. A., Ciou, S. C., Lin, L. I., Ou, D. L. (2015). Zebrafish as a disease model for studying human *hepatocellular carcinoma*. World Journal of Gastroenterology, 21(42), 12042–12058.

Lu, M., Grove, E. A., Miller, R. J. (2002). Abnormal development of the hippocampal dentate gyrus in mice lacking the CXCR4 chemokine receptor. Proceedings of the National Academy of Sciences of the United States of America, 99(10), 7090–7095.

Lu, R., Medina, K. L., Lancki, D. W., Singh, H. (2003). IRF-8 orchestrate the pre-B-to-B transition in lymphocyte development. Genes and Development, 17(14), 1703–1708.

Lull, M. E., Block, M. L. (2010). Microglial activation and chronic neurodegeneration. Neurotherapeutics, 7(4), 354–365.

Lynn, L. M., Kelsh, R. N., Wakamatsu, Y., Ozato, K. (2005). Pigment pattern formation in the medaka embryo. Pigment Cell Research, 18(2), 64-73.

Mackintosh, J. A. (2001). The antimicrobial properties of melanocytes, melanosomes and melanin and the evolution of black skin. Journal of theoretical biology. 211(2), 101-113.

Mandrell, D., Truong, L., Jephson, C., Sarker, M. R., Moore, A., Lang, C.,Tanguay, R. L. (2012). Automated zebrafish chorion removal and single embryo placement: optimizing throughput of zebrafish developmental toxicity screens. Journal of Laboratory Automation, 17(1), 66–74.

Maneu, V., Noailles, A., Meg´ıas, J., G´omez-Vicente, V., Carpena, N., Gil, L., Gozalbo, D., Cuenca, N. (2014). Retinal microglia are activated by systemic fungal infection. Investigation Ophthalmol and Visual Science. 55(6)3578– 3585.

Mantovani, A., Cassatella, M. A., Costantini, C., Jaillon, S. (2011). Neutrophils in the activation and regulation of innate and adaptive immunity. Nature Reviews Immunology, 11(8), 519–531

Marvin, J. M., Matthew, P., Satwik, K., Jacqueline, D., Gennadiy, I. P., Molly, K. H., Marshall, L. M., Beverly, A. R., Karl, J. M., Betsy, S. P., Mihir, D. P., Deborah, A. M., Scott A. Long., John J. P., David R. A., Atli, T. (2010). Structure-based drug design enables conversion of a DFG-in binding CSF-1R kinase inhibitor to a DFG-out binding mode. Bioorganic and Medicinal Chemistry Letters, 20 (5), 1543-1547.

Masazumi, S. (2002). Morphological color changes in fish: regulation of pigment cell density and morphology. Microscopy Research and Technique, 58(6), 496–503.

Masoud, R., Bizouarn, T. and Houee-Levin, C. (2014). Cholesterol: A modulator of the phagocyte NADPH oxidase activity - A cell-free study, Redox Biology. Elsevier, 3, 16–24.

May, C. R. (1974). Effects of temperature and salinity on yolk utilization in Bairdiella icistia (Jordan & Gilbert) (Pisces: sciaenidae). Journal of Experimental Marine Biology Ecology, 16(3), 213-225.

Mayer, D. (2009). Antimicrobial drug resistance clinical and epidemiological aspects. Antimicrobial Drug Resistance, 2, 692.

Mayer, F. L., Wilson, D., Hube, B. (2013). *Candida albicans* pathogenicity mechanisms. Virulence, 4(2), 119–128.

McCallum, K. C., Garsin, D. A. (2016). The role of reactive oxygen species in modulating the *Caenorhabditis elegans* immune response. PLoS Pathogens, 12(11), e1005923.

McKenzie, C. G. J., Koser, U., Lewis, L. E., Bain, J. M., Mora-Montes, H. M., Barker, R. N., Erwig, L. P. (2010). Contribution of *Candida albicans* cell wall components to recognition by and escape from murine macrophages. Infection and Immunity, 78(4), 1650–1658.

Medzhitov, R., Janeway, C. A. (1997). Innate Immunity: The virtues of a nonclonal system of recognition. Cell, 91(3), 295 - 298

Mehdi, B., Marziyhe, R., Sayed, A. H., Majid, K., Milad, M. (2012). Reproduction of *Aphanius dispar dispar* (Rüppell, 1829) in Dalaki River, Bushehr, south of Iran. World Journal of Fish and Marine Sciences, 4(6), 594-596.

Mesa-Arango, A. C., Forastiero, A., Bernal-Martinez, L., Cuenca-Estrella, M., Mellado, E., Zaragoza, O. (2013). The non-mammalian host *Galleria mellonella* can be used to study the virulence of the fungal pathogen *Candida tropicalis* and the efficacy of antifungal drugs during infection by this pathogenic yeast. Medical Mycology, 51(5), 461-72.

Messer, S. A., Diekema, D. J., Boyken, L., Tendolkar, S., Hollis, R. J., Pfaller, M. A. (2006). Activities of micafungin against 315 Invasive clinical isolates of fluconazole-resistant Candida spp. Journal of Clinical Microbiology, 44(2), 324–326.

Miceli, M. H., Díaz, J. A., Lee, S. A. (2011). Emerging opportunistic yeast infections. Lancet infectious disease, 11(2), 142-51.

Miller, R. J., Banisadr, G., Bhattacharyya, B. J. (2008). CXCR4 signalling in the regulation of stem cell migration and development. Journal of Neuroimmunology, 198(0), 31–38.

Mogensen, T. H. (2009). Pathogen recognition and inflammatory Ssgnalling in innate immune defenses. Clinical Microbiology Reviews, 22(2), 240–273.

Molano, J., Bowers, B., Cabib, E. (1980). Distribution of chitin in the yeast cell wall. An ultrastructural and chemical study. Journal of Cell Biology, 85(2), 199- 212.

Mora-Montes, H. M., Bates, S., Netea, M. G., Castillo, L., Brand, A., Buurman, E. T., Díaz-Jiménez, D. F., Kullberg, B. J., Brown, A. J. P., Odds, F. C., Gow, N. A. R. (2010). A multifunctional mannosyltransferase family in *candida albicans* determines cell wall mannan structure and host-fungus interactions', Journal of Biological Chemistry, 285(16), 12087–12095.

Moran, G., Coleman, D., and Sullivan, D. (2012). An Introduction to the Medically Important Candida Species. Candida and Candidiasis, Second Edition. Chapter 2.

Morley, S. C. (2012). The Actin-Bundling Protein L-Plastin: A Critical Regulator of Immune Cell Function. International Journal of Cell Biology, 2012, 10 pages.

Mosser, D. M., Edwards, J. P. (2008). Exploring the full spectrum of macrophage activation. Nature Reviews. Immunology, 8(12), 958–969.

Mounier, R., Théret, M., Arnold, L., Cuvellier, S., Bultot, L., Göransson, O., Sanz, N., Ferry, A., Sakamoto, K., Foretz, M., Viollet, B., Bénédicte Chazaud. (2013). Regulates macrophage skewing at the time of resolution of inflammation during skeletal muscle regeneration. Cell Metabolism, 18(2), 251 – 264.

Mourabit, S., Edenbrow, M., Croft, D. P., Kudoh, T. (2011). Embryonic development of the self-fertilizing mangrove killifish *Kryptolebias marmoratus*. Developmental Dynamics, 240(7), 1694-1704.

Mourabit, S., Michael, W M., Smith, E., Ronny van, A., Kudoh, T. (2014). Bmp Suppression in Mangrove Killifish Embryos Causes a Split in the Body Axis. PLOS, 9(1), e84786.

Mukaremera, L., Lee, K. K., Mora-Montes, H. M., and Gow, N. A. R. (2017). *Candida albicans* Yeast, pseudohyphal, and Hyphal morphogenesis differentially affects immune recognition. Front Immunol, 8, 629.

Munro, C. A., Bates, S., Buurman, E. T., Hughes, H. B., MacCallum, D. M., Bertram, G., Gow, N. A. R. (2005). Mnt1p and Mnt2p of *Candida albicans* are partially redundant *α*-1, 2-mannosyltransferases that participate in *O*-linked Mannosylation and Are Required for Adhesion and Virulence. The Journal of Biological Chemistry, 280(2), 1051–1060.

Murciano, C., Moyes, D. L., Runglall, M., Islam, A., Mille, C., Fradin, C., Naglik, J. R. (2011). *Candida albicans* cell wall glycosylation may be indirectly required for activation of epithelial cell proinflammatory responses. Infection and Immunity, 79(12), 4902–4911.

Nadeem, S. G., Shafiq, A., Hakim, S. T., Anjum, Y. T., Kazm, S. U. (2013). Effect of growth media, pH and temperature on yeast to hyphal transition in *Candida albicans*. Open Journal of Medical Microbiology, 3(3), 185-192.

Nagao, y., Suzuki, T., Shimizu, A., Kimura, T., Seki, R., Adachi, T., Inoue, C., Omae, Y., Kamei, Y., Hara, I., Taniguchi, Y., Naruse, K., Wakamatsu, Y., Kelsh, R. N., Hibi, M., Hashimoto, H. (2014). Sox5 functions as a fate switch in medaka pigment cell development. PLoS Genet, 10(4), e1004246.

Naglik, J. R., (2014) Candida Immunity. New Journal of Science; 27p. Review article.

Naglik, J. R., Challacombe, S. J., Hube, B. (2003). *Candida albicans* secreted aspartyl pro-teinases in virulence and pathogenesis. Microbiology and Molecular Biology Reviews, 67(3), 400–428.

Naglik, J. R., Moyes, D., Makwana, J., Kanzaria, P., Tsichlaki, E., Weindl, G., Hube, B. (2008). Quantitative expression of the *Candida albicans* secreted aspartyl proteinase gene family in human oral and vaginal candidiasis. Microbiology (Reading, England), 154(11), 3266–3280.

Naglik, J. R., Richardson, J. P., Moyes, D. L. (2014) *Candida albicans* Pathogenicity and Epithelial Immunity. PLoS Pathog, 10(8), e1004257.

Namba, Y., Ito, M., Zu, Y., Shigesada, K., Maruyama, K. (1992). Human T cell L-plastin bundles actin filaments in a calcium dependent manner. Biochemistry, 112(4), 503-507.

Navarro-Arias, M. J., Defosse, T. A., Dementhon, K., Csonka, K., Mellado-Mojica, E., Dias Valério, A., Mora-Montes, H. M. (2016). Disruption of protein mannosylation affects *Candida guilliermondii* cell wall, Immune Sensing, and Virulence. Frontiers in Microbiology, 7, 1951.

Netea, M. G., Brown, G. D., Kullberg, B. J., Gow, N. A. R. (2008). An integrated model of the recognition of *Candida albicans* by the innate immune system. Nature Review Microbiology, 6(1), 67–78.

Netea, M. G., Gow, N. A. R., Munro, C. A., Bates, S., Collins, C., Ferwerda, G., Kullberg, B. J. (2006). Immune sensing of *Candida albicans* requires cooperative recognition of mannans and glucans by lectin and Toll-like receptors. Journal of Clinical Investigation, 116(6), 1642–1650.

Nobile, C. J., Johnson, A. D. (2015). *Candida albicans* biofilms and human disease. Annual Review of Microbiology, 69, 71–92.

Ogira, P G., Liti, D., James Wanga, J. (2012). Effects of temperature on embryonic development time and yolk absorption period of *Oreochromis Niloticus*. International Journal of Science and Research, 3(9), 2319-7064.

Ogle, M. E., Segar, C. E., Sridhar, S., Botchwey, E. A. (2016). Monocytes and macrophages in tissue repair: Implications for immunoregenerative biomaterial design. Experimental Biology and Medicine, 241(10), 1084–1097.

Olson, J., K. (2010). Immune response by microglia in the spinal cord. Annals New York Academy Science, 1198(1), 271-278.

Onishi, J., Meinz, M., Thompson, J., Curotto, J., Dreikorn, S., Rosenbach, M., Douglas, C., Abruzzo, G., Flattery, a, Kong, L., Cabello, a, Vicente, F., Pelaez, F., Diez, M. T., Martin, I., Bills, G., Giacobbe, R., Dombrowski, a, Schwartz, R., Morris, S., Harris, G., Tsipouras, a, Wilson, K. and Kurtz, M. B. (2000) 'Discovery of novel antifungal (1,3)-beta-D-glucan synthase inhibitors.', Antimicrobial agents and chemotherapy, 44(2), 368–377.

Osorio, F., Sousa, C. S. (2011). Myeloid C-type lectin receptors in pathogen recognition and host defense. Immunity, 34(5), 651-64.

Ostrosky-Zeichner, L., Casadevall, A., Galgiani, J.N., Odds, F.C., Rex, J.H. (2010). An insight into the antifungal pipeline: selected new molecules and beyond. Nature Reviews Drug Discovry, 9, 719–727.

Ota, S., Hisano, Y., Ikawa, Y., Kawahara, A. (2014). Multiple genome modifications by the CRISPR/Cas9 system in zebrafish. Genes Cells, 19(7), 555-64.

Paik, Y. H., Iwaisako, K., Seki, E., Inokuchi, S., Schnabl, B., Osterreicher, C. H., Brenner, D. A. (2011). The nicotinamide adenine dinucleotide phosphate oxidase homologues NOX1 and NOX2/gp91phox mediate hepatic fibrosis in mice. Hepatology (Baltimore, Md.), 53(5), 1730–1741.

Panday, A., Sahoo, M. K., Osorio, D., and Batra, S. (2015). NADPH oxidases: an overview from structure to innate immunity-associated pathologies, Cellular and Molecular Immunology, 12(1), 5–23.

Panopoulos, A. D., Watowich, S. S. (2008). Granulocyte colony-stimulating factor: Molecular mechanisms of action during steady state and 'emergency' hematopoiesis. Cytokine, 42(3), 277-288.

Papon N., Savini V., Lanoue A., Simkin A. J., Crèche J., Giglioli-Guivarc'h N. (2013). *Candida guilliermondii*: biotechnological applications, perspectives for biological control, emerging clinical importance and recent advances in genetics. Current. Genetics, 59(3), 73–90.

Park, J. S., Mathison, B. D., Hayek, M. G., Massimino, S., Reinhart, G. A., Chew, B. P. (2011). Astaxanthin stimulates cell-mediated and humoral

immune responses in cats. Veterinary Immunology Immunopathology, 144(3-4), 455-61.

Patrick, V., Selene, F., Alix, C. (2012). Antifungal Resistance and New Strategies to Control Fungal Infections. International journal of microbiology, 26 pages.

Paulovicova, L., Paulovicova, E., Karelin, A. A., Tsvetkov, Y. E., Nifantiev, N. E., Bystricky. S. (2015). Immune cell response to Candida cell wall mannan derived branched α-oligomannoside conjugates in mice. Journal of Microbiology, Immunology and Infection, 48(1), 9-19.

Paumann-Page, M., Furtmüller, P. G., Hofbauer, S., Paton, L. N., Obinger, C., Kettle, A. J. (2013). Inactivation of human myeloperoxidase by hydrogen peroxide. Archives of Biochemistry and Biophysics, 539(1), 51–62.

Perry, V.H., Nicoll, J.A.R., Holmes, C. (2010) Microglia in neurodegenerative disease. Nature Reviews Neurology, 6(4) 193-201.

Peter, F. Z., Christine, S., Danny, K., Shanshan, L. (2011). Immune escape of the human facultative pathogenic yeast *Candida albicans*: The many faces of the Candida Pra1 protein. International Journal of Medical Microbiology, 301(5), 423-430.

Pfaller, M. A., Diekema, D. J. (2007). Epidemiology of Invasive Candidiasis: a Persistent Public Health Problem. Clinical Microbiology Reviews, 20(1), 133–163.

Pixley, F. J and Stanly, E. R. (2004). CSF-1 regulation of the wandering macrophage: complexity in action.Trends in Cell Biology, 14(11), 628 – 638.

Plaut, I. (2000). Resting metabolic rate, critical swimming speed, and routine activity of the *Euryhaline Cyprinodontid*, *Aphanius dispar*, acclimated to a wide range of salinities. Physiological and Biochemical Zoology, 73(5), 590-596.

Porazinski, S. R., Wang, H., Furutani-Seiki, M. (2010). Dechorionation of medaka embryos and cell transplantation for the generation of chimeras. Journal of visualized experiments, (46), 2055.

Prill, R. J., Iglesias, P. A., Levchenko, A. (2005). Dynamic properties of network motifs contribute to biological network organization. PLoS Biology, 3(11), e343.

Pukkila-Worley, R., Peleg, A. Y., Tampakakis, E., Mylonakis, E. (2009). *Candida albicans* hyphal formation and virulence assessed using a *Caenorhabditis elegans* infection model. Eukaryotic Cell, 8(11), 1750–1758.

Pukkila-Worley, R., Ausubel, F. M., and Mylonakis, E. (2011). *Candida albicans* infection of *Caenorhabditis elegans* induces antifungal immune defenses. PLoS Pathogens, 7(6), e1002074.

Qin, A., Coffey, D. G., Warren, E. H., Ramnath, N. (2016). Mechanisms of immune evasion and current status of checkpoint inhibitors in non-small cell lung cancer. Cancer Medicine, 5(9), 2567–2578.

Qin, Y., Zhang, L., Xu, Z., Zhang, J., Jiang, Y. Y., Cao, Y., Yan, T. (2016). Innate immune cell response upon *Candida albicans* infection, Virulence, 7(5), 512–526.

Qin, Y., Zhang, L., Xu, Z., Zhang, J., Jiang, Y. Y., Cao, Y. and Yan, T. (2016). Innate immune cell response upon *Candida albicans* infection. Virulence, 7(5), 512–526.

Rauta, P. R., Nayak, B., and Das, S. (2012). Immune system and immune responses in fish and their role in comparative immunity study: A model for higher organisms. Immunology Letters, 148(1), 23-33.

Raz, E., Mahabaleshwar, H. (2009). Chemokine signalling in embryonic cell migration: a fisheye view. Development, 136(8), 1223-1229.

Reutter, K. (1986). Chemoreceptors. Biology of the Integument, 586-604.

Richardson, J. P., and Moyes, D. L. (2015). Adaptive immune responses to *Candida albicans* infection. Virulence, 6(4), 327–337.

Richardson, K., Brammer, K. W., Marriott, M. S., Troke, P. F. (1985). Activity of UK-49,858, a bis-triazole derivative, against experimental infections with *Candida albicans* and Trichophyton mentagrophytes. Antimicrobial Agents and Chemotherapy, 27(5), 832–835.

Rida, P. C. G., Nishikawa, A., Won, G. Y., Dean, N. (2006). Yeast-to-hyphal transition triggers formin-dependent Golgi localization to the growing tip in *Candida albicans*. Molecular Biology of the Cell, 17(10), 4364–4378.

Rigden, D. J., Mello, L. V., Galperin, M. J. (2004). The PA14 domain, a conserved all-β domain in bacterial toxins, enzymes, adhesins and signalling molecules. Trends in Biochemical Sciences, 29(7), 335-339.

Rogers, T. E., Galgiani, J. N. (1986). Activity of fluconazole (UK 49,858) and ketoconazole against *Candida albicans* in vitro and in vivo. Antimicrobial Agents and Chemotherapy, 30(3), 418–422.

Rolston, K. M. D. (2001). Overview of systemic fungal infections. Oncology, 15(11), 11-14.

Rosemore, B. J., Welsh, C. A. (2012). The Effects of rearing density, salt concentration, and Incubation temperature on Japanese Medaka, 9(4), 185–190.

Ruiz-Herrera, R., Elorza, M. V., Valent´ın, E., Sentandreu, R. (2006). Molecular organization of the cellwall of *Candida albicans* and its relation to pathogenicity. Federation of European Microbiological Societies, 6(1), 14–29.

Saeed, S., Al-Naema, N., Butler, J., Febbo, E. (2015). Arabian killifish (*Apanius dispar*) embryos: A model organism for the risk assessment of the Arabian Gulf coastal water. Environmental Toxicology Chemistry, 34(12), 2898–2905.

Saito, H., Tomioka, H., Watanabe, T., Sato, K. (1986). Mechanisms of phagocytosis of *Mycobacterium leprae* and other mycobacteria by human oligodendroglial cells. Infection and Immunity, 51(1), 163–167.

Sampermans, S., Mortier, Soares, E. V. (2005). Flocculation onset in *Saccharomyces cerevisiae*: the role of nutrients. Journal of Applied Microbiology, 98(2), 525–531.

Savage, D. C., Dubos, R. J. (1967). Localization of indigenous yeast in the murine stomach. Journal of Bacteriology, 94(6), 1811–1816.

Schaller, M., Borelli, C., Korting, H.C., Hube, B. (2005). Hydrolytic enzymes as virulence factors of *C. albicans*. Mycoses, 48(6), 365-377.

Schmit, J. P. (2014). Fungal biodiversity: What do we know? What can we predict? Biodiversity and Conservation, 16(1), 1-5.

Segal, A. W. (2008). The function of the NADPH oxidase of phagocytes and its relationship to other NOXs in plants, invertebrates, and mammals.

International Journal of Biochemistry and Cell Biology. Elsevier Ltd, 40(4), 604–618.

Selders, G. S., Fetz, A. E., Radic, M. Z., and Bowlin, G. L. (2017). An overview of the role of neutrophils in innate immunity, inflammation and host-biomaterial integration. Regen Biomater, 4(1), 55–68.

Selemidis, S., iunn Seow, H., Broughton, B. R. S., Vinh, A., Bozinovski, S., Sobey, C., Drummond, G.R., Vlahos, R. (2013). Nox1 oxidase suppresses influenza a virus-induced lung Inflammation and oxidative stress. PLoS ONE 8(4), e60792.

Shapiro, R. S., Uppuluri, P., Zaas, A. K., Collins, C., Senn, H., Perfect, J. R., Cowen, L. E. (2009). Hsp90 Orchestrates temperature-dependent *Candida albicans* morphogenesis via Ras1-PKA signaling. Current biology, 19(8), 621–629.

Sheehan, D. J., Hitchcock, C. A., Sibley, C. M. (1999). Current and emerging azole antifungal agents. Clinical Microbiology Reviews, 12(1), 40–79.

Shen, J. Q., Yang, Q. L., Xue, Y., Cheng, X. B., Jiang, Z. H., Yang, Y. C., Chen, Y. D. and Zhou, X. (2015). Inducible nitric oxide synthase response and associated cytokine gene expression in the spleen of mice infected with *Clonorchis sinensis*. Parasitology Research, 114(5), 1661-1670.

Shi, C., Zhu, Y., Ran, X., Wang, M., Su, Y., Cheng, T. (2006). Therapeutic Potential of Chitosan and Its Derivatives in Regenerative Medicine. Journal of Surgical Research, 133(2), 185 – 192.

Shi, M. M., Chong, I. W., Long, N. C., Love, J. A., Godleski, J. J., Paulauskis, J. D. (1998) Functional characterization of recombinant rat macrophage inflammatory protein-1 alpha and mRNA expression in pulmonary inflammation. Inflammation, 22(1), 29-43.

Shin, D.-M., Lee, C.-H., Morse, H. C. (2011). IRF8 governs expression of genes involved in innate and adaptive immunity in human and mouse germinal center B cells. PLoS ONE, 6(11), e27384.

Shinomiya, H. (2012). Plastin family of actin-bundling proteins: Its functions in leukocytes, neurons, intestines, and cancer. International Journal of Cell Biology, 2012, 8.

Shoham, S. and Levitz, S. M. (2005). The immune response to fungal infections. Journal of haematology, 129(5), 569-582.

Silva, M. T., Correia-Neves, M. (2012). Neutrophils and macrophages: the main partners of phagocyte cell systems. Frontiers in Immunology, 3, 174.

Simona-Adriana, M., Constantin, A., Manda, G., Sasson, S., Manea, A. (2015). Regulation of Nox enzymes expression in vascular pathophysiology: Focusing on transcription factors and epigenetic mechanisms. Redox Biology, 5, 358-366.

Sohnle, P. G., Hahn, B. L. (2002). Effect of prolonged fluconazole treatment on Candida albicans in diffusion chambers implanted into mice. Antimicrobial Agents and Chemotherapy, 46(10), 3175–3179.

Startford M. (1992). Yeast flocculation: a new perspective. Microbiology Physiology, 33, 2-71.

Stiller, R. L., Bennett, J. E., Scholer, H. J. (1983), Correlation of in vitro susceptibility test results with in vivo response: flucytosine therapy in a systemic candidiasis model. The Journal of Infectious Diseases, 147(6), 1070–1077.

Stratford, M. (1992). Lectin-mediated aggregation of yeasts — yeast flocculation. Biotechnology and Genetic Engineering Reviews, 10(1), 283-342

Stuart, M. L., Charles, S. (2009). Recognition of the fungal cell wall by innate immune receptors. Current Fungal Infection Reports, 3(3), 179-185.

Sundstrom, P. (2002). Adhesion in Candida spp. Cellular Microbiology, 4(8), 461-469.

Swanson, C. (1998). Interactive effects of salinity on metabolic rate, activity, growth, and osmoregulation in the euryhaline milkfish, *Chanos chanos*. Journal of Experimental Biology, 201, 3355–3366.

Takahashi, K. G., A. Nakamura, and K. Mori. (2000). Inhibitory effects of ovoglobulins on bacillary necrosis in larvae of the pacific oyster, Crassostrea gigas. Journal of Invertebrate Pathology, 75(3), 212–217.

Tapia, C. V., Falconer, M., Tempio, F., Falcón, F., López, M., Fuentes, M., Alburquenque, C., Amaro, J., Bucarey, S. A., Nardo, A. D. (2014). Melanocytes and melanin represent a first line of innate immunity against

Candida albicans, Medical Mycology, 52(5), 445–452.

Teresa, V. B., Leonard, I. Z. (2010). Swimming into the Future of Drug Discovery: In Vivo Chemical Screens in Zebrafish. ACS Chemistry Bioliology. 5 (2), 159–161.

Thompson, J., Hayes, N., Gevaria, H., Harris, Y. (2017). The role of microglia and monocyte-derived macrophages in Toxoplasma gondii infection of the brain. Immunology, 198(1), 68.16.

Timpel, C., Strahl-Bolsinger, S., Ziegelbauer, K., Ernst, J.F. (1998). Multiple functions of Pmt1p-mediated protein O-mannosylation in the fungal pathogen *Candida albicans*. Journal of Biological Chemistry, 273(33), 20837–20846

Tissenbaum, H. A. (2015). Using *C. elegans* for aging research. Invertebrate Reproduction and Development, 59(1), 59–63.

Torosantucci, A., Bromuro, C., Chiani, P., De Bernardis, F., Berti, F., Galli, C., Norelli, F., Bellucci, C., Polonelli, L., Costantino, P., Rappuoli, R. and Cassone, A. (2005). A novel glyco-conjugate vaccine against fungal pathogens. The Journal of Experimental Medicine, 202(5), 597–606.

Torraca, V., Masud, S., Spaink, H. P., Meijer, A. H. (2014). Macrophage-pathogen interactions in infectious diseases: new therapeutic insights from the zebrafish host model. Disease Models and Mechanisms, 7(7), 785–797.

Toshiaki, J., Hara. (1971). 4 Chemoreception. Fish Physiology. 5, 79-120.

Tripathi, P., Tripathi, P., Kashyap, L., Singh, V. (2007). The role of nitric oxide in inflammatory reactions, 51 (3), 443–452.

Tsai, C. J.Y., Loh, J. M. S., and Proft, T. (2016). *Galleria mellonella* infection models for the study of bacterial diseases and for antimicrobial drug testing. Virulence, 7(3), 214–229.

Turner, S. A., Butler, G. (2014). The *Candida* pathogenic species complex. Cold Spring Harbor Perspectives in Medicine, 4(9), a019778.

Ueno, M., Fujita, Y., Tanaka, T., Nakamura, Y., Kikuta, J., Ishii, M., Yamashita, M. (2013). Layer V cortical neurons require microglial sup-port for survival during postnatal development. Nature Neurosci-ence, 16(5), 543–551.

Vanherp, L., Poelmans, J., Hillen, A., Govaerts, K., Belderbos, S., Buelens, T., Lagrou K., Himmelreich, U., Vande Velde, G. (2018). Bronchoscopic fibered confocal fluorescence microscopy for longitudinal in vivo assessment of pulmonary fungal infections in free-breathing mice. Scientific Reports. 8, 3009.

Vazquez-Torres, A., Balish, E. (1997). Macrophages in resistance to candidiasis. Microbiology Molecular Biology Review, 61(2), 170-92.

Verstrepen, k. j., Klis, F. M. (2006). Flocculation, adhesion and biofilm formation in yeasts. Molecular biology, 60(1), 5-15.

Victor, F., Menachem, G. (2000). Factors affecting growth of killifish, *Aphanius dispar*, a potential biological control of mosquitoes. Aquacultire, 184(3-4):255-265.

Vylkova, S., Carman,A. J., Danhof, H. A., Collette, J. R., Zhou, H., Lorenz, M. C. (2011). The fungal pathogen *Candida albicans* autoinduces hyphal morphogenesis by raising extracellular pH. mBio, 2 (3),1-12.

Walker, L. A., MacCallum, D. M., Bertram, G., Gow, N. A. R., Odds, F. C., Brown, A. J. P. (2009). Genome-wide analysis of *Candida albicans* gene expression patterns during infection of the mammalian kidney. Fungal Genetics and Biology, 46(2), 210–219.

Walsh, T. J., Garrett, K., Feurerstein, E., Girton, M., Allende, M., Bacher, J., Francesconi, A., Schaufele, R., Pizzo, P. A. (1995). Therapeutic monitoring of experimental invasive pulmonary aspergillosis by ultrafast computerized tomography, a novel, noninvasive method for measuring responses to antifungal therapy. Antimicrobial agents and chemotherapy, 39(5), 1065–1069.

Walters, K. B., Green, J. M., Surfus, J. C., Yoo, S. K., Huttenlocher, A. (2010). Live imaging of neutrophil motility in a zebrafish model of WHIM syndrome. Blood, 116(15), 2803–2811.

Wang, A., Fairhurst, A. M., Tus, K., Subramanian, S., Liu, Y., Lin, F., Igarashi, P., Zhou, X.J., Batteux, F., Wong, D., Wakeland, E. K., Mohan, C. (2009). CXCR4/CXCL12 hyperexpression plays a pivotal role in the pathogenesis of lupus. J Immunol, 182(7), 4448-4458.

Wang, N., Liang, H., Zen, K. (2014). Molecular Mechanisms That Influence the Macrophage M1–M2 Polarization Balance. Frontiers in Immunology, 5, 614.

Weerasekera, M. M., Wijesinghe, G. K., Jayarathna, T. A., Gunasekara, C. P., Fernando, N., Kottegoda, N. and Samaranayake, L. P. (2016). Culture media profoundly affect *Candida albicans* and *Candida tropicalis* growth, adhesion and biofilm development, Memorias do Instituto Oswaldo Cruz, 111(11), 697–702.

Wei, D., Zhang, X. L., Wang, Y. Z., Yang, C. X., Chen, G. (2010). Lipid peroxidation levels, total oxidant status and superoxide dismutase in serum, saliva and gingival crevicular fluid in chronic periodontitis patients before and after periodontal therapy. Australian Dental Journal, 55(1), 70–78

Wellington, M., Dolan, K., and Krysan, D.J. (2009). Live *Candida albicans* Suppresses Production of Reactive Oxygen Species in Phagocytes. Infection and immunity, 77(1), 405–413.

Westerfield, M. (2000). The zebrafish book. A guide for the laboratory use of zebrafish (*Danio rerio*), 4th ed. University of Oregon Press, Eugene, OR.

Wheeler, R. T., Fink, G. R. (2006). A drug-sensitive genetic network masks fungi from the immune system. PLoS Pathogens, 2(4), 328–339.

Whiteway, M., Bachewich, C. (2007). Morphogenesis in *Candida albicans.* Annual Reviews Microbiology, 61, 529–553.

Wiederhold, N. P., Lewis, R. E. (2003). The echinocandin antifungals: an overview of the pharmacology, spectrum and clinical efficacy. Expert Opin Investig Drugs, 12(8), 1313-33.

Wisplinghoff, H., Bischoff, T., Tallent, S. M., Seifert, H., Wenzel, P. R., Edmond, M. B. (2004). Nosocomial Bloodstream Infections in US Hospitals: Analysis of 24,179 Cases from a Prospective Nationwide Surveillance Study. Clinical Infectious Diseases, 39(3), 309–317.

Wu-Hsieh, B. A., Chen, W., Lee, H. J. (1998). Nitric oxide synthase expression in macrophages of Histoplasma capsulatum-infected mice is associated with splenocyte apoptosis and unresponsiveness. Infection and Immunity, 66(11), 5520–5526.

Yanai, H., Negishi, H., Taniguchi, T. (2012). The IRF family of transcription factors: Inception, impact and implications in oncogenesis. Oncoimmunology, 1(8), 1376–1386.

Yang, Y. (2003). Virulence factors of Candida species, Journal of microbiology, immunology, and infection = Wei mian yu gan ran za zhi, 36(4), 223–228.

Yona, S., Kim, K. W., Wolf, Y., Mildner, A., Varol, D., Breker, M., Jung, S. (2013) Fate mapping reveals origins and dynamics of monocytes and tissue macrophages under homeostasis. Immunity, 38(1), 79–91.

Yoshinari, N., Ando, K., Kudo, A., Kinoshita, M., Kawakami, A. (2012). Colored medaka and zebrafish: Transgenics with ubiquitous and strong transgene expression driven by the medaka b-actin promoter. Develop. Growth Differ, 54(9), 818–828.

Zeidler, D., Zahringer, U., Gerber, I., Dubery, I., Hartung, T., Bors, W., Hutzler, P. and Durner, J. (2004). Innate immunity in Arabidopsis thaliana: Lipopolysaccharides activate nitric oxide synthase (NOS) and induce defense genes. Proceedings of the National Academy of Sciences, 101(44), 15811–15816.

Zhang, J., Van Lanen, S. G., Ju, J., Liu, W., Dorrestein, P. C., Li, W., Shen, B. (2008). A phosphopantetheinylating polyketide synthase producing a linear polyene to initiate enediyne antitumor antibiotic biosynthesis. Proceedings of the National Academy of Sciences of the United States of America, 105(5), 1460–1465.

Zhang, S., Barros, S. P., Niculescu, M. D., Moretti, A. J., Preisser, J. S. and Offenbacher, S. (2010). Alteration of PTGS2 promoter methylation in chronic periodontitis. Journal of Dental Research, 89(2), 133–137.

Zhao, F., Shi, Y., Huang, Y., Zhan, Y., Zhou, L., Li, Y., Wan, Y., Li, H., Huang, H., Ruan, H., Luo, L., Li, L. (2017). Irf8 regulates the progression of myeloproliferative neoplasm (MPN)-like syndrome via Mertk signaling in zebrafish. Leukemia, 32(1), 149-158.

Zhu, W., Filler, S. G. (2010). Interactions of *Candida albicans* with epithelial cells. Cellular Microbiology, 12(3), 273-282.

Appendix 1: plasmid maps

Appendix 1: A) Plasmid map and features of destination vector 16AC2PSC_A_ptgs2_PMA-T3137 bp. **B)** Ad_ptgst2 sequence. The high-lighted sequence indicates EcoR, Xba and sp6_promoter sequence at the 5' end and T3_promoter, NotI and ApaI sequence at the 3' end.

A

Quality Assurance Documentation:16AC2PSC
Ref. No: 1960872
Designation: *E. coli* K12 OmniMAXTM 2T1
Gene name: Ad_ptgs2
Gene size: 757 bp
Vector backbone: PMA-T
Cloning sites: SfiI/SfiI

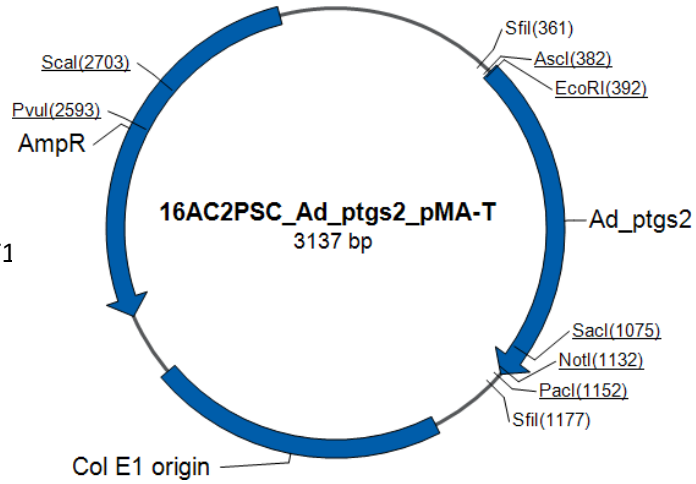

B

```
>Ad_ptgs2
CCGAATTCTCTAGAGATTTAGGTGACACTATAGAA
TGTTGGCCACGAGGCGTTCGGCCTGGTCCCGGGCCTCATGATGTACGCCACCATCTGGCT
CCGTGAACACAACCGAGTGTGTGATGTTTTGAAGGAAGTACACCCAGACTGGGATGATGA
AAGACTCTTTCAGACCACTCGACTCATCCTCATTGGCGAAACCATCAAGATCGTGATCGA
GGACTACGTGCAGCACCTGAGTGGATATAACTTCAAACTCAAGTTTGACCCAGAGCTGCT
CTTCAGCCAGCGTTTCCAGTACCAGAACCGCATCGCGTCTGAGTTCAACACCCTGTACCA
CTGGCACCCTCTGATGCCTGACAGCTTCCACATCGAGGAGAGGGATTACAGCTACAAAGA
GTTTGTCTTCAACACCACTGTCATGACTGAGCACGGCATTGGCAACCTGGTAGATTCCTT
CAGCAAGCAGATTGCAGGACGGGTCGCCGGTGGTCGGAACGTTCCGGGAGCCATCTTGTA
TGTTGCCATCAAGTCCATCGAAAACAGTAGAAAAATGCGTTACCAATCCCTGAATGCCTA
CAGGAAGAGATTCTCCATGAAGCCCTACACTTCATTTGAAGACATGACAGGAGAGAAAGA
AATGGCCGCCATACTGGAGGAGCTGTACGGGGACATTGACGCTGTGGAGCTCTACCCCGG
CCTGCTGGTGGAGAAACCCCGGCCAA
CCCTTTAGTGAGGGTTAATTGCGGCCGCGGGCCCGG
```

Appendix 2: A) Plasmid map and features of destination vector 16AC2PTC_Ad_mpx_pMA-T3354 bp. **B)** Ad_mpx(N-ter) sequence. The highlighted

Sequence indicates EcoR, Xba and sp6_promoter sequence at the 5' end and T3_promoter, NotI and ApaI sequence at the 3' end. The red nucleotides are the start codon.

A

Quality Assurance Documentation:16AC2PTC
Ref. No: 1960873
Designation: *E. coli* K12 OmniMAX™ 2T1R
Gene name: Ad_mpx
Gene size: 980 bp
Vector backbone: PMA-T
Cloning sites: SfiI/SfiI

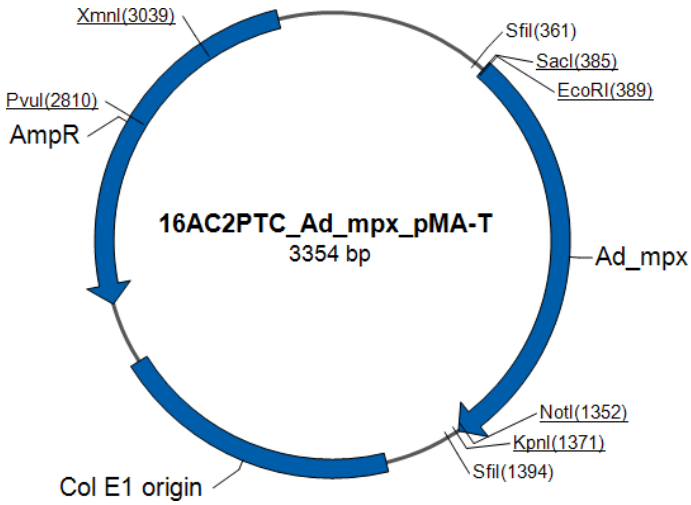

B

```
> Ad_mpx
CCGAATTCTCTAGAGATTTAGGTGACACTATAGAA
ATGCATCTC
TCTGTCTTTTTTATCCTGGGCCTCAGCCTGGTGACCAGCCACTCCAAACCCACAGGGGAA
GGACTTGGCGGTCCTTTCCTGCAAAAATGCTTTGAAGAAGCAAAAAAAATTGTAGATGAC
GCATACAAGTACTCCAGAGAAGAGAGCCTCAGACGAGTGCGCAGAGATGTGGTGCAGCCT
CATGATGCTCTTCGTCTCCTGAAGCAGCCCCGCGGCGATACTCGTTCAGCTGTGCGTTCG
GCCGACTACATGGCACAGACTCTACGTTTGGTCCAGGACAAAGTTCATCGGGTGCACAAG
CGCTCTCTCAATGCAACAGATTTGCTCACGGACCAAGATATGATAGAGCTTGCAAGAATT
ACTGGATGTGAGGCTCGAATTAGGAATCCATCTTGTGTCACCACTCCAAATATTAACAAG
TATCGCACAGCCACCAGCGTCTGCAACAACCTAAAAAACCCTCGCCTTGGAGCTGCCAAC
ACCCCATTCACCCGCTGGCTGCCCTCCGAGTACGACGACAGCATCTCCCAACCAAAAGGA
TGGGACAGAAACCGCAAATTCAACAACTTCTTACTCCCACTGGTGCGACAGGTGTCCAAC
AATATTTTGAGCACAACAGACGCAGGCGTGGTCAATGACACAGAGTACACTCACATGGTG
ACCTTGTTTGGTCAGTGGAATGACCATGACCTGTCCTTCACACCGTTCTCCCCCAGCATC
CGCTCCTTTAGCAACGGCGTGAACTGTGCTGACAGTTGCGAACACACTGAGCCATGCATC
CCTATCCCGATACCCCGTGGAGACCCCCGCCTTCCCTCCCGCCCAGACAGCTGCATCCCA
GCCTTTAGATCTGCTCCTGCCTGTGGAACCGGCTACTCTGCATTTAATTTTGGTGGAGAA
CCCTTTAGTGAGGGTTAATTGCGGCCGCGGGCCCGG
```

Appendix 3: A) Plasmid map and features of destination vector 16AC2PUC_Ad_Mfap1_pMK_RQ3249 bp. **B)** Ad_Mfap1 C-ter sequence. The highlighted sequence indicates EcoR, Xba and sp6_promoter sequence at the 5' end and T3_promoter, NotI and ApaI sequence at the 3' end. The red nucleotides are the stop codon and the green nucleotide is the 3'UTR.

A

Quality Assurance Documentation:16AC2PUC
Ref. No: 1960874
Designation: *E. coli* K12 OmniMAX^{TM} 2T1R
Gene name: Ad_mfap1
Gene size: 971 bp
Vector backbone: PMK-RQ (KnaR)
Cloning sites: SfiI/SfiI

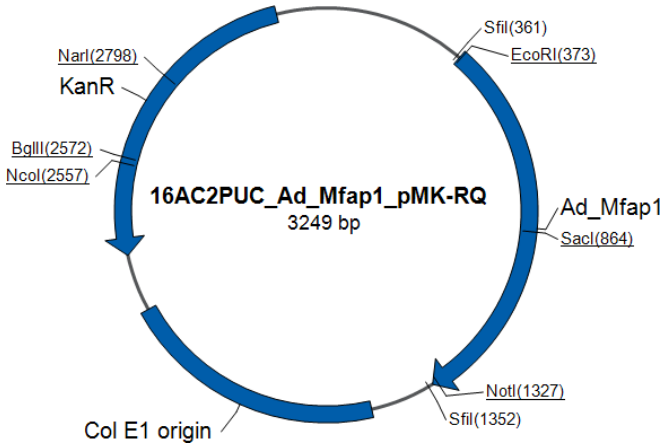

B

```
>Ad_Mfap1
CCGAATTCTCTAGAGATTTAGGTGACACTATAGAA
TATGGAGGTGGAGGAGGAGGGGAAGTCGGGGGAGGAGTCCGAGTCGGAATCGGAATACGA
GGAATACACGGACAGCGAGGACGAAGCGGAGCCGCGCCTCAAACCCGTCTTCATCCGCAA
GAAGGACAGAGTCACGGTGGCAGAGCGCGAAGCTGAGGAGCAGAAGCAGCGGGAGCTGGA
GGCCGAGGCCAAGCGACAGGCGGAGGAGCGCCGCCGCTACACCCTGAAAATCGTCGAGGA
GGAGGCAAAGAAGGAGTTCGAGGAGAATCGGCGCTCGCTGGCCGCCCTGGAAGCCCTGGA
CACGGACGGCGAGAACGAGGAGGAGGAATACGAGGCCTGGAAGGTCCGGGAGCTGAAACG
CATCAAGAGGGACAGAGAGGCCCGGGAAACGATGGAGAAGGAGAAGGCCGAGATCGAGCA
CTTCCACAACCTGACGGAGGAGGAGCGCCGGGCGGAGCTCCGGAACAGCGGCAAGGTCGT
CACCAACAAGGCCCAGAAGGGCAAATACAAGTTCCTGCAGAAGTACTACCACAGAGGGGC
GTTCTTCATGGATGAGGAGGAGGACGTCTATAAGAGAGACTTCAGCGCTCCCACGCTGGA
GGATCACTTCAACAAAACCATCTTACCCAAAGTCATGCAGGTCAAGAACTTCGGTCGGTC
GGGACGCACCAAGTACACCCACCTGGTGGACCAGGACACCACTTCGTTCGACTCGGCCTG
GGCTCAGGAGAGCGCTCAGAACAGCAAGTTCTTCAAGCAGAAGGCGGCAGGCGTGAGGGA
CGTGTTTGATCGCCCCACGGTGAAGAAGAGGAAGACCTAAGACGACCTAAGGTCCCGGTG
GCGTCGGCGAGCGCTCGGCACGCCGCCTCCAGACTGTTAAAGTGAAACTAAATCCACACA
CCCTTTAGTGAGGGTTAATTGCGGCCGCGGGCCCGG
```